DOCTORAL THESIS

On Design Principles and Calculation Methods Related to Air Leakages and Thermal Bridges in Well-insulated Building Envelopes

Jaanus Hallik

TALLINNA TEHNIKAÜLIKOOL
TALLINN UNIVERSITY OF TECHNOLOGY
TALLINN 2022

On Design Principles and Calculation Methods Related to Air Leakages and Thermal Bridges in Well-insulated Building Envelopes

JAANUS HALLIK

TALLINN UNIVERSITY OF TECHNOLOGY
School of Engineering
Department of Civil Engineering and Architecture
This dissertation was accepted for the defence of the PhD degree 20/05/2022

Supervisor: Prof. Targo Kalamees
                                    Nearly Zero Energy Buildings Research Group
                                    Department of Civil Engineering and Architecture
                                    School of Engineering
                                    Tallinn University of Technology
                                    Tallinn, Estonia

Opponents: Prof. Tore Kvande
                                    Department of Civil and Environmental Engineering
                                    Faculty of Engineering
                                    Norwegian University of Science and Technology
                                    Norway

                                    Prof. Raimondas Bliūdžius
                                    Institute of Architecture and Construction
                                    Kaunas University of Technology
                                    Lithuania

Defence of the thesis: 17/06/2022, Tallinn

Declaration:
Hereby I declare that this doctoral thesis, my original investigation and achievement, submitted for the doctoral degree at Tallinn University of Technology has not been submitted for doctoral or equivalent academic degree elsewhere.

Jaanus Hallik

                                    _____
                                                        Signature

European Union
European Regional
Development Fund

Investing
in your future

Õhulekete ja külmasildade mõju hindamise ja arvutamise põhimõtted hästi soojustatud piirdetarindite projekteerimisel

JAANUS HALLIK

Contents

Abbreviations

ach	Air change per hour, m^{-1}
ASHRAE	American Society of Heating, Refrigerating and Air-Conditioning Engineers
CFD	Computational fluid dynamics
EPC	Energy performance certificate
EPS	Expanded polystyrene
ETICS	External thermal insulation composite system
FD	Finite difference
FE	Finite element
IL 0	Installation level 0
IL 1	Installation level 1
IL 2	Installation level 2
IWEC	International Weather for Energy Calculations
LBNL	Lawrence Berkley National Laboratory
nZEB	Nearly zero energy building
PIR	Polyisocyanurate
PU	Polyurethane
PU OCF	Polyurethane one-component foam
PVC	Polyvinyl chloride
PW	Planed wooden surface
SW	Sawn wooden surface

Symbols

A	Area, m^2
C	Flow coefficient, $m^3/(h \cdot Pa^n)$
$\Delta U''$	Correction factor based on the level of insulation installation quality, $W/(m^2 \cdot K)$
ΔU_g	Correction term for air cavities, $W/(m^2 \cdot K)$
h_{add}	Additional length of the point thermal bridge, m
h_{eq}	Equivalent length of the point thermal bridge, m
h_{TB}	Actual length of the point thermal bridge, m
H_d	Direct heat transfer coefficient, W/K
H_{tr}	Transmission heat transfer coefficient, W/K
H_{ve}	Air leakage heat transfer coefficient, W/K
K	Number of point thermal bridges
L	Length, m
L_{2D}	Thermal coupling coefficient obtained from a two-dimensional numerical calculation, $W/(m \cdot K)$
L_{2Dref}	Thermal coupling coefficient obtained from a two-dimensional numerical calculation without thermal bridge, $W/(m \cdot K)$
L_{3D}	Thermal coupling coefficient obtained from a three-dimensional numerical calculation, W/K
L_{3Dref}	Thermal coupling coefficient obtained from a three-dimensional numerical calculation without thermal bridge, W/K
n	Number of measurements
n	Flow exponent, -
n_{50}	Leakage air change rate at 50 Pa air pressure difference, h^{-1}
P	Air pressure, Pa
q	Heat flux, W/m^2
q_{50}	Air leakage rate at 50 Pa air pressure difference, $m^3/(h \cdot m^2)$
$q_{50,base}$	Base value of air leakage rate, $m^3/(h \cdot m^2)$
Q_H	Annual heat loss through 1 m^2 of the building envelope, kWh/(m²·a)
q_v	Air leakage rate through the building envelope, m^3/s
R_1	Thermal resistance of insulation layer, $(m^2 \cdot K)/W$
c_p	Specific heat capacity of air, $J/(Kg \cdot K)$
R_{se}	Thermal resistance of external surface, $(m^2 \cdot K)/W$
R_{si}	Thermal resistance of internal surface, $(m^2 \cdot K)/W$

R_{tot}	Total thermal resistance of building envelope component, (m²·K)/W
U	Thermal transmittance, W/(m²·K)
U_c	Corrected thermal transmittance according to EN ISO 6946, W/(m²·K)
U_{c0}	Corrected thermal transmittance for installation quality level 0 according to EN ISO 6946, W/(m²·K)
U_{c1}	Corrected thermal transmittance for installation quality level 1 according to EN ISO 6946, W/(m²·K)
U_{c2}	Corrected thermal transmittance for installation quality level 2 according to EN ISO 6946, W/(m²·K)
U_{CFD}	Corrected thermal transmittance according to numerical calculation, W/(m²·K)
U_{Ch}	Variable thermal transmittance of the building envelope depending on the temperature difference between the interior and exterior temperatures, W/(m²·K)
V_{100}	Leakage air flow rate at 100 Pa air pressure difference, m³/h
V_{400}	Leakage air flow rate at 400 Pa air pressure difference, m³/h
V_{50}	Leakage air flow rate at 50 Pa air pressure difference, m³/h
$\dot{V}$	Air flow, m³/h

Greek letters

Δ	Delta, difference
χ	Point thermal transmittance, W/K
λ	Thermal conductivity, W/(m·K)
σ	Standard deviation
Ψ	Linear thermal transmittance, W/m²·K
Θ_e	Exterior temperature, °C
Θ_i	Interior temperature, °C
ρ_{air}	Density of air, kg/m³

Abstract
On design principles and calculation methods related to air leakages and thermal bridges in well-insulated building envelopes

Minimising heat transfer through the building envelope in nZEBs assumes careful optimisation of building fabric performance. Increased insulation thickness introduces new challenges because thermal bridges and air leakages contribute to a significantly high proportion of overall heat loss while also creating a risk of moisture accumulation inside the construction and deterioration of the building structure.

Underestimation of air leakages, thermal bridging and the effect of nonidealities inside the insulation layer along with non-ideal workmanship can lead to significantly higher heat losses than estimated for otherwise well-insulated building envelopes. This contributes to a performance gap, where targeted energy performance of the building is not met in practice. Minimising heat loss through air leakages and thermal bridging is challenging, mainly because widely used methods and empirical solutions are too imprecise in the case of well-insulated building envelopes while experimental knowledge and more detailed methods are too complex and time-consuming to implement in practical design process.

The objective of this thesis is to assess and further develop current normative methods used to estimate the heat loss through gaps, cavities and other nonidealities along with penetrating thermal bridging elements in well-insulated building envelopes with greater accuracy in limited time and resource conditions. For future practical use and predictive modelling the whole building and joint air leakage rates were measured, statistically assessed and tabulated by effecting factors for situations where direct measurement is not possible.

According to field measurements the airtightness of Estonian wooden buildings has improved by a factor of 10 since the minimum requirements for energy efficiency took effect. The median air leakage rate for buildings erected since 2009 is 1.1 $m^3/(h \cdot m^2)$ with base value for energy performance calculation of 3.0 $m^3/(h \cdot m^2)$. Prefabrication with the light-weight timber construction technology seems to be superior to on-site or traditional timber log building with the lowest calculated base value of 1.6 $m^3/(h \cdot m^2)$ for this group of buildings. The compactness factor and number of storeys did not have a significant effect on air leakage referring to the fact that if systematic quality assurance with a proper airtightness concept is used, the geometric and structural complexity of the building envelope will no longer be a key factor for achieving airtightness.

Wooden test specimens representing typical joints in building envelope with planed, sawn and plastic-coated cavities and two cavity thicknesses were filled with three different polyurethane (PU) foams and tested for air leakages according to standard EN 12114 in laboratory conditions. The surface property and thickness of the joint had a significant effect on the air leakage of joints filled with PU foam. In laboratory conditions consistent and a very low air leakage rate was obtained with planed timber surfaces. Joints with plastic-coated and sawn timber surfaces performed worse by a factor of 2 or more on average and contributed to a very variable airtightness with up to 28 % and 50 % test specimens failing the airtightness testing.

Even if air leakages are minimised through proper sealing, additional heat loss will still occur in small gaps and cavities inside the insulation layer caused by varying

manufacturing tolerances, thermal contraction of the material and poor workmanship, especially in the case of more complex building geometry. Numerical analysis indicated that the additional heat loss induced by air cavities between insulation boards due to nonidealities is highly dependent on the cavity diameter and temperature difference. Penetrating vertical air cavities with 5 mm, 10 mm and 20 mm diameters will increase the thermal transmittance in the wall construction by up to 10 %, 33 % and 59 % at 40 K temperature difference. In roof construction the effect is even more adverse, and a simplified method presented in EN ISO 6946 Annex F fails to describe this. The current thesis points out certain insulation solutions that should be reclassified in the standard that is in force today.

Parametric numerical assessment of different thermal bridges in a well-insulated construction was carried out to study the effect of minimal flanking element length in the numerical heat flow calculation and the possibility of simplifying the assessment of combined thermal bridges in steady-state conditions. In the case of a well-insulated building envelope, the sufficient length of the flanking element to adequately describe the linear thermal transmittance in a steady-state situation is equal to approximately its thickness. The shorter distance to the adiabatic cut-off plane suggested in this study can be used to disaggregate more complex thermal bridges with multiple combined junctions, allowing the separation of the thermal bridges, which can then be summed up arithmetically and thus reducing the need for separate calculation by up to 76 %.

The current thesis proposes a new method for the estimation of point thermal transmittance of composite (metal + other materials) elements, such as metal angles with plastic thermal brakes or timber, fixation anchors etc. inside the wall construction by combining results from two separate two-dimensional numerical heat flow calculations.

Lühikokkuvõte
Õhulekete ja külmasildade mõju hindamise ja arvutamise põhimõtted hästi soojustatud piirdetarindite projekteerimisel

Piirdetarindite soojuskadude vähendamine energiatõhusates liginullenergiahoonetes eeldab piirdetarindi toimivuse hoolikat kavandamist. Paksema soojustuskihi ning suurenenud soojustakistuse tõttu suureneb õhulekete ja külmasildade olulisus tarindi kogusoojuskaos.

Õhulekete ja külmasildade tegeliku mõju alahindamine ning soojustuskihi ebaideaalsustega mitte arvestamine võib kaasa tuua oluliselt suurema soojuskao kui paksu soojustuskihiga piirdetarindi puhul eeldada võiks ning eesmärgiks seatud hoone energiatõhususe tase jääb seetõttu praktikas saavutamata. Külmasildadest ja õhuleketest tingitud soojuskadude hindamine on praktikas probleemiks, sest kasutusel olevad tavapärased lihtmeetodid jäävad hästi soojustatud piirdetarindite puhul ebatäpseks ning detailsemad analüüsimeetodid on sageli liiga komplekssed ja aeganõudvad tavaprojekteerimisel rakendamiseks.

Käesoleva doktoritöö eesmärk on hinnata soojustusesiseste pragude ja külmasildade mõju arvestamisel praegu kasutusel olevate standardiseeritud meetodite adekvaatsust ning neid edasi arendada moel, mis võimaldaks hästi soojustatud piirdetarindite korral soojuskadude kiiret ja täpsemat analüüsi. Õhulekkearvu ennustamiseks või modelleerimiseks olukorras, kus hoone otsene mõõtmine ei ole võimalik määrati ja tabuleeriti suure hulga mõõtmiste baasil olulisemate mõjutegurite järgi õhulekkearvu baasväärtused nii tervikhoonete kui paisuva polüuretaanvahuga täidetud vuugilahenduste kohta.

Käesolevast doktoritööst selgus, et Eesti puithoonete õhupidavus on pärast energiatõhususe miinimumnõuete kehtestamist 2009. aastal ligi kümnekordselt paranenud. Uuemate puithoonete õhulekkearv on keskmiselt (mediaanväärtus) 1.1 m^3/(h·m^2) ning sellele vastav õhulekkearvu baasväärtus 3.0 m^3/(h·m^2) hõlmates 75 % valimist 84 % usaldusintervalliga. Kergkonstruktsioonis hoonete tehaseline tootmine tagab seejuures oluliselt parema õhupidavuse võrreldes platsiehitusega või traditsiooniliste tehaseliselt toodetud palkhoonetega, tagades vaadeldud mõjutegurite lõikes madalaima õhulekkearvu baasväärtuse tasemel 1.6 m^3/(h·m^2). Hoone kompaktsus ja korruselisus hoone õhupidavusele olulist mõju ei avaldanud, mis näitab, et läbimõeldud tihenduslahenduste ning süsteemse kvaliteedikontrolli tingimustes ei sõltu hoone õhupidavus enam oluliselt hoone arhitektuurse lahenduse või konstruktsiooni keerukusest.

Paisuva polüuretaanvahuga täidetud vuukide õhulekke laboratoorsel mõõtmisel leiti, et vuugi pinna omadused ning vuugi laius mõjutavad oluliselt vahuga täidetud vuugi õhupidavust. Hööveldatud puitpinnaga vuukide puhul täheldati laboritingimustes väga madalat õhulekkemäära ühtlaselt kõigi katsekehade lõikes. Plastikkattega ning saetud puitpinnaga vuukide puhul oli õhulekkemäär enam kui kaks korda kõrgem ning kuni 28 % ja 50 % vastavatest katsekehadest lekkisid seejuures kontrollimatult.

Lisaks otsesele õhulekkele tekib hästi soojustatud piirdetarindis täiendav soojuskadu ka soojustusplaatide vahel esinevate suletud õhutühimike tõttu. Sellised tühimikud tekivad materjali toomisel ja lõikamisel esinevate võimalike tolerantside, mahukahanemise ning ebaühtlase töökvaliteedi tõttu ning võivad varieeruda mõnest

mõnekümne millimeetrini. Arvutuslik analüüsi näitas, et tühimikusisesest õhuringlusest ja kiirgusülekandest tingitud täiendav soojuskadu on tugevalt sõltuv tühimiku laiusest ja temperatuuride erinevusest sise- ja väliskeskkonnna vahel. Läbivad vertikaalsed 5 mm, 10 mm ja 20 mm laiusega praod välisseina soojustuskihis suurendavad soojusläbivust vastavalt 10 %, 33 % ja 59 % kui temperatuuride erinevus sise- ja väliskeskkonna vahel on 40 K. Katusekonstruktsioonis on mõju veelgi suurem ning EN ISO 6946 standardi lisas F toodud lihtsustatud parandid alahindavad seda olulisel määral. Käesolev doktoritöö kirjeldab erineva ristlõikega osaliselt või täielikult soojustuskihti läbivate pragudest tingitud täiendavat soojusläbivust ning toob välja soojustuslahendused, mis tuleks standardi lisas ümber klassifitseerida.

Parameetrilisel arvutuslikul analüüsil vaadeldi mudeli katkestustasapindade minimaalse kauguse vähendamise mõju erinevate külmasildade joonsoojusläbivuse arvutamisel eesmärgiga lihtsustada omavahel kombineeritud külmasildade normatiivset analüüsi. Arvutustulemused näitasid, et hästi soojustatud piirdetarindi puhul on minimaalne vahekaugus külmasilla keskse elemendi ja katkestustasapinna vahel võrdne tarindi paksusega ilma arvutustäpsuse olulise vähenemiseta. See võimaldab keerukamad kombineeritud külmasillad katkestustasapindadega omavahel lahutada ning kasutada joonsoojusläbivuste aritmeetilist liitmist, vähendades nii praktikas oluliselt arvutustele kuluvat aega. Uuritud hoonegeomeetria puhul vähenes eraldi analüüsi vajavate sõlmede hulk kuni 76 %.

Käesolevas doktoritöös pakuti välja uudne meetod metallist fassaadikinnitite ja muude analoogsete väiksemate külmasildade punktsoojusläbivuse täpseks arvutamiseks kasutades kahemõõtmelist temperatuurivälja arvutusmeetodit.

List of publications

The list of the author's publications on the basis of which the thesis has been prepared:

I   Hallik, J.; Kalamees, T. (2019). Development of airtightness of Estonian wooden buildings. Journal of Sustainable Architecture and Civil Engineering, 24 (1), 36−43. DOI: 10.5755/j01.sace.24.1.23231.

II Hallik, J.; Gustavson, H.; Kalamees, T. (2019). Air leakage of joints filled with polyurethane foam. Buildings, 9 (7), 172. DOI: 10.3390/buildings9070172.

III Hallik, J.; Kalamees, T. (2020). A new method to estimate point thermal transmittance based on combined two-dimensional heat flow calculation. 12th Nordic Symposium on Building Physics, NSB 2020, Tallinn; Estonia; 6 Sept - 9 Sept 2020. EDP Sciences, #08005. (E3S Web of Conferences; 172). DOI: 10.1051/e3sconf/202017208005.

IV Hallik, J.; Kalamees, T. (2021). The effect of flanking element length in thermal bridge calculation and possible simplifications to account for combined thermal bridges in well insulated building envelopes. Energy and Buildings, 252 (111397). DOI: 10.1016/j.enbuild.2021.111397.

V   Hallik, J.; Klõšeiko, P.; Piir, R.; Kalamees, T. (2022). Numerical analysis of additional heat loss induced by air cavities between insulation boards due to non-ideality. (Under review, submitted to: Journal of Building Engineering 06.04.2022)

These publications are referred to in the thesis by their Roman numbers

Author's Contribution to the Publications

The author of the thesis is the principal author of all five publications with the following contribution:

I   Data curation and preparation and statistical analysis were carried out by the author. A number of air leakage tests in the large Estonian air leakage database were carried out by the author. Compilation of the methodology of statistical analysis and original draft preparation were carried out by the author. The review and editing of the paper were carried out and research principles of the study were developed in cooperation with the author's supervisor T.K.

II Data curation, statistical analysis and original draft preparation and review of the publication were carried out by the author. Compilation of the testing methodology, preparation of the test specimens, practical laboratory measurements and data acquisition were done by co-authors T.K and H.G.

III Conceptualisation of the study, compilation of the methodology, preparation of calculation models and conducting all numerical calculations were carried out by the author. Data visualisation and original draft preparation were carried out by the author. The review and editing of the paper were carried out in cooperation with the author's supervisor T.K.

IV The preparation of calculation models and conducting numerical calculations was carried out by the author. Original draft preparation was carried out by the author. The conceptualisation of this study, compilation of methodology and the review and editing of the paper were carried out in cooperation with author's supervisor T.K.

V   Calculation models were prepared and numerical calculations were carried out by the author. Experimental measurements in the climate chamber and validation of numerical models were done by co-authors P.K and R.P. Data visualisation and original draft preparation were conducted by the author. The review and editing were done in cooperation with P.K and T.K. The conceptualisation of this study, compilation of methodology and the review and editing of the paper were carried out in cooperation with the co-authors and author's supervisor.

1 Introduction

1.1 Background

A well-insulated, airtight and thermal bridge free building envelope is a key factor for nearly zero energy buildings (nZEBs) mandatory in the European Union from the year 2021 (EPBD, 2018). Minimising heat losses and combining a thermally optimised building envelope with the passive use of solar energy allows a significant reduction in the heat load and heating energy demand of residential buildings during the heating period. Minimising heat transfer through the building envelope in nZEBs requires careful optimisation of building fabric performance, thermal bridges and air leakages through the building envelope. These key factors related to heat loss are interconnected in practice and contribute to the three-dimensional transient heat loss through the building envelope.

The heat loss through the plane building envelope is defined and well described in EN ISO 6946 (2017), showing that increased insulation thickness corresponds to decreased heat loss. The thermal performance of the plane building envelope is well studied and the difference between mathematical ideal and construction practice is shown in (Gullbrekken, Kvande, et al., 2017; Kivioja & Vinha, 2020; O'Hegarty et al., 2021).

For older buildings a wide range of topics concerning airtightness of the building envelope have been studied in the past and the phenomenon along with affecting factors in older buildings have been sufficiently described. Increased insulation thickness in energy efficient buildings introduces new challenges when accounting for air leakages as infiltration and exfiltration airflows contribute to a higher proportion of heat loss while also creating the risk of moisture accumulation inside the construction and deterioration of the building structure if the air leakages are not minimised or avoided. In practice it is problematic to estimate the air leakages in the design phase of the building process. This is especially important in the case of timber constructions where the materials are more sensitive to extensive moisture and deterioration.

Thermal bridges and other nonidealities are present in the building envelope decreasing its overall thermal transmittance and increasing the heat losses locally. Penetrating structural elements with low thermal resistance in facade systems and air voids or cavities inside the insulation layer introduced by material tolerances and non-ideal workmanship can cause significantly higher heat losses than estimated for an otherwise well insulated building envelope. Increased insulation thickness and minimised air leakages in modern energy efficient buildings and nZEBs increase the effect of thermal bridges on the overall heat loss of the building envelope (Ge & Baba, 2015). The fraction of heat loss due to thermal bridge effects is highly dependent on architectural complexity and constructional solutions used in the building envelope, but is usually significant in nZEBs and can be as high as 30 % or more (Erhorn et al., 2010).

Underestimation of thermal bridging, the effect of nonidealities inside the insulation layers and air leakages leads to a performance gap, where the estimated energy performance is not met in practice. Minimising heat loss through air leakages and thermal bridging is challenging, mainly for two reasons:
1. the existing methods and empirical solutions are too imprecise in the case of well insulated building envelopes, and
2. the existing knowledge and more detailed methods are too complex and time-consuming to implement in the practical design process.

This PhD thesis studies the effect of air leakages and thermal bridges along with other nonidealities in the context of well-insulated building envelopes in order to provide robust, updated and more accurate methods to estimate the heat loss through air leakages and several types of thermal bridges that could be implemented in the design process of nZEBs and used to reduce the performance gap. This is especially important in the case of modular building prefabrication because of excessive junctions in the building envelope, prevailing use of timber elements which are prone to moisture damage and very limited time during the design process for thorough assessment of solutions.

1.2 Objectives and content of the study

The objective of the present thesis is to further develop current normative methods used to estimate the heat losses through gaps, cavities and other nonidealities along with penetrating thermal bridging elements in well-insulated building envelopes with a greater accuracy in limited time and resource conditions as well as heat loss through air leakages when direct measurement is not possible.

The specific objectives of the thesis were the following:

- To determine the airtightness and its variation and subsequent base values of Estonian wooden buildings for several grouping factors such as building envelope, construction process, number of storeys, compactness, energy performance, etc.
- To determine the air leakage of joints filled with different products of polyurethane (PU) foam with different typical joint surface properties and width.
- To assess the effect of additional heat loss through unintentional cavities in the insulation layer and provide suggestions for improving standardised methods.
- To determine the minimal length of flanking elements in numerical models used to calculate the linear thermal transmittance in the case of combined thermal bridges under steady-state conditions.
- To create a new method to assess the heat loss through small three-dimensional thermal bridges with a two-dimensional numerical heat flow calculation method.

The results of the thesis, described in the following chapters, are published in four journal articles and one conference paper. A graphical overview of the research contribution in relation to the system of European norms related to heat loss in building envelope is given in Figure 1.

It is expected that the airtightness of the building envelope has been improved over the years, especially after the minimum requirements for energy performance were set by legislation (MTMm nr 58, 2015). Several publications seem to conclude that the overall air leakage of the building envelope, even in modern buildings, depends mostly on the building quality and on subsequent factors that affect the building quality (Colijn et al., 2017; Kalamees, 2007; Mortensen & Bergsøe, 2017). There have been attempts to estimate the airtightness of the building envelope without measuring, based on component measurements and subsequent calculations, but no reliable method for estimation has been found (T. O. Relander et al., 2012). This means that in the design phase, or when calculating the energy use of existent buildings with no means of direct measurements, the statistical average values for different building techniques, construction types and different time frames must be used. The average airtightness of the existing building stock and the variation within subgroups can differ between regions as the building process and quality assurance measures are different.
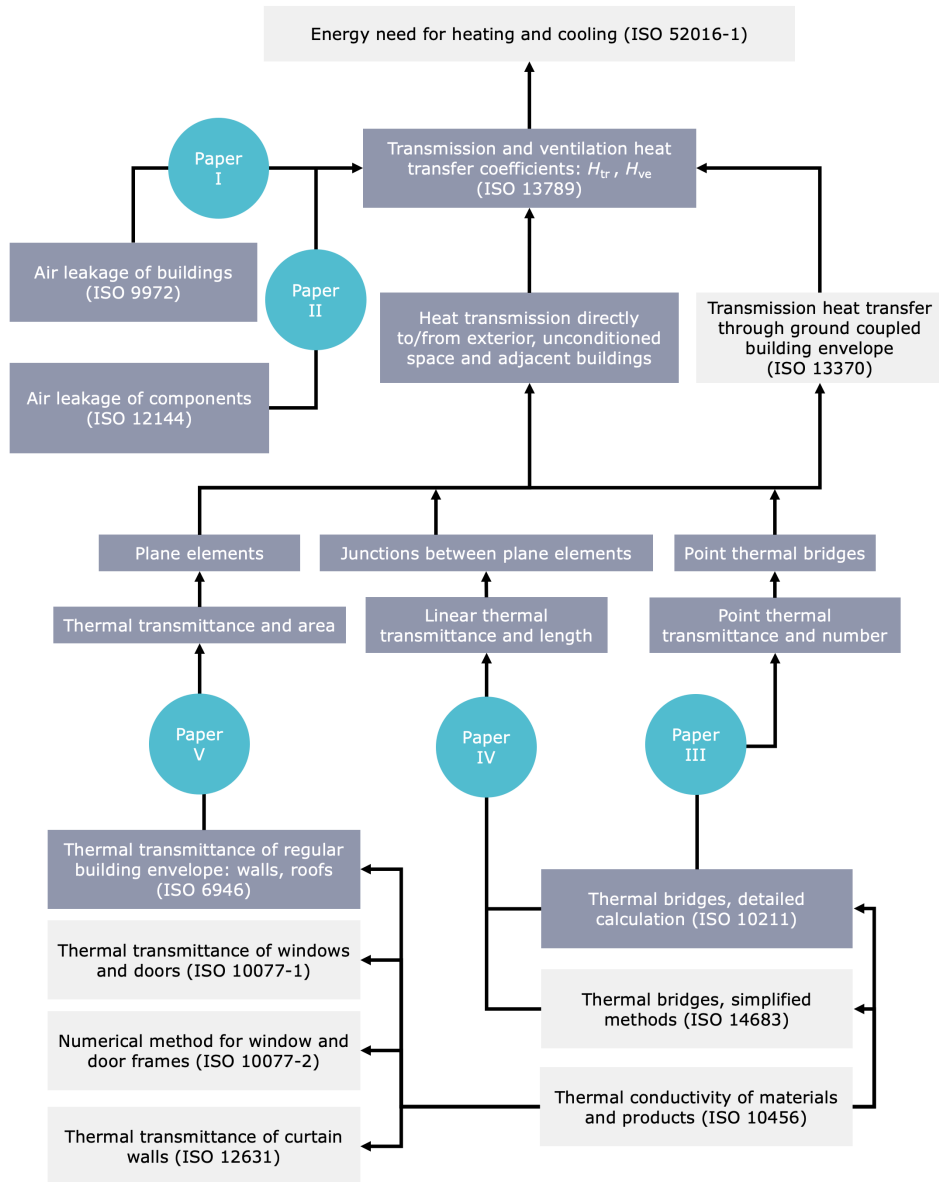
Figure 1. Research contribution of this thesis in relation to European norms related to heat loss in building envelope.

In PUBLICATION I a large number of whole-building airtightness measurements of Estonian wooden buildings are statistically analysed to determine the average (median) air leakage rates at 50 Pa and tested for significant differences within the grouping factors related to building complexity and quality assurance. Additionally, the base values of air leakage are calculated to include the effect of variation within the measured

groups to give practitioners a possibility of using construction specific estimation if airtightness testing is not yet feasible.

In existing buildings and for major renovations specific airtightness products, such as special sealing tapes for different surface materials, airtight membranes, rubber collars, adhesive sealing glues and joining elements, are frequently omitted in favour of expanding montage foams although the existing literature shows only variable success and sealing the gaps in the building envelope using only montage foam is generally not regarded as an infallible solution. Nevertheless, for accurate estimation of air leakages there is a need for detailed data about specific leakage rates depending on the width and type of the gaps in the building envelope, typically connections between wall and roof elements, window and door connections, etc. The expansion of foam cannot be fully controlled and therefore successful results can be highly dependent on surface properties along with foam properties and environmental conditions. In PUBLICATION II the air leakage of joints filled with PU foam and factors influencing it are studied to see if consistent airtightness can be achieved under varying conditions. Three typical surface properties common in prefabricated building envelopes are studied. Air leakage measurements through different joint configurations were conducted under laboratory conditions, based on the standardised method (EN 12114, 2000) and statistical analysis was used to retrieve the specific air leakages for joints with 10 mm and 30 mm diameter, three types of coating and three separate PU foam products.

Air leakages are just one aspect of additional heat loss caused by gaps and nonidealities between building envelope parts and within the insulation layer. Many studies in the existing literature describe the effect of air convection in and around insulation systems and conclude that there is a substantial increase of thermal transmittance if air circulation between the warm and the cold side around the insulation layer is enabled (Bankwall, 1972; Chebil et al., 2003; Huttunen & Vinha, 2013; Šadauskiene et al., 2009; Stankevičius et al., 2013). Therefore, it is crucial to seal the gaps between the rigid insulation boards to minimise the additional heat loss through the natural convection inside the construction. However, small gaps, slits and cavities between rigid insulation boards can contribute to higher heat loss even if the internal or external surfaces are sealed with tapes and air circulation between the warm side and the cold side around the insulation layer is avoided and the natural buoyancy-driven circulation is localised inside small cavities. A simplified method is described in EN ISO 6946 (2017) to include these effects into the thermal transmittance of an insulated structure; however, it is expected that the effect is underestimated in the case of well insulated building envelopes. In PUBLICATION V the effect of penetrating and partly penetrating differently shaped air cavities inside the insulation layer is studied. These systematically occurring cavities are caused by the varying tolerances of the insulation boards during the production process, on-site cutting and assembling as well as by poor workmanship, especially in the case of more complex building geometry. The numerical steady-state computational fluid dynamics (CFD) method is used to derive additional heat loss caused by the convective air movement and radiation inside a 200 mm thick insulation layer depending on the cavity thickness, thermal conductivity of the insulation material and temperature difference between the warm and the cold side of the structure. Correction factors given in EN ISO 6946 Annex F (EN ISO 6946, 2017) are compared to the study results and reclassification of the solutions and respective

correction factors in the standard is recommended to consider higher than expected heat loss through irregular air voids and cavities.

The overall heat loss of the building envelope is strongly dependent on thermal bridging elements that partly or fully penetrate the insulation layer. With many modern facade systems, the external cladding needs repeated fixation points and metal elements that penetrate the insulation and contribute to higher heat loss. Although several more prominent linear thermal bridges are accounted for in practice, the three-dimensional heat flow through the vast array of fixation elements and other point thermal bridges is usually neglected. Based on experience with less insulated structures it is usually expected that various point thermal bridges have a small contribution to the overall heat loss, but several recent studies have shown that within a highly insulated building envelope the extremely conductive metal fixing elements and cladding systems have a considerable impact on the effectiveness of thermal insulation layers (Theodosiou et al., 2019). Although the detailed numerical calculation methodology for steady-state three-dimensional heat flow is described in European standard EN ISO 10211 (2017) along with other related standards not implemented in general practice due to the time-consuming model preparation routine, lack of input data as well as the high number of different thermal bridges that have to be assessed for a single project. Additionally, the selection of software tools for three-dimensional numerical heat flow modelling is often limited due to their high price and steep learning curve compared to numerical heat flow calculation tools in two dimensions where several open source or free to use tools are generally available. There is a great need for simple methods and workflows to implement the three-dimensional thermal bridge effects in practice. In PUBLICATION III a new method is proposed to estimate three-dimensional heat loss and point thermal transmittances based on multiple two-dimensional calculations to provide a faster and more accessible solution for accurate estimation of all necessary thermal bridge elements in a well-insulated building envelope.

In complex situations, where multiple thermal bridges are in close proximity the calculation of linear thermal transmittance strictly according to the standard should be conducted separately for each such combination. This poses a practical problem as the number of different combinations (mainly related to window to wall connections in combination with corners, intermediate ceiling, etc.) is too large to follow in practice the standardised procedure. Furthermore, most whole building energy simulation tools do not usually have an interface for the highly fragmented input of linear thermal transmittances required to realistically model the overall thermal transfer value of an entire building envelope. In PUBLICATION IV a parametric numerical assessment of different thermal bridges in well-insulated constructions is carried out to study the effect of the flanking element in the numerical heat flow calculation to determine the minimal flanking element length for combined thermal bridges in numerical models that has minimal or no effect on the accuracy in estimating the linear thermal transmittance in steady-state conditions.

1.3 New knowledge and practical application

New knowledge discussed in this thesis relates to
- reconsideration of the factors affecting air leakages in building envelopes in the case of newer well insulated buildings;
- quantification of the air leakages through joints in building envelopes tightened with PU foam without additional sealing with tapes depending on joint geometry and surface properties;
- additional heat loss due to the buoyancy-driven air flow in cavities within the insulation layer arising from nonidealities in the building process and assessment of adequacy of the simplified method given in EN ISO 6946 (2017) to estimate the necessary correction factor for thermal transmittance with suggested reclassification of the described construction solutions;
- specification of a standard calculation method with proven performance for quick and accurate assessment of additional heat loss due to thermal bridges inside well-insulated building envelopes by simplifying the assessment of combined thermal bridges
- new method proposed for predicting three-dimensional heat flow and the point thermal transmittance of thermal bridges caused by full or partial penetration of the building envelope with metal elements with uniform geometry in the third dimension using two-dimensional numerical calculation.

Practical application discussed in this thesis relates to
- quantification of air leakages for the whole building simulation by statistically derived tabulated median and base values of total building air leakage rates for buildings of different age groups and construction technologies for use in practical application where the building's airtightness is not known or cannot be measured
- defining the surface properties of joints in the building envelope that contribute to failing airtightness when filled with PU foam without additional sealing with tapes
- suggested reclassification of different insulation solutions in EN ISO 6946 (2017) Annex F to incorporate the higher than estimated heat loss to the simplified correction factor for air cavities
- use of a significantly reduced flanking element length compared to the current method in EN ISO 10211 (2017) for steady-state numerical assessment of combined linear thermal bridges without substantial reduction in accuracy thus reducing the number of complex thermal bridges that need separate analysis and thereby the working hours of practitioners
- possibility of estimating the point thermal transmittance of different mounting brackets etc using two-dimensional software in cases where the three-dimensional calculation procedure is not possible due to lack of time, software tools or skills within the design team.

1.4 Limitations of the study

In PUBLICATION I the air leakage database of only wooden buildings was assessed as these buildings are more prone to failures and have a higher moisture related risk of deterioration. The degradation of airtightness over time is not considered.

In PUBLICATION II the air leakage of joints filled with PU foam was measured in laboratory conditions and premium quality PU foams were applied by skilled workers. The skill level of workers and real-life application conditions can induce significant differences between different foams and cause higher air leakages compared to laboratory measurements. However, this needs further research. The ageing of the freshly applied foam over a longer period of time and degradation due to thermal and dynamic shrinking were not taken into account.

In PUBLICATION III the assessment is based on highly conductive metal point thermal bridges. Application of the proposed method with penetrating concrete columns etc. needs further research.

In PUBLICATION III, PUBLICATION IV and PUBLICATION V the analysis was based on insulation layer thickness of 200 mm with a variable thermal conductivity to cover a wide range of thermal transmittances of well-insulated building envelopes. This thickness corresponds to the typical timber element length.

2 Heat loss of building envelopes

2.1 In general

The heat loss through building envelopes is a three-dimensional dynamic process where different physical phenomena such as conduction, convection and radiation take place simultaneously. These processes are strongly determined by the size, shape and thermal properties of the building envelope as well as the environmental conditions inside and outside of the building. For practical implementation these interconnected processes are usually broken up and assessed separately, typically by using more or less simplified approaches. In the building design process the estimation of heat loss through the building envelope is described in EN ISO 13789 (2017) where the transmission heat transfer coefficient H_{tr} and air leakage heat transfer coefficient H_{ve} are defined for the entire building. These values are necessary for estimating the energy need for heating and cooling a building. The coefficient H_{tr} includes the heat transfer through the plane elements, junctions between the plane elements where linear thermal bridges emerge and point thermal bridges while H_{ve} includes the heat transfer through the infiltrating and exfiltrating airflow. For both coefficients additional standards are needed to describe the necessary methods for calculating the heat transfer through windows and doors (EN ISO 10077-1, 2017; EN ISO 10077-2, 2017), curtain wall systems (EN ISO 12631, 2017), regular plane elements (EN ISO 6946, 2017), linear and point thermal bridges (EN ISO 10211, 2017) and ground coupled envelopes (EN ISO 13370, 2017) for component-wise assessment.

When the heat loss between the conditioned space and the external environment is considered the direct heat transfer coefficient H_d is calculated either directly for the whole building envelope by numerical methods using the modelling rules given in EN ISO 10211 (2017) or by using the simplified component based approach according to equation (1) defined in EN ISO 13789 (2017).

$$H_d = \sum_{i=1}^{N_i} U_i \cdot A_i + \sum_{k=1}^{N_k} \Psi_k \cdot l_k + \sum_{j=1}^{N_j} \chi_j \qquad , \text{W/K} \qquad (1)$$

where U_i is the thermal transmittance of element i of the building envelope in W/(m²·K), A_i is the area of element i of the building envelope in m², Ψ_k is the linear thermal transmittance of thermal bridge k in W/(m·K), l_k is the length of linear thermal bridge k in m, χ is the point thermal transmittance of point thermal bridge j in W/K.

The thermal transmittance of these plane elements of building envelope depends directly on the thermal resistance of the individual layers. Increasing the thickness of the insulation layer and decreasing the thermal conductivity of the insulation material reduce the thermal transmittance and the direct heat transfer coefficient accordingly. To account for the additional heat loss due to thermally inhomogeneous layers, mechanical fasteners and cavities within the insulation layer corrections to thermal transmittance shall be applied according to simplified methods described in EN ISO 6946 (2017).

The effect of air leakages through the building envelope is included in a separate heat transfer coefficient H_{ve} according to equation (2). However, if the infiltration air flow rate is known, this does not account for collateral effects of air leakages such as moisture condensation (Janssens & Hens, 2003) or cold air movement (Chebil et al., 2003) inside the insulation layer.

$$H_{ve} = \rho_{air} \cdot c_p \cdot q_v \qquad \text{, W/K}$$

<div align="right">(2)</div>

where q_v is the air leakage rate through the building envelope in m³/s and $\rho_{air} \cdot c_p$ is the heat capacity of air per volume in J/(m³·K).

2.2 Heat loss and thermal transmittance in well insulated building envelopes

The energy performance requirements have gradually become more stringent in the European Union (EU) after the Energy Performance Building Directive (EPBD, 2018) recast forced the member states to fully adopt the nZEB requirements for all new buildings and major renovations. Depending on the climatic conditions, availability of renewable energy sources and national differences the cost optimal levels of insulation differ between the member states. In Estonian climate the cost optimal insulation thickness in combination with triple-glazed windows is 200 mm (Pikas et al., 2014). Zangheri et al. (2018) calculated the cost-optimal retrofit measures to reach nZEB levels in different European countries and found that a typical nZEB building should have a well-insulated envelope (including insulation layers of 10–30 cm and double or triple low emissivity (low-e) windows) depending on climatic conditions. The necessary thermal transmittance of wall and roof constructions is in a range of 0.12–0.33 W/(m²·K) for Spain and Italy and 0.09–0.18 W/(m²·K) for all other countries corresponding to at least 200 mm thick insulation layer considering typical insulation materials.

Historically the heat loss of the building envelope has been mainly determined by the heat loss through plane elements due to a low thermal resistance of uninsulated walls, roofs and floor slabs. When the thermal resistance of the insulation is increased in modern buildings, the overall heat loss will be reduced and the proportion of other heat transfer components will become more prominent.

The effect of air leakages on thermal transmittance and heat losses of well-insulated buildings is strongly affected by their location (climate conditions and sheltering from wind), architectural and structural solutions (compactness, construction type, height), ventilation systems and overall building quality. The airtightness of buildings with different envelope structure has been shown to differ by a factor of 4 or more (Górzeński et al., 2014; Paap et al., 2012; Vinha et al., 2015). Jokisalo et al. (2009) showed that in Finnish cold climate air leakages through the building envelope cause about 15–30 % of the energy use of space heating including ventilation in a detached house with typical airtightness (n_{50} = 3.9 ach) and 30–50 % in the case of a leaky house (n_{50} = 10 ach). The resultant change in the energy use of space heating is 7 % on average, when the value of the building leakage rate n_{50} changes by one unit (1 ach).

Minimised air leakages in well-insulated and energy efficient buildings increase the effect of thermal bridges on the overall heat loss of the building envelope even more (Ge & Baba, 2015). The fraction of the heat loss due to thermal bridge effects is highly dependent on the architectural complexity and constructional solutions used in the building envelope, but it is usually significant in nZEBs and can be as high as 30 % or more (Erhorn et al., 2010).

While the heat losses through air leakages and dominating two- and three-dimensional thermal bridges are accounted for separately from the thermal transmittance of the building envelope according to EN ISO 13789 (2017) recent studies have shown that affecting factors have to be reconsidered when estimating the thermal

transmittance of a well-insulated building envelope. It is important to acknowledge that the method defined in EN ISO 6946 (2017) is based on the ideal electrical-thermal analogy and therefore, it is necessary to consider corrections to the thermal transmittance that include different aspects of nonidealities present in built solutions. In their review of building wall thermal characterisation, Evangelisti et al. (2018) showed that the measured thermal transmittance is about 20 % higher than the calculated one. O'Hegarty et al. (2021) reviewed 14 past studies and conducted additional experiments to study in-situ U-value (thermal transmittance) performance gap. A total of 13 tests from 7 different sites were conducted, 10 of which were on envelopes with theoretical thermal transmittances below $U{\leq}0.2$ W/(m$^2{\cdot}$K). It was shown that the deviation between theoretical and measured thermal transmittances increases considerably (127 % increase on average) at lower thermal transmittances corresponding to an increase in thermal transmittance by 0.2 W/(m$^2{\cdot}$K). Deviations of up to 297 % were observed and these cannot be explained by uncertainties in material properties or minor defects in the insulation layer.

When the insulation thickness is increased the role of different physical processes will become more prominent and will start to limit the actual thermal resistance of the insulation layer. Kivioja & Vinha (2020) studied natural convection inside 300 mm and 600 mm thick insulation layers of roof constructions and observed a 10 %–46 % increase in the heat flux inside a blown-in glass wool (density 25 kg/m^3) layer in the case of 20 K temperature difference and a 10 %– 63 % increase in the case of 35 K temperature difference. With a blown-in wood fibre insulation (density 40 kg/m^3) the increase of the heat flux in the range of 2 %–16 % was observed only in the case of 35 K temperature difference. Previous studies have also shown heat flux increase of similar magnitude and a strong effect of temperature difference on air convection inside thick insulation layers (Gullbrekken et al., 2019; Gullbrekken, Uvslokk, et al., 2017; Shankar & Hagentoft, 2000). A convection barrier in the middle of the insulation layer is recommended both in wall and pitched roof structures if the insulation thickness exceeds 200 mm to effectively decrease the temperature difference across each layer and limit the additional heat loss (Gullbrekken, Uvslokk, et al., 2017). Discrepancies between modelling and experimental data suggest that workmanship quality and material properties related to ageing and deformations can have a significant effect on the natural convection and additional heat loss at the border regions of the insulation layer (Wahlgren, 2005, 2007). Huttunen & Vinha (2013) observed unexpectedly large thermal transmittances from well-insulated wall elements filled with cellulose explaining the difference from estimated values by unexpected creep of material forming penetrating air gaps at the edges of test specimens. They emphasised that the natural convection inside this kind of cavities can have a significant effect on thermal transmittance. This effect is not limited to air-permeable insulation materials and can be especially problematic in the case of rigid insulation boards, where varying measurement tolerances (Šadauskiene et al., 2009), shrinkage due to ageing as well as thermal expansion and contraction (Tatara & Ricketts, ,2017) and poor workmanship in the case of more complex building geometry will incur partly or fully penetrating air cavities. The simplified method in EN ISO 6946 (2017) Annex F to correct for this effect underestimates the additional heat loss in the case of well-insulated building envelopes. Therefore, further research is needed to quantify the effect of air cavities with different width and geometry on the thermal transmittance.

The contribution of thermal bridges to overall heat loss is highly dependent on architectural and structural solutions but can easily be as high as 30–40 % of the total

heat loss of the building envelope (Al-Sanea & Zedan, 2012; Berggren & Wall, 2013, 2018; Capozzoli et al., 2013). A wide array of highly conductive metal fixing elements and composite cladding systems have to be included in calculating thermal transmittance according to EN ISO 6946 (2017). These can have a considerable impact on the effectiveness of thermal insulation layers (Theodosiou et al., 2019) However, not enough numerically derived product-specific data are available for all possible situations.

Consequently, for well-insulated building envelopes the thermal transmittance has to be corrected to include the effect of convection, multidimensional conduction as well as all nonidealities present on the building site. In practice this means that current methods must be reassessed and improved in order to accurately estimate the actual heat loss through air leakages, thermal bridges and nonidealities inside the insulation layer.

2.2.1 Airtightness and factors affecting it

In Estonia, lightweight timber-frame envelopes are common for detached houses. Today timber structures have become more and more common for apartment buildings and non-residential buildings (Ministry of Economic Affairs and Communications, 2022). Structures built from timber logs have been historically widespread and are still used for some projects. It is expected that the airtightness of the building envelope has been improved over the years as the knowledge and specific sealing products are generally available, especially since the minimum requirements for energy performance were set by legislation (MTMm nr 58, 2015). Several publications seem to conclude that in general the air leakage of the building envelope, even in modern buildings, depends on the quality of construction works and on factors that affect this process (Colijn et al., 2017; Kalamees, 2007; Mortensen & Bergsøe, 2017). For example, the number of storeys, compactness of the building volume etc. have been shown to increase the complexity of the work needed to achieve the required airtightness. Prignon & Van Moeseke (2017) conducted a thorough literature review to gather data and knowledge from 14 different countries and to rank the factors that have an influence on building airtightness based on their significance. While the envelope structure, building method, ventilation system and all aspects related to guidance and supervision are acknowledged as highly significant influencing factors, many other parameters related to insulation type and position, foundation and ceiling type etc. are not considered significant or are not enough discussed in previous research. Various parameters related to building geometry (building volume, number of storeys, floor area etc.) are often considered important, but significant inconsistency is present between different studies and air leakage pathways are not directly linked with building geometry (Prignon & Van Moeseke, 2017).

Attempts have been made to estimate the airtightness of the building envelope without measuring, based on component measurements and subsequent calculations, but no reliable method for such estimation has been found (T. O. Relander et al., 2012). Prignon & Van Moeseke (2017) also discuss this and conclude that lack of standardisation at different levels and the impact of workmanship and supervision partially explain why reliable and suitable models for predicting airtightness are difficult to develop. This means that in the design phase, or when calculating the energy use of existent buildings with no means of direct measurements, statistical average values for different building techniques, construction types and different time frames must be used. The average airtightness of the existing building stock and the variation within subgroups can be different in different countries as the building process and quality assurance measures are different. Therefore, data for similar regions are needed.

2.2.2 Air leakages of joints between building components

There are several different technical solutions for sealing the cracks, joints and penetrations through the building envelope. Special sealing tapes for different surface materials, airtight membranes, rubber collars, adhesive sealing glues and various montage foams, etc. are used with varying degrees of success. Although it has been shown that the overall airtightness of new buildings has improved significantly (Górzeński et al., 2014; T. O. Relander et al., 2012), the actual leakage rate and its variation are strongly related to overall quality assurance mechanisms and local building techniques (Vinha et al., 2015), especially for window related air leakages (Cuce, 2017). Polyurethane one-component foams (PU OCF) are self-adhesive and self-hardening sealing materials often used for door and window installation and filling other joints and gaps in the building envelope. Despite their widespread use it is not known if the necessary airtightness can be consistently achieved without the use of additional sealing tapes. The volume of PU OCF expands after application to fill all hollow spaces and hardens on contact with air humidity. The expansion of foam cannot be fully controlled and therefore successful results can be highly dependent on surface properties along with foam properties and environmental conditions. Different joints in the building envelope can have different surface materials. Depending on the construction technology, a cap between different envelope elements can have sawn wooden surface (wooden studs and beams at the end of wall and roof elements etc.), planed wooden surface (connection between wooden window frame, plywood and other similar wood-based products, planed wooden elements etc.) or plastic surface (connection between PVC window frame and wall). Air leakage of joints filled with PU foam in the case of all three surface types was measured under laboratory conditions (published in PUBLICATION II) to quantify the differences due to surface roughness and material as well as joint width and specific foam product and to determine if consistent airtightness can be achieved under varying conditions.

2.2.3 Additional heat loss due to air cavities inside the insulation layer

Air leakages are just one aspect of additional heat loss caused by gaps and nonidealities between building envelope parts and within the insulation layer. Previous studies have described the effect of air convection in and around insulation systems to conclude that there is a substantial increase of thermal transmittance if air circulation between warm and cold sides around the insulation layer is enabled (Bankwall, 1972; Chebil et al., 2003; Huttunen & Vinha, 2013; Šadauskiene et al., 2009; Stankevičius et al., 2013). It is therefore crucial to seal the gaps between the rigid insulation boards to minimise the additional heat loss through natural convection around the insulation layer. The remaining isolated small gaps, slits and cavities between insulation boards or between the insulation matt and structural elements can still contribute to higher heat loss due to the natural buoyancy-driven air circulation in localised small cavities. These air cavities inside an insulation layer can vary in size and shape and may lack filling or tightening with montage foam or a similar agent, especially when rigid insulation boards, such as many common external thermal insulation composite systems (ETICS) are used. The size, shape and distribution of this type of cavities are affected by varying tolerances of the boards during the production process, on-site cutting and assembling as well as due to poor workmanship, especially in the case of more complex building geometry. According to EN 13163 (2016) and EN 825 (2013), the allowed tolerances of board width and length are up to 5 mm and of board squareness up to 1, 2 and 5 mm/m. Such production

tolerances can in the worst case lead to up to a 15 mm wide cavity between 3 m long insulation boards.

Similar issues with manufacturing tolerances occur in the case of mineral wool boards. Deviations in the board length of up to 20 mm and board width of up to 5 mm in the manufacturing process were observed in a previous study about dual density rockwool boards (Šadauskiene et al., 2009); the observed deviation from squareness according to the width and the length was up to 3 mm/m. The observed width of actual vertical air cavities forming due to these deviations was up to 5 mm when insulation boards were installed (Šadauskiene et al., 2009). When an insulation layer is installed between timber or steel battens, additional cavities can occur due to non-ideal cutting and placement of insulation material.

Additionally, expanded polystyrene (EPS) is prone to shrinkage due to ageing as well as thermal expansion and contraction (Tatara & Ricketts, 2017). The alternating heating and cooling cycles cause changes in the cavity width between boards with increasing permanent deformation (Ricketts, 2018; Tatara & Ricketts, 2017). Altogether, the heat loss through a building envelope featuring all the irregularities of that kind is higher due to radiation and natural convection that occur inside these cavities and is highly dependent on cavity dimensions as well as the temperature difference between the internal and the external environment.

Several empirical studies have been conducted to give an insight into the approximate effect of penetrating cavities inside insulation layers. In 1972, in the first study conducted in Sweden, heat flow plates were used to test the change in local thermal resistance caused by penetrating cavities with 5, 10 and 30 mm width within an insulation layer; as the study concentrated mainly on the natural convection inside the insulation material itself, the overall effect of air cavities on the thermal transmittance was not quantified (Bankwall, 1972). Under the heat flow plate, the thermal resistance decreased locally by up to 8 % at a 5 mm wide cavity, up to 21 % at a 10 mm wide cavity and by up to 64 % at a 30 mm wide cavity (Bankwall, 1972). Although the effect on the entire wall area with fewer cavities will be significantly lower, the study showed that the natural convection inside such air cavities can have a significant impact on the thermal transmittance, depending strongly on the cavity width.

Similarly, Lowe et al. (2007) and Miles-Shenton et al. (2010, 2015) showed through field measurements in Great Britain that differently sized and shaped air cavities caused by poor workmanship can increase the observed thermal transmittance by a factor of 2 while the effect is strongly dependent on the actual observed nonideality.

Huttunen & Vinha (2013) conducted hot-box measurements to study the natural convection inside the exterior wall with air-permeable insulation and to assess the effect of horizontal cavities within an insulation layer caused by material displacement after installation or by non-ideal workmanship, resulting in rounded edges of insulation wool batts that form vertical air cavities between the edge of the insulation wool batt and the structural timber element. It was reported that negligent installation of insulation wool can cause horizontal air cavities at the upper or lower edges of the wall insulation layer and in the case of wet-sprayed cellulose insulation, these may be formed due to creep of the material (Huttunen & Vinha, 2013). Contrary to previous studies, it was concluded that air cavities formed due to poor workmanship do not dramatically increase (observed increase 5 % to 10 %) the thermal transmittance at no provision of air circulation from the hot side to the cold side referring to rounded edges of wool batts (Huttunen & Vinha, 2013). Creeps at the edge of wet-sprayed cellulose, which enable air circulation between

hot and cold sides, showed a significantly greater effect (Huttunen & Vinha, 2013): an up to 34 % increase compared to the ideal thermal transmittance calculated according to EN ISO 6946 (2017). However, the dimensions of the air cavities and their effect compared to standardised installation quality levels were not quantified.

A simplified method is described in EN ISO 6946 Annex F (2017) to include all these effects into the thermal transmittance of insulated structures. However, this method is expected to underestimate the effect in the case of well-insulated building envelopes. Additionally, the installation quality levels and the examples given in the standard are only descriptive and the limiting cavity widths and cavity length-to-area ratio are not quantified.

Further research is needed to quantify the effect of air cavities with different width and geometry on the thermal transmittance depending on the temperature difference between the interior and exterior sides of the insulation layer as well as to describe the cavity types and geometries with respective dimensions that correspond to simplified correction factors assigned to each installation level given in EN ISO 6946 (2017). Numerical simulation of computational fluid dynamics (CFD) with preliminary validation against the climate chamber experiment described in PUBLICATION V was used in this thesis to parametrically assess the additional heat loss caused by buoyancy-driven air circulation and radiation inside air cavities with different width, geometry and location in a well-insulated building envelope.

2.2.4 Thermal bridging

Thermal bridges are defined as part of the building envelope where the otherwise uniform thermal resistance is significantly changed by full or partial penetration of the building envelope by materials with higher thermal conductivity (EN ISO 10211, 2017). Typically, these represent different junctions in the building envelope where two or more building components are connected and form linear thermal bridges along the connection, e.g., exterior wall connection to roof, intermediate ceiling or floor, window and door perimeters etc. Additionally point thermal bridges with a localised effect occur when highly conductive metal fixing elements and cladding systems are used to attach an insulation layer and external cladding to a structural part of the building envelope. The fraction of heat loss due to these thermal bridge effects is highly dependent on architectural complexity and constructional solutions used in the building envelope.

Over the years there has been a lot of research to propose different ways to reduce the workload related to thermal bridge effects in building envelopes. Robust coefficients for defining the thermal transmittances have been used (EN ISO 13790, 2008), but these can underestimate the actual heat loss (Bergero & Chiari, 2018; Theodosiou et al., 2021; Theodosiou & Papadopoulos, 2008). A large number of thermal bridge catalogues have been composed for typical or approximate geometries (EN ISO 14683, 2017) for both national and international implementation along with specific attention to optimised window to wall connections (Adamus & Pomada, 2018; Cappelletti et al., 2011; Kalbe & Kalamees, 2019), special construction types (Chang et al., 2019; Viot et al., 2015), etc. Alternatively, there have been attempts to generate statistical models for typical junctions that would allow the estimation of linear thermal transmittance based on other building envelope parameters (Borelli et al., 2020; Capozzoli et al., 2013; Larbi, 2005), but these are bound to specific geometrical and constructional solutions and are not universally applicable. Despite this collective effort, a standardised numerical calculation is often still necessary and in the case of complex building geometry and window layout,

the number of combined thermal bridges is too large to follow the standardised procedure in practice. Moreover, for very complex junctions where highly conductive elements create a need for very fine meshing of the finite element model it may happen that those larger models with multiple combined junctions cause extended simulation duration as well as models reaching the maximum mesh size limitations.

In practice, junctions with two or more combined thermal bridges are sometimes handled as the sum of individual thermal bridges, but this is not allowed by EN ISO 10211 (2017) and not backed up by previous studies. It is expected that building envelope parts with variable layer properties related to thermal resistances as well as geometric dimensions need different minimal flanking element length to reach a uniform thermal distribution at the cut-off boundary condition. In EN ISO 10211 (2017) methodology, it is defined that for all regular building envelope elements (excluding ground coupled elements) the minimum flanking element length is 1.0 m or 3 times the thickness of the flanking element itself. Previous studies related to simplification of dynamic properties of thermal bridges through the equivalent wall (Martin et al., 2012) and mixed equivalent wall methods (Quinten & Feldheim, 2019) show that shorter flanking element lengths for those specific junctions can be used to describe the heat loss and surface temperatures without significant loss of accuracy compared to EN ISO 10211 (2017) methodology. The current thesis builds on these findings to detect the minimal flanking element lengths (PUBLICATION IV) through parametric numerical assessment of different well-insulated constructions and to use these shorter lengths to simplify the assessment of combined thermal bridges by arithmetically combining the linear thermal transmittances of unitary thermal bridges and thus reducing the required working hours of practitioners and the time and computing power for more complex numerical finite element (FE) or finite difference (FD) models due to smaller model geometry.

Although several more prominent linear thermal bridges are accounted for in the practice the three-dimensional heat flow through the vast array of fixation elements and other point thermal bridges is often neglected. Based on experience with less insulated structures it is usually expected that various point thermal bridges have a small contribution to the overall heat loss. However, several recent studies show that within well-insulated building envelopes the highly conductive metal fixing elements and cladding systems have a considerable impact on the effectiveness of thermal insulation layers (Theodosiou et al., 2019). Although the detailed numerical calculation methodology for steady-state three-dimensional heat flow is described in European standard EN ISO 10211 (2017) along with other related standards, it is not implemented in general practice due to the time-consuming model preparation routine, lack of input data as well as the large number of different thermal bridges that have to be assessed for a single project. Additionally, the selection of software tools for three-dimensional numerical heat flow modelling is limited due to their high price and steep learning curve (e.g. ANSYS (ANSYS inc., 2020), COMSOL Multiphysics (Comsol inc., 2020), PHYSIBEL Trisco and Solido (PHYSIBEL, 2020), etc.) compared to numerical heat flow calculation tools in two dimensions where several open source or free to use tools like LBNL Therm software package (LBNL Therm, 2020) and others are generally available.

Omission of numerical assessment of different point thermal bridges introduces great uncertainty in estimating the overall heat loss of highly insulated building envelopes and different parametric or simplified calculation procedures are needed for general practice to avoid the performance gap. Several efforts have been made to generalise the thermal bridge effects of different fixation elements inside the insulating layer with sensitivity

analysis to show the effect of different technical parameters contributing to the heat flow through these thermal bridges such as thermal conductivity of bridging elements and the surrounding insulation layer, thermal resistances of adjoining layers etc. (Lorenzati et al., 2016; Theodosiou et al., 2019; Theodosiou et al., 2015). Stonkuvienė et al. (2021) conducted hot-box measurements of steel ties and connectors inside 200 mm and 300 mm thick insulation layers and compared the results with numerical three-dimensional steady-state calculations as well as with the simplified procedure described in EN ISO 6946 (2017) to propose a method and predefined tabulated coefficients for the simplified method given in EN ISO 6946 (2017) depending on the fixed insulation layer thickness and material properties and height of connectors.

The current thesis proposes an additional method for accurate estimation of point thermal transmittance of composite (metal + other materials) elements, such as metal angles with plastic thermal brakes or timber, fixation anchors etc. inside the wall construction layer, by combining results from two separate two-dimensional numerical heat flow calculations.

The method is based on the hypothesis that the difference between the actual length of the thermal bridge in the third dimension and the equivalent length of the thermal bridge are strongly correlated to the difference between the thermal coupling coefficients derived from the respective cross sections (i.e., the central plane of the thermal bridge and the reference plane without it) and that the difference partially involves the effect of varying geometry and conductivities to the heat flow in the third dimension. The proposed methodology (PUBLICATION III) can be useful in general practice where the design team lacks the skills or software tools for conducting detailed numerical analysis in three dimensions.

3 Methods

3.1 Airtightness in Estonian wooden buildings

3.1.1 Studied buildings

The database of buildings with measured airtightness was constructed based on the results of different building envelope (Figure 2) airtightness measurements according to EN ISO 9972 (2015) and EN 13829 (2000) carried out between 2003 and 2017 (in total 522 buildings). The subset of all wooden buildings (in total 313 buildings) was used for further analysis. The buildings were classified based on building structure (log houses versus lightweight timber frame), the number of storeys (single-storey versus multi-storey), year of construction (built before 1945, built between 1946 and 1994, built between 1995 and 2008, built since 2009), energy classification (energy performance certificate A and B versus minimum requirements (EITMn nr. 63, 2018)) and compactness factors (envelope area ratio to volume and envelope area ratio to floor area). Additionally, companies (producers or building companies) with five or more measurements were grouped to analyse the effect of systematic measurements.
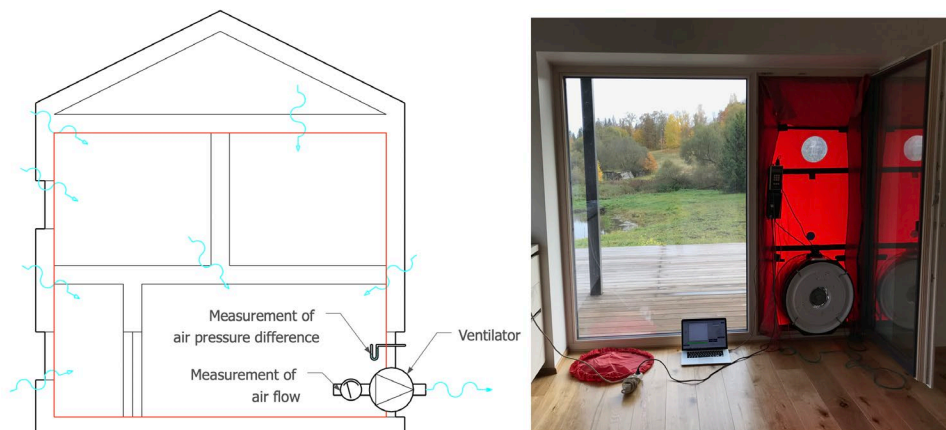

Figure 2. Measurement of building envelope airtightness with pressurization and depressurization test according to ENS ISO 9972 and EN 13829.

For all buildings built since 2009 an additional grouping based on production technology was described to compare on-site building practice to prefabrication for lightweight timber construction and hand-made building logs to prefabricated building logs for log houses. The prefabrication level for lightweight timber construction differs between companies. For volumetric modules the building envelope is typically finished internally and externally, and airtightness is controlled with vapour control membranes separately for each module. Prefabricated separate roof and wall elements are typically structurally complete but the internal finishing layers and external cladding are completed on site allowing for additional taping to connect the vapour control membranes between the separate elements. For both construction types, the vapour control layer (polyethylene sheet) is used on the interior side of the load bearing structures (Figure 3).
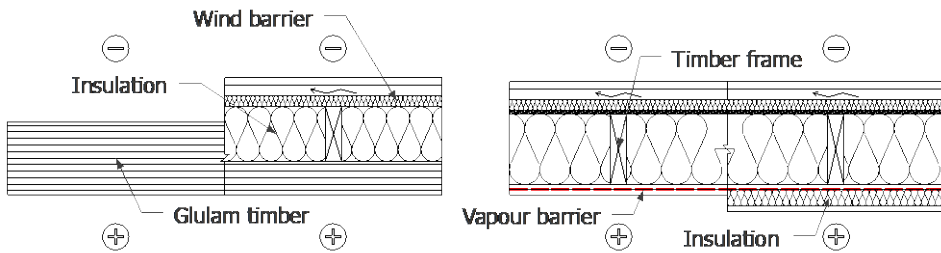
Figure 3. A typical solution for prefabricated glulam timber log structures (left) and lightweight external wall timber structure with and without additional installation layer (right) for better airtightness and moisture safety used in Estonia. The airtight layer is marked with a red dashed line.

For log houses the prefabricated glulam timber logs are assembled on site and typically no additional insulation nor separate airtightness layers are used. The energy performance requirements of those buildings are fulfilled through a more efficient heating system and a well-insulated lightweight roof structure with a similar vapour control membrane for airtightness. For glulam log structures with a thickness less than 200 mm an additional external insulation layer with a timber frame in combination with a wind-barrier layer, ventilated cavity and cladding is used for better energy performance.

3.1.2 Measurements

The air leakage measurements were carried out using a standardised pressurisation test according to method B (the test of the building envelope where all the intentional openings (for natural and mechanical ventilation) shall be sealed, the doors, windows and trapdoors being closed) described in EN ISO 9972 (2015) and EN 13829 (2000). The airtightness of the building envelope was tested in a range of pressure differences between 10 Pa and 60 Pa and reported with a standardised pressure difference of 50 Pa. At standardised pressure difference the air flow rate (V_{50}), the air leakage rate (q_{50}) and air change rate (n_{50}) were calculated by dividing the measured air flow rate by the external envelope area or by the internal volume of the building respectively.

For all buildings, a depressurisation test was carried out to test the airtightness of the building envelope. For some buildings an additional pressurisation test was performed to measure air leakage in reversed pressure conditions. For these buildings, the average leakage rate and other relevant test results were calculated as arithmetic means.

3.1.3 Statistical analysis and calculation of base values

The preliminary analysis of the data showed that the distribution of the measured air leakage (q_{50}) data is non-normal. Because of this, the median value along with 0.16 and 0.84 quantiles were used to describe the distribution within the different subsets of the data. The non-parametric Kruskal–Wallis rank test was used to determine statistical differences between different groups of the measured data. In case of a significant difference, subsequent pairwise comparison of subsets was carried out using the post-hoc Conover *test*. For the analysis, the statistical analysis software R (version 3.5.1) (R Core Team, 2018) was used with several add-on packages to allow non-parametric analysis and visualisation.

Along with median values, the mean value of the air leakage rate ($q_{50,mean}$) and standard deviation (σ_{q50}) of all groups were calculated to allow the estimation of the base value of the air leakage rate ($q_{50,base}$) for different groups of buildings.

The base value of the air leakage rate was calculated according to the method described in the Finnish quality assurance manual for airtightness of building envelope (RT 80-10974, 2009). The calculated base value depends on the group size and the variation within the group, so that 75 % of the measured buildings will be below the base value with a confidence interval of 84 % in the case of normal distribution of the means. The base value is calculated according to equation (*3*) as follows:

$$q_{50,base} = q_{50,mean} + 0.674 \cdot \sigma_{q50} + \sigma_{q50} \div \sqrt{n} \quad , \text{m}^3/(\text{h} \cdot \text{m}^2) \qquad (3)$$

where $q_{50,base}$ – estimated base value of air leakage rate [$\text{m}^3/(\text{h} \cdot \text{m}^2)$]; $q_{50,mean}$ – measured value of mean air leakage rate of the group considered [$\text{m}^3/(\text{h} \cdot \text{m}^2)$]; σ_{q50} – standard deviation of mean air leakage rate of the group considered [$\text{m}^3/(\text{h} \cdot \text{m}^2)$]; n – number of measured buildings in the group considered.

3.2 Air leakage of joints

3.2.1 Studied joints

In laboratory conditions 95 mm deep joints with two different widths (10 mm and 30 mm) and three different surface treatments (sawn wooden laths (SW), planed wooden laths (PW) and plastic surface (PVC)) filled with three different PU foam products (product L, product S, product K, all with high elastic recovery dimensional stability) from different producers were studied. To reduce measurement uncertainty three identical test specimens were prepared for each combination, totalling to 54 test specimens. Foam was applied to each joint twice, once from each side.

The width and surface material of studied joints represent typical situations in different building envelope structures (some examples given in Figure 4) where PU montage foams are used to limit air leakages. To improve measurement accuracy multiple joints with same width, surface properties and foam filling were incorporated into single test specimen. Depending on number of joints in each test specimen the cumulative length of joints was 5.89 m (10 mm) and 9.82 m (30 mm) for sawn timber surface and 6.93 m (10 mm) and 10.89 m (30 mm) for other surfaces.
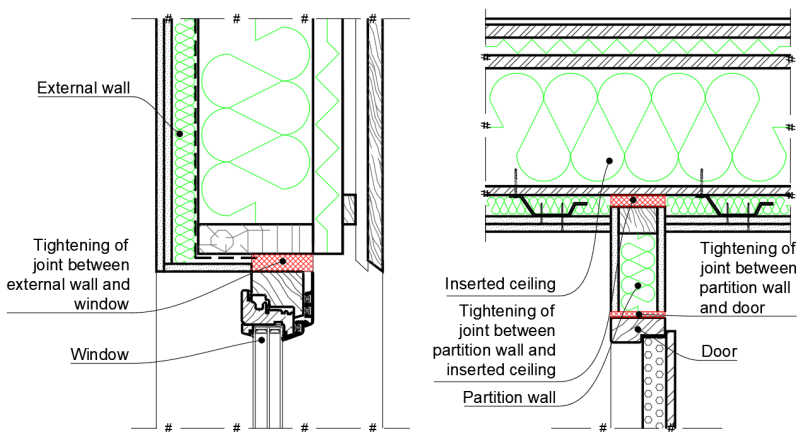

Figure 4. Joints in the building envelope where polyurethane filling is typically used.

Joints were filled in laboratory conditions by professional workers (provided by PU foam producers) according to filling instructions (Figure 5 a). It was targeted that foam should fill the joint through the width (Figure 5 b).

(a)   (b)

Figure 5. Filling the joints in a wooden frame (a) and an example of the cross section (from above) of the frame with filled joints (b).

3.2.2 Measurements

Measurements of the air leakage from the building envelope joints were conducted under laboratory conditions, based on the EN 12114 (2000) standard. The air flow rate and static air pressure differences were measured and recorded at each step automatically.

Air leakage test equipment shown in Figure 6 and Figure 7 consists of the following:

- hermetic chamber (3 mm steel plate) with the test area at a width of 334 mm, a height of 1000 mm and a depth of 100 mm
- fan (Elmo Rietschle G-BH1, positive pressure difference ≤100 kPa, negative pressure difference ≤90 kPa, air flow 2450 m³/h) for creating air flow
- frequency converter (EATON DC1-S24DNN-A20N) to regulate air flow
- air flow calibrator (Dwyer: GFC 1109 for 0-–5 l/min, GFC 1131 for 0–30 l/min, GFC 1144 for 0–500 l/min, with an accuracy of ±1.5 %)
- differential manometer (Produal PEL-DK for 0–1000 Pa and Dwyer Magnesense MS for 0–100 Pa, with an accuracy of ±1 %) for pressure difference measurements
- temperature and relative humidity sensor (Rotronic HygroClip SC05);
- data-logger (Grant Squirrel SQ2010, 8 channels) for automatic and simultaneous data reading and saving.
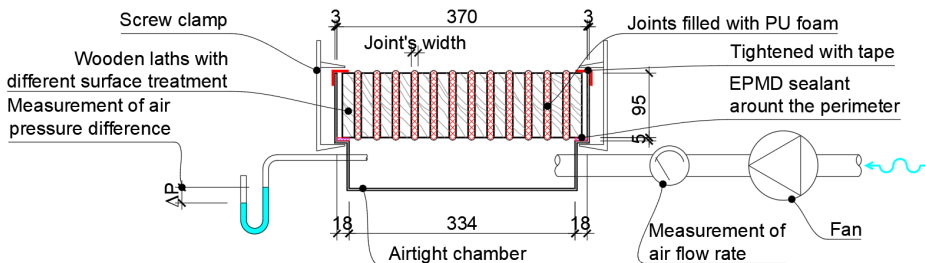

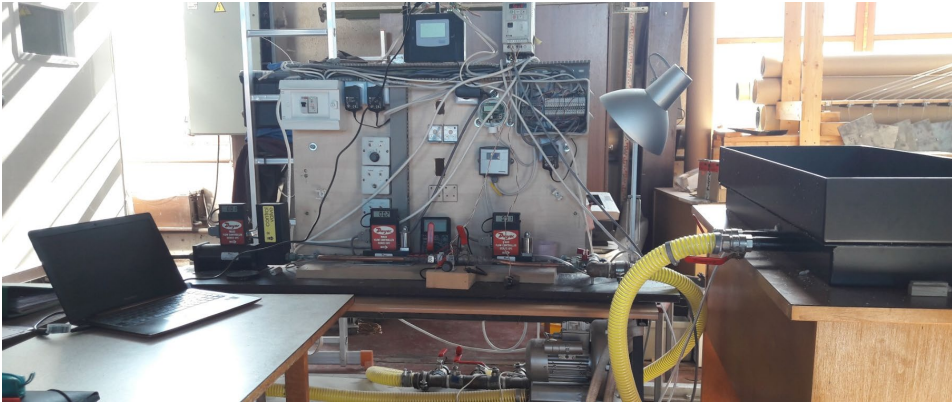*Figure 6. Schematic of equipment for air leakage tests (dimensions in mm).*

Figure 7. Equipment for air leakage tests

The air leakage through test specimens was measured at various air pressure differences, depending on the individual test, of up to ±600 Pa together with three pressure pulses (Figure 8 a) according to EN 12114 (2000) standard. The test sequence was carried out for each individual test specimen so that air flow rate was recorded for specific combination of joint width, lath surface treatment and foam product each time. The relation between the pressure difference and the air flow through the building envelope (Figure 8 b) allowed the results to be presented using the power law (equation (4)).

$$\dot{V} = C \cdot \Delta P^n \quad , \text{m}^3/\text{h} \qquad (4)$$

where $\dot{V}$ [m³/h] is the air flow, ΔP is the air pressure difference [Pa], and C [m³/(h·Pa^n)] and n [-] are constants obtained from curve fitting, with n ranging from 0.5 to 1.

The air leakage of each test specimen was measured at positive and negative pressure difference (different flow direction) with separate curve fitting.
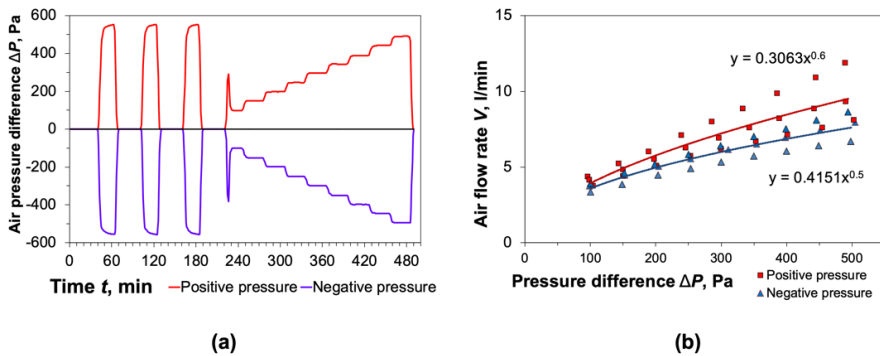

| (a) | (b) |

Figure 8. Air pressure difference over the studied joint (a) and its influence on the air flow rate (b).

3.2.3 Statistical analysis

The measurement data were combined into a database and analysed to test the significance of different factors. To allow comparison of test specimens with different lath and joint dimensions, the measured air flow rate was divided by cumulative joint length of each test specimen to obtain air leakage rates V_{100} … V_{500} [l/(min·m)]. Preliminary analysis of the measured air leakages over a wide range of pressure differences showed that some test specimens with the same foam, joint width and surface treatment had significantly larger air leakage rates. These test results were marked as 'failing specimens' and were omitted from more detailed statistical analysis. The failing criteria was defined as $V_{100} > 1.5$ l/(min·m). Nevertheless, all measurement results were used to determine the ratio of failed specimens grouped by foam, lath surface treatment and joint width. The cumulative distribution of leakage rates at 100 Pa pressure difference for different joint surface types along with graphical representation of failing test specimens is shown in Figure 9.
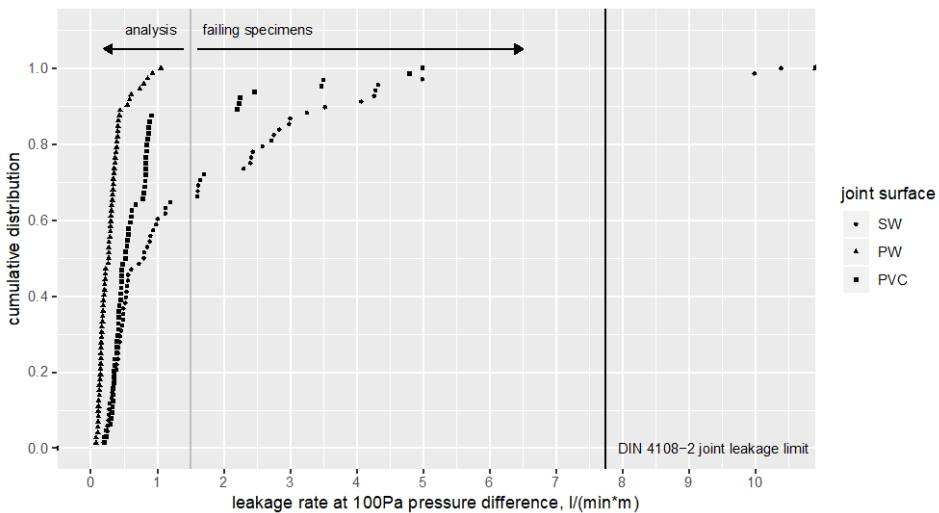

Figure 9. Cumulative distribution of leakage rates for different joint surface types at 100 Pa pressure difference and the limiting value for failing specimens.

The general limiting value of air leakage for airtight joints [0.1 m³/(m·h·(ΔPa)$^{2/3}$)] according to German standard DIN 4108-2 is also shown in the figure for corresponding pressure difference (Beuth-Verlag, 2013).

Due to measurement sensitivity, the air leakage rate of some test specimens could not be measured for the full range of pressure differences. Some test specimens were too tight for stable measurements at lower pressure differences while some test specimens with higher leakage did not sustain stable pressure difference at 500 Pa and 600 Pa pressure difference. Therefore, more detailed statistical analysis was done with air leakage rates at 400 Pa pressure difference. For the analysis a power law between pressure difference and air flow through the envelope (equation (4)) was linearised and statistically fitted on measured leakage rates and pressure differences separately for each test specimen. The respective flow coefficient C and exponent n derived for each test specimen were used according to estimate air leakage rates at exactly 400 Pa pressure difference (according to equation (4)). The mean air leakage rate (V_{400}) per

metre length of joint along with standard deviation (σ_{V400}) was calculated and tested for significant differences (One-Way ANOVA with 95 % confidence interval) between the different grouping factors (joint width, lath surface treatment, foam product). Additionally, air leakage rates at 50 Pa pressure difference were estimated from the same power curves to allow comparison with previous studies. For the analysis, the statistical analysis software R (version 3.5.1) was used with several add-on packages to allow statistical analysis and data visualisation (Kassambara, 2018; R Core Team, 2018).

3.3 Heat loss due to cavities within the insulation layer

Parametric steady-state numerical CFD analysis was used to assess the effect of gravity induced natural convection on heat and particle transfer inside differently shaped cavities within a 200 mm thick insulation layer.

3.3.1 Experimental study in a climate chamber for model validation

To validate the numerical CFD model measurement data from a climate chamber experiment were used to gather temperature and heat flux data with a penetrating cavity of 10 mm thickness. The test wall incorporated 200 mm thick polyisocyanurate (PIR) insulation boards with measured thermal conductivity of 0.019 W/(m^2·K) and a 0.3 mm thick duct tape covering was used to seal the cavities between insulation boards and to form a closed space. Interior and exterior temperatures along with the interior surface heat flux were measured at the cavity location as well as at one reference point away from the joints corresponding to the one-dimensional situation. The following sensors and loggers were used:

- temperature sensor Onset Hobo TMC20-HD (accuracy ±0.15°C) fastened using tape and hot glue with logger UX120-006M
- heat flux plate greenTEG gSKIN-XP (accuracy ±3 %) fastened using thermal paste and tape with logger Grant Squirrel SQ2020 1F8
- heat flux plate Hukseflux HFP03 (accuracy ±6 %) fastened using thermal paste with logger Grant Squirrel SQ2020 1F8 for PIR 1D conductivity measurements
- temperature sensor Pico PT100 1/10 DIN (accuracy ±0.03°C) with logger Pico PT-104 for the calibration of the Onset temperature sensors
- temperature sensor Siemens QFA3171 (accuracy ±0.6°C) built into the climate chamber for boundary condition measurements.

The temperature and heat flux measurements were taken at the central plane of the penetrating cavity at different heights measured from bottom of the cavity. The scheme of the experimental setup is shown in Figure 10.
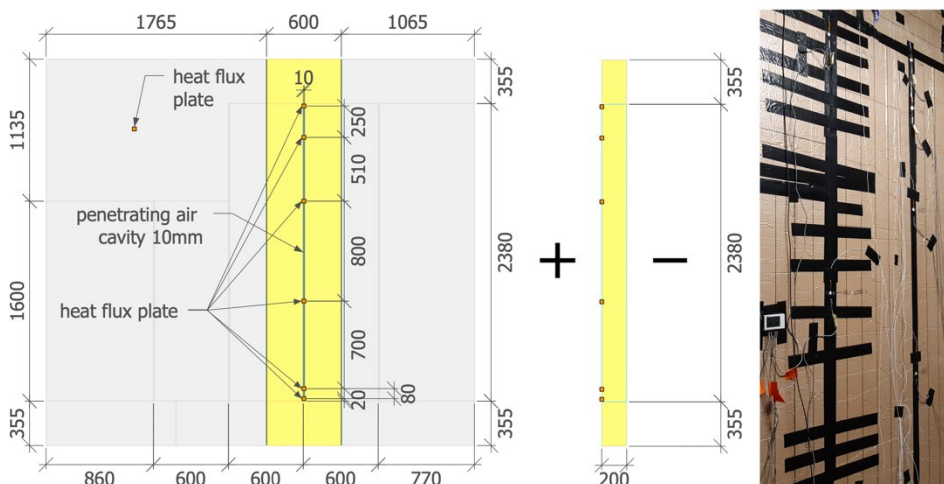
Figure 10. Scheme of the of test wall: sensor placement on the internal chamber side (left); cross section of the test wall (middle); photo of the test wall (right)

The heat flux plates with sensing dimension of 10 x 10 mm were fixed to the internal chamber side of the joint using thermal paste and tape. Heat flux values were recorded at 20 mm, 100 mm, 800 mm, 2110 mm and 2360 mm height. The exterior chamber temperatures ranged from –30 °C to +10 °C (with 10 °C intervals); the interior chamber temperature was set at +20 °C. Measurement results were averaged over periods of stable ambient temperatures for analysis.

The measurements regarding the air cavity with metal diagonal tie and additional filling with mineral wool, foam tape and PU foam were part of the study of thermal bridge effects of vertical diagonal tie connectors in precast concrete sandwich panels and are published in (Klõšeiko et al., 2020).

3.3.2 Simplified thermal transmittance correction (EN ISO 6946)

European standard EN ISO 6946 (2017) describes a simplified method to account for the effect of air cavities within an insulation layer. Three levels of installation quality are defined in EN ISO 6946 (2017) with appropriate correction factors $\Delta U''$ for installation levels 0 (IL 0), 1 (IL 1) and 2 (IL 2) shown in Table 1.

Table 1. Correction factors for air voids given in EN ISO 6946 Annex F

Installation level	Description	Correction factor $\Delta U''$, W/(m²·K)
IL 0	No air voids within the insulation, or where only minor air voids are present that have no significant effect on the thermal transmittance.	0.00
IL 1	Air gaps bridging between the hot and cold side of the insulation, but not causing air circulation between the warm and cold side of the insulation.	0.01
IL 2	Air gaps bridging between the hot and cold side of the insulation, combined with cavities resulting in free air circulation between the warm and cold sides of the insulation.	0.04

These correction factors are used to calculate the correction term for air cavities ΔU_g according to equation (5).

$$\Delta U_g = \Delta U'' \cdot \left(\frac{R_1}{R_{tot}}\right)^2 \qquad , \text{W/(m}^2\cdot\text{K)} \tag{5}$$

where R_1 is the thermal resistance of the layer containing the cavities, (m²·K)/W; R_{tot} is the total thermal resistance of the component ignoring any thermal bridging (thermally homogeneous building envelope), (m²·K)/W; $\Delta U''$ is the correction factor based on the level of insulation installation quality, W/(m²·K).

The correction term is then used to estimate the corrected thermal transmittance U_c of the building envelope according to equation (6).

$$U_c = U + \Delta U_g \qquad , \text{W/(m}^2\cdot\text{K)} \tag{6}$$

where U is the thermal transmittance of a component ignoring any air cavities and thermal bridging, W/(m²·K); ΔU_g is the correction term for air cavities in accordance with equation (5), W/(m²·K).

It is difficult to implement this simplified method correctly in real life conditions as the descriptions given for each installation level are limited in detail, have changed in different redactions of the same standard and do not quantify the amount and location of air cavities. For example, depending on the width of the installed insulation panels, the recurring distance between the penetrating air cavities differs and therefore also the average length per unitary envelope area is different. Additionally, the convective heat flow inside penetrating cavities is caused by the buoyancy-driven air flow, but it is not clearly described if and in which range of temperature differences this flow is accounted for in tabulated correction factors.

In our study, the numerical modelling is used to calculate detailed values for correction factors $\Delta U''$ depending on the temperature difference, thermal transmittance of the penetrated insulation material as well as the geometric characteristics of the assessed air cavities.

3.3.3 Description of model geometry

A simplified construction type of a single insulation layer with a thickness of 200 mm was used for the assessment with alternative thermal conductivities of 0.019 W/(m·K), 0.031 W/(m·K) and 0.040 W/(m·K), corresponding to the typical range of insulation materials used in nZEBs. The numerical domain is 600 mm wide, corresponding to the typical ETICS panel, and 3110 mm long, corresponding to the full storey height of a building (Figure 11). The numerical domain encloses one cavity between insulation boards along the length of the domain symmetric to cut-off planes, corresponding to an average cavity length-to-area ratio of 1.67 m/m². The dimensions of the numerical domains for the roof and floor constructions were kept the same for sake of comparison.
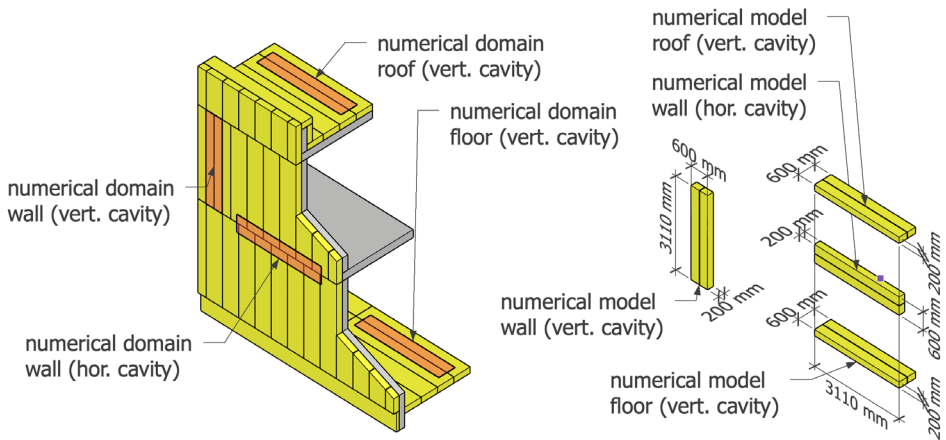
Figure 11. Location of numerical domains and respective calculation models with dimensions.

The thermal transmittance of this building component without the effect of thermal bridging and air cavities corresponding to EN ISO 6946 (2017) installation level 0 is U_{c0} = 0.194 W/(m²·K) with thermal conductivity of 0.040 W/(m·K). The simplified normative method suggests corrected thermal transmittance U_{c1} = 0.203 W/(m²·K) and U_{c2} = 0.231 W/(m²·K) for installation levels 1 and 2 with the same insulation material. With thermal conductivity of 0.031 W/(m·K) the respective values are U_{c0} = 0.151 W/(m²·K), U_{c1} = 0.161 W/(m²·K) and U_{c2} = 0.189 W/(m²·K) and with thermal conductivity of 0.019 W/(m²·K), U_{c0} = 0.094 W/(m²·K), U_{c1} = 0.103 W/(m²·K) and U_{c2} = 0.132 W/(m²·K).

For each location in the building envelope, CFD analysis was carried out on five main types of potential air cavities, as seen in Figure 12, totalling 483 numerical models:
a) penetrating cavity with rectangular cross section
b) rectangular cavity filled by PU foam (50 mm) from the external side
c) cavities in 2-layer insulation with rebate, tongue and groove edge
d) penetrating cavity with wedge-shaped cross section
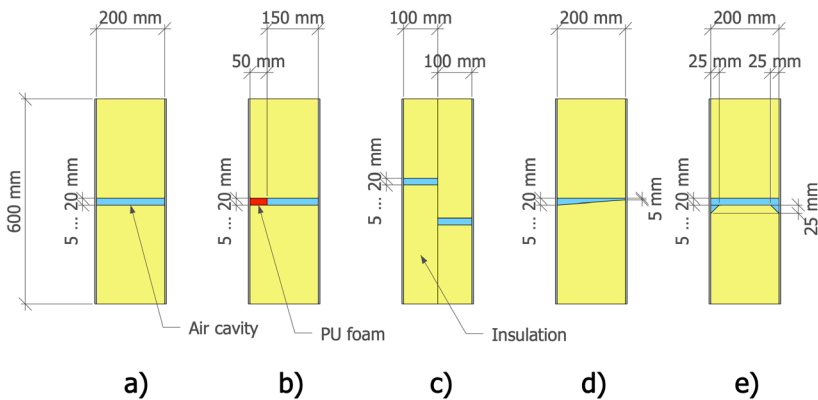e) penetrating cavity with additional triangular cut-outs.

Figure 12. Assessed geometric cases of different cavities.

3.3.4 Computational fluid dynamics analysis

Numerical parametric steady-state three-dimensional CFD calculation software ANSYS® Fluent Academic Student 2021 R2 (ANSYS inc., 2020) was used to assess the effect of radiation- and gravity-induced natural convection on heat and particle transfer inside cavities between rigid insulation boards and within the insulation material.

The models were set up with an adaptive computational mesh with very fine element size inside the air cavity and in its vicinity and in coarser elements near the cut-off surfaces (Figure 13) of the model as the number of finite elements was limited by the used software package.
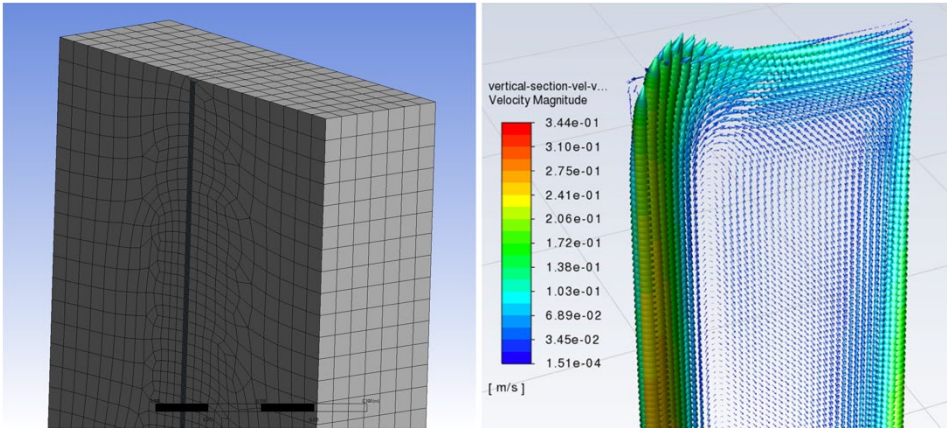

Figure 13. Example of an adaptive computational mesh (left) and calculated air velocities inside the penetrating air cavity (right). Screenshots courtesy of ANSYS, Inc.

The calculation model with 10 mm penetrating air cavity with a uniform cross section was validated with climate chamber measurements described in more detail in our previous study (Klõšeiko et al., 2020). The thermal resistances R_{si} = 0.08 (m²·K)/W and R_{se} = 0.08 (m²·K)/W for all calculations were defined according to the values measured in that study. Incompressible ideal gas and laminar flow were assumed for each calculation.

The convergence criterion defined in EN ISO 10211 (2017) was used to limit the number of iterations, i.e., the sum of all heat flows entering the object divided by half the sum of the absolute values of all heat flows shall be less than 0.0001. Continuity, velocity and energy absolute residual criteria were set to ≤0.00001.

The sum of all heat flows entering the object was then divided by the reference area of the geometric model to quantify the respective heat flux for each assessed case. The heat flux was then divided by the temperature difference used between opposite boundary conditions to quantify the corrected thermal transmittance U_{CFD} for each case and to calculate the correction factor ΔU_g by subtracting the nominal thermal transmittance U_{c0} without air cavities.

3.3.5 Calculation of annual heat loss in different climate conditions

As the increase in the thermal transmittance of a building envelope due to natural convection inside penetrating air cavities is strongly related to the temperature difference, the effect on overall heat loss of the building envelope is different in different climates. To assess this difference, a simplified heat loss calculation utilising heating degree days was used for five different locations across Europe, as shown in Figure 14.

For Estonian climate (Tartu), hourly temperature data from national test reference year for energy calculations were used (Kalamees & Kurnitski, 2006); for all other locations, hourly temperature data from ASHRAE International Weather for Energy Calculations (IWEC) data (ASHRAE, 2001) were used.
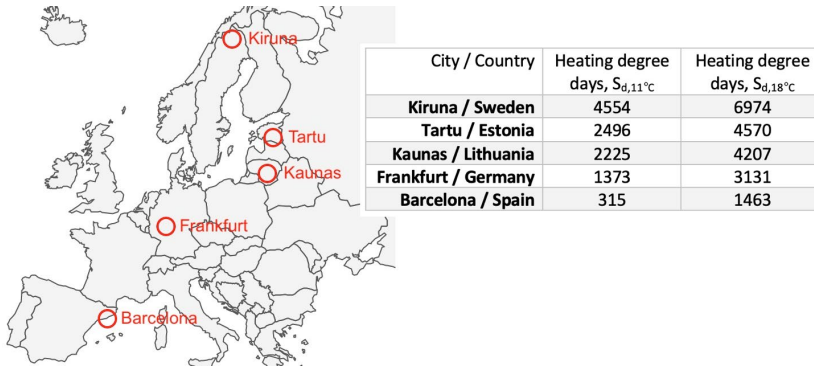

City / Country	Heating degree days, $S_{d,11°C}$	Heating degree days, $S_{d,18°C}$
Kiruna / Sweden	4554	6974
Tartu / Estonia	2496	4570
Kaunas / Lithuania	2225	4207
Frankfurt / Germany	1373	3131
Barcelona / Spain	315	1463

Figure 14. Locations with different heating degree days in a typical year used for the assessment.

For each assessed cavity type and insulation combination, a linear regression was used to retrieve slope and intercept for the numerically derived relationship between U_{CFD} and the temperature difference in the range of 10 K to 40 K. Based on regression parameters, the temperature dependent thermal transmittance U_{Ch} was calculated for each hour of the typical year and respective heat loss through the unitary area of the building envelope was accumulated for all hours where the exterior temperature is below the thermal balance point according to equation (7). The thermal balance point of a building will depend on overall heat loss of the building, available solar and internal heat gains etc, which are not defined in this study, because only a theoretical unitary area of external envelope is considered. In this study the value of thermal balance point was defined at 11 °C corresponding to 10 K below the interior temperature of 21 °C.

$$Q_H = 0.001 \cdot \sum (\Theta_i - 10 - \Theta_e) \cdot U_{Ch} \quad \text{if } \Theta_e < (\Theta_i - 10) \quad , \text{kWh/(m}^2\cdot\text{a)} \quad (7)$$

where Q_H is annual heat loss through 1 m^2 of the building envelope, kWh/(m²·a); Θ_i interior temperature, °C; Θ_e exterior temperature, °C; U_{Ch} variable thermal transmittance of the building envelope depending on the temperature difference between the interior and exterior temperatures, W/(m²·K).

3.4 Assessment of combined thermal bridges

Parametric steady-state finite element (FE) numerical assessment of different thermal bridges in a well-insulated construction was carried out (PUBLICATION IV) to study the effect of minimal flanking element length in the numerical heat flow calculation to determine the minimal flanking element length that has negligible or no effect on accuracy in calculating the linear thermal transmittance in steady-state conditions.

3.4.1 Numerical finite element analysis

Thermal bridges are defined as part of the building envelope where the otherwise uniform thermal resistance is significantly changed by full or partial penetration of the building envelope by materials with higher thermal conductivity (EN ISO 10211, 2017).

The linear thermal transmittance Ψ of an additional thermal bridge was calculated as described in equation (8).

$$\Psi = L_{2D} - \sum_{j=1}^{N_j} U_j \cdot l_j \qquad , W/(m \cdot K) \qquad (8)$$

where L_{2D}, W/(m·K), is the thermal coupling coefficient obtained from a separate two-dimensional numerical calculation; U_j, W/(m^2·K), is the thermal transmittance of the building envelope adjoining the thermal bridge and l_j, m, is the respective length of the adjoining part of the building envelope (i.e., flanking element length) described in the numerical model.

The thermal coupling coefficients L_{2D} for each case were obtained from two-dimensional numerical models with the respective heat flows divided by the temperature difference used in the model. The heat flow and thermal bridge calculations were carried out according to the methodology, boundary conditions and modelling rules described in EN ISO 10211 (2017). The software package LBNL Therm (LBNL Therm, 2020), which utilises steady-state finite element methods to numerically calculate two-dimensional heat flows in complex geometrical models, was used. This software package was selected because of programmable input and output and the author of this thesis has already developed pre- and post-processing workflows for this specific software that enables parametric study.

3.4.2 Studied geometry of thermal bridges

For the assessment were used three well-insulated construction types with three different insulation materials with an equal overall wall thickness of 480 mm:

A. lightweight timber construction with a 417 mm layer of insulation and repeating wooden c-beams as load bearing structures (Figure 15 - A; Figure 16 - 1, 2, 5, 6) with thermal transmittance between 0.060 and 0.094 W/(m^2·K) depending on the thermal conductivity of the insulation material

B. lightweight concrete (thermal conductivity 0.24 W/(m·K)) sandwich element with a 200 mm layer of insulation (Figure 15 – B, Figure 16 – 3, 4, 7, 8) with thermal transmittance 0.096–0.158 W/(m^2·K) depending on the insulation material

C. heavyweight concrete (thermal conductivity 2.3 W/(m·K)) sandwich element with a 200 mm layer of insulation (Figure 15 – C, Figure 16 – 3, 4, 7, 8) with thermal transmittance between 0.106 and 0.189 W/(m^{2}K) depending on the thermal conductivity of the insulation material.
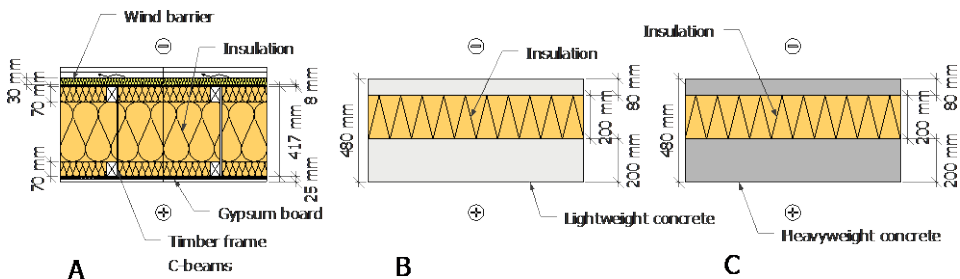

Figure 15. Three different wall construction types used in numerical analysis: A – lightweight timber construction, B – lightweight concrete sandwich element, C – heavyweight concrete sandwich element.

Assessment was carried out on five main types of thermal bridges connected to the external wall part for each construction type. The slab on the ground construction and the foundation geometry below the ground were similar for all assessed cases with 200 mm of heavyweight concrete on top of 250 mm insulation and thermal conductivity corresponding to that of the external wall insulation layer. In the case of ground coupled junctions the length of terrain and soil depth were set to 20 m and the length of the floor slab inside the building to 4 m according to EN ISO 10211 and the characteristic dimension of the floors of the model buildings used in this study. An overview of the assessed geometries is shown in Figure 16 and Figure 17:

- regular external wall to external wall connection (Figure 16 – 1 and 3)
- inverted external wall to external wall connection (Figure 16 – 2 and 4)
- window to external wall connection (Figure 16 – 5 and 7)
- external wall to slab on ground connection (Figure 16 – 6 and 8)
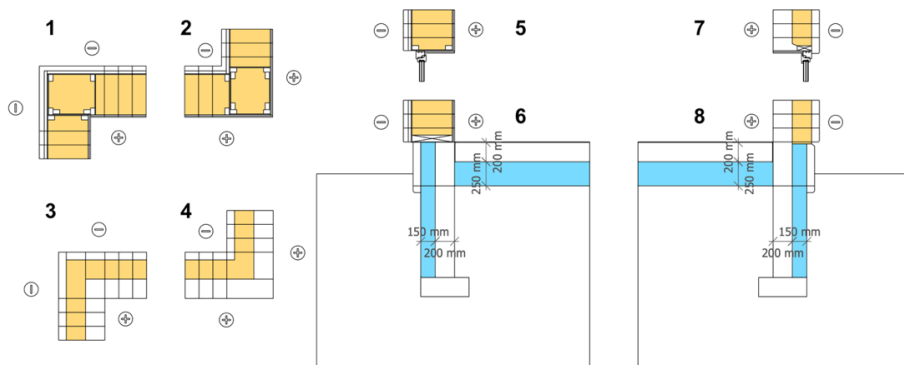- external wall to intermediate ceiling connection (Figure 17 – A).

Figure 16. Assessed geometry in main analysis: 1 and 3 – regular corner, 2 and 4 – inverted corner, 5 and 7 – window to wall connection, 6 and 8 – floor slab to external wall connection.

The flanking element length for each assessed thermal bridge was varied between 10 % and 100 % (corresponding to 1/3 and 3 times the thickness of the flanking element) with steps of 10 % (i.e., 0.144 m) totalling 10 different numerical models with flanking element lengths between 0.144 m and 1.44 m.

An additional geometry was included for further numerical analysis for the external wall with heavyweight concrete sandwich elements to study thermal bridges with significantly higher linear thermal transmittances. For this, two suboptimal levels ('medium' and 'high') of thermal bridges were described for the external wall to window connection and the external wall to balcony connection, as illustrated in Figure 17. The balcony connection junction with a 'high' thermal bridge corresponds to a fully protruding balcony slab while the junction with a 'medium' thermal bridge has a special decoupling element (ISOKORB) (Schöck bauteile GmbH, 2012) with an effective thermal conductivity of 0.124 W/(m·K) separating the balcony slab and the intermediate floor slab. The window connection with 'medium' and 'high' thermal bridges correspond to the suboptimal positioning of the window frame halfway or fully into the internal load bearing layer. The thermal conductivity λ of different materials used in the numerical analysis is described in Table 2.
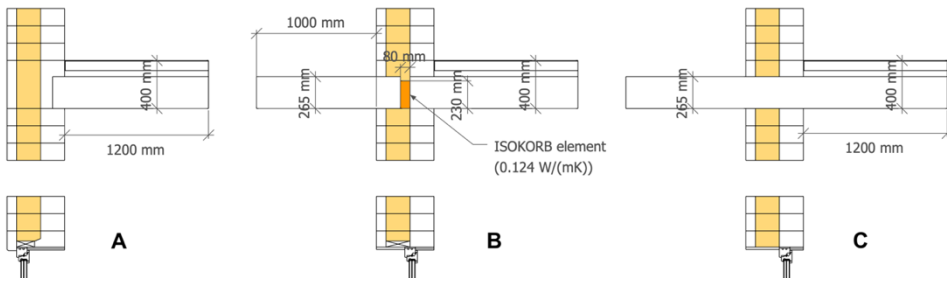
Figure 17. Additional geometry for follow-up analysis: A – junctions with 'low' thermal bridge, B – junctions with 'medium' thermal bridge, C – junctions with 'high' thermal bridge.

Table 2. Variable layer properties in assessed geometric cases

Construction type	Material layer	Thermal conductivity λ, W/(m·K)
Lightweight timber construction	0.03 m wind barrier board	0.031
	0.008 m fibreboard (OSB)	0.130
	0.417 m insulation layer	0.022 / 0.031 / 0.040
	0.012 m fibreboard (OSB)	0.130
	0.013 m gypsum board	0.210
Heavyweight concrete sandwich element	0.08 m heavyweight concrete	2.300
	0.2 m insulation layer	0.022 / 0.031 / 0.040
	0.2 m heavyweight concrete	2.300
Lightweight concrete sandwich element	0.08 m lightweight concrete	0.240
	0.2 m insulation layer	0.022 / 0.031 / 0.040
	0.2 m lightweight concrete	0.240
Slab on ground	0.2 m heavyweight concrete	2.300
	0.25 m insulation layer	0.022 / 0.031 / 0.040
	20.0 m soil layer	2.000
	0.15 m edge insulation layer	0.022 / 0.031 / 0.040

The assessed different insulation materials correspond, for example, to two typical mineral wool types, along with the PU foam insulation, that are used for nZEBs. In the scope of this study alternative insulation materials with the same thermal conductivity can be considered as interchangeable.

3.4.3 Description of whole building model geometry

To assess the potential for simplifications in real life situations, two existing buildings of different size and geometry were described, featuring several combined thermal bridges in the thermal envelope. A large non-residential four-storey office building (Figure 18 A) with mixed construction was used as a model building for bigger and more complex building geometry featuring 11 regular junctions with a single linear thermal bridge and 73 junctions with two or more combined thermal bridges according to the minimum flanking element length required by EN ISO 10211 (2017). A prefabricated two-storey wooden reference building (Figure 18 B) with a well-insulated lightweight timber frame wall and roof elements was used as an alternative example of detached houses featuring 8 regular junctions with a single linear thermal bridge and 26 junctions with two or more

combined thermal bridges. For both buildings, the number of combined thermal bridges was calculated based on the minimum distance between the different junctions according to EN ISO 10211 (2017).
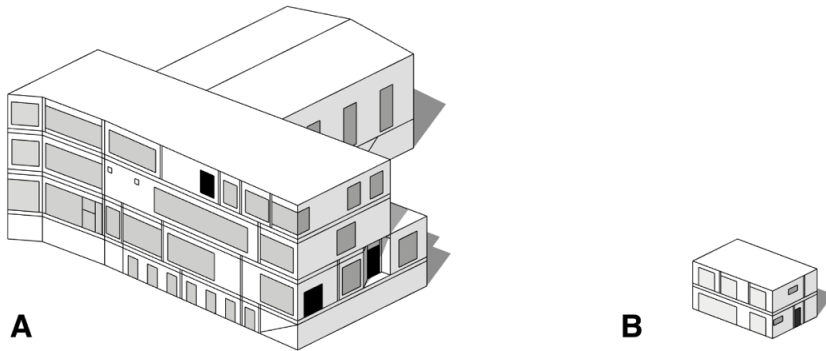

Figure 18. Model building envelope geometry of the large non-residential office building (A, 3 storeys + basement) and of the detached house (B, 2 storeys) used for assessment.

Subsequently, a new minimum distance between all junctions was defined based on numerical cases with the relative deviation of linear thermal transmittances of up to 0.5 %, 1.0 % or 2.0 %. Then the reduced number of combined thermal bridges was calculated by using these shorter flanking element lengths. This allows estimating the reduction of working hours for general practitioners when unitary linear thermal transmittances are combined for overall heat loss calculation.

3.5 A new method for estimating point thermal transmittance

A new methodology, published in PUBLICATION III for estimating the three-dimensional heat flow caused by a point thermal bridge is based on multiple two-dimensional numerical heat flow calculations. A multiple regression model was used to estimate the equivalent length of the thermal bridging element based on several parameters related to the heat flow through the building envelope.

3.5.1 Numerical finite element analysis

The point thermal transmittance χ, which represents the additional heat flow per 1 K air temperature difference between the internal and the external environment of this kind of penetrations is calculated as in equation (9).

$$\chi = L_{3D} - \sum_{i=1}^{N_i} U_i \cdot A_i - \sum_{k=1}^{N_k} \Psi_k \cdot l_k \qquad \text{, W/K} \tag{9}$$

where L_{3D} is the thermal coupling coefficient obtained from a three-dimensional numerical calculation, U_i is the thermal transmittance of the building envelope adjoining the thermal bridge, A_i is the respective area of the adjoining part of the building envelope in the calculation model, Ψ_k is the linear thermal transmittance of the additional thermal bridge if present derived from equation (8) and l_j is the respective length of the additional linear thermal bridge.

When the three-dimensional reference calculation without the assessed penetrating element already contains the effect of the additional linear thermal bridge, the point

thermal transmittance of an assessed thermal bridge can also be derived as in equation (10)

$$\chi = L_{3D} - L_{3Dref} \qquad , W/K \qquad (10)$$

where L_{3Dref} is the thermal coupling coefficient obtained from a separate three-dimensional numerical calculation model with identical boundary conditions, cut-off planes etc., but without considering the presence of the assessed point thermal bridge.

The thermal coupling coefficients L_{2D} and L_{2Dref} as well as L_{3D} and L_{3Dref} obtained from two- and three-dimensional numerical models are calculated as respective heat flows divided by the temperature difference used in the model.

The heat flow and thermal bridge calculations in this study were carried out according to the methodology, boundary conditions and modelling rules described in EN ISO 10211 (2017) by applying the software package Physibel Trisco (PHYSIBEL, 2020), which uses the finite difference method to numerically calculate three-dimensional heat flows in complex geometrical models. For each assessed thermal bridge case four heat flows were numerically derived:

- three-dimensional heat flow for the actual point thermal bridge
- three-dimensional reference heat flow for the same model omitting the thermal point penetration
- two-dimensional heat flow for the horizontal cross section taken from the central plane of the point thermal bridge element and
- two-dimensional reference heat flow for the horizontal cross section omitting the thermal point penetration.

To avoid the uncertainty generated by using different numerical software tools for two- and three-dimensional calculation, the two-dimensional heat flow was obtained from the three-dimensional calculation model in which the third dimension was set to unitary length (1 m) and modelled with uniform geometry in that dimension.

3.5.2 Description of the assessed thermal bridging elements

An external wall construction with an external insulation layer, wind barrier layer and ventilated cladding with a penetrating metal bracket fixed to the vertical timber elements was assessed. Schematic horizontal cross sections for thermal bridge cases and reference cases are shown in Figure 19.
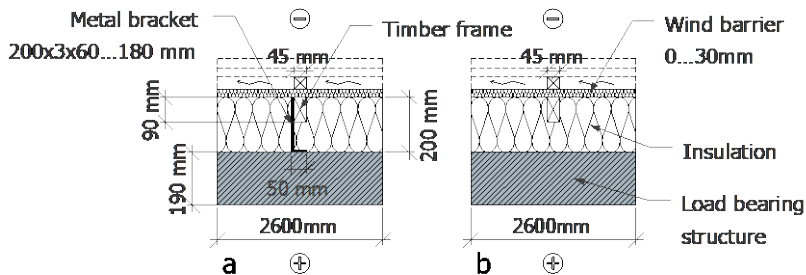

Figure 19. Horizontal cross section of the assessed external wall for calculating the thermal coupling coefficient L2D with a thermal bridge (a) and L2Dref for reference cases (b) without a thermal bridge.

Previous studies have shown that along with the thermal conductivity of the penetrating element itself the thermal conductivity of the insulation material and its layer thickness used in the building envelope as well as the resistances of the layers covering the penetrating element on the internal and external sides have a significant effect on point thermal transmittance (Theodosiou et al., 2019; Theodosiou et al., 2015). In the current study the thermal conductivity λ of the internal load bearing structure, insulation layer and wind barrier layer as well as the metal thermal bridging element was varied as described in Table 3. The assessed insulation materials correspond to two different typical mineral wool types along with polyurethane foam insulation that are used in this kind of construction in nZEBs.

Table 3. Variable parameters used in numerical heat flow analysis

Parameter	Description	Thermal conductivity λ, W/(m·K)
Load bearing structure	0.19 m reinforced concrete	2.50
	0.19 m aerated concrete	0.15
Insulation layer	typical mineral wool	0.040
	good mineral wool	0.031
	polyurethane foam	0.023
Wind barrier	0.009 m gypsum board	0.250
	0.030 m gypsum board	0.250
	0.030 m mineral wool board	0.031
	0.030 m fibreboard	0.055
	only wind barrier membrane	(-)
Metal bracket	regular steel	55
	reinforced steel	17
	aluminium	160

In addition to variable thermal conductivity and layer thickness the length of metal bracket in third dimension was varied to include brackets with the following lengths: 0.06 m, 0.12 m and 0.18 m. The thickness of metal brackets was set to 0.003 m in all calculated cases. Altogether 102 different combinations were calculated.

The cut-off planes for two- and three-dimensional models were selected according to EN ISO 10211 (2017) to eliminate the effect of thermal bridges on the heat flow distribution near the cut-off planes of the calculation model. The total width of the two-dimensional calculation model was 2.60 m while the width and height of the three-dimensional calculation model were both 2.60 m as shown in Figure 20.

Based on three-dimensional thermal coupling coefficients, point thermal transmittance was calculated as in equation (10). The acquired point thermal transmittance was divided by the difference of two-dimensional thermal coupling coefficients to obtain the equivalent length h_{eq} of the thermal bridge. The equivalent length of thermal bridge therefore expresses the hypothetical length of 2D thermal bridge cross section which amounts to heat loss equal to point thermal transmittance of real 3D thermal bridge. As the point thermal transmittance of the bridging element is directly related to the actual thermal bridge length, this effect is omitted from further analysis by subtracting the actual physical length of the considered thermal bridge h_{TB} from the equivalent

length of the thermal bridge h_{eq}. The effect of different parameters is tested against the additional length of the thermal bridge h_{add} as in equation (11).
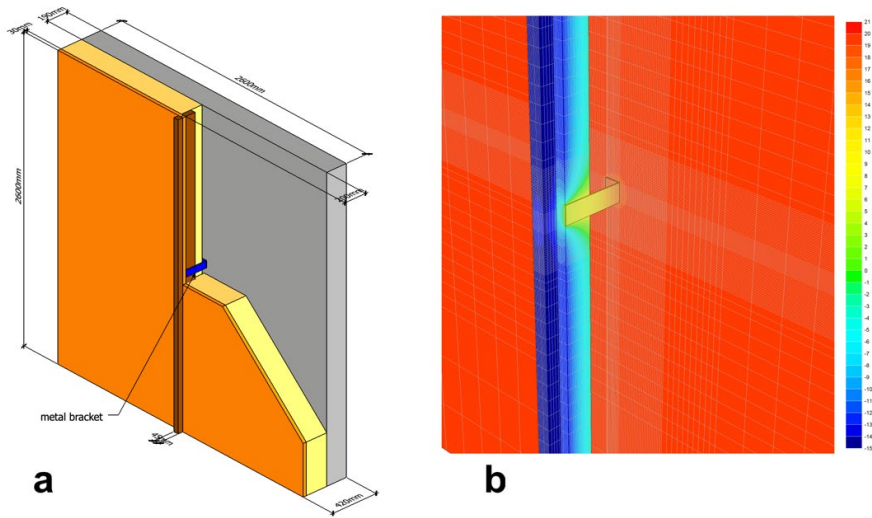

Figure 20. Geometric model of the assessed external wall part containing a thermal bridge (a) and central part of three-dimensional FED model of the assessed external wall containing a thermal bridge (b) with indicated mesh density and temperature distribution (the parts of wind barrier and insulation layers are cut off for visualisation purpose).

$$h_{add} = h_{eq} - h_{TB} \qquad , \text{m} \qquad\qquad (11)$$

The half amount of the additional length of thermal bridge can be considered as an extra length on both sides of the bridging element to compensate for the heat flows in the third dimension as shown in Figure 21.
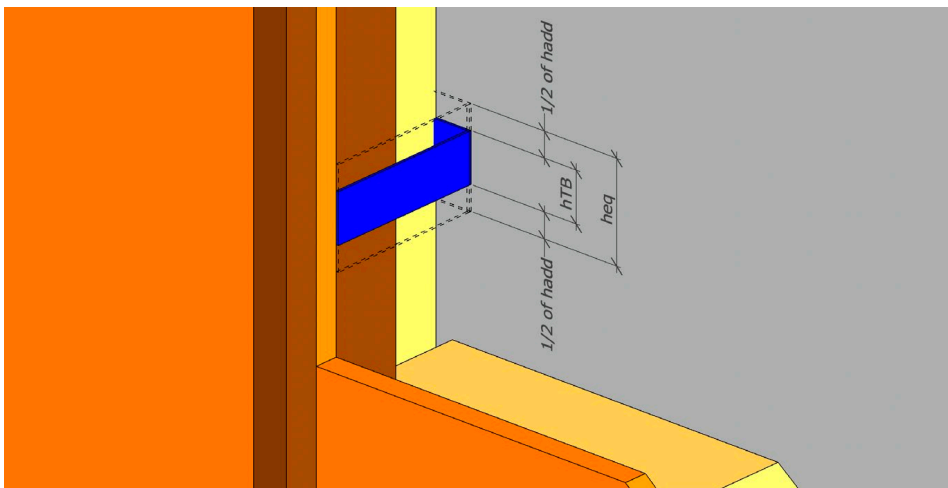

Figure 21. Schematic view of the assessed point thermal bridge with actual length (h_{TB}), equivalent length (h_{eq}) and additional length (h_{add}) of the thermal bridge in the third dimension.

3.5.3 Statistical analysis

The heat flows and thermal coupling coefficients for each combination of input variables were combined into a database. Based on the calculated point thermal transmittances and differences of two-dimensional thermal coupling coefficients, several multiple linear regression models were fitted to the numerically calculated data by using the R software package (R Core Team, 2018). As a first step, the simple linear regression was fitted as described in equation (12), but additional terms to the basic multiple linear regression equation were added to improve the model fit as given in equations (13), (14) and (15) based on preliminary numerically calculated data (altogether 12 different equations were fitted, but only 4 most relevant are given here).

$$h_{add} = c_1 \cdot \left(L_{2D} - L_{2Dref} \right) + c_n \tag{12}$$

$$h_{add} = c_1 \cdot \left(L_{2D} - L_{2Dref} \right) + c_2 \cdot \lambda_{TB} + c_3 \cdot R_{il} + c_4 \cdot R_{el} + c_n \tag{13}$$

$$h_{add} = c_1 \cdot \left(L_{2D} - L_{2Dref} \right) + c_2 \cdot \lambda_{TB} + c_3 \cdot h_{TB} + c_4 \cdot R_{el} \cdot \left(L_{2D} - L_{2Dref} \right) + c_n \tag{14}$$

$$h_{add} = c_1 \cdot \left(L_{2D} - L_{2Dref} \right) + c_2 \cdot \lambda_{TB} + c_3 \cdot h_{TB} + c_4 \cdot R_{el} \cdot \left(L_{2D} - L_{2Dref} \right) + c_5 \\ \cdot R_{il} + c_n \tag{15}$$

where R_{il}, R_{el} are respectively the thermal resistances of the layers adjoining the thermal bridging element from the internal and external sides, λ_{TB} is the thermal conductivity of the thermal bridging element, h_{tb} is the actual length of the thermal bridging element and c_1, c_2, c_3, c_4, c_5 and c_n are the estimated coefficients from the regression model.

The goodness of fit was assessed by considering the adjusted R-squared for each model and the *p*-value for each coefficient estimate. For the analysis and model fitting by the least squares method the statistical analysis software R (version 3.5.1) (R Core Team, 2018) was used with several add-on packages to allow statistical analysis and data visualisation.

4 Results

4.1 Airtightness in Estonian wooden buildings

As expected, the median air leakage (q_{50}) of older buildings, which was between 10.7 m³/(h·m²) and 13.9 m³/(h·m²), has decreased to 1.1 m³/(h·m²) after the minimum requirements for energy performance took effect in 2008 (Table 4). The development is similar in detached houses and apartment buildings (Figure 22). The variation within the age groups has also decreased significantly in new wooden buildings allowing the use of the base value $q_{50} = 3.0$ m³/(h·m²) for new wooden buildings when no additional information is available during energy performance calculation.
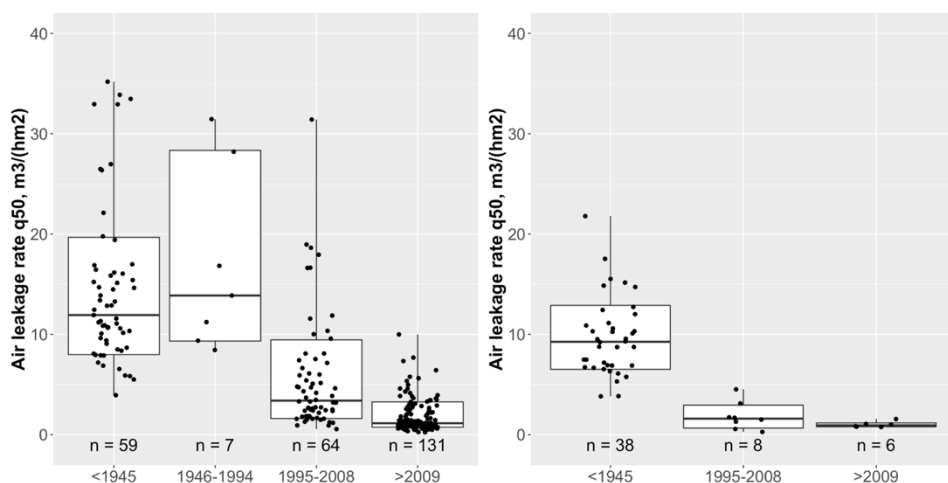

Figure 22. Air leakage rates of detached (left) and apartment buildings (right) based on the construction year. The median values with 0.16 / 0.84 quantiles are marked.

Table 4. Air leakage rate and its distribution depending on the time of construction

	Number of buildings	Air leakage rate q_{50}, m³/(h·m²)					
		Median	16 % percentile	84 % percentile	Mean	σ_{q50}	$q_{50,base}$
All wooden buildings							
Built before1945	97	10.7	6.9	16.4	12.5	6.9	17.8
Built in 1946–1994	7	13.9	9.3	28.3	17.1	9.2	26.8
Built in 1995–2008	72	3.2	1.5	8.1	5.2	5.5	9.5
Built since 2009	137	1.1	0.8	3.1	1.8	1.6	3.0

   A more detailed analysis on buildings (137 in total) built since 2009 describes the effect of additional factors on air leakage (Table 5).

Table 5. Effect of different factors on the air leakage rate and its distribution in the group of buildings built since 2009

	Number of buildings	Air leakage rate q_{50}, m³/(h·m²)					
		Median	16 % percentile	84 % percentile	Mean	σ_{q50}	$q_{50,base}$
Wooden buildings built since 2009							
Single-storey	34	1.1	0.8	3.1	1.9	1.9	3.4
Multi-storey	103	1.1	0.7	3.2	1.8	1.5	3.0
EPC class A	6	0.5	0.3	1.5	0.9	1.0	2.0
EPC class B	10	0.7	0.4	1.4	1.0	1.1	2.1
EPC class C (minimum requirement)	121	1.2	0.8	3.3	1.9	1.7	3.2
Log building	46	2.2	1.0	3.9	2.5	1.7	3.9
Lightweight timber	91	0.9	0.7	1.6	1.4	1.5	2.6
Irregular measurements	35	2.8	0.9	5.5	3.1	2.4	5.1
Systematic measurements (>5)	102	1.0	0.7	2.1	1.3	0.9	2.0

The energy performance certificate (EPC) classification A or B contributed to a slightly lower median air leakage (0.5 and 0.7 m³/(h·m²) respectively) than in the case of buildings designed to meet minimum requirements (EPC "C") (1.2 m³/(h·m²)). The lightweight timber construction (median 0.9 m³/(h·m²)) had significantly lower median air leakage compared to log houses (2.2 m³/(h·m²)). This can be due to the fact that airtightness has been predominantly measured in prefabricated buildings not on site. The companies that systematically conduct air leakage measurements (5 or more measurements in dataset) have significantly lower air leakage rates in buildings (1.0 m³/(h·m²)) compared to the buildings in the irregular measurement group (2.8 m³/(h·m²)). All those differences were statistically significant (p-value < 0.05, Kruskal-Wallis, post-hoc Conover).

As Table 5 illustrates, the number of storeys did not influence the air leakage of the building envelope. Both groups have equal median air leakage rates (1.1 m³/(h·m²)). Surprisingly, the analysis showed no significant difference between buildings with different compactness factors or different number of storeys (Figure 23) although a lower air leakage rate was expected for buildings with better compactness through a favourable ratio of the external envelope area to the internal volume and a generally smaller number of junctions related to a simpler form factor.

As the construction technique had a great effect on the average air leakage, both groups (log buildings and lightweight timber buildings) were further analysed to see if prefabrication has a significant effect as expected. Indeed, as Table 6 shows, the prefabricated log buildings (median 1.6 m³/(h·m²)) are 55 % more airtight than hand-made log buildings (median 3.6 m³/(h·m²)). In the case of lightweight timber buildings, prefabrication has even a larger effect: the air leakage rate of prefabricated buildings (median 0.9 m³/(h·m²)) is 74 % lower compared to on-site construction (median 3.4 m³/(h·m²)).
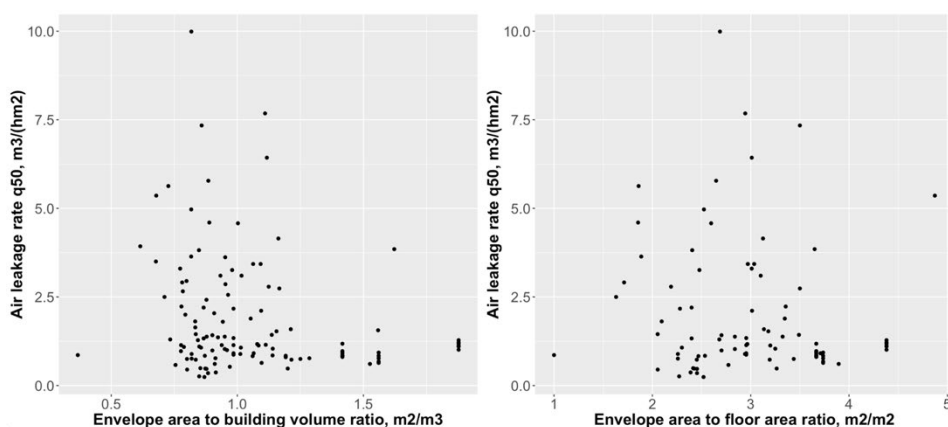
Figure 23. Correlation of air leakage rate (q_{50}) and building compactness for buildings built since 2009. The envelope area to volume ratio (left) and the envelope area to floor area ratio (right) are given.

Table 6. Effect of prefabrication on the air leakage rate and its distribution for different construction subtypes

	Number of buildings	Air leakage rate q_{50}, m³/(h·m²)					
		Median	16 % percentile	84 % percentile	Mean	σ_{q50}	$q_{50,base}$
All log buildings built since 2009							
Handmade logs	13	3.6	2.7	5.8	4.2	1.9	5.9
Prefabricated logs	33	1.6	0.9	3.1	1.9	1.1	2.8
All lightweight timber buildings built since 2009							
Prefabricated elements	80	0.9	0.7	1.3	1.1	0.7	1.6
On-site building	11	3.4	1.4	6.0	4.0	2.7	6.7

The effect of systematic measurement practice within manufacturing or building companies was further analysed separately for log buildings and lightweight timber construction. Like in the case of the full dataset, the effect of systematic measurements was significant in both groups of construction technologies, but the differences were smaller (Table 7). Within log buildings the systematic measurements showed 37 % lower air leakage rates. Within lightweight timber buildings the systematic measurements showed 47 % lower air leakage rates. This means that systematic measurements give manufacturers and building companies good feedback about air leakages, thus fostering improvement of the airtightness and quality control systems used.

	Number of buildings	Air leakage rate q_{50}, m³/(h·m²)					
		Median	16 % percentile	84 % percentile	Mean	σ_{q50}	$q_{50,base}$
All log buildings built since 2009							
Irregular measurements	11	3.0	1.9	6.3	3.9	2.3	6.1
Systematic measurements (> 5)	35	1.9	0.9	3.5	2.1	1.2	3.1
All lightweight timber buildings built since 2009							
Irregular measurements	24	1.7	0.8	4.6	2.7	2.4	4.8
Systematic measurements (> 5)	67	0.9	0.7	1.3	1.0	0.4	1.2

For visual comparison between different building technologies within companies that conduct systematic measurements on their buildings the average (median) air leakage rates along with 16 % and 84 % percentiles are given in Figure 24. It can be seen that log buildings have a significantly higher variation within the same company compared to prefabricated lightweight elements.
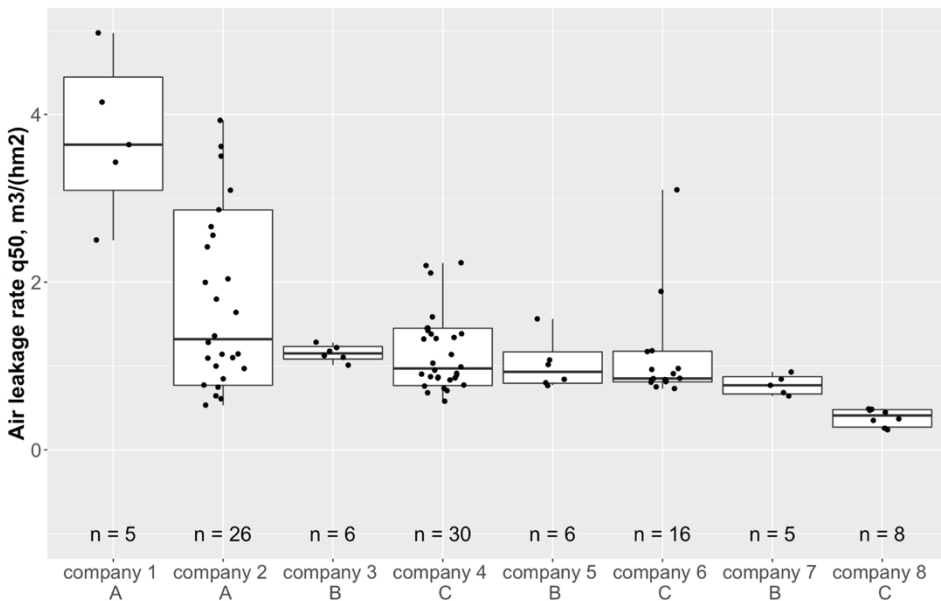

Figure 24. Comparison of air leakage rates and their distribution between companies that conduct systematic measurements (A – log buildings, B – volumetric prefabricated modules, C – prefabricated wall/roof elements).

The prefabricated volumetric and regular modules have a lower variation, and the median values of air leakages are around q_{50} = 1.0 m³/(h·m²) or even lower. The higher

variation in measurements affects significantly the base values of air leakage rates for these construction technologies. For handmade log buildings the base value $q_{50,base}$ = 5.9 m³/(h·m²). For prefabricated log buildings the base value of air leakage is 53 % lower: $q_{50,base}$ = 2.8 m³/(h·m²). Both these construction technologies cannot compete with prefabricated modular technology, where the base value of the air leakage rate $q_{50,base}$ = 1.6 m³/(h·m²). For comparison, the base value of the air leakage rate $q_{50,base}$ for all timber buildings built since 2009 was 3.0 m³/(h·m²).

4.2 Air leakage of joints sealed with PU foam

Preliminary analysis of the measured air leakages over a full range of pressure differences showed that some test specimens with otherwise identical foam, joint width and surface treatment had significantly larger air leakage rates. These measurement results are classified as 'failing specimens' and omitted from more detailed statistical analysis. The failing criterion was defined at 100 Pa pressure difference as V_{100} > 1.5 l/(min·m). Nevertheless, all measurement results were used to determine the ratio of failed specimens grouped by foam, lath surface treatment and joint width. The cumulative distribution of leakage rates at 100 Pa pressure difference for different joint surface types along with graphical representation of failing test specimens is shown in Figure 25. The general limiting value of air leakage for airtight joints (0.1 m³/(m·h·(ΔPa)^{2/3})) according to German standard DIN 4108-2 is also shown in the figure for the corresponding pressure difference (Beuth-Verlag, 2013).
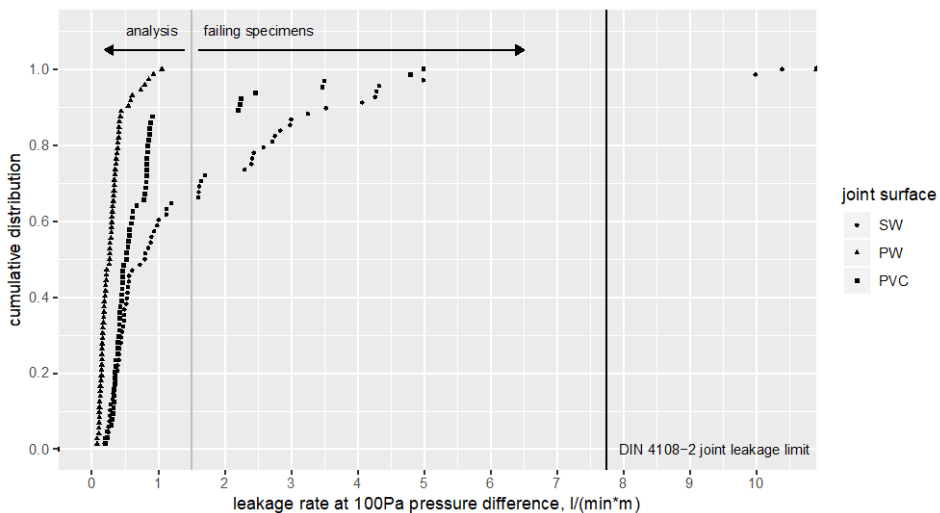

Figure 25. Cumulative distribution of leakage rates for different joint surface types at 100 Pa pressure difference and the limiting value for failing specimens.

The proportion of the test specimens with failed airtightness depended mainly on lath surface properties. Figure 26 shows that in the case of planed timber, the airtightness did not fail. In the case of the PVC surface, the proportion of failed test specimens was 16 % and 28 % respectively for 10 mm and 30 mm wide joints. Joints with a sawed wooden surface performed significantly worse with a failure rate of 33 % and 50 % for 10 mm and 30 mm wide joint respectively.

A greater joint width also contributed to a higher failure rate of airtightness. Grouping by specific foam products had no significant effect on the failure rate of test specimens.
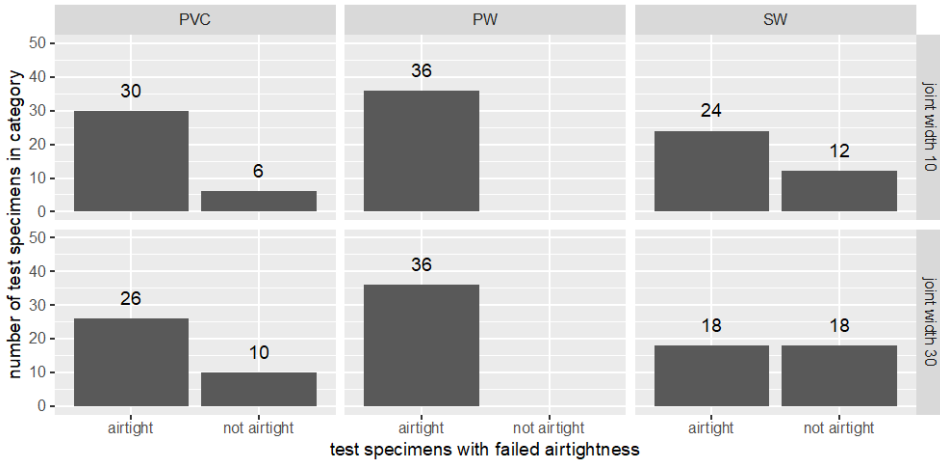

Figure 26. Number of test specimens with failed airtightness depending on lath surface treatment grouped by joint width (10 mm or 30 mm).

The mean air leakage rates at 400 Pa and 50 Pa pressure differences grouped by foam product, joint width and lath surface treatment are given in Table 8 along with variation (standard deviation) within test specimens and under- and overpressure conditions. For statistical testing air leakage rates at 400 Pa pressure difference were used.

Table 8. Air leakage rates and standard deviation at 400 Pa and 50 Pa pressure difference

| Surface | Joint type | | Air leakage rate at 400 and 50 Pa air pressure difference | | | |
| | Width, mm | Foam product | V_{400}, l/(min·m) | | V_{50}, l/(min·m) | |
			Mean	σ_{V400}	Mean	σ_{V50}
Planed wood (PW)	10	K	0.301	0.141	0.203	0.109
		L	0.604	0.229	0.203	0.076
		S	0.299	0.169	0.156	0.054
	30	K	0.606	0.618	0.214	0.092
		L	1.090	0.713	0.404	0.191
		S	0.398	0.374	0.172	0.068
PVC	10	K	1.413	0.477	0.293	0.118
		L	1.084	0.172	0.233	0.078
		S	1.007	0.229	0.251	0.070
	30	K	1.603	0.601	0.313	0.134
		L	1.758	0.438	0.441	0.123
		S	2.067	0.311	0.483	0.071
Sawn wood (SW)	10	K	0.616	0.290	0.252	0.097
		L	1.164	0.334	0.381	0.129
		S	1.216	0.657	0.329	0.147
	30	K	1.880	0.217	0.565	0.027
		L	1.165	0.714	0.392	0.207
		S	1.298	0.787	0.402	0.195

Figure 27 shows that the mean air leakage rate for joints with a planed wood surface (V_{400} = 0.549 l/(min·m)) was significantly ($p < 0.0001$, Anova) lower, by a factor of 2 or more, compared to sawn wood surfaces (V_{400}= 1.132 l/(min·m)) and plastic surfaces (V_{400}= 1.438 l/(min·m)). Also, the deviation was lower for joints with a planed wood surface (σ_{V400} = 0.501 l/(min·m)) compared to sawn wood surfaces (σ_{V400} = 0.635 l/(min·m)) and plastic surfaces (σ_{V400} = 0.524 l/(min·m)), meaning higher reliability in achieving the target result. It was expected that the smooth wood surface would enable better bonding between the wood surface and PU foam whereas in the case of the sawn wood surface the foam cannot fill all the small grooves.

Symbols in figure: n − number of observations in group, ns − p > 0.05, * − p < 0.05, ** − p < 0.01, *** − p < 0.001
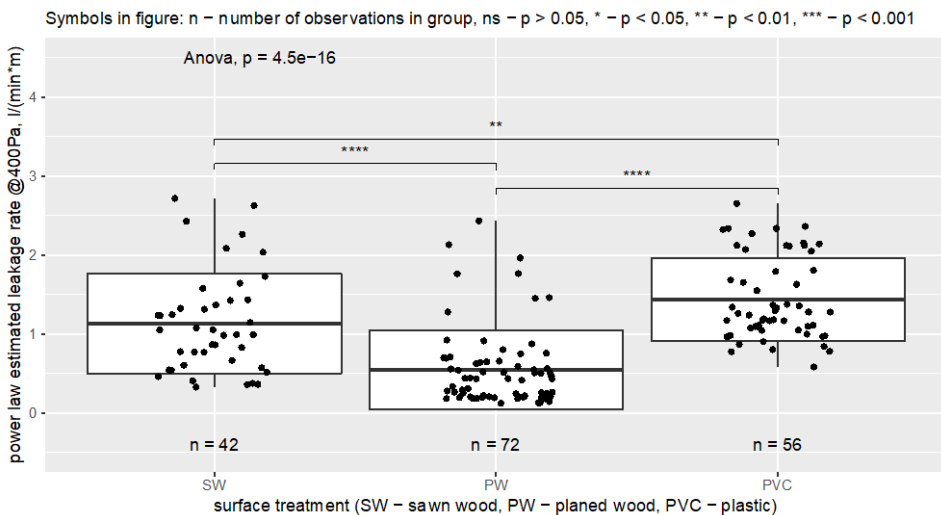
Figure 27. Mean air leakage rate (bold line) and standard deviation (white box) at 400 Pa depending on lath surface treatment (joints of both widths are included).

For plastic coated laths the foam can expand similarly to planed wood laths, but the humidity transport from surface to foam is limited, which inhibits foam expansion. This is usually compensated by moistening the plastic surface before applying the foam; however, exact guidelines with quantities are not given by foam producers. If the plastic surface is moistened before the foam is applied, water droplets on the plastic surface may cause random leakage pathways depending on the spraying technique and the amount of water used. The difference between PVC coating and sawn wood was small, but still significant ($p < 0.01$, Anova) contributing on average to approximately 27 % higher air leakages in the case of plastic coating.

Comparison between different surface treatments within groups of the same foam product and joint width is illustrated in Figure 28. The air leakage rate in the case of the planed timber surface stayed significantly lower than for the two other surface treatment groups even when considering the effect of joint width (10 mm versus 30 mm) and specific foam products, except for test specimens with 30 mm wide joints and foam product 'L', where all measurements had large variations and the average air flow differences between all foam products were small. The difference between the sawn wooden surface and the plastic surface was not significant in most cases.

Symbols in figure: n − number of observations in group, ns − p > 0.05, * − p < 0.05, ** − p < 0.01, *** − p < 0.001
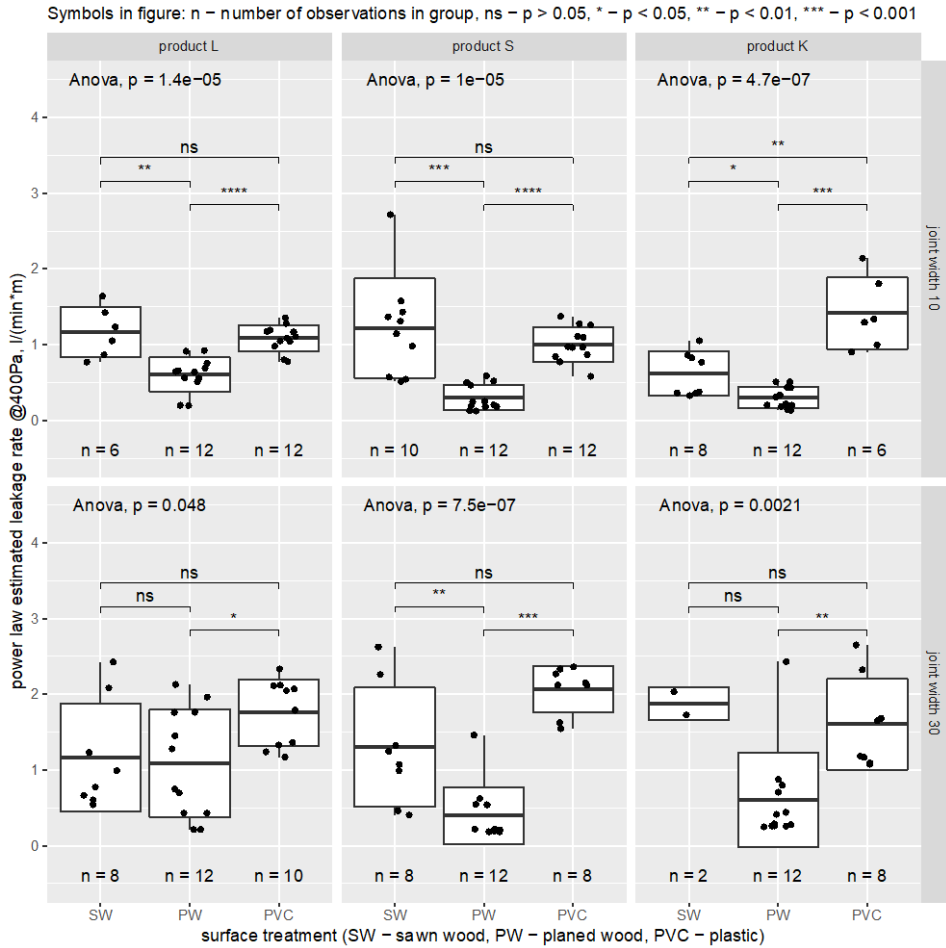
Figure 28. Mean air leakage rate (bold line) and standard deviation (white box) at 400 Pa pressure difference depending on lath surface treatment grouped by joint width (10 mm or 30 mm) and foam product (K, L and S).

Mean air leakage rate and its variation increase with the increase in joint width (Figure 29). The mean air leakage through a 10 mm joint with all surfaces filled with all foams (V_{400} = 0.801 l/(min·m)) was significantly lower ($p < 0.0001$, Anova) than the mean air leakage through a 30 mm joint (V_{400}= 1.194 l/(min·m)). The same was observed when the different lath surface treatments were assessed separately, but for sawn wooden surfaces the difference was not statistically significant due to the large variation in measurement results (Figure 30).

Even though different analysed foam products performed slightly differently in the case of the wider joint width, the overall difference between these products was not statistically significant, mainly due to a large variation in measured performance of test specimens. This shows that there are no major differences between specific premium-class PU foams.
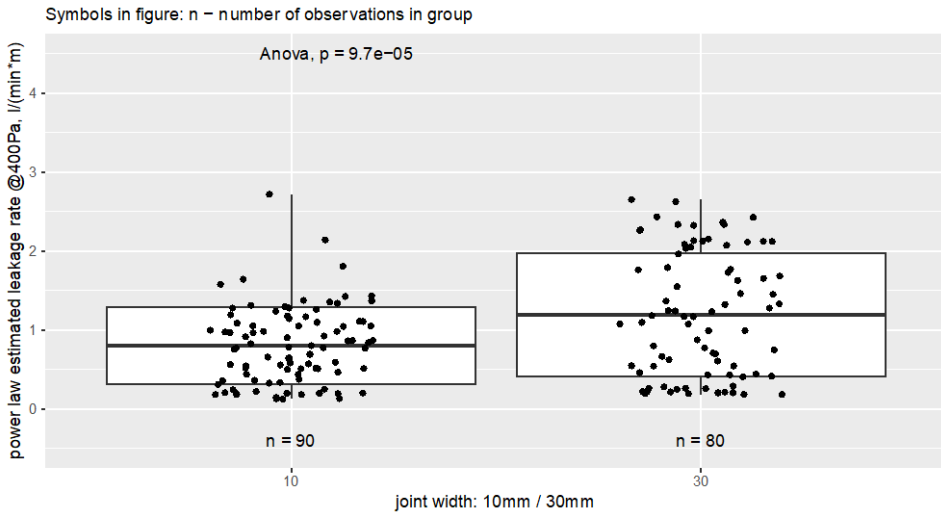
Figure 29. Mean air leakage rate (bold line) and standard deviation (white box) at 400 Pa depending on joint width (10 mm (left) or 30 mm (right)).
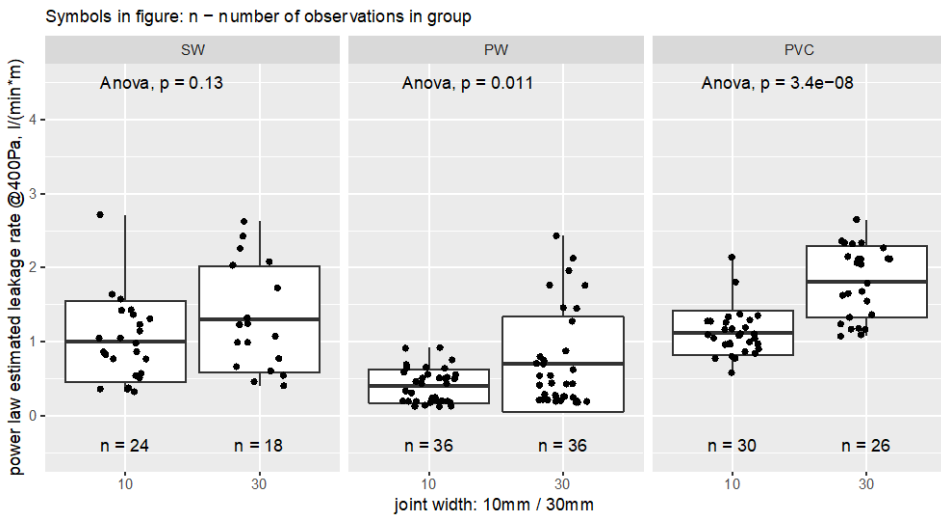

Figure 30. Mean air leakage rate (bold line) and standard deviation (white box) at 400 Pa depending on joint width (10 mm or 30 mm) grouped by lath surface treatment.

4.3 Heat loss due to cavities within the insulation layer

4.3.1 Observed installation situations

Hundreds of photos taken on building sites and in prefabrication factories in Estonia were qualitatively assessed to identify the most typical situations where cavities and other nonidealities occur. Based on observations, typical situations for different kinds of insulation materials and construction types are presented below to show ideal workmanship compared to typical nonideality as well as defective installation solutions commonly found on construction sites or in prefabrication.

Figure 31. Ideal workmanship (left) and typical nonideality (right) for a timber frame construction with mineral wool insulation batts.

Most typical nonidealities in the case of wool insulation batts with a lightweight timber frame construction are small cavities between the wool batt and the timber frame and rounded corners that form when a slightly wider insulation batt is tucked between the timber frame (Figure 31). When the formed cavity does not penetrate the entire layer and does not enable air circulation between the warm and cold sides, the effect on measured thermal transmittance is low, corresponding to an increase of 5–10 % at 35 K temperature difference (Huttunen & Vinha, 2013). Other observed workmanship failures related to wool insulation, such as shown in Figure 32, are not typical, should be classified as defective work and are not covered by EN ISO 6946 (2017) or assessed in this study.

Figure 32. Non-acceptable installation of mineral wool insulation batts in timber framed construction.

An example of nonideality for rigid insulation boards used in an ETICS system on masonry or a similar structural layer contains vertical and horizontal cavities, which may occur due to several factors. Smaller cavity widths of up to 5–10 mm can be caused by material shrinkage through ageing or cycling exposure to high temperatures in dark coloured facades or roofs or by squareness tolerance of insulation boards. Wider cavities are typically caused by poor workmanship but may also occur in the case of complex building envelopes with curved or otherwise non-uniform geometry when insulation boards must be precisely cut to a specific size on the building site. It is recommended that PU foam be used to fill the cavities between the rigid insulation boards during the installation (Figure 33 left), but this is often omitted in practice (Figure 33 right). The most typical nonideality observed on site occurs within the wall insulation layer where up to 10 mm wide vertical cavities between insulation boards running along the full floor height are not filled with foam.

Figure 33. Ideal workmanship (left) and typical nonideality (right) for rigid insulation boards of walls (above) and roof (below).

When PU foam is used to close such cavities, it is not technically possible to fill the entire cavity in a well-insulated building envelope, due to layer thickness. The nozzle of the foam gun does not fit properly into thinner cavities and if the cavity is deep and narrow, only its small external part can be filled. According to montage foam manufacturers, the PU foam applied through the nozzle to the cavity between insulation boards can fill approximately 50 mm deep outermost part of the cavity if the cavity width is below 20 mm. A typical penetrating air cavity formed due to cyclic thermal expansion and shrinkage is shown in Figure 34.

Figure 34. Penetrating air cavity formed due to aging and cyclic thermal expansion and shrinkage in the roof insulation layer.

4.3.2 Validation of the CFD model

The measured heat fluxes from the climate chamber experiment are given in Table 9. The heat flux at the top of the penetrating cavity is small but increases significantly towards the lower part of the cavity. Due to the natural convection occurring inside the penetrating cavity, the cooling air moves downwards at the external side of the cavity and creates a large temperature gradient on the bottom end corresponding to the maximum measured heat flux. The heat flux on the bottom part of the cavity depends significantly on the temperature difference between the internal and external environments. In the case of approximately 10 K temperature difference the maximum heat flux was 16.1 W/m^2 while in the case of approximately 50 K temperature difference the maximum heat flux increased up to 151.2 W/m^2.

Table 9. Average measured heat fluxes through a penetrating air cavity between insulation boards

Temperature difference, K	Measured average heat flux at different heights from bottom of cavity, W/m^2					
	20 mm	100 mm	800 mm	1600 mm	2110 mm	2360 mm
9.8	16.1	14.0	3.5	2.8	2.1	2.6
19.7	38.0	35.6	10.1	6.4	4.0	3.1
29.5	61.6	59.5	18.8	10.9	6.1	4.0
39.5	111.9	95.2	28.6	15.5	7.4	3.0
49.3	151.2	122.2	35.9	19.0	8.6	2.6

The experimental and computational heat fluxes through the penetrating air cavities of the test wall were found to be in relatively good agreement as shown in Figure 35.
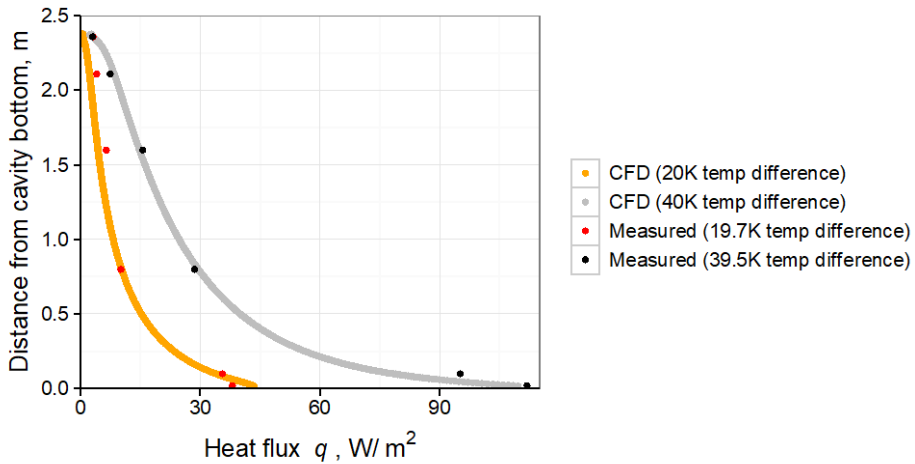
Figure 35. Comparison of simulated and measured interior surface heat fluxes at different heights of the penetrating air cavity at 20 K and 40 K ambient temperature difference.

4.3.3 Convective heat loss of penetrating air cavities

The results from numerical models show that the heat loss through a penetrating air cavity within the insulation layer is strongly dependent on the temperature difference across the building envelope. Figure 36 shows the numerically derived thermal transmittance U_{CFD} for a wall, roof and floor construction with 200 mm of insulation with the thermal conductivity of 0.040 W/(m·K), including the effect of 5, 10 and 20 mm penetrating rectangular air cavities.
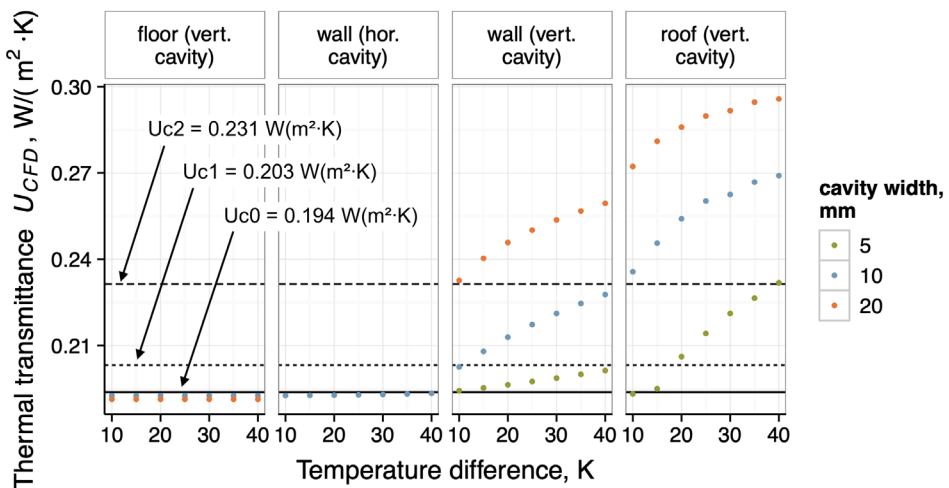

Figure 36. Corrected thermal transmittance U_{CFD} of a building envelope (insulation thermal conductivity 0.040 W/(m·K)) incorporating the effect of air cavities depending on the temperature difference and penetrating cavity width and location.

The results from numerical models show that penetrating vertical air cavities inside the floor construction and horizontal air cavities in the wall construction have no significant effect on the thermal transmittance. In the case of vertical air cavities inside

the wall and roof construction, the convective heat flow inside the cavity increases the corrected thermal transmittance U_{CFD} well over the normative correction level at higher temperature differences. At 40 K temperature difference and a 20 mm wide vertical cavity, the corrected thermal transmittance U_{CFD} = 0.296 W/(m^2·K) for the roof construction and U_{CFD} = 0.259 W/(m^2·K) for the wall construction. These values correspond to 53 % and 34 % increase in the respective thermal transmittances.

For better comparison, instead of corrected thermal transmittances correction factors $\Delta U''$ were derived for thermal transmittance from the numerical models for penetrating air cavities in different locations. Figure 37 depicts these factors depending on the cavity width, insulation material and temperature difference across the entire building envelope.
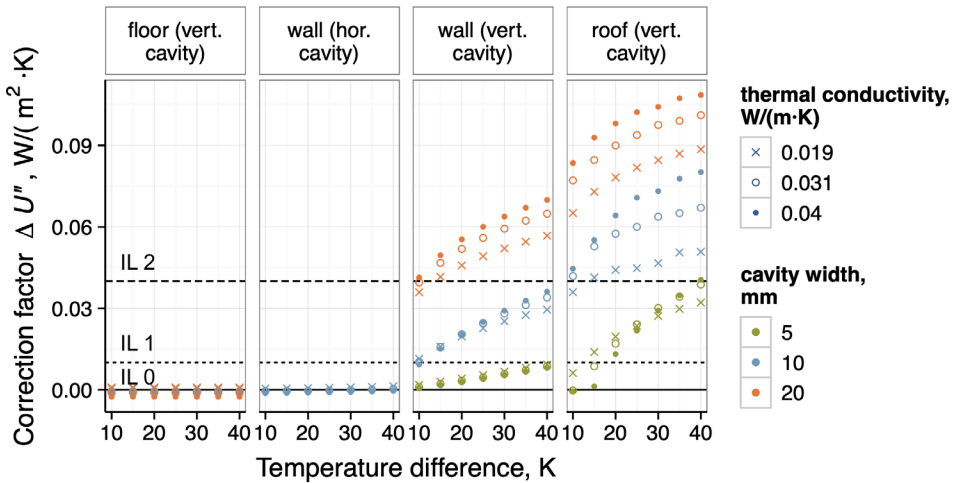

Figure 37. Correction factor of air cavities $\Delta U''$ depending on the temperature difference, thermal conductivity of the insulation layer and penetrating cavity width and location (IL 0 … IL 2 refer to installation levels described in EN ISO 6946).

Horizontal penetrating cavities within the wall insulation layer do not affect the thermal conductivity of the wall because no convective air flow between the warm internal and the cold external side takes place due to the very small height of the air cavity. In the case of some insulation materials with a higher thermal conductivity, the air cavity even slightly decreases the heat loss due to the lower thermal conductivity of still air. A similar situation can be seen with vertical air cavities in the floor construction, where thermal stratification takes place between the warm boundary on the top and the cold boundary at the bottom and convective air flow is suppressed. Similarly to horizontal air cavities, the still air with lower thermal conductivity decreases the heat loss in cases with inferior insulation materials.

In the case of vertical penetrating air cavities within a wall insulation layer, the convective heat flow is strongly dependent on the temperature difference and cavity width. At 10 K temperature difference, the numerically estimated correction factor $\Delta U''$ was similar to simplified values according to EN ISO 6946 (2017) but increased from 0.002 to 0.010 W/(m^2·K) for 5 mm and from 0.010 to 0.035 W/(m^2·K) for 10 mm wide penetrating air cavities at the 40 K temperature difference. This corresponds approximately to one level of increase in the normative installation level. For a wider penetrating cavity, the estimated correction factor increases from 0.040 up to

0.070 W/(m²·K) and at the 40 K temperature difference, is well over the maximum correction level proposed by EN ISO 6946 (2017). The increase of the thermal transmittance due to a higher temperature difference is greater in the roof construction for all assessed cases with the estimated correction factor $\Delta U''$ value over 0.1 W/(m²·K) in a worst-case scenario. The simplified procedure defined in EN ISO 6946 (2017) is unable to describe this for any of the cases where the penetrating cavity is wider than 5 mm.

The effect of the insulation material is small for 5 mm and 10 mm wide cavities. In the case of wider cavities (20 mm), the heat loss increases with the increase in thermal conductivity. This effect is more prominent in vertical cavities inside the roof construction.

4.3.4 The effect of air cavities in dual-layer insulation with a rebate edge or partial filling with PU foam

Additionally, cases with non-penetrating cavities were assessed to see if their effect on the thermal transmittance is significantly lower when the air circulation between internal and external boundaries is prevented by partial filling with PU foam or with the use of dual-layer insulation with a rebate edge (Figure 12 in Methods chapter). The results from both geometric cases in comparison with fully penetrating air cavities are given in Figure 38.
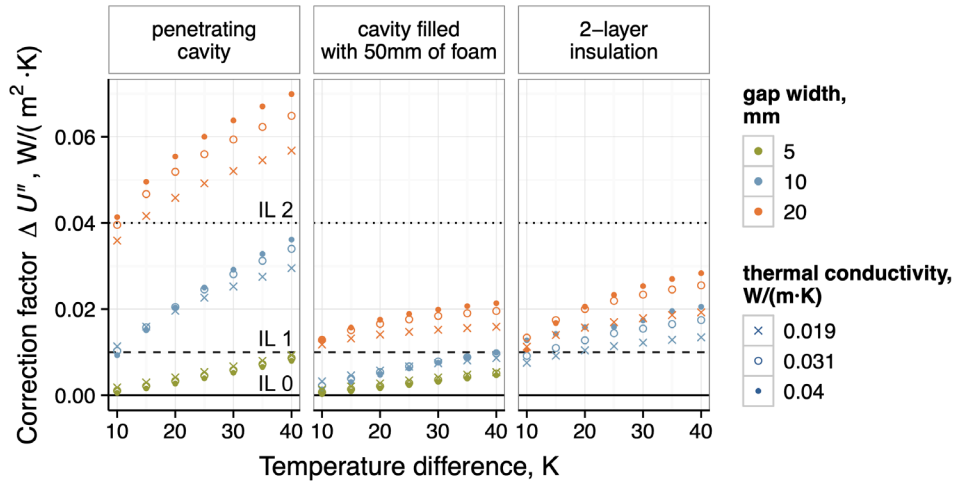

Figure 38. Correction factor of air cavities $\Delta U''$ depending on the temperature difference, the thermal conductivity of the insulation layer and the penetrating cavity width at a dual insulation layer or partially foamed cavity(IL 0 … IL 2 refer to installation levels described in EN ISO 6946).

Compared to both two-layer insulation and partial foaming, the penetrating air cavity decreased the correction factor $\Delta U''$ by a factor of 2 or more depending on the temperature difference. However, at the temperature difference of $\Delta t = 35$ K, the numerically derived correction factor was still above the normative installation levels 0 and 1 although both alternatives are listed as level 0 installation solutions in EN ISO 6946 (2017). Nevertheless, compared to the penetrating cavity, the additional heat loss through these cavities was only slightly dependent on the temperature difference across the entire building envelope, which is to be expected.

4.3.5 The effect of triangular air cavities

Additionally, the effect of the penetrating triangular (wedge-shaped) air cavity and penetrating air cavity with additional triangular cut-outs (Figure 12 in Methods chapter) on the thermal conductivity was assessed (Figure 39).
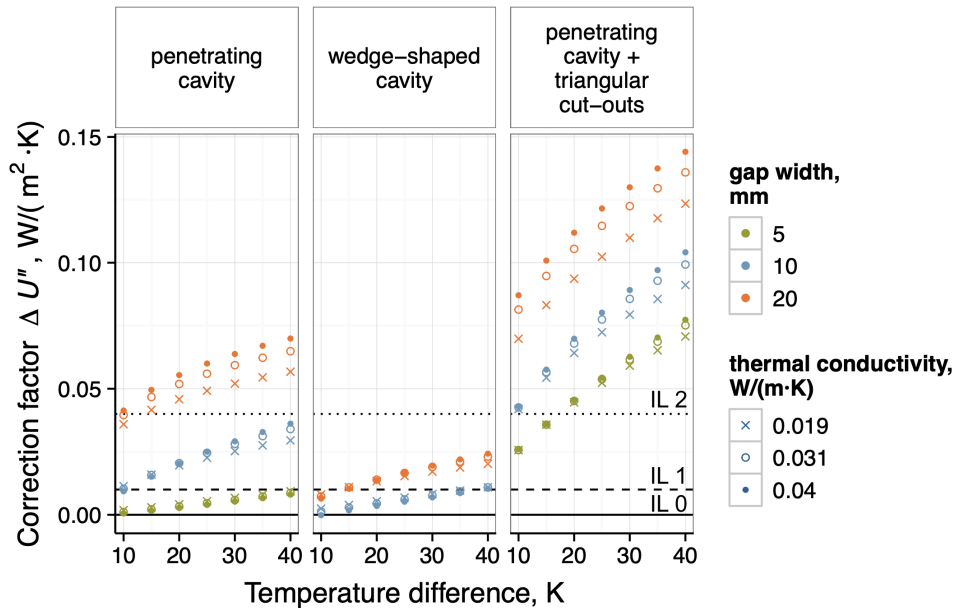

Figure 39. Correction factor of air cavities ΔU'' depending on the temperature difference and on the thermal conductivity of the insulation layer in the case of triangular air cavities (IL 0 ... IL 2 refer to installation levels described in EN ISO 6946).

As Figure 37 shows, additional heat loss will be notably reduced if the penetrating air cavity is wedge-shaped so that the width decreases perpendicular to the insulation layer down to 5 mm. The effect of a vertical 10 mm wide cavity in the wall construction is in the range of normative installation level 1 and the effect of a vertical 20 mm wide cavity is well below normative installation level 2 where the correction factor will remain between 0.01 and 0.025 W/(m²·K) in the wall insulation layer. This is roughly a reduction by one level compared to a rectangular penetrating air cavity. Compared to the penetrating cavity, the additional heat loss through the wedge-shaped air cavity depends only slightly on the temperature difference across the entire building envelope.

If additional triangular cut-outs are added to the penetrating air cavity, the correction factor will increase significantly and for all cases the additional thermal transmittance will be well above normative correction values. This suggests that errors of that kind during installation should be classified as inadequate workmanship.

4.3.6 Heat loss of a building envelope with cavities in different climate conditions

The natural convection and radiation inside assessed air cavities was found to be strongly dependent on the temperature difference between the warm and cold sides. Therefore, the actual increase in the heat loss will vary depending on the location and climate. To account for cumulative temperature differences and their effect in different climates,

the heat loss through a wall or roof construction with a unitary area including vertical penetrating air cavities was calculated for five different locations in Europe, including Barcelona (Spain) from Southern Europe, Kiruna (Sweden) from cold Northern Europe and Tartu (Estonia), Kaunas (Lithuania) and Frankfurt (Germany) in between these locations.

The linear model was fitted using the results from previous sections for each assessed case, and the intercept along with the slope parameter from the regression model were used to calculate the corrected thermal transmittance U_{ch} for each hour of the year based on outdoor temperature in a typical year in each location. The estimated heat losses using the corrected thermal transmittance in the case of an insulation material with thermal conductivity of 0.019 W/(m·K) are given below as an example (Figure 40).
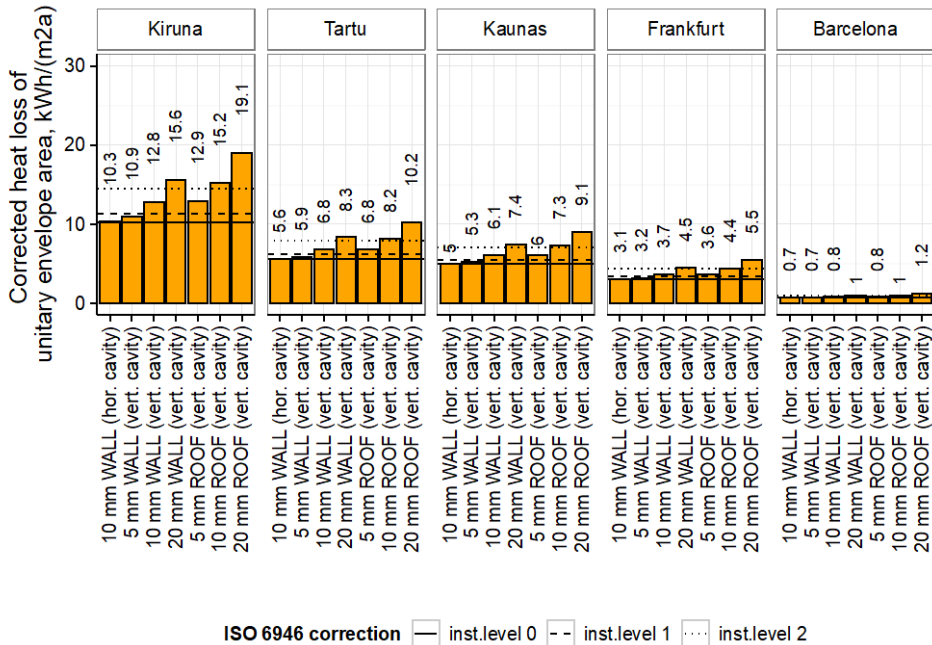

Figure 40. Heat loss of a unitary envelope area with a vertical penetrating air cavity in different climates depending on the air cavity configuration inside the insulation layer.

In the warm climate (Barcelona), the difference in the estimated annual heat loss is marginal. In Frankfurt (Germany) and Kaunas (Lithuania), the annual heat loss through the unitary envelope area is in the range of 3.1 to 9.1 kWh/(m²·a), depending on the air cavity width and location. In Tartu (Estonia), the estimated annual heat loss in a typical year is between 5.6 to 10.2 kWh/(m²·a) and in northernmost part of Europe (Kiruna, Sweden), it is in the range of 10.3 to 19.1 kWh/(m²·a). The relative increase in annual heat loss for a worst-case scenario (20 mm wide air cavity in the roof construction) ranges from 75 % to 86 %, depending on the climate (Figure 41). The absolute increase of heat loss in Kiruna (Sweden) is 8.8 kWh/(m²·a) for each square metre of the envelope area.

Compared to a regular penetrating 10 mm and 20 mm wide air cavities, the use of PU montage foam to fill the outermost 50 mm of the cavity will reduce the heat loss respectively by 0.8 and 1.9 kWh/(m²·a) in Estonian climate.
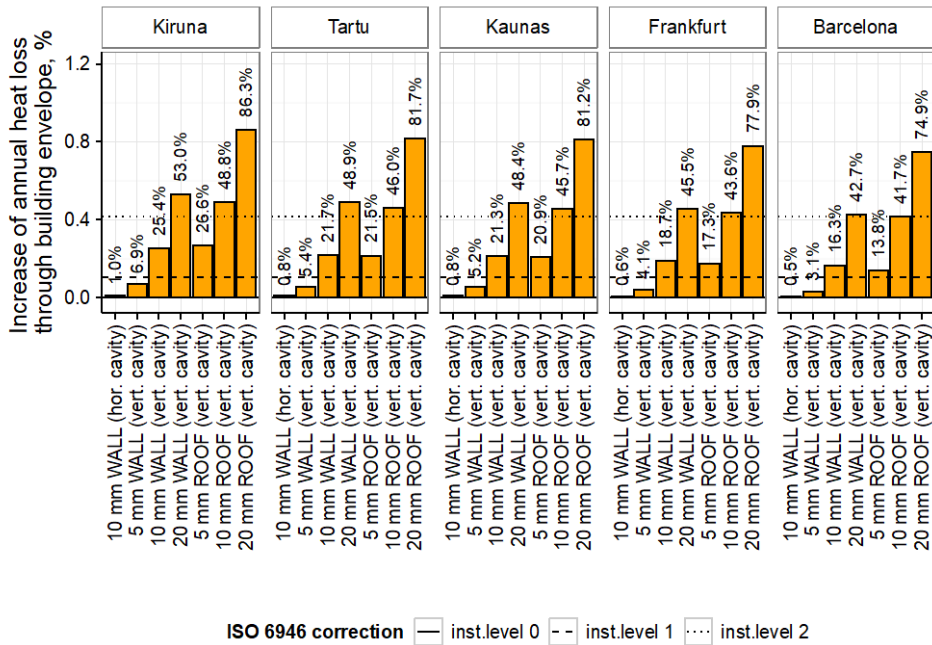
Figure 41. Relative increase of the heat loss of the unitary envelope area in different climates depending on the air cavity configuration inside the insulation layer.

4.4 Assessment of combined thermal bridges

Altogether, 5 typical junctions with 3 different insulation materials and 3 construction types were numerically assessed with 10 different flanking element lengths, totalling to 450 models. The linear thermal transmittance of these junctions considering the flanking element length according to EN ISO 10211 (2017) requirements was between -0.130 and 0.341 W/(m·K) depending on the junction, construction type and thermal conductivity of the insulation layer.

Additional analysis included more severe thermal bridges in the window to wall connection and balcony slab to wall connection with 3 different insulation materials and with 10 different flanking element lengths for the construction type with heavyweight concrete as the internal load bearing layer. The calculated linear thermal transmittance was between 0.101 and 1.111 W/(m·K).

The tabulated linear thermal transmittance values of all assessed thermal bridge combinations are given in PUBLICATION III in full detail along with the corresponding deviations at different relative flanking element lengths.

4.4.1 The effect of flanking element length

The numerical analysis of different junctions showed that the minimum flanking element lengths for well-insulated wall construction were significantly lower than defined in the EN ISO 10211 standard. The deviation of linear thermal transmittance compared to a reference case according to EN ISO 10211 for the external wall corner was less than 3 %. For a regular wall corner (Figure 42), the construction with a highly conductive internal structural layer (200 mm heavyweight concrete) had a higher deviation compared to the

lightweight timber construction. In the case of an inverted (inward) corner with a highly conductive internal structural layer (Figure 43) the effect was inverted, but negligible. For both junctions, the insulation material with higher thermal conductivity caused a slightly higher deviation from the normative calculation results. The absolute deviation of linear thermal transmittance $\Delta\Psi$ for all assessed cases was less than 0.002 W/(m·K).
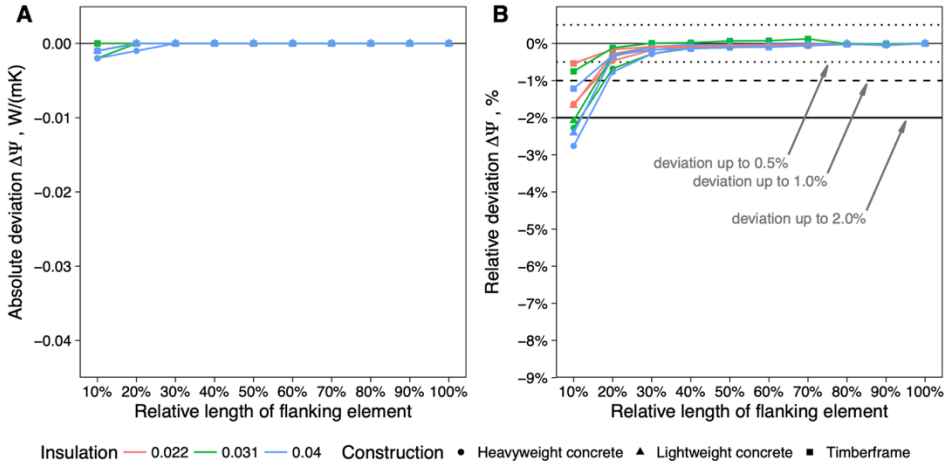

Figure 42. Effect of flanking element length on linear thermal transmittance of external wall corner with relative and absolute deviations shown.
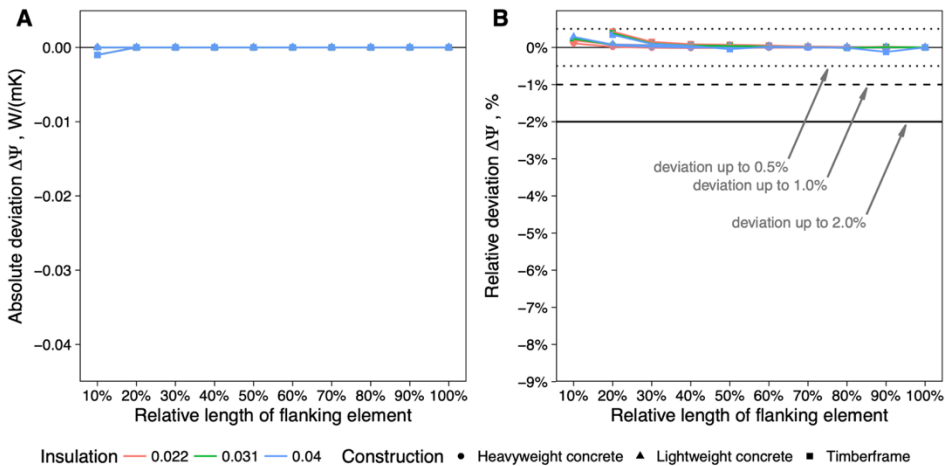

Figure 43. Effect of flanking element length on linear thermal transmittance of inverted external wall corner with relative and absolute deviations shown.

In the case of window to external wall connections (Figure 44), the deviation from the standardised calculation was less than 2 % for constructions with a highly conductive internal structural layer (heavyweight concrete) and similar for all assessed insulation materials. In the case of lightweight timber frame construction, the relative deviation varied more and for very short flanking element lengths (10 % of the standardised flanking element length) the deviation was in the range of 6 % to 8 %. However, the absolute deviation for all cases was 0.002 W/(m·K) or less.
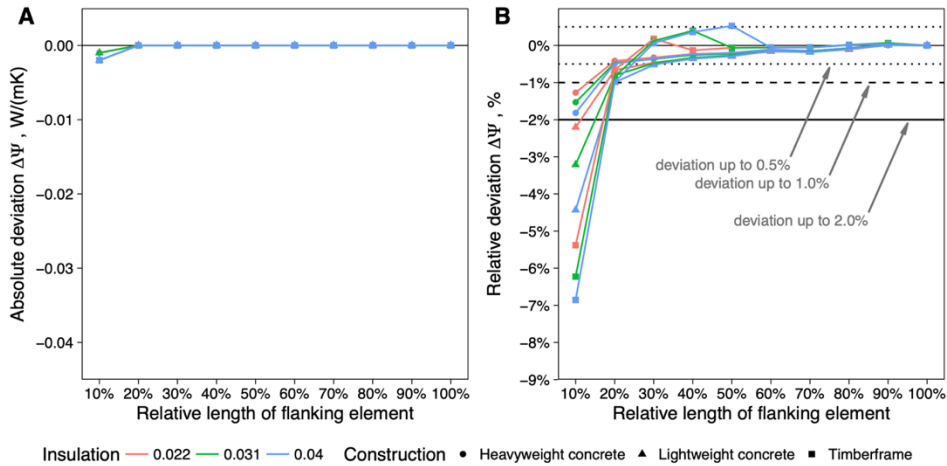
Figure 44. Effect of flanking element lengths on linear thermal transmittance of window to wall connection.

When a ground coupled element such as a slab on the ground is part of the numerical model, the deviation from the standardised case is significantly higher (Figure 45). When both flanking element lengths (i.e., of the external wall part and the slab on the ground part) decrease, at least two different processes seem to affect the heat flows.
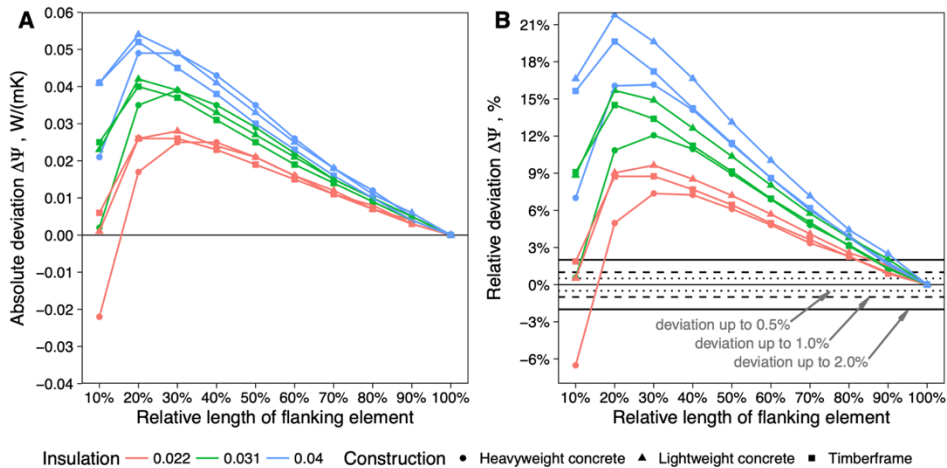

Figure 45. Effect of flanking element lengths on linear thermal transmittance of the ground floor slab to wall connection (the flanking element length for both the external wall and ground floor slab was changed).

The steady increase of the calculated linear thermal transmittance is caused by the increasing edge effect when the length of the slab on the ground part is reduced, which is expected (Hagentoft, 1988). Nevertheless, for all assessed material and construction combinations, the deviation of linear thermal transmittance is rapidly decreasing when the ground slab length in the model is 30 % or less from the standardised slab length (i.e., 4 m). This can be caused by the mutual effect of vertical foundation insulation and very short geometric boundaries of the floor slab and the ground domain, meaning that in

these small models, the heat must travel a significantly longer path to reach exterior conditions. This is highly dependent on the foundation geometry and the subsoil insulation and shows that it is not possible to decrease the length of ground coupled flanking elements without introducing a lot of uncertainty.

To exclude this effect another set of calculations were performed with a constant slab on ground length of 4 m and only the flanking element length of the external wall was altered (Figure 46). As expected, the effect of ground losses was eliminated and only the effect of wall part length is seen. The effect is similar to that of other junctions where linear thermal transmittance in the case of short flanking element lengths is lower than for the full-size model. However, the difference between different construction types is significant. For lightweight timber frame construction, the deviation is less than 1 % for all cases but a highly conductive internal structural layer (heavyweight concrete) coupled to the floor slab and foundation causes deviations of up to 8 % at very short wall lengths (0.144 m) due to the limited heat flow at the internal boundary condition compared to the standard geometry of the model. Absolute values of deviation are in the range of -0.03 to -0.02 W/(m·K), underestimating the actual linear thermal transmittance.
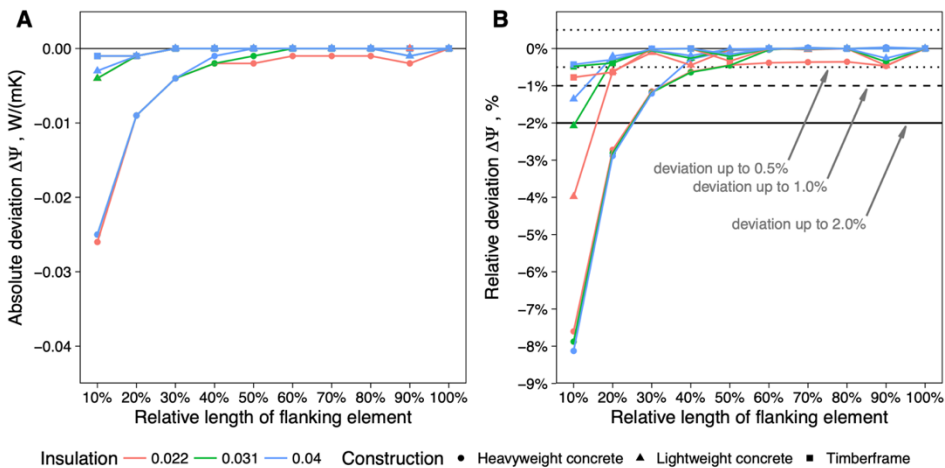

Figure 46. Effect of flanking element lengths on linear thermal transmittance of the ground floor slab to wall connection.

To confirm these findings for thermal bridges with higher thermal transmittance, a wall construction with a highly conductive internal load bearing layer was further assessed in combination with junctions where the insulation layer was significantly reduced by a protruding balcony slab or by suboptimal positioning of the window frame as described in the Methods chapter (see Figure 17). The results are given in Table 10 along with linear thermal transmittances and corresponding deviations for all assessed junctions and combinations.

Table 10. Deviation of linear thermal transmittance ΔΨ depending on the flanking element length in the numerical model for with medium and high linear thermal transmittance

Junction	$\lambda_{insulation}$, W/(m·K)	Ψ, W/(m·K)	ΔΨ, W/(m·K) at different relative lengths of flanking element l_j					
			10 %	20 %	30 %	40 %	50 %	60 %–100 %
Window–wall connection (medium thermal bridge)	0.022	0.105	-0.006	-0.002	-0.001	0	0	0
	0.031	0.104	-0.006	-0.002	-0.001	0	0	0
	0.040	0.101	-0.006	-0.002	-0.001	0	0	0
Window–wall connection (high thermal bridge)	0.022	0.422	-0.076	-0.025	-0.009	-0.003	-0.001	0
	0.031	0.418	-0.074	-0.025	-0.008	-0.003	-0.001	0
	0.040	0.415	-0.073	-0.024	-0.008	-0.003	-0.001	0
Wall–inter. ceiling connection (medium thermal bridge)	0.022	0.300	-0.006	-0.002	-0.001	0	0	0
	0.031	0.308	-0.006	-0.002	-0.001	0	0	0
	0.040	0.316	-0.005	-0.002	-0.001	0	0	0
Wal–inter. ceiling connection (high thermal bridge)	0.022	1.111	-0.089	-0.029	-0.01	-0.003	-0.001	0
	0.031	1.104	-0.086	-0.028	-0.01	-0.003	-0.001	0
	0.040	1.097	-0.082	-0.027	-0.009	-0.003	-0.001	0

The deviation of the linear thermal transmittance for medium thermal bridges was similar to previous results with deviations occurring at 30 % relative length of the flanking element compared to EN ISO 10211 (2017) requirements. Although the absolute deviation of the linear thermal transmittance of high thermal bridges was higher at very short flanking element lengths, the deviation at 40 % and 50 % of the required flanking element was negligible compared to the linear thermal transmittance of the junction itself.

These findings indicate that for a well-insulated building envelope and for a wide range of thermal bridges and construction types, the minimum flanking element length can be significantly lower than required by EN ISO 10211 (2017). For most of the assessed junctions, using 50 % of the standard flanking element length provided the same numerical results for linear thermal transmittance. In Figure 47 the required length of the flanking element is shown for each assessed combination of connection, construction and insulation that keeps the deviation ΔΨ below three limiting values – i.e., the allowed deviation from the standard calculation for the same junctions is less than 0.5 %, 1.0 % or 2.0 %.

For minimal deviation, a flanking element length around 40 % to 50 % should be used compared to EN ISO 10211 (2017) requirements. If a deviation of up to 2 % is allowed, a junction with a minimum flanking element length of 20 % can be used for junctions with linear thermal transmittance Ψ < 0.2 W/(m·K) and 30 % for junctions with higher linear thermal transmittance. In this case, the required flanking element length in the numerical model corresponds roughly to the flanking element thickness or less.
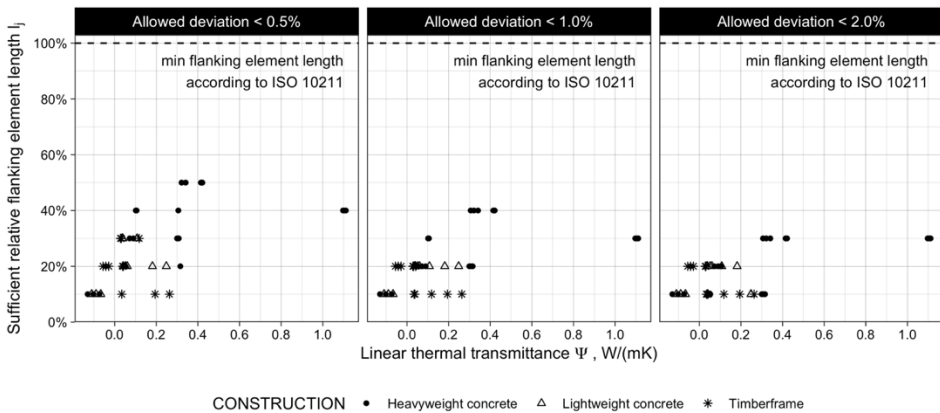
Figure 47. Minimal relative length of flanking elements in all assessed junctions that keep the deviation of linear thermal transmittance below 0.5 % (left), 1.0 % (middle) or 2.0 % (right) compared to EN ISO 10211 reference case depending on linear thermal transmittance of the junction.

This shows that for well-insulated building envelopes, the effect of thermal bridges seems to be localised near the junction and interaction of multiple thermal bridges is very small at distances corresponding roughly to wall or roof thickness. This is to be expected as a thicker insulation layer and a higher thermal resistance of the wall or roof part reduce the proportion of perpendicular heat flow through the flanking elements compared to the theoretical heat flow limited by surface resistances as well as provide higher and more even surface temperatures along the flanking element length.

4.4.2 Simplification of combined thermal bridges

Based on these findings, the linear thermal transmittances of single connections can be arithmetically pooled to estimate the linear thermal transmittance of combined thermal bridges with good accuracy. For ground coupled flanking elements such as slab on grade etc. this simplification is not possible and flanking element length according to EN ISO 10211 (2017) must be used.

To estimate the potential of this simplification on time and effort for general practitioners a number of regular and combined thermal bridges were identified on two different building geometries as described in Methods chapter (Figure 18). The assessed building envelopes included a total of 84 office building junctions and 34 detached house junctions. By using shorter flanking element lengths based on the previous section corresponding to three alternative levels of accuracy, the number of different junctions was recalculated. As Table 11 illustrates, in the case of office buildings the numerical calculation of linear thermal transmittance is needed for only 45 different junctions (46 % reduction) when deviation of up to 0.5 % is allowed. If deviation of up to 2.0 % is allowed, the reduction in the number of different junctions will be 76 %, which will significantly reduce the time needed for thermal bridge calculation. For detached houses, the reduction in the number of different thermal bridge combinations is lower as expected, but still between 35 % and 50 %.

Table 11. Number of thermal bridges that need separate numerical calculation when considering different flanking element lengths

Thermal bridge type	Allowed relative deviation	Office building	Detached house
Regular thermal bridges	According to EN ISO 10211	11	8
Combined thermal bridges	According to EN ISO 10211	73	26
	< 0.5 %	34	14
	< 1.0 %	28	10
	< 2.0 %	19	9

4.5 Simplified estimation of point thermal transmittance

4.5.1 The effect of thermal properties

Altogether 102 different combinations of thermal bridging situations were numerically calculated. For testing the effect of thermal bridge length in the third dimension, a concrete wall with a regular steel fixation bracket of 60 mm length combined with three alternative insulation materials and a 9 mm gypsum wind barrier layer was selected as the base case. Other variable parameters were tested in all possible combinations. The correlation between the point thermal transmittance and the difference of two-dimensional thermal coupling coefficients can be seen in Figure 48.
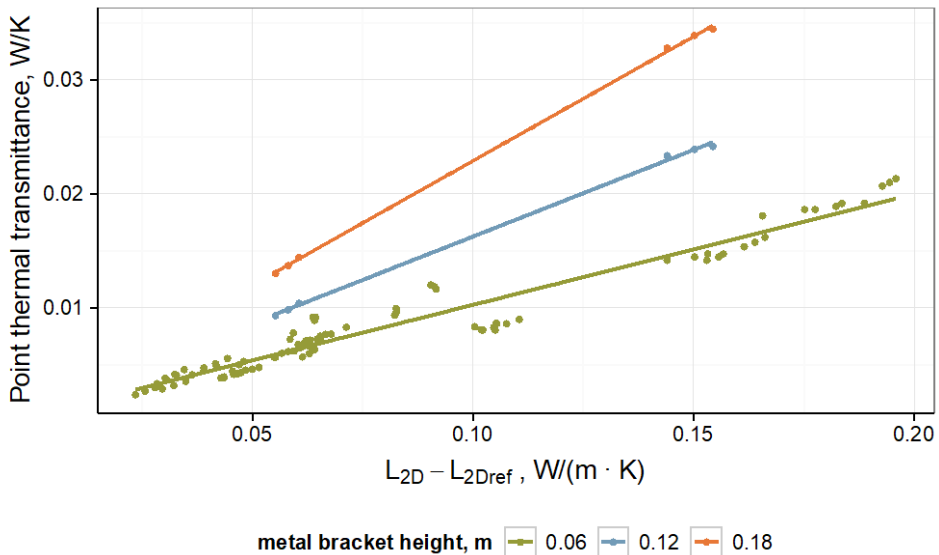

Figure 48. Correlation between the point thermal transmittance and the difference of two-dimensional thermal coupling coefficients.

The difference caused by bracket length is expected as the thermal bridge itself has a greater length, but other factors causing variation need further analysis. To omit the direct effect of bracket length in the third dimension, the additional length of the thermal

bridge h_{add} (i.e, the difference between equivalent length h_{eq} and actual length h_{TB} of the thermal bridge in the third dimension) is used instead of point thermal transmittance to test the correlation between different input variables and the additional heat loss from the third dimension. The additional length of the thermal bridge increases when the difference between two-dimensional thermal coupling coefficients decreases (Figure 49). However, the variation due to other factors is high and is mainly described by the thermal conductivity of the bridging element and the thermal resistance of the external (i.e., the wind barrier) layer (Figure 50).
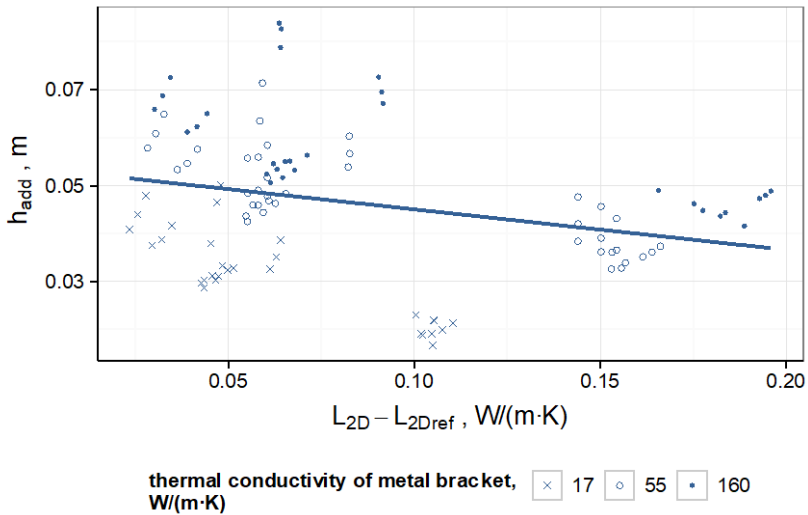

Figure 49. Correlation between the additional thermal bridge length h_{add} and the difference of two-dimensional thermal coupling coefficients.
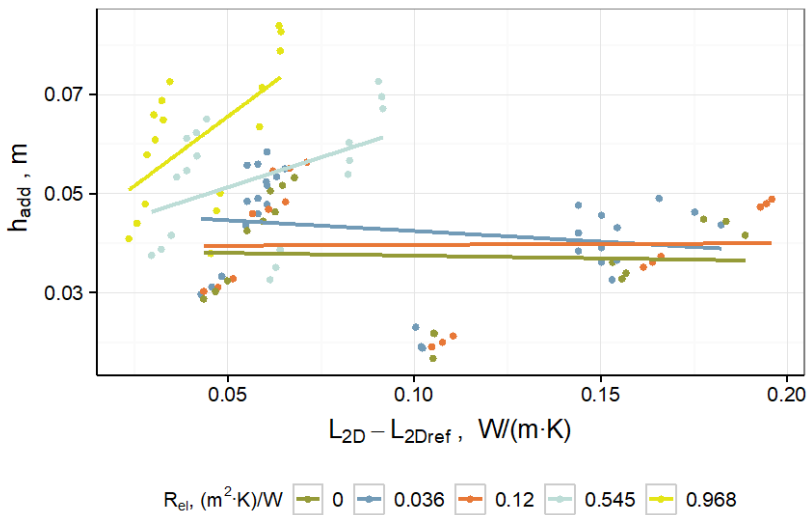

Figure 50. Correlation between the additional thermal bridge length h_{add} and the difference of two-dimensional thermal coupling coefficients grouped by the thermal resistance of the external wind barrier.

The correlation between the additional length of the thermal bridge and the difference between thermal coupling coefficients is strongly affected by the thermal resistances of the outermost layers. With higher thermal resistances (mineral wool or wood fibre wind barrier) the additional length of the thermal bridge has a strong positive correlation with the difference between respective thermal coupling coefficients. With low thermal resistance (wind barrier membrane or gypsum board) this effect is not present. This means that the interaction of these variables must be described when fitting the model.

Surprisingly, the thermal resistance of the load bearing layer and other internal layers adjoining the thermal bridge as well as the thermal conductivity of the insulation layer have no significant effect on the additional thermal bridge length. Although the point thermal transmittance depends on these parameters, the effect is already included in the thermal coupling coefficients and the additional length of the thermal bridge is not directly affected. This allows more simplification in the multiple regression model fitting as these parameters can be omitted.

4.5.2 Model fitting

Altogether 12 different model fits were tested to find a satisfactory balance between a good fit and the minimum number of terms in the multiple linear regression equation. As the difference between two-dimensional thermal coupling coefficients and the additional model length is strongly related to the thermal conductivity of the point thermal bridge and the thermal resistance of the wind barrier layer, it was expected that like in equation (*12*) the simple correlation has no predictive power (adjusted $R^2 = 0.072$). Other models, based on equations (*13*), (*14*) and (*15*), had better predictive power. The final empiric equation with estimated coefficients (all parameters with *p*-value < 0.001) that can be used to derive the additional thermal bridge length is given as equation (16).

$$h_{add} = -1.078 \cdot \left(L_{2D} - L_{2Dref} \right) + 0.001732 \cdot \lambda_{TB} + 1.480 \cdot h_{TB} + 4.162 \cdot R_{el} \quad (16)$$
$$\cdot \left(L_{2D} - L_{2Dref} \right) + 0.2529$$

The point thermal transmittance of a given thermal bridge can then be calculated according to equation (17).

$$\chi = \left(h_{add} - h_{TB} \right) \cdot \left(L_{2D} - L_{2Dref} \right) \quad (17)$$

Point thermal transmittances retrieved from three-dimensional numerical calculations are plotted against estimated point thermal transmittances in Figure 51 for the same thermal bridges.
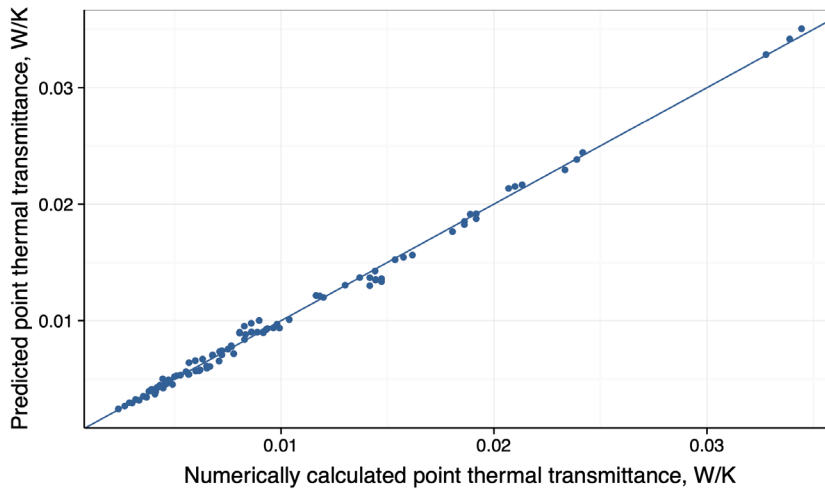
Figure 51. Correlation between calculated and estimated point thermal transmittance (the blue line represents x=y).

The relative error varies between −9.2 % (underestimation) and +15.1 % (overestimation) although typical deviations from the numerically calculated values were significantly lower with 0.25 and 0.75 quantiles at −2.7 % and +3.2 %, respectively.

The equation and the calculation methodology can be used for thermal bridges which embrace similar situations with local point thermal bridges incorporating metal penetrations through the insulation layer, such as metal brackets supporting or fixing the window frame to the load bearing structure etc. Analysis showed that the thermal conductivity of the insulation material of the layer that is penetrated and the thermal resistance of the internal (load bearing) structure have no significant effect on the equivalent length of the thermal bridge. This makes it possible to use the method on a wide array of different envelope configurations. A detailed calculation example using the proposed method to estimate the point thermal transmittance of a metal sheet in window-to-wall connection is given in PUBLICATION III.

5 Discussion

5.1 Airtightness in Estonian wooden buildings

The results confirm that buildings constructed after the energy performance requirements took effect have significantly lower air leakage than older buildings with the median q_{50} of 1.1 m³/(h·m²) and range from 0.8 to 3.1 m³/(h·m²), which correspond to 16 % and 84 % quantiles. This conforms well with other countries where new buildings had similar air leakage rates. In Poland, typical new building construction is characterised by airtightness n_{50} in the range of 1.6 to 2.6 h⁻¹ (Górzeński et al., 2014). Similar results have been achieved for timber-frame low-energy houses in Norway, where measured apartments had airtightness n_{50} in the range of 0.5 to 1.3 h⁻¹ (Holøs & Relander, 2010).

According to a previous study of the Estonian building stock, the most significant factors affecting the airtightness are the quality of workmanship and supervision as well the number of storeys of the house, both showing a more than a two-fold effect (Kalamees, 2007). This study shows that, for newer buildings, the number of storeys no longer has any effect on airtightness. This refers to the fact that a systematic approach to designing the airtight envelope avoids large air leakages characteristic of external wall and intermediate ceiling junctions in older buildings. Furthermore, the non-existent correlation between airtightness and compactness of the building envelope suggests that if a systematic quality assurance procedure with a proper airtightness concept in all junctions is followed, the geometric and structural complexity of the building envelope will no longer be a key factor for achieving airtightness. It must be noted that similar studies in Finland have shown significant differences in building airtightness depending on the number of storeys, with timber-frame multi-storey buildings (4.8 m³/(h·m²)) having higher air leakage rates than single-storey buildings (3.4 m³/(h·m²)), referring to the fact that such effects are related to local building technologies and overall quality assurance mechanisms (Vinha et al., 2015).

The quality of workmanship through systematic measurements as well as prefabrication showed significant improvement in the full dataset and in both subgroups (log buildings and lightweight timber buildings) corresponding to a 37 % to 74 % improvement, depending on the factor and group. The differences in other grouping factors were significantly smaller. For buildings with more ambitious airtightness targets, including buildings with higher designed energy efficiency and quality management, similar sealing measures are taken. Such measures include systematic use of specialised membranes and sealing tapes with a significant attention to connections between openings and external walls.

The results from this study give an overview of average air leakage rates along with the variation of different grouping factors related to building geometry and construction technology. Assuming consistency in construction technologies and in quality assurance mechanisms, these average values with appropriate safety margins can be used for energy calculation in Estonian conditions for new buildings as well as buildings in respective age groups. The base values calculated (*see* Table 4, Table 5 and Table 6) take into consideration the variation of the measured results and try to give estimates for each grouping factor with a 75 % margin and 84 % confidence interval. Due to the high variation in measured values, the base values are much higher than median or mean air leakage rates. The base values for buildings built since 2009 are in a range of 1.6 to 3.9 m³/(h·m²) with a value of 3.0 m³/(h·m²) for all measured buildings. The lowest base

value of the air leakage rate is for the group of prefabricated lightweight timber buildings with a value of $q_{50,base}$ = 1.6 m³/(h·m²). The groups with an energy classification target of A or B energy class, or systematic measurement practice within a single company achieved a base value $q_{50,base}$ around 2.0 m³/(h·m²), while on-site construction and handmade log buildings achieved a base value $q_{50,base}$ 6.7 m³/(h·m²) and 5.9 m³/(h·m²), respectively.

5.2 Air leakage of joints sealed with PU foam

Although the airtightness properties of foam joints have been previously tested and proved to be almost perfect (Ift Rosenheim, 2007) and good airtightness performance of the window-to-wall interface in cavity brick walls was reported (Van Den Bossche et al., 2012), the current study showed that the airtightness of actual joints could vary a lot and depends strongly on many parameters. A previous study in Belgium (Van Den Bossche et al., 2012) assessed the airtightness of PU foam joints among other insulating and sealing techniques (tapes, mineral wool). Several joints with PU foam filling half of the cavity, full cavity and full cavity with plaster coating were measured for airtightness. Air leakage rates in the range of 1.06 to 1.77 m³/(h·m) were measured at 50 Pa pressure difference for test specimens with pure PU foam treatment, which correspond respectively to 17.6 to 29.5 l/(min·m). Additional coating with plaster or additional sealing with caulking lowered the air leakages below 0.10 m³/(h·m), which corresponds to 1.67 l/(min·m). In this study the air leakages at 50 Pa pressure difference remained in the range of 0.156 to 0.565 l/(min·m) depending on surface treatment and joint width. Other studies of window-to-wall interfaces sealed with PU foam have also shown somewhat higher air leakages ranging from 0.0 to 0.155 (mean 0.03) m³/(h·m) (Proskiw, 1995) and 0.10 m³/(h·m) (Höglund & Bengt, 1984). Compared to other joint sealing measures studied by Relander et al. (2008a) the PU foam performed worse than well installed sealing tape but was comparable to backer rod and vapour barrier technique as well as sealing tapes with few holes. Self-expanding sealing strips and more traditional use of nailed vapour barrier was found to cause significantly higher leakage rate in the case of 15 mm wide joint in a range of 1.09 to 3.02 l/(min·m) at 50 Pa pressure difference.

Expanding montage foams need additional moisture from the air and through adjacent surfaces to fully expand and fill the grooves and concavities. It was expected that the smooth planed surface of timber joints would provide good conditions for foam bonding, and the measured results confirmed this. The air leakages in the case of planed timber surfaces were significantly lower compared to other surface types averaging V_{400} = 0.549 l/(min·m) at 400 Pa pressure difference. During repetitive testing with three identical test specimens for each configuration there were no measurements with failing airtightness. The joints with sawn timber laths performed worse by more than a factor of 2 averaging V_{400} = 1.132 l/(min·m) at 400 Pa pressure difference and the failure rate under repetitive testing was huge, totalling 33 % and 50 % for 10 mm and 30 mm joint widths, respectively. This shows that the studied foams were often unable to bond with the uneven surface and although some test specimens have comparable air leakages to planed timber surfaces, the foam–timber interface is systematically not airtight.

The failure rate of plastic-coated laths was significantly lower compared to sawn timber. However, a failure rate of more than 28 % in the case of the wider joint width still contributes to a situation where a foam–PVC interface has some bonding problems. The surface of PVC-coated laths is smooth, but the inhibited transport of moisture

through the plastic surface and water droplets caused by moistening the surfaces can, in some cases, create pathways for air leakages. Although this does not always cause major air leakages, the systematic effect contributes to even higher average air leakage rates compared to sawn timber (V_{400} = 1.438 l/(min·m) at 400 Pa pressure difference).

The leakage rate through the window–wall interface can be compared to the leakage rate of the window itself to assess the additional effect of leakages on overall airtightness. A large number of window products were tested in Belgium to assess the distribution and average airtightness of different window types (Van Den Bossche & Janssens, 2016). Although the variation within the test specimens was high, the median airtightness of single and double frame windows (independently from their material) was respectively 0.82 m³/(h·m²) and 1.36 m³/(h·m²) for 50 Pa pressure difference. For a hypothetical window with a size of 1.0 m × 1.0 m (joint length 4.0 m) this corresponds to air leakages of 0.82 and 1.36 m³/(h·m²), respectively, for single and double frame windows at 50 Pa pressure difference. The average air leakage rate of joints in the range of 0.156 to 0.565 l/(min·m) would, according to this study, add 0.04 m³/(h·m²) to 0.14 m³/(h·m²), corresponding to a 5 % to 17 % increase in the case of a single window and a 5 % to 10 % increase in the case of a double window. For larger windows with a favourable aspect ratio, the additional effect of the window–wall interface would be lower.

Similarly, the potential effect of measured joint air leakage can be calculated for an entire building envelope. For this a cumulative joint length for all connections between the building envelope elements was calculated for a prefabricated two-storey wooden reference building with very good airtightness and optimised window connection details (Kalbe & Kalamees, 2019). The good airtightness was achieved with systematic use of special tapes and on-site quality assurance measures. The building was included in a larger study (PUBLICATION I) of airtightness of Estonian wooden buildings. Its average measured air leakage rate q_{50} = 0.24 m³/(h·m²) at 50 Pa pressure difference, which corresponds to the measured air flow rate V_{50} = 91 m³/h. According to this study, with the cumulative joint length of 206 m and external envelope area of 373.5 m² the average air leakage rate of joints in the range of 0.156 to 0.565 l/(min·m) at 50 Pa pressure difference would contribute to additional 1.93 m³/h to 6.98 m³/h respectively corresponding to less than 0.02 m³/(h·m²) increase in the air leakage of an entire building envelope. In PUBLICATION I it was shown that the actual average air leakage rate of the envelope in newer wooden buildings is around 1.1 m³/(h·m²) with a very high (standard deviation 1.6 m³/(h·m²)) variation. This strongly suggests that the actual air leakage of the building envelope mainly depends on the 'failure rate' of sealing measures rather than on the leakage properties of the sealed joints. Previous studies have found that workmanship quality plays a critical role in achieving adequate airtightness. Kalamees et al. (2017) showed that comparison of air leakage readings measured in field conditions and those calculated based on laboratory measurements have significant differences. Relander et al., (2008b, 2008a) studied 7 different sealing techniques typical in Norway to assess the air leakage effect in the case of wall to window connection and showed that tapes provide most airtight solution with other sealing measures performing significantly worse. It was stated that for all the measures the effect of faulty workmanship can higher than expected air leakages.

Joint width and thus the volume of the joint are important factors when considering the use of expanding PU foam to achieve airtight connections. Although more foam is used for wider joints, the pressure during foam expansion is expected to be higher in the

case of a smaller volume. This can be systematically seen from the measurements, where the 10 mm wide joints performed significantly better for all surface types. The variation of measured air leakages along with the failure rate during repetitive testing was always higher with a 30 mm joint width compared to a 10 mm joint width. The effect of long-term expansion and periodic movement of building elements should be further studied as a wider joint width with the same elasticity can withstand larger movements. It is shown that PU foams are prone to fast chemical degradation (Pellizzi et al., 2014), which changes the mechanical properties of the foam. In this study the measurements were carried out within a few months after the foam was applied and the effect of ageing and chemical degradation was not considered.

Different foam products were compared in this study and although detailed analysis within subgroups of different lath surfaces and joint widths indicated some differences between specific foam products in some cases, no statistically significant differences were found. It should be noted that top-of-the-line high quality PU foams from each producer applied by skilled workers in a laboratory setup were measured in this study. The skill level of workers and real-life application conditions can induce significant discrepancies between different foams and cause higher air leakages compared to laboratory measurements. However, this needs to be further studied.

5.3 Heat loss due to cavities within the insulation layer

The current study showed that in a fully penetrating vertical air cavity within a wall insulation layer, the convective heat flow was strongly dependent on the temperature difference and cavity width. At a small temperature difference (Δt = 10 K), the correction factor $\Delta U''$ was similar to simplified values defined in EN ISO 6946 (2017), but at a higher temperature difference (Δt = 40 K) the heat loss significantly increased, corresponding approximately to one level of increase in the standardised installation level. For a 20 mm wide fully penetrating cavity, the correction factor at the 40 K temperature difference was well over the maximum correction level proposed by EN ISO 6946 (2017). Although direct comparison is not possible, an older empirical study in Sweden (Bankwall, 1972) measured the reduction of thermal resistance under a heat flow plate over vertical and horizontal 5 mm, 10 mm and 30 mm cavities in a 95 mm thick insulation layer and found similar effects. At the temperature difference around 20 K, the thermal resistance decreased up to 5 %, 21 % and 55 % on average under the heat flow plate respective to the cavity width from 5 mm to 30 mm (Bankwall, 1972). If approximate length-to-area ratios are derived from the assessed cavity widths and the measurement plate diameter of 100 mm, the scaled down increase in thermal transmittance will be very similar to our study. In the current study, the numerically calculated correction factors for vertical air cavities $\Delta U''$ were 0.004 and 0.015 W/(m^2·K) for 5 mm and 10 mm wide air cavities and 0.055 W/(m^2·K) for 20 mm wide air voids. In the Swedish study, the results for penetrating horizontal cavities in the insulation layer did not differ from vertical cavities, which could not be reproduced in our study. In their study Huttunen & Vinha (2013) also concluded that horizontal air cavities have no significant effect on the overall thermal transmittance.

The increase of the thermal transmittance due to higher temperature differences was higher in the roof construction for all assessed cases. The simplified procedure defined in EN ISO 6946 (2017) is unable to describe this problem for all cases with cavities wider than 5 mm. Šadauskiene et al. (2009) studied cavities within the roof insulation layer and showed that cavity widths below 5 mm have no significant effect on thermal transmittance;

however, their measurements were conducted only with the temperature difference of Δt = 20 K. Our study showed that a further rise of temperature difference significantly increased the additional heat loss due to a 5 mm wide cavity in the roof construction. In the case of roof construction, the external surface temperature may be even higher and the temperature difference may be even greater (Tatara & Ricketts, 2017). For wider cavities in the roof insulation layer Šadauskiene et al. (2009) found an up to 20 % increase of thermal transmittance considering the least favourable estimated combination of air cavity length-to-area ratios of 0.25 m/m^2 (1.3 mm wide cavity), 0.25 m/m^2 (3.0 mm wide cavity), 0.556 m/m^2 (9.0 mm wide cavity) and 0.556 m/m^2 (18.0 mm wide cavity). Our study determined the correction factor for 10 mm and 20 mm air cavities for the thermal conductivity of 0.040 W/(m·K) around 0.07 and 0.10 W/(m^2·K) when the cavity length-to-area ratio was 1.67 m/m^2. For the 3 lower cavity length-to-area ratio, this means an approximately 12 % increase in the thermal transmittance due to a 10 mm cavity and 17 % increase due to a 20 mm cavity. In general, the increase is similar to that reported by Šadauskiene et al. (2009).

According to Kuusk et al. (2021), in the case of circular use of materials the possible deviation from nominal material dimensions could be larger than set for new materials: up to 2 % for mineral wool (EN 13162, 2016) or 3 % for expanded PU (EN 13163, 2016). Therefore, estimation of crack dimensions in the construction of the building envelope from materials from urban mines or reused material banks should be even more conservative.

The effect of insulation material is small for 5 mm and 10 mm wide penetrating cavities. For wider cavities (20 mm), the heat loss increases with the increase in the thermal conductivity. This effect is more prominent in vertical cavities inside the roof construction. This also suggests that additional heat loss in wider penetrating cavities occurring between the edge of the insulation board and the timber frame or steel battens can be even higher due to conductive materials. Still, this needs to be studied further.

Two types of non-penetrating cavities were assessed to see if the effect on the thermal transmittance is significantly lower when the air circulation between internal and external boundaries is prevented by partial filling with PU foam or with the use of dual-layer insulation with rebate edge. Both alternatives decreased the correction factor $\Delta U''$ by a factor of 2 or more depending on the temperature difference. In the case of a 10 mm wide cavity the correction factor stayed slightly below normative installation level 1, which corresponds to 4.6 % to 9.5 % increase in the thermal transmittance depending on the insulation material. A previous study showed that cavities formed due to poor workmanship do not dramatically increase (observed increase 5 % to 10 %) thermal transmittance if they prevent air circulation from the hot side to the cold side (Huttunen & Vinha, 2013). Nevertheless, at the temperature difference of Δt = 35 K, the numerically derived correction factor for a 10 mm wide cavity was above normative installation level 0 and for a 20 mm wide cavity above normative installation level 1. Both alternatives are listed as level 0 installation solution in EN ISO 6946 (2017), which should be updated.

The current study and previous studies show that along with the temperature difference, the length-to-area ratio (average cavity length for unitary envelope area) has a significant effect on additional heat loss through the building envelope. Our study was based on typical dimensions of insulation boards and typical timber frame step size with an approximate width of 600 mm corresponding to the cavity length-to-area ratio of 1.67 m/m^2 when only vertical cavities are accounted for. If the step size between timber or steel battens is smaller due to architectural or structural constraints, the length-to-area

ratio will increase along with additional heat loss. The average step size of 400 mm, for example, increases the additional losses through vertical cavities by 50 %. Currently, the correction factors for air cavities defined in EN ISO 6946 do not quantify the number of cavities and should be updated.

Our study showed that there are smaller or larger cavities present between the insulation boards and batts installed on construction sites and in the factory of the prefabricated building elements, so the insulation does not always fill the space provided. According to our results, the actual heat loss due to cracks and cavities is higher than the calculated ideal situation. Hamburg & Kalamees (2019) showed that the performance gap between the measured and the calculated energy consumption is 2 % to 30 %, and the delivered energy for room heating after refurbishment works is on average more than 35 % larger than the calculated values in the design phase. In addition to higher room temperature, energy for heating depends directly also on the heat loss of the building envelope (Hamburg & Kalamees, 2018). The standard EN ISO 6946 (2017) is based on the ideal electrical-thermal analogy and it is necessary to consider appropriate corrections to the thermal transmittance in the calculations of the heat loss of the building envelope.

The results are summed up in Table 12 where for each assessed situation the suitable normative installation level is given, which does not underestimate the actual heat loss in the case of typical insulation panel width of 600 mm.

Table 12. Proposal for standardised installation levels (EN ISO 6946) for each assessed case (cc 600 mm) that can be used and will not underestimate the actual thermal transmittance caused by air cavities inside the insulation layer in well-insulated building envelopes.

Cavity width	Reclassified standardised installation levels according to cavity geometry (*see* Figure 12) for floor, wall and roof construction										
	Penetrating cavity with rectangular cross section				Cavity filled with PU foam (50 mm) from external side		Cavities in 2-layer insulation with rebate, tongue and groove edge		Penetrating cavity with wedge-shaped cross-section		Penetrating cavity with additional triangular cut-outs
	Floor	Wall (hor.)	Wall (vert.)	Roof	Wall	Roof	Wall	Roof	Wall	Roof	Wall
= 5 mm	0	0	1	2	1	1	1	2	1	2	n/a
≤ 10 mm	0	0	2	n/a	1	2	2	2	1	2	n/a
> 10 mm (20 mm)	0	0	n/a	n/a	2	n/a	2	n/a	2	n/a	n/a

n/a – not applicable

Previous research shows that in the case of impermeable insulation materials convective heat transfer can take place in air gaps wider than 5 mm (Šadauskiene et al., 2009; Stankevičius et al., 2013), but the influence of natural convection on general heat transfer is insignificant when a joining small air gap of up to 3 mm thickness occurs around the thermal-insulating layer. Therefore, cavities with the thickness below 5 mm are not assessed in this study. In practice, insulation installation level 0 (i.e., no effect due to cavities) is not achievable with most insulation solutions where the formation of vertical cavities with the thickness around 5 mm or more is expected. A few notable exceptions to this in practice would be spray-on foam insulation and blown-in cellulose insulation inside wall and roof elements when high density blow in insulation is used to avoid the forming of creeps and cavities through vibration and ageing. Many other insulation solutions should be reclassified (currently level 0) to levels 1 or 2: dual layer insulation, sealed or partly foamed cavities within single insulation layers. The effect is strongly climate dependent; however, the current definition of the thermal transmittance neglects this.

5.4 Possible simplifications regarding thermal bridging

The current study confirmed that for well-insulated constructions, the minimum flanking element length required in the numerical model is significantly lower than described in EN ISO 10211 (2017) without compromising the accuracy of steady-state calculations of linear thermal transmittance. Similar findings have been reported in previous studies related to dynamic modelling of thermal bridges with equivalent wall and mixed equivalent wall methods where new shorter flanking element lengths were accompanied by a limited change in surface temperature along the flanking element (Martin et al., 2012; Quinten & Feldheim, 2016, 2019). The length of equivalent wall parts in these studies was strictly related to fixed geometry and material layers; nevertheless, compared to the requirements of EN ISO 10211 (2017), only 40 % to 50 % of the flanking element length was needed (Ge & Baba, 2015) to define equivalent wall parts.

The current study shows that even shorter flanking element lengths are acceptable for most junctions. In the case of regular junctions adjacent to external air within well-insulated constructions with linear thermal transmittance below 0.1 W/(m·K), the reduction of flanking element length from 1.44 m to 0.288 m (80 % reduction) had no effect on numerically calculated linear thermal transmittance. For junctions with significantly higher linear thermal transmittance, especially above 0.3 W/(m·K) and up to 1.1 W/(m·K), a reduction of only half of the flanking element length (0.72 m) was possible without a change in calculated linear thermal transmittance, but this occurred only in constructions with a highly conductive internal load bearing layer (heavyweight concrete in this study). The junctions with lightweight concrete or timber frame construction behaved similarly to thermally good junctions, with the deviation of the linear thermal transmittance $\Delta\Psi$ around 0.001 W/(m·K) when the flanking element length was reduced from 1.44 m to 0.288 m (80 % reduction). The thermal conductivity of insulation material had no significant effect on $\Delta\Psi$ in all assessed cases.

Contrary to the objective of the equivalent wall method, the shorter distance to the adiabatic cut-off plane in this study was used to disaggregate more complex thermal bridges with multiple combined junctions, allowing the separation of the thermal bridges, which can then be summed up arithmetically. The results show that when minimum flanking element lengths identified in this study are used instead of standard values, the amount of different complex thermal bridges in two reference buildings can

be reduced by 35 % to 76 % depending on the allowed deviations in the range of 0.5 % to 2.0 %. This would significantly reduce the working hours of practitioners.

A previous study on the application of infrared thermography for the assessment of combined thermal bridges also suggests that despite EN ISO 10211 requirements the adjacent thermal bridges can be assumed to interact only if the surface temperature between the thermal bridges remains lower than the uniform surface temperature and shorter flanking elements are possible depending on the detail (O'Grady et al., 2018). The authors refer to the remark in a BRE report (Ward et al., 2016) that allows separate assessment of combined thermal bridges if these are more apart from each other than the thickness of the building element.

For point thermal bridges in building facades the current study proposes a new method for predicting three-dimensional heat flow and the point thermal transmittance of thermal bridges caused by full or partial penetration of the building envelope with metal elements with uniform geometry in the third dimension using two-dimensional numerical calculation. This would enable estimation of the point thermal transmittance of different mounting brackets etc. in cases where a three-dimensional calculation procedure is not possible due to lack of time, software tools or skills within the design team.

Analysis revealed that the effect of insulation material as well as the thermal resistance of the internal layers (load bearing part of the building envelope) did not have any significant effect on the linear regression between the additional length of the thermal bridge and the difference in thermal coupling coefficients derived from the respective cross sections.

6 Conclusions

This thesis studied the effect of air leakages and thermal bridges along with other nonidealities in the context of well-insulated building envelopes in order to provide input for robust, updated and more accurate methods to estimate the heat loss through building envelopes.

Based on field measurements it was concluded that the airtightness of Estonian wooden buildings has improved by a factor of 10 since the minimum requirements for energy efficiency took effect.

The improved quality of workmanship has helped to significantly reduce air leakages. Prefabrication with the light-weight timber construction technology provides substantially better airtightness compared to traditional timber log building construction technology. Besides, prefabrication improves airtightness also within log wood and lightweight timber building groups, because on-site building or the use of handmade logs corresponds to significantly higher air leakages.

The compactness factor and number of storeys did not have a significant effect on air leakage. This refers to the fact that if systematic quality assurance with a proper airtightness concept is used, the geometric and structural complexity of the building envelope will no longer be a key factor for achieving airtightness.

The tabulated base values of the air leakage rate for buildings erected since 2009 are in a range of 1.6 to 3.9 $m^3/(h·m^2)$ with a value of 3.0 $m^3/(h·m^2)$ for all buildings. The lowest base value of air leakage rate is for a group of prefabricated lightweight timber buildings with $q_{50,base}$ = 1.6 $m^3/(h·m^2)$. The groups with an energy classification target of A or B energy class and systematic measurement practice within a single company achieved a base value $q_{50,base}$ around 2.0 $m^3/(hm^2)$, while on-site construction along with handmade log buildings achieved a base value $q_{50,base}$ 6.7 $m^3/(h·m^2)$ and 5.9 $m^3/(h·m^2)$, respectively. Assuming consistency in construction technologies and in quality assurance mechanisms, these tabulated base values can be used for energy calculation in Estonian conditions for new buildings or buildings in the respective age groups.

Based on laboratory measurements in this study, it can be concluded that thickness and surface property of the joints in building envelope had a significant effect on the air leakage of joints filled with PU foam. In laboratory conditions consistent and a very low air leakage rate was obtained with planed timber surfaces. Joints with plastic-coated and sawn timber surfaces performed worse by a factor of 2 or more on average and contributed to a very variable airtightness with up to 28 % and 50 % test specimens failing the airtightness testing.

Increasing the joint width increased the air leakage along with its variation within all other analysed factors. Contrary to assumption, no significant differences between different premium class foam products could be shown. Comparison of estimated and previously measured overall airtightness of an entire building envelope showed dependence on the 'failure rate' rather than on the average measured leakage rate. It should be taken into consideration that the results obtained in laboratory conditions may be better than the ones obtained on site. Besides, the effect of ageing needs to be further studied. The tabulated joint air leakage rates grouped by main effecting factors can be useful for predictive leakage modelling in the future.

Air convection through gaps and nonidealities between building envelope parts and within the insulation layer causes additional heat loss of the building envelope. Numerical analysis of additional heat loss induced by air cavities between insulation

boards due to nonidealities led to the conclusion that certain insulation solutions described in EN ISO 6946 Annex F should be reclassified (currently level 0), e.g., dual layer insulation, sealed or partly foamed cavities within single insulation layers. While the additional heat loss is insignificant through a penetrating horizontal air cavity, the heat loss through vertical air cavities inside wall and roof insulation layers is highly dependent on the cavity diameter and temperature difference. The rise of the temperature difference from 10 K to 40 K increased the correction factor for air cavities one level up compared to the estimation based on EN ISO 6946. For an upward heat flow (roof construction), the effect was even more adverse. Insulation material has only a marginal effect (higher thermal conductivity contributes to a slightly higher additional heat loss). The presence of penetrating air cavities with 5 mm, 10 mm and 20 mm diameters will increase the thermal transmittance in the wall construction by up to 10 %, 33 % and 59 % at 40 K temperature difference. This phenomenon is not adequately covered in the current standard. Penetrating cavities with a width of more than 10 mm inside roof insulation have a huge effect and should be classified as inadequate workmanship and an inappropriate solution.

The results from numerical assessment of different thermal bridges in lightweight and heavyweight constructions show that the minimal flanking element length can be significantly reduced. This simplifies the assessment of combined linear thermal bridges where two or more separate simple junctions are in close proximity such as window connection to intermediate ceiling, ground floor slab and several short wall segments in between. In the case of a well-insulated building envelope, the sufficient length of the flanking element to adequately describe the linear thermal transmittance in a steady-state situation is equal to approximately its thickness. Compared to EN ISO 10211 requirements, this makes it possible to reduce the proportion of different complex thermal bridges from between 35 % to 76 %, depending on the allowed deviations in the range of 0.5 % to 2.0 %. This would significantly reduce the working hours of practitioners.

A new method was proposed for predicting the three-dimensional heat flow and the point thermal transmittance of thermal bridges caused by full or partial penetration of the building envelope with metal elements with uniform geometry in the third dimension using two-dimensional numerical calculation. This would make it possible to estimate the point thermal transmittance of different mounting brackets etc. in cases where the three-dimensional calculation procedure is not possible due to lack of time, software tools or skills within the design team. The results of this thesis can be used as input to further research on this topic to generate a generalised set of requirements for a future version of EN ISO 10211 standards and provide a more detailed workflow for the assessment of combined thermal bridges in steady-state calculations.

References

Adamus, J., & Pomada, M. (2018). Analysis of heat flow in composite structures used in window installation. *Composite Structures*, *202*, 127–135. https://doi.org/10.1016/j.compstruct.2017.12.077

Al-Sanea, S. A., & Zedan, M. F. (2012). Effect of thermal bridges on transmission loads and thermal resistance of building walls under dynamic conditions. *Applied Energy*, *98*, 584–593. https://doi.org/10.1016/j.apenergy.2012.04.038

ANSYS inc. (2020). *ANSYS finite element analysis software*. https://www.ansys.com/products

ASHRAE. (2001). *International Weather for Energy Calculations (IWEC Weather Files) Users Manual and CD-ROM*. Amer Society of Heating. https://books.google.ee/books?id=tcaVuAAACAAJ

Bankwall, C. G. (1972). Natural convective heat transfer in insulated structures. *ASME Pap*, *72-WA/HT-63*.

Bergero, S., & Chiari, A. (2018). The influence of thermal bridge calculation method on the building energy need: a case study. *Energy Procedia*, *148*, 1042–1049. https://doi.org/10.1016/J.EGYPRO.2018.08.056

Berggren, B., & Wall, M. (2013). Calculation of thermal bridges in (Nordic) building envelopes – Risk of performance failure due to inconsistent use of methodology. *Energy and Buildings*, *65*, 331–339. https://doi.org/10.1016/j.enbuild.2013.06.021

Berggren, B., & Wall, M. (2018). State of Knowledge of Thermal Bridges—A Follow up in Sweden and a Review of Recent Research. *Buildings*, *8*(11), 154. https://doi.org/10.3390/buildings8110154

Beuth-Verlag. (2013). *DIN 4108-2:2013-02 Wärmeschutz und Energie-Einsparung in Gebäuden - Teil 2: Mindestanforderungen an den Wärmeschutz*. Beuth-Verlag.

Borelli, D., Cavalletti, P., Marchitto, A., & Schenone, C. (2020). A comprehensive study devoted to determine linear thermal bridges transmittance in existing buildings. *Energy and Buildings*, *224*, 110136. https://doi.org/10.1016/j.enbuild.2020.110136

Capozzoli, A., Gorrino, A., & Corrado, V. (2013). A building thermal bridges sensitivity analysis. *Applied Energy*, *107*, 229–243. https://doi.org/10.1016/j.apenergy.2013.02.045

Cappelletti, F., Gasparella, A., Romagnoni, P., & Baggio, P. (2011). Analysis of the influence of installation thermal bridges on windows performance: The case of clay block walls. *Energy and Buildings*, *43*(6), 1435–1442. https://doi.org/10.1016/j.enbuild.2011.02.004

Chang, S. J., Wi, S., & Kim, S. (2019). Thermal bridging analysis of connections in cross-laminated timber buildings based on ISO 10211. *Construction and Building Materials*, *213*, 709–722. https://doi.org/10.1016/J.CONBUILDMAT.2019.04.009

Chebil, S., Galanis, N., & Zmeureanu, R. (2003). Computer simulation of thermal impact of air infiltration through multilayered exterior walls. *Eighth International IBPSA Conference*, 155–162. http://www.ibpsa.org/%5Cproceedings%5CBS2003%5CBS03_0155_162.pdf

Colijn, M., Entrop, A. G., & Toxopeus, M. E. (2017). Evaluating the effectiveness of improved workmanship quality on the airtightness of Dutch detached houses. *Energy Procedia*, *132*(June), 843–848. https://doi.org/10.1016/j.egypro.2017.09.670

Comsol inc. (2020). *The COMSOL Multiphysics Software Product Suite*. https://www.comsol.com/products

Cuce, E. (2017). Role of airtightness in energy loss from windows: Experimental results from in-situ tests. *Energy and Buildings*, *139*, 449–455. https://doi.org/10.1016/j.enbuild.2017.01.027

EITMn nr. 63. (2018). Hoone energiatõhususe miinimumnõuded. In *[in Estonian. Decree of the Minister of Foreign Trade and Information Technology No 63 (11.12.2018) Minimum energy performance requirements of the building]*. Riigi Teataja. https://www.riigiteataja.ee/akt/113122018014

EN 12114. (2000). *Thermal performance of buildings - Air permeability of building components and building elements - Laboratory test method*. CEN.

EN 13162. (2016). *Thermal insulation products for buildings - Factory made mineral wool (MW) products - Specification*.

EN 13163. (2016). *Thermal insulation products for buildings - Factory made expanded polystyrene (EPS) products - Specification* (EN 13163:2). European committee of Standardization.

EN 13829. (2000). *Thermal performance of buildings - Determination of air permeability of buildings - Fan pressurization method*.

EN 825. (2013). *Thermal insulating products for building applications - Determination of flatness* (EVS-EN 825). European committee of Standardization.

EN ISO 10077-1. (2017). *Thermal performance of windows, doors and shutters — Calculation of thermal transmittance — Part 1: General*.

EN ISO 10077-2. (2017). *Thermal performance of windows, doors and shutters — Calculation of thermal transmittance — Part 2: Numerical method for frames*.

EN ISO 10211. (2017). *ISO 10211:2017 Thermal bridges in building construction. Heat flows and surface temperatures. Detailed calculations*. https://www.iso.org/standard/65710.html

EN ISO 12631. (2017). *Thermal performance of curtain walling — Calculation of thermal transmittance*.

EN ISO 13370. (2017). *Thermal performance of buildings — Heat transfer via the ground — Calculation methods*.

EN ISO 13789. (2017). *Thermal performance of buildings — Transmission and ventilation heat transfer coefficients — Calculation method*.

EN ISO 13790. (2008). *ISO 13790:2008 Energy performance of buildings — Calculation of energy use for space heating and cooling*.

EN ISO 14683. (2017). *Thermal bridges in building construction — Linear thermal transmittance — Simplified methods and default values*.

EN ISO 6946. (2017). *Building components and building elements — Thermal resistance and thermal transmittance — Calculation Method* (2017th ed.). ISO Copyright office. www.iso.org

EN ISO 9972. (2015). *Thermal performance of buildings - Determination of air permeability of buildings - Fan pressurization method*.

EPBD. (2018). Directive (EU) 2018/844 of the European Parliament and of the Council of 30 May 2018 amending Directive 2010/31/EU on the energy performance of buildings and Directive 2012/27/EU on energy efficiency. *Official Journal of the European Union*, *30 May*. https://eur-lex.europa.eu/legal-content/EN/TXT/HTML/?uri=CELEX:32018L0844&from=EN

Erhorn, H., Erhorn-Kluttig, H., Citterio, M., Cocco, M., Van Orshoven, D., Tilmans, A., Schild, P., Bloem, P., Thomsen, K. E., & Rose, J. (2010). *An effective Handling of Thermal Bridges in the EPBD Context*. *March*. www.asiepi.eu

Evangelisti, L., Guattari, C., & Asdrubali, F. (2018). Influence of heating systems on thermal transmittance evaluations: Simulations, experimental measurements and data post-processing. *Energy and Buildings*, *168*, 180–190. https://doi.org/10.1016/j.enbuild.2018.03.032

Ge, H., & Baba, F. (2015). Dynamic effect of thermal bridges on the energy performance of a low-rise residential building. *Energy and Buildings*, *105*, 106–118. https://doi.org/10.1016/j.enbuild.2015.07.023

Górzeński, R., Szymański, M., Górka, A., & Mróz, T. (2014). Airtightness of buildings in Poland. *International Journal of Ventilation*, *12*(4), 391–400. https://doi.org/10.1080/14733315.2014.11684032

Gullbrekken, L., Grynning, S., & Gaarder, J. E. (2019). Thermal performance of insulated constructions-experimental studies. *Buildings*, *9*(2). https://doi.org/10.3390/buildings9020049

Gullbrekken, L., Kvande, T., & Time, B. (2017). Ventilated wooden roofs: Influence of local weather conditions-measurements. *Energy Procedia*, *132*, 777–782. https://doi.org/10.1016/j.egypro.2017.10.029

Gullbrekken, L., Uvslokk, S., Kvande, T., & Time, B. (2017). Hot-Box measurements of highly insulated wall, roof and floor structures. *Journal of Building Physics*, *41*(1), 58–77. https://doi.org/10.1177/1744259116669516

Hagentoft, C.-E. (1988). *Heat loss to the ground from a building : slab on the ground and cellar* [Byggnadsfysik LTH, Lunds Tekniska Högskola]. https://lup.lub.lu.se/search/ws/files/4896022/8056211.pdf

Hamburg, A., & Kalamees, T. (2018). The Influence of Energy Renovation on the Change of Indoor Temperature and Energy Use. *Energies*, *11*(11), 3179. https://doi.org/10.3390/en11113179

Hamburg, A., & Kalamees, T. (2019). How well are energy performance objectives being achieved in renovated apartment buildings in Estonia? *Energy and Buildings*, *199*, 332–341. https://doi.org/https://doi.org/10.1016/j.enbuild.2019.07.006

Höglund, I., & Bengt, J. (1984). *Joint Sealing Between Window (Door) Frames and Walls– Development of New Types of Synthetic Rubber Stuffing Strips*. Division of Building Technology, Stockholm, Sweden.

Holøs, S. B., & Relander, T.-O. (2010). Airtightness Measurements of Wood Frame Low Energy Row Houses. *BEST Conference*, 1–11.

Huttunen, P., & Vinha, J. (2013). Effect of natural convection on the thermal transmittance of exterior walls with air-permeable insulation. *Thermal Performance of the Exterior Envelopes of Whole Buildings - 12th International Conference*.

Ift Rosenheim. (2007). *Air permeability of montage foam. Test report 10533428*.

Janssens, A., & Hens, H. (2003). Interstitial Condensation Due to Air Leakage: A Sensitivity Analysis. *Journal of Building Physics*, *27*(1), 15–29. https://doi.org/10.1177/1097196303027001002

Jokisalo, J., Kurnitski, J., Korpi, M., Kalamees, T., & Vinha, J. (2009). Building leakage, infiltration, and energy performance analyses for Finnish detached houses. *Building and Environment*, *44*(2), 377–387. http://www.sciencedirect.com/science/article/pii/S0360132308000516

Kalamees, T., & Kurnitski, J. (2006). Estonian climate analysis for selecting the test reference year. *HB 2006 - Healthy Buildings: Creating a Healthy Indoor Environment for People, Proceedings, 5*, 207–212.

Kalamees, Targo. (2007). Air tightness and air leakages of new lightweight single-family detached houses in Estonia. *Building and Environment, 42*(6), 2369–2377. https://doi.org/10.1016/j.buildenv.2006.06.001

Kalamees, Targo, Alev, Ü., & Pärnalaas, M. (2017). Air leakage levels in timber frame building envelope joints. *Building and Environment, 116*, 121–129. https://doi.org/10.1016/j.buildenv.2017.02.011

Kalbe, K., & Kalamees, T. (2019). Influence of Window Details on the Energy Performance of an nZEB. *Journal of Sustainable Architecture and Civil Engineering, 1*(24), 61–70. https://doi.org/10.5755/j01.sace.24.1.22052

Kassambara, A. (2018). *ggpubr: "ggplot2" Based Publication Ready Plots*. https://cran.r-project.org/package=ggpubr

Kivioja, H., & Vinha, J. (2020). Hot-box measurements to investigate the internal convection of highly insulated loose-fill insulation roof structures. *Energy and Buildings, 216*, 109934. https://doi.org/10.1016/j.enbuild.2020.109934

Klõšeiko, P., Piir, R., Jeltsov, M., & Kalamees, T. (2020). Thermal bridge effect of vertical diagonal tie connectors in precast concrete sandwich panels: An experimental and computational study. *E3S Web of Conferences, 172*, 1–7. https://doi.org/10.1051/e3sconf/202017208001

Kuusk, K., Kullerkupp, K., Pihelo, P., Ritzen, M., Tisov, A., & Kalamees, T. (2021). Circularity concepts for offsite prefabricated energy renovation of apartment buildings. *The 8th International Buildings Physics Conference*.

Larbi, A. Ben. (2005). Statistical modelling of heat transfer for thermal bridges of buildings. *Energy and Buildings, 37*(9), 945–951. https://doi.org/10.1016/j.enbuild.2004.12.013

LBNL Therm. (2020). *Therm*.

Lorenzati, A., Fantucci, S., Capozzoli, A., & Perino, M. (2016). Experimental and numerical investigation of thermal bridging effects of jointed Vacuum Insulation Panels. *Energy and Buildings, 111*, 164–175. https://doi.org/10.1016/j.enbuild.2015.11.026

Lowe, R. J., Wingfield, J., Bell, M., & Bell, J. M. (2007). Evidence for heat losses via party wall cavities in masonry construction. *Building Services Engineering Research and Technology, 28*(2), 161–181. https://doi.org/10.1177/0143624407077196

Martin, K., Escudero, C., Erkoreka, A., Flores, I., & Sala, J. M. (2012). Equivalent wall method for dynamic characterisation of thermal bridges. *Energy and Buildings, 55*, 704–714. https://doi.org/10.1016/j.enbuild.2012.08.024

Miles-Shenton, D., Gorse, C., & Thomas, F. (2015). *External walls partially filled with insulation, and the potential to "top-up" the residual cavity*. http://eprints.leedsbeckett.ac.uk/5067/

Miles-Shenton, D., Wingfield, J., Sutton, R., & Bell, M. (2010). *Temple Avenue field trial – Evaluation of design & construction process and measurement of fabric performance of new build dwellings*. 1–32.

Ministry of Economic Affairs and Communications. (2022). *Register of Buildings*.

Mortensen, L. H., & Bergsøe, N. C. (2017). Air tightness measurements in older Danish single-family houses. *Energy Procedia, 132*(June), 825–830. https://doi.org/10.1016/j.egypro.2017.10.016

MTMm nr 58. (2015). Hoonete energiatõhususe arvutamise metoodika (Methodology for calculating the energy performance of buildings). In *Riigi Teataja - State Gazette of the Republic of Estonia*. https://www.riigiteataja.ee/akt/109062015021?leiaKehtiv

O'Grady, M., Lechowska, A. A., & Harte, A. M. (2018). Application of infrared thermography technique to the thermal assessment of multiple thermal bridges and windows. *Energy and Buildings*, *168*, 347–362. https://doi.org/10.1016/J.ENBUILD.2018.03.034

O'Hegarty, R., Kinnane, O., Lennon, D., & Colclough, S. (2021). In-situ U-value monitoring of highly insulated building envelopes: Review and experimental investigation. *Energy and Buildings*, *252*, 111447. https://doi.org/10.1016/j.enbuild.2021.111447

Paap, L.; Mikola, A.; Kõiv, T.-A.; Kalamees, T. (2012). Airtightness and ventilation of new Estonian apartments constructed 2001-2010. *Proceedings of the Joint Conference 33rd AIVC Conference and 2nd TightVent Conference Optimising Ventilative Cooling and Airtightness for [Nearly] Zero-Energy Buildings, IAQ and Comfort, Copenhagen*.

Pellizzi, E., Lattuati-Derieux, A., Lavédrine, B., & Cheradame, H. (2014). Degradation of polyurethane ester foam artifacts: Chemical properties, mechanical properties and comparison between accelerated and natural degradation. *Polymer Degradation and Stability*, *107*, 255–261. https://doi.org/10.1016/j.polymdegradstab.2013.12.018

PHYSIBEL. (2020). *Physibel finite difference calculation tools*.

Pikas, E., Thalfeldt, M., & Kurnitski, J. (2014). Cost optimal and nearly zero energy building solutions for office buildings. *Energy and Buildings*, *74*, 30–42. https://doi.org/10.1016/j.enbuild.2014.01.039

Prignon, M., & Van Moeseke, G. (2017). Factors influencing airtightness and airtightness predictive models: A literature review. *Energy and Buildings*, *146*, 87–97. https://doi.org/10.1016/j.enbuild.2017.04.062

Proskiw, G. (1995). *Air leakage characteristics of various rough-opening sealing methods for windows and doors*.

Quinten, J., & Feldheim, V. (2016). Dynamic modelling of multidimensional thermal bridges in building envelopes: Review of existing methods, application and new mixed method. *Energy and Buildings*, *110*, 284–293. https://doi.org/10.1016/j.enbuild.2015.11.003

Quinten, J., & Feldheim, V. (2019). Mixed equivalent wall method for dynamic modelling of thermal bridges: Application to 2-D details of building envelope. *Energy and Buildings*, *183*, 697–712. https://doi.org/10.1016/J.ENBUILD.2018.11.004

R Core Team. (2018). *R: A Language and Environment for Statistical Computing*. https://www.r-project.org/

Relander, T.-O., Thue, J. V., & Gustavsen, A. (2008a). Air tightness performance of different sealing methods for windows in wood-frame buildings. *Proceedings of the 8th Symposium on Building Physics in the Nordic Countries*, *1994*, 417–424.

Relander, T.-O., Thue, J. V., & Gustavsen, A. (2008b). The influence of different sealing methods of window and door joints on the total air leakage of wood-frame buildings. *Proceedings of the 8th Symposium on Building Physics in the Nordic Countries*, 497–504.

Relander, T. O., Holøs, S., & Thue, J. V. (2012). Airtightness estimation - A state of the art review and an en route upper limit evaluation principle to increase the chances that wood-frame houses with a vapour- and wind-barrier comply with the airtightness requirements. *Energy and Buildings*, *54*, 444–452. https://doi.org/10.1016/j.enbuild.2012.07.012

Ricketts, L. (2018). Impact of Insulation Dimensional Stability on Conventional Roof Performance. *33rd RCI International Convention and Trade Show*, 161–173.

RT 80-10974. (2009). *Teollisesti valmistettujen asuinrakennusten ilmanpitävyyden laadunvarmistusohje [Air- tightness management manual for prefabricated residential buildings]*.

Šadauskiene, J., Buska, A., Burlingis, A., Bliüdžius, R., & Gailius, A. (2009). The effect of vertical air gaps to thermal transmittance of horizontal thermal insulating layer. *Journal of Civil Engineering and Management*, *15*(3), 309–315. https://doi.org/10.3846/1392-3730.2009.15.309-315

Schöck bauteile GmbH. (2012). *Building Physics Report No .: 1 - Building Physics Analyses and Isokorb Specifications* (Issue 1). https://www.laros.com.au/wp-content/uploads/2017/03/LAROS-Schöck-Isokorb-BuildingPhysicsReportNo1_Mar12.pdf

Shankar, V., & Hagentoft, C. E. (2000). A Numerical Study of Effect of Natural Convection on Thermal Properties of Horizontal Oriented Porous Insulation. *Journal of Building Physics*, *24*(2), 155–167. https://doi.org/10.1106/BLW6-JKJA-VNN4-MH62

Stankevičius, V., Paukštys, V., Bliudžius, R., Šadauskiene, J., Turskis, Z., & Samajauskas, R. (2013). Convection in mineral wool used as insulation for buildings. *Journal of Civil Engineering and Management*, *19*(2), 296–304. https://doi.org/10.3846/13923730.2013.775182

Stonkuvienė, A., Bliūdžius, R., Burlingis, A., & Ramanauskas, J. (2021). The impact of connector's thermal and geometrical characteristics on the energy performance of facade systems. *Journal of Building Engineering*, *35*(July 2020). https://doi.org/10.1016/j.jobe.2020.102085

Tatara, J., & Ricketts, L. (2017). Impact of Heating and Cooling of Expanded Polystyrene and Stone Wool Insulations on Conventional Roof Performance. *IMPACT OF HEATING AND COOLING OF EXPANDED POLYSTYRENE AND STONE WOOL INSULATIONS ON CONVENTIONAL ROOF PERFORMANCE*, 1–16.

Theodosiou, T. G., & Papadopoulos, A. M. (2008). The impact of thermal bridges on the energy demand of buildings with double brick wall constructions. *Energy and Buildings*, *40*(11), 2083–2089. https://doi.org/10.1016/j.enbuild.2008.06.006

Theodosiou, T., Tsikaloudaki, K., Kontoleon, K., & Giarma, C. (2021). Assessing the accuracy of predictive thermal bridge heat flow methodologies. *Renewable and Sustainable Energy Reviews*, *136*(October 2020), 110437. https://doi.org/10.1016/j.rser.2020.110437

Theodosiou, T., Tsikaloudaki, K., Tsoka, S., & Chastas, P. (2019). Thermal bridging problems on advanced cladding systems and smart building facades. *Journal of Cleaner Production*, *214*, 62–69. https://doi.org/10.1016/J.JCLEPRO.2018.12.286

Theodosiou, Theodoros G., Tsikaloudaki, A. G., Kontoleon, K. J., & Bikas, D. K. (2015). Thermal bridging analysis on cladding systems for building facades. *Energy and Buildings*, *109*, 377–384. https://doi.org/10.1016/j.enbuild.2015.10.037

Van Den Bossche, N., Huyghe, W., Moens, J., Janssens, A., & Depaepe, M. (2012). Airtightness of the window-wall interface in cavity brick walls. *Energy and Buildings*, *45*, 32–42. https://doi.org/10.1016/j.enbuild.2011.10.022

Van Den Bossche, N., & Janssens, A. (2016). Airtightness and watertightness of window frames: Comparison of performance and requirements. *Building and Environment*, *110*, 129–139. https://doi.org/10.1016/j.buildenv.2016.09.034

Vinha, J., Manelius, E., Korpi, M., Salminen, K., Kurnitski, J., Kiviste, M., & Laukkarinen, A. (2015). Airtightness of residential buildings in Finland. *Building and Environment*, *93*(P2), 128–140. https://doi.org/10.1016/j.buildenv.2015.06.011

Viot, H., Sempey, A., Pauly, M., & Mora, L. (2015). Comparison of different methods for calculating thermal bridges: Application to wood-frame buildings. *Building and Environment*, *93*, 339–348. https://doi.org/10.1016/j.buildenv.2015.07.017

Wahlgren, P. (2005). Variation in onset of natural convection in loose-fill attic insulation due to geometry and materials. *7th Symposium on Building Physics in the Nordic Countries, Reykjavik*.

Wahlgren, P. (2007). Overview and literature survey of natural and forced convection in attic insulation. *Journal of Building Physics*, *30*(4), 351–370. https://doi.org/10.1177/1744259106075947

Ward, T., Hannah, G., & Sanders, C. (2016). *Conventions for Calculating Linear Thermal Transmittance and Temperature Factors: (br 497)*. IHS BRE Press. https://books.google.ee/books?id=iR10jwEACAAJ

Zangheri, P., Armani, R., Pietrobon, M., & Pagliano, L. (2018). Identification of cost-optimal and NZEB refurbishment levels for representative climates and building typologies across Europe. *Energy Efficiency*, *11*(2), 337–369. https://doi.org/10.1007/s12053-017-9566-8

Acknowledgements

First of all, I would like to thank my supervisor Targo Kalamees for the guidance, exceptional support, patience and trust in me throughout my studies. I would also like to thank Tiia Kaare for thoroughly revising and editing this thesis at such short notice.

My sincere gratitude goes out to all my lovely colleagues from Tallinn University of Technology – Paul Klõšeiko, Endrik Arumägi, Karl-Villem Võsa, Raimo Simson, Tuule-Mall Parts, Alo Mikola, Laura Kadaru, Martin Kiil, Villu Kukk, Kalle Kuusk, Kristo Kalbe, Simo Ilomets, Helena Kuivjõgi, Meril Tamm, Eero Tuhkanen and many others. Thank you for fruitful discussions, collaborations and sharing your knowledge no matter the topic or time. And thank you for sharing all those early mornings and late evenings on the trails running, skiing and cycling that kept the spirit high throughout these years.

I would like to thank all my friends for the greatest support imaginable, for all the smiles and laughter in-between the working hours.

My gratitude goes out to my parents and family for all the support, encouragement and freedom to find my own path.

Above all, my greatest gratitude goes out to my loved ones. My daughter Anette for showing exceptional talent in many fields and determination in pursuing her dream to become a scientist – greetings to University of Groningen. My son Lennart for keeping the spark in my eyes with all the talks and walks together, for showing such a great knowledge and understanding of space and beyond at such a young age. And finally, to my lovely wife for inspiring me and leading the way in academic life and for all the deep and meaningful conversations, advice and good words over the years.

PUBLICATION I
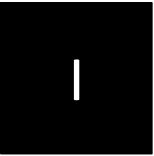
Development of Airtightness of Estonian Wooden Buildings

Jaanus Hallik*

Tallinn University of Technology, Department of Civil Engineering and Architecture, Nearly Zero Energy Buildings Research Group, Ehitajate tee 5, Tallinn 19086, Estonia

Sense OÜ, Estonia

Targo Kalamees

Tallinn University of Technology, Department of Civil Engineering and Architecture, Nearly Zero Energy Buildings Research Group, Ehitajate tee 5, Tallinn 19086, Estonia

*Corresponding author: **jaanus.hallik@taltech.ee**

The field measurements of airtightness in Estonian detached and apartment buildings conducted between 2003 – 2017 were combined into a large dataset for further analysis. The buildings were classified based on building structure, number of storeys, year of construction, energy classification and compactness factors. A subset with all wooden buildings (313 in total) was statistically analysed to determine the average (median) air leakage rates at 50 Pa and tested (Kruskal-Wallis test with post-hoc Conover test) for significant differences within the grouping factors. As expected, the median air leakage (q_{50}) of older buildings between 10.7 and 13.9 $m^3/(hm^2)$ has decreased to 1.1 $m^3/(hm^2)$ after the minimum requirements for energy efficiency have taken effect. A more detailed analysis on newer buildings showed that quality of the workmanship combining systematic measurement routines as well as prefabrication, yields significantly lower median air leakages compared to on-site construction. The buildings with better energy classification targets also achieved lower median air leakages compared to buildings designed to meet minimum requirements. Further analysis showed significant differences between buildings with lightweight timber construction and those with log construction. This can be due to fact that the airtightness has been predominantly measured in prefabricated buildings compared to on-site building technology. Surprisingly, the analysis showed no significant difference between buildings with a different compactness factor or a different number of storeys. For use in energy calculations, the base values of air leakage rates for each group are calculated and presented accounting for variation of measurements.

Keywords: airtightness, air leakage, pressurisation test.

Introduction

A well-insulated, airtight and thermal bridge free building envelope is a key factor for nearly zero energy buildings (nZEB) that becomes mandatory from year 2021. Minimising heat losses and combining a thermally optimised building envelope with the passive use of solar energy allows a significant reduction in the heat load and heating energy demand of residential buildings. However, increased insulation thickness in timber constructions creates a serious risk of moisture accumulation inside the construction and deterioration of the building structure if the air leakages are not minimised or avoided. This is especially important in the case of timber construction where the materials are more sensitive to extensive moisture and deterioration.

In Estonia, lightweight timber-frame envelopes are common for single-family detached houses. Today timber structures have become more and more common for apartment buildings and non-res-

ktu
1922

Journal of Sustainable
Architecture and Civil Engineering
Vol. 1 / No. 24 / 2019
pp. 36-43
DOI 10.5755/j01.sace.24.1.22167

idential buildings. Structures built from timber logs have been historically very common and are still used for some projects. It is expected that the air-tightness of the building envelope has been improved over the years, especially after the minimum requirements for energy efficiency have been set by legislation. However, several publications seem to conclude that the overall air leakage of the building envelope, even in modern buildings, depends mostly on the building quality and on subsequent factors that affect the building quality (Mortensen and Bergsøe 2017, Colijn *et.al* 2017, Kalamees 2007). For example, the number of storeys, compactness of the building volume etc has been shown to increase the complexity of the work needed to achieve the necessary air-tightness. There have been attempts to estimate the air-tightness of the building envelope without measuring, based on component measurements and subsequent calculations, but no reliable method for estimation has been found (Relander *et.al* 2012). This means that in the design phase, or when calculating the energy use of existent buildings with no means of direct measurements, the statistical average values for different building techniques, construction types and different time frames have to be used. The average air-tightness of existing building stock and the variation within subgroups can be different in different countries as the building process and quality assurance measures are different. In this study a large number of air tightness measurements of Estonian wooden buildings are statistically analysed to determine the average (median) air leakage rates at 50 Pa and tested for significant differences within the grouping factors related to building complexity and quality assurance. Additionally, the base values of air leakage are calculated including the effect of variation within the measured groups.

Studied buildings

The database of air leakages was combined based on the results of different measurements carried out between 2003 and 2017 (in total 522 buildings). The subset of all wooden buildings (in total 313 buildings) were used for further analysis. The buildings were classified based on building structure (log houses versus lightweight timber frame), the number of storeys (single-storey versus multi-storey), year of construction (built before 1945, built between 1946-1994, built between 1995-2008, built since 2009), energy classification (energy classes A and B versus minimum requirements) and compactness factors (envelope area ratio to volume and envelope area ratio to floor area). Additionally, those companies (producers or building companies) with 5 or more measurements were grouped to analyse the effect of systematic measurements on them.

For all buildings built since 2009 an additional grouping based on production technology was described to compare on-site building practice to prefabrication for lightweight timber construction, and hand-made building logs to prefabricated building logs for log-houses. The prefabrication level for lightweight timber construction differs between different companies. For volumetric modules the building envelope is typically finished internally and externally and air-tightness is controlled with vapour control membranes separately for each module. Prefabricated separate roof and wall elements are typically structurally complete but the internal finishing layers and external cladding are completed on-site allowing for additional taping to connect the vapour control membranes between the separate elements. For both production types the vapour control layer (polyethylene sheet) is used on the interior side of the load bearing structures (Fig. 1).

For log houses the prefabricated glulam timber logs are assembled on-site and typically no additional insulation nor separate air tightness layers are used. The energy performance requirements of those buildings are fulfilled through more efficient heating system and well insulated lightweight roof structure with similar vapour control membrane for air tightness. For glulam log structures with thickness less than 200mm an additional external insulation layer with timber frame in combination with wind-barrier layer, ventilated cavity and cladding is used for better energy performance.

Measurements

The air leakage measurements were carried out using a standardised pressurisation test according to method B (the test of the building envelope where all the intentional openings (for natu-

Methods

Fig. 1

A typical solution for prefabricated glulam timber log structures (left) and lightweight external wall timber structure with and without additional installation layer (right) for better air tightness and moisture safety used in Estonia. The air tightness layer is marked with black dashed line
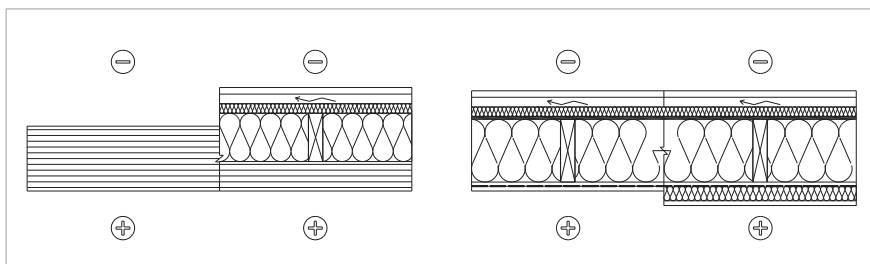
ral and mechanical ventilation) shall be sealed, the doors, windows and trapdoors being closed) described in EN ISO 9972:2015 and EN 13829:2001. The air tightness of the building envelope was tested in a range of pressure differences between 10 Pa and 60 Pa and reported with a standardised pressure of 50 Pa. At an air flow rate of 50 Pa the pressure difference (V_{50}), the air leakage rate (q_{50}), and air change rate (n_{50}) were calculated by dividing the measured air flow rate by the external envelope area or by the internal volume of the building respectively.

For all buildings, a depressurisation test was carried out to test the airtightness of the building envelope. For some buildings an additional pressurisation test was carried out to measure air leakage in reversed pressure conditions. For these buildings, the average leakage rate and other relevant test results were calculated as arithmetic means.

Statistical analysis

The preliminary analysis of the data showed that the distribution of the measured air leakage (q50) data is non-normal. Because of this, the median value and 0.16 / 0.84 quantiles were used to describe the distribution within the different subsets of the data and the non-parametric Kruskal-Wallis rank test was used to determine statistical differences between different groups of the measured data. In case of significant difference, a subsequent pairwise comparison of subsets was carried out using a post-hoc Conover test. For the analysis, the statistical analysis software R (version 3.5.1) was used with several add-on packages to allow non-parametric analysis and visualisation.

Along with median values, the mean value of air leakage rate ($q_{50,mean}$) and standard deviation (σ_{q50}) of all groups were calculated to allow the estimation of base value of air leakage rate ($q_{50,base}$) for different groups of buildings.

Calculation of the base value

The base value of air leakage rate was calculated according to the method described in the Finnish quality assurance manual for airtightness of building envelope [RT 80-10974, 2009]. The calculated base value depends on the group size and the variation within the group, so that 75 percent of the measured buildings will be below the base value with a confidence interval of 84 percent in the case of normal distribution of the means. The base value is calculated according to equation 1 as follows.

$$q_{50,base} = q_{50,mean} + 0.674 \cdot \sigma_{q50} + \sigma_{q50} : \sqrt{n} \qquad (1)$$

where: $q_{50,base}$ – estimated base value of air leakage rate (m³/(hm²)); $q_{50,mean}$ – measured value of mean air leakage rate of the group considered (m³/(hm²)); σ_{q50} – standard deviation of mean air leakage rate of the group considered (m³/(hm²)); n – number of measured buildings in the group considered.

Results

As expected, the median air leakage (q_{50}) of older buildings between 10.7 and 13.9 m³/(hm²) has decreased to 1.1 m³/(hm²) after the minimum requirements for energy efficiency have taken effect (Fig. 2). A more detailed analysis on buildings (137 in total) built since 2009 described the effect of different factors on air leakage (Table 1).
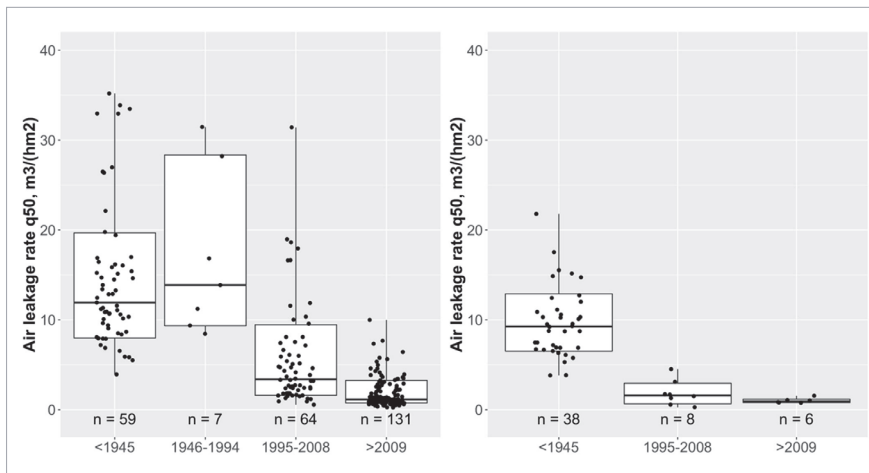
Fig. 2

Air leakage rates of detached (left) and apartment buildings (right) based on year of construction. The median values with 0.16 / 0.84 quantiles are marked

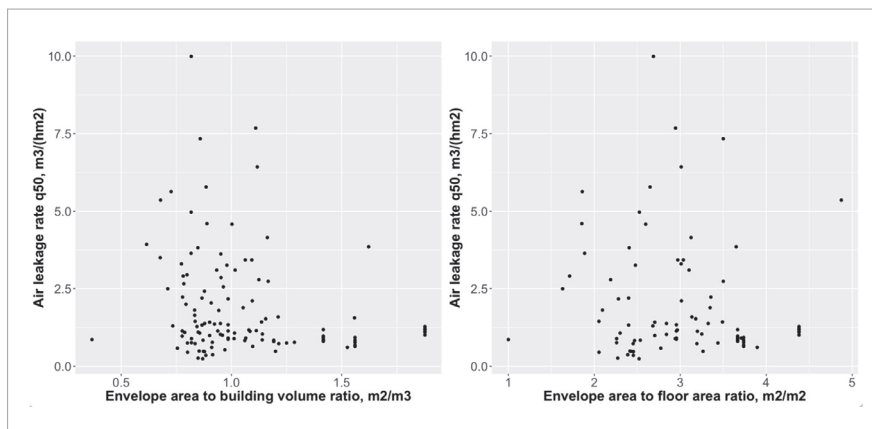|	Number of buildings median	Air leakage rate q_{50}, m³/(h·m²)					
		median	16% percentile	84% percentile	mean	σ_{q50}	$q_{50,base}$
All wooden buildings							
<1945	97	10.7	6.9	16.4	12.5	6.9	17.8
1946-1994	7	13.9	9.3	28.3	17.1	9.2	26.8
1995-2008	72	3.2	1.5	8.1	5.2	5.5	9.5
>2009	137	1.1	0.8	3.1	1.8	1.6	3.0
Wooden buildings 2009+							
1-storey	34	1.1	0.8	3.1	1.9	1.9	3.4
multi-storey	103	1.1	0.7	3.2	1.8	1.5	3.0
Energy class A	6	0.5	0.3	1.5	0.9	1.0	2.0
Energy class B	10	0.7	0.4	1.4	1.0	1.1	2.1
Energy class C (minimum)	121	1.2	0.8	3.3	1.9	1.7	3.2
Log-building	46	2.2	1.0	3.9	2.5	1.7	3.9
Lightweight timber	91	0.9	0.7	1.6	1.4	1.5	2.6
irregular measurements	35	2.8	0.9	5.5	3.1	2.4	5.1
systematic measurements (>5)	102	1.0	0.7	2.1	1.3	0.9	2.0

Table 1

Effect of different factors on air leakage rate and its distribution

The energy classification A or B contributed to slightly lower median air leakage (0.5 / 0.7 m³/(hm²)) than buildings designed to meet minimum requirements (1.2 m³/(hm²)). The lightweight timber construction (0.9 m³/(hm²)) had significantly lower air leakage compared to log houses (2.2 m3/(hm²)). This can be due to fact that the airtightness has been predominantly measured in prefabricated buildings compared to on-site building. The companies which are systematically conducting air leakage measurements (5 or more measurements in dataset) have significantly lower air leakage rates in those buildings (1.0 m³/(hm²)) compared to buildings in the irregular measurement group (2.8 m³/(hm²)). All those differences were statistically significant with p-value < 0.05.

As can be seen from the **Table 1**, the number of storeys did not have an effect on air leakage of the building envelope. Both groups have equal air leakage (1.1 m³/(hm²)). Surprisingly, the analysis showed no significant difference between buildings with different compactness factors or different number of storeys (**Fig. 3**) although a lower air leakage rate was expected for buildings with better compactness through favourable ratio of the external envelope area to internal volume and a generally smaller number of junctions related to a more simple form factor.

As the construction technique had a great effect on an average air leakage, both groups (log-buildings and lightweight buildings) were further analysed to see if prefabrication has a significant effect as expected. As can be seen from **Table 2**, the prefabricated log-buildings (1.6 m³/(hm²)) are 55% more airtight than hand-made log-buildings (3.6 m³/(hm²)). In the case of lightweight timber buildings, the prefabrication has even larger effect and prefabricated buildings (0.9 m³/(hm²)) have 74% lower air leakage rate compared to on-site building (3.4 m³/(hm²)).

	Number of buildings median	Air leakage rate q_{50}, m³/(h·m²)					
		median	16% percentile	84% percentile	mean	σ_{q50}	$q_{50,base}$
All log buildings 2009+							
Handmade logs	13	3.6	2.7	5.8	4.2	1.9	5.9
Prefabricated logs	33	1.6	0.9	3.1	1.9	1.1	2.8
All lightweight timber buildings 2009+							
Prefabricated elements	80	0.9	0.7	1.3	1.1	0.7	1.6
On-site building	11	3.4	1.4	6.0	4.0	2.7	6.7

The effect of systematic measurement practice within manufacturing or building companies were further analysed separately for log-buildings and lightweight timber construction. Similarly to the full dataset, the effect of systematic measurements in both groups of different construction technologies was significant, but the differences were smaller (**Table 3**). Within log-buildings the systematic measurements showed 37% lower air leakage rates. Within lightweight timber buildings the systematic measurements showed 47% lower air leakage rates. This means that systematic measurements give good feedback to manufacturers and building companies about the air leakages, with possibilities to improve the air-tightness system used and quality control system used.

	Air leakage rate q_{50}, m³/(h·m²)						
	n	median	16% percentile	84% percentile	mean	σ_{q50}	$q_{50,base}$
All log buildings 2009+							
irregular measurements	11	3.0	1.9	6.3	3.9	2.3	6.1
systematic measurements (>5)	35	1.9	0.9	3.5	2.1	1.2	3.1
All lightweight timber buildings 2009+							
irregular measurements	24	1.7	0.8	4.6	2.7	2.4	4.8
systematic measurements (>5)	67	0.9	0.7	1.3	1.0	0.4	1.2

Table 3

The effect of systematic measurements on air leakage rate and its distribution for sub-construction types

For visual comparison between different building technologies within companies that conduct systematic measurements on their buildings the average (median) air leakage rates along with 16% and 84% percentiles are given in **Fig. 4**. It can be seen from **Fig. 4** that log-buildings have a significantly higher variation within the same company compared to prefabricated lightweight elements.
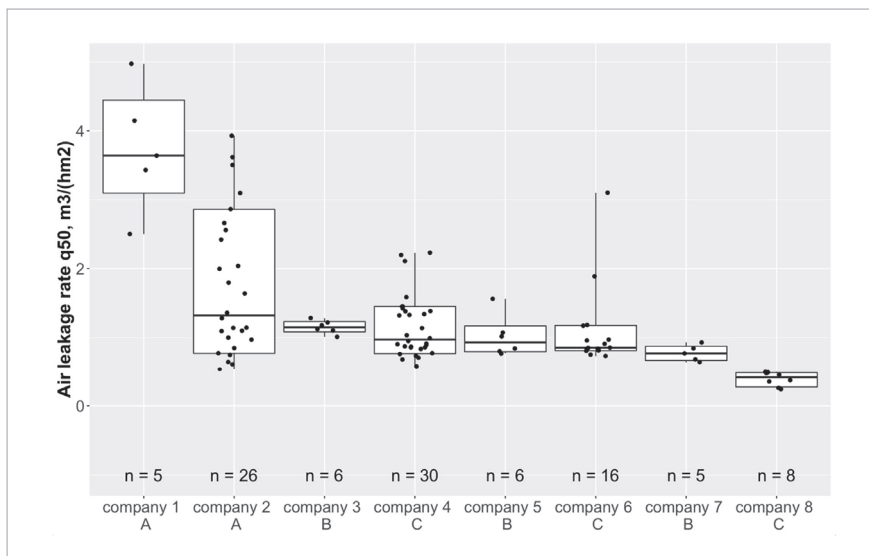
Fig. 4

Comparison of air leakage rates and its distribution between companies that conduct systematic measurements (A – log buildings, B – volumetric prefabricated modules, C – prefabricated wall/roof elements)

The prefabricated volumetric and regular modules have a lower variation and the median values of air leakages are around q_{50} = 1.0 m³/(hm²) or even lower. The higher variation in measurements is significantly affecting the base values of air leakage rates for these construction technologies. For handmade log buildings the base value $q_{50,base}$ = 5.9 m³/(hm²). For prefabricated log buildings the base value of air leakage is 53% lower resulting in $q_{50,base}$ = 2.8 m³/(hm²). Both construction technologies cannot compete with prefabricated modular technology, where base value of air leakage rate $q_{50,base}$ = 1.6 m³/(hm²). For a comparison, the base value of air leakage rate $q_{50,base}$ for all timber buildings built since 2009 is 3.0 m³/(hm²).

The results confirm that buildings built after the energy performance requirements have taken effect have significantly lower air leakage than older buildings with median q50 of 1.1 (m³/(hm²)) and range of 0.8 – 3.1 (m³/(hm²)) corresponding to 16% and 84% quantiles. This corresponds well with

Discussion

other countries where new buildings had similar air leakage rates. In Poland, typical new building construction was characterised by airtightness n_{50} in the range of 1.6 to 2.6 h^{-1} (Górzeński *et.al* 2016). Similar results have been achieved for timber-frame low-energy houses in Norway, where measured apartments had airtightness n_{50} in the range of 0.5 to 1.3 h^{-1} (Relander and Holøs 2018).

According to the previous study of Estonian building stock, the most significant factors affecting the air tightness were the quality of workmanship and supervision, as well the number of storeys of the house, both showing a more than a two-fold effect (Kalamees 2007). This study shows that, for newer buildings, the number of storeys no longer has any effect on air-tightness. This refers to the fact that a systematic approach to designing the air-tight envelope avoids large air leakages related to external wall and intermediate ceiling junctions in older buildings. Furthermore, non-existent correlation between airtightness and compactness of the building envelope refers to the assumption that if systematic quality assurance with a proper air tightness concept in all junctions is used, the geometric and structural complexity of the building envelope is no longer a key factor while achieving air tightness in Estonia. It has to be noted that similar studies in Finland have shown significant differences in building airtightness depending on the number of storeys, with timber-frame multi-storey buildings (4.8 m^3/(hm^2)) having higher air-leakage rates than single-storey buildings (3.4 m^3/(hm^2)), referring to the fact that these kinds of effects are related to local building technologies and overall quality assurance mechanisms (Vihna *et.al* 2015).

The quality of workmanship through systematic measurements as well as prefabrication showed significant improvement in the full dataset and in both subgroups (log-buildings and lightweight timber buildings) corresponding to a 37% to 74% improvement, depending on the factor and group. The differences in other grouping factors were significantly smaller. For buildings with better air tightness target including buildings with higher designed energy efficiency and quality management similar sealing measures are utilised including systematic use of specialised membranes and sealing tapes with a significant attention to connections between openings and external wall.

The results from this study give an overview of average air leakage rates along with the variation for different grouping factors related to building geometry and construction technology. Assuming consistency in construction technologies and in quality assurance mechanisms, these average values with appropriate safety margins can be used for energy calculation in Estonian conditions for new buildings, or buildings in respective age groups. The base values calculated and stated in **Tables 1**, **2** and **3** take into account the variation of the measured results and try to give estimates for each grouping factor with a 75% margin and 84% confidence interval. Due to the high variation in measured values, the base values are much higher than median or mean air leakage rates. The base values for buildings built since 2009 are in a range of 1.6 to 3.9 m^3/(hm^2) with a value of 3.0 m^3/(hm^2) for all buildings. The lowest base value of air leakage rate is for a group of prefabricated lightweight timber buildings with a value of $q_{50,base}$ = 1.6 m^3/(hm^2). The groups with an energy classification target of A or B energy class, or systematic measurement practice within a single company achieved a base value $q_{50,base}$ around 2.0 m^3/(hm^2), while on-site construction along with handmade log-buildings achieved a base value $q_{50,base}$ 6.7 m^3/(hm^2) and 5.9 m^3/(hm^2) respectively.

Conclusions

The air-tightness of Estonian wooden buildings has improved by a factor of 10 since the minimum requirements for energy efficiency have taken effect. Buildings with a higher energy efficiency target also have a slightly better air leakage rate. Prefabrication with light-weight timber construction technology seems to be superior to traditional log-wood building and notably, prefabrication improves air-tightness even within log-wood building or lightweight building groups, meaning that on-site building or the use of handmade logs corresponds to significantly higher air leakages. The compactness factor and number of storeys did not have a significant effect on air leakage referring to the fact that if systematic quality assurance with a proper air tightness concept is used, the geometric and structural complexity of the building envelope is no longer a key factor while achieving air tightness.

References

Colijn M., Entrop A.G., Toxopeus M.E. Evaluating the effectiveness of improved workmanship quality on the airtightness of Dutch detached houses. Energy Procedia, 2017; 132: 843-848. https://doi.org/10.1016/j.egypro.2017.09.670

Górzeński R., Szymański M., Górka A., Mróz T. Airtightness of Buildings in Poland. International Journal of Ventilation, 2014; 12: 391-400. https://doi.org/10.1080/14733315.2014.11684032

Relander T.O., Holøs S. Airtightness Measurements of Wood Frame Low Energy Row Houses. Building Enclosure Science & Technology (BEST2) conference proceedings, 2018.

Kalamees T. Air tightness and air leakages of new lightweight single-family detached houses in Estonia. Building and Environment, 2007; 42: 2369–2377. https://doi.org/10.1016/j.buildenv.2006.06.001

Mortensen L.H., Bergsøe N.C. Air tightness measurements in older Danish single-family houses.

Energy Procedia, 2017; 132: 825–830. https://doi.org/10.1016/j.egypro.2017.10.016

RT 80-10974 Teollisesti valmistettujen asuinrakennusten ilmanpitävyyden laadunvarmistusohje [Airtightness management manual for prefabricated residential buildings], Rakennustieto OY. 2009.

Relander T.O., Holøs S., Thue J.V. Airtightness estimation—A state of the art review and an en route upper limit evaluation principle to increase the chances that wood-frame houses with a vapour- and wind-barrier comply with the airtightness requirements. Energy and Buildings, 2012; 54: 444–452. https://doi.org/10.1016/j.enbuild.2012.07.012

Vinha J., Manelius E., Korpi M., Salminen K., Kurnitski J., Kiviste M., Laukkarinen A. Airtightness of residential buildings in Finland. Building and Environment, 2015; 93: 128-140. https://doi.org/10.1016/j.buildenv.2015.06.011

About the Authors

JAANUS HALLIK

PhD canditate

Tallinn University of Technology, Department of Civil Engineering and Architecture, Nearly Zero Energy Buildings Research Group

Main research area

Minimising of heat loss of nZEB building envelope

Address

Ehitajate tee 5,
Tallinn 19086, Estonia
Tel. +372 5021841
E-mail: jaanus.hallik@taltech.ee

TARGO KALAMEES

Professor

Tallinn University of Technology, Department of Civil Engineering and Architecture, Nearly Zero Energy Buildings Research Group

Main research area

Building envelope structures; renovation of buildings; hygrothermal behaviour of buildings structures (computer simulations, laboratory experiments, field studies); moisture safety of buildings; boundary conditions for hygrothermal simulations and experiments; building energy consumption and healthy building design; indoor climate and indoor air quality of residential-, office-, and historic buildings

Address

Ehitajate tee 5,
Tallinn 19086, Estonia
Tel. +3726202403
E-mail: targo.kalamees@taltech.ee

PUBLICATION II

II

Hallik, J.; Gustavson, H.; Kalamees, T. (2019). Air Leakage of Joints Filled with Polyurethane Foam. Buildings, 9 (7), 172. DOI: 10.3390/buildings9070172.

Air Leakage of Joints Filled with Polyurethane Foam

Jaanus Hallik [1],*, Heleen Gustavson [2] and Targo Kalamees [1]

[1]   Nearly Zero Energy Buildings Research Group, Department of Civil Engineering and Architecture,
      Tallinn University of Technology, Ehitajate tee 5, 19086 Tallinn, Estonia

[2]   School of Engineering, Department of Civil Engineering and Architecture, Tallinn University of Technology,
      Ehitajate tee 5, 19086 Tallinn, Estonia

*   Correspondence: jaanus.hallik@taltech.ee; Tel.: +372-5021-841

Abstract: Air leakage through the building envelope joints is usually one of the main reasons why airtightness targets are not achieved. The objective of this study was to analyse the air leakage of joints filled with polyurethane foam and its influencing factors. Wooden test specimens (54 in total) with planed, sawn and plastic-coated cavities and two cavity thicknesses were filled with three different polyurethane foams and tested according to standard EN 12114. The surface type and thickness of the joint had a significant effect on the air leakage of joints filled with polyurethane foam. In laboratory conditions, a consistent and very low air leakage rate was obtained with planed timber surfaces. Joints with plastic-coated and sawn timber surfaces performed worse, on average, by a factor of two or more and contributed to very variable airtightness, with up to 28% and 50% of the test specimens failing the airtightness testing. On the basis of the high 'failure rate', polyurethane foam may classify as a not completely trustworthy solution in guaranteeing the airtightness of construction joints. A comparison of estimated and previously measured overall airtightness of an entire building envelope showed dependency on 'failure rate' rather than on average measured leakage rate.

Keywords: airtightness; air leakage; polyurethane foam; timber joints

---

1. Introduction

An airtight and well-insulated building envelope is a key factor for achieving the requirements set for nearly zero energy buildings (nZEB) becoming mandatory in the European Union (EU) from the year 2021. Increased insulation thickness in timber constructions creates a serious risk of moisture accumulation inside the construction and deterioration of the building structure, if air leakages are not minimised or avoided. This is especially important in the case of timber constructions where the materials are more sensitive to extensive moisture and deterioration. There are several different technical solutions for sealing the cracks, joints and penetrations through the building envelope. Special sealing tapes for different surface materials, airtight membranes, rubber collars, adhesive sealing glues and different montage foams are used with varying degrees of success. Although it has been shown that the overall airtightness of new buildings has improved significantly [1–3], the actual leakage rate and its variation is strongly related to overall quality assurance mechanisms and local building techniques [1,4], especially for window-related air leakages [5].

Polyurethane (PU) one-component foams (OCF) are self-adhesive and self-hardening sealing materials that are often used for door and window installation and filling other joints and gaps in the building envelope. Despite their widespread use, it is not known if the necessary airtightness can be consistently achieved without the use of additional sealing tapes. The volume of PU OCF expands after application, filling all hollow spaces and hardens on contact with the air humidity. The expansion of the foam cannot be fully controlled, and therefore successful results can be highly dependent on the surface properties along with the foam properties and the environmental conditions. Different joints in

the building envelope can have different surface materials. Depending on the construction technology, a cap between different envelope elements can have a sawn wooden surface (wooden studs and beams at the end of walls, roof elements, etc.), a planed wooden surface (connection between wooden window frame, plywood and other similar wood-based products, planed wooden elements etc.) or a plastic surface (connection between wall and a window frame manufactured from polyvinyl chloride (PVC)). All three surface types were analysed in this study to quantify the differences due to surface treatment.

The objective of this study was to analyse the air leakage of joints filled with polyurethane foam and their influencing factors to see if consistent airtightness can be achieved under varying conditions. The first part of the study consisted in estimating experimentally the air leakage rates over test specimens prepared so to analyse the influence of different foams, joint widths and surface treatments. Inferential statistics was then used in the second part of the paper for the analysis and interpretation of the data. The following hypotheses were studied:

- A joint between sawn wooden surfaces is leakier than a joint between planed wooden surfaces because the sawn surface is rougher;
- A joint with a PVC surface has larger leakage than the other tested joints because the foam is not exposed to humidity, and water droplets on the plastic surface may cause leakage pathways;
- A wider joint has larger air leaks because the pressure exerted by the expanding foam is lessened;
- Different foams have different air leakage properties.

2. Methods

2.1. Studied Joints

In this study, 95 mm-deep joints with two different widths (10 mm and 30 mm) and three different surface treatments (sawn wooden laths (SW), planed wooden laths (PW), and plastic surface (PVC)) filled with three different polyurethane foam products (product L, product S, product K, all with high elastic recovery dimensional stability) from different producers were studied. Three identical test specimens were prepared for each combination to reduce measurement uncertainty, totalling 54 test specimens. Foam was applied to each joint twice, once on each side.

The studied joints may represent joints in different building envelope structures, where achieving airtightness is necessary, and montage foams are generally used for this purpose. Some examples are presented in Figure 1.
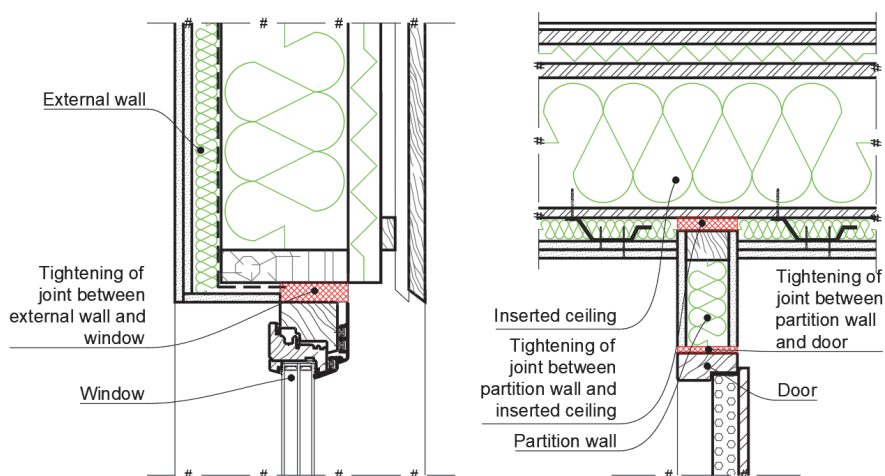

Figure 1. Some joints of the building envelope where polyurethane filling may be used.

The joints were filled in laboratory conditions by professional workers (provided by the PU-foam producers) according to the filling instructions (Figure 2a). Joint filling was carried out so that the foam filled the joint in its width (Figure 2b). Excessive foam was removed after the first round of measurements to allow repeated measurements of the test specimens with a cut foam surface.

(**a**)　　　　　　　　　　　　　　　　　　　　　　　(**b**)

Figure 2. Filling the joints in a wooden frame (**a**) and example of a cross section (from above) of a frame with filled joints (**b**).

2.2. Measurements

The measurements of air leakage from the building envelope joints were conducted under laboratory conditions, based on the EN 12114 standard [6]. The air leakage test equipment (Figures 3 and 4) consisted of the following:

- A hermetic chamber (Tallinn University of Technology, Tallinn, Estonia) (3 mm steel plate with ethylene propylene diene monomer (EPDM) rubber sealant) with the test area having a width of 334 mm, a height of 1000 mm and a depth of 100 mm;
- A fan (Elmo Rietschle G-BH1, positive pressure difference ≤100 kPa, negative pressure difference ≤90 kPa, air flow 2450 m^3/h, Gardner Denver, Inc, Milwaukee, USA) for creating an air flow;
- A frequency converter (EATON DC1-S24DNN-A20N, Eaton Industries GmbH, Bonn, Germany) to regulate the air flow;
- An air flow calibrator (Dwyer: GFC 1109 for 0–5 L/min, GFC 1131 for 0–30 L/min, GFC 1144 for 0–500 L/min, with an accuracy of ±1.5%, Dwyer Instruments International, Michigan, USA);
- A differential manometer (Produal PEL-DK for 0–1000 Pa and Dwyer Magnesense MS for 0–100 Pa, with an accuracy of ±1%) for pressure difference measurements;
- A temperature and relative humidity sensor (Rotronic HygroClip SC05, Rotronic AG, Bassersdorf, Switzerland);
- A data-logger (Grant Squirrel SQ2010, 8 channels, Grant Instruments, Cambridge, United Kingdom) for automatic and simultaneous data reading and saving.

Kalamees et al. (2010) [7] analysed the air pressure conditions in typical Finnish residences using data from field measurements and computer simulations and showed that for detached houses, the design value of the air pressure difference across the building envelope for moisture convection analysis should be at least ±10 Pa. To avoid the disruptive effect of normal air pressure variation, air leakage measurements have to be conducted at a higher air pressure difference. According to ISO 9972 [8], the air leakage measurement of the whole building envelope is performed between 10 Pa and typically up to 60 Pa and 100 Pa, while the reference pressure difference for the declared air leakage rate is usually equal to 50 Pa. European standard EN 12114 [6] about air permeability of building components and building elements aims for the maximum pressure difference up to 1000 Pa

during measurements, while the reference pressure difference for classifying the air permeability of windows and doors is 100 Pa, according to EN 12207 [9]. The climatic conditions (e.g., wind speed) corresponding to different pressure differences significantly depend on the wind direction, building height and shape, etc. The typical reference pressure difference of 50 Pa corresponds roughly to a wind speed in the range of 9 to 10 m/s.
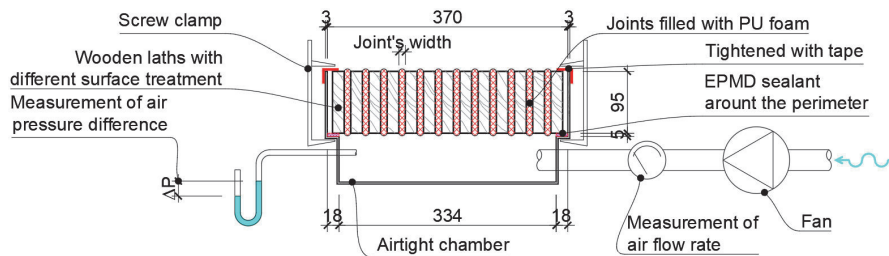

Figure 3. Schematic of the equipment for the air leakage tests (dimensions in mm).

Figure 4. Equipment for the air leakage tests.

In this study, air leakage measurements were conducted at different air pressure differences, depending on the individual test, up to ±600 Pa, together with three pressure pulses (Figure 5a) according to EN 12114 standard. The air flow rate and static air pressure differences were measured and recorded at each step automatically. The relation between the pressure difference and the airflow through the building envelope (Figure 5b) allowed to present the results using the power law (Equation (1)):

$$\dot{V} = C \cdot \Delta P^n, \text{ m}^3/\text{h} \tag{1}$$

where $\dot{V}$ (m^3/h) is the airflow, ΔP is the air pressure difference (Pa), and C (m^3/(h·Pa^n)) and n (-) are constants obtained from curve fitting, with n ranging from 0.5 to 1.

The air leakage of each test specimen was measured at positive and negative pressure differences (different flow direction) with separate curve fitting. After removing the excessive foam, all measurements were repeated at positive and negative pressure differences to account for both situations in real-life conditions. During this repetitive testing phase, each test specimen was measured four times totalling 216 separate measurement sequences.
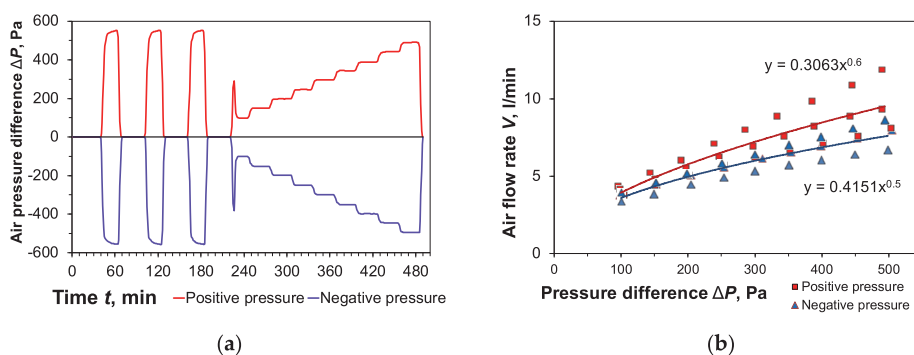
Figure 5. Air pressure difference over the studied joint (**a**) and its influence on the air flow rate (**b**).

2.3. Statistical Analysis

The measurement data were combined into a database and analysed to test the significance of different factors. To allow the comparison of test specimens with different lath and joint dimensions, the measured air flow rate was divided by the cumulative joint length of each test specimen to obtain the air leakage rates (V_{100} ... V_{500}, L/(min·m)). Preliminary analysis of the measured air leakages over a wide range of pressure differences showed that some test specimens with the same foam, joint width and surface treatment had significantly larger air leakage rates and therefore were marked as 'failing specimens' and omitted from more detailed statistical analysis. The failing criterion was defined as $V_{100} > 1.5$ L/(min·m). Nevertheless, all measurement results were still used to determine the ratio of failed specimens grouped by foam, lath surface treatment and joint width. The cumulative distribution of leakage rates at 100 Pa pressure difference for different joint surface types along with a graphical representation of the failing test specimens is shown in Figure 6. The general limiting value of air leakage for airtight joints (0.1 m^3/(m·h·(daPa)$^{2/3}$)) according to German standard DIN 4108-2 is also shown in the figure for the corresponding pressure difference [10].

Due to measurement sensitivity, the air leakage rate of some test specimens could not be measured for the full range of pressure differences. Some test specimens were too tight for stable measurements at lower pressure differences, while some test specimens with higher leakage did not sustain a stable pressure difference at 500 Pa and 600 Pa pressure difference. For this purpose, more detailed statistical analysis was done with air leakage rates at 400 Pa pressure difference. For the analysis, a power law between pressure difference and airflow through the envelope (Equation (1)) was linearized and statistically fitted to the measured leakage rates and pressure differences separately for each test specimen. The respective flow coefficients and exponents derived for each test specimen were used according to the estimated air leakage rates at exactly 400 Pa pressure difference (according to Equation (1)). The mean air leakage rate (V_{400}) per metre length of joint along with the standard deviation (σ_{V400}) was calculated and tested for significant differences (One-Way ANOVA with 95% confidence interval) between the different grouping factors (joint width, lath surface treatment, foam product). Additionally, air leakage rates at 50 Pa pressure difference were estimated from the same power curves to allow comparisons with previous studies.

For the analysis, the statistical analysis software R (version 3.5.1, The R Foundation for Statistical Computing, Vienna, Austria) was used with several add-on packages to allow statistical analysis and data visualisation [11,12].
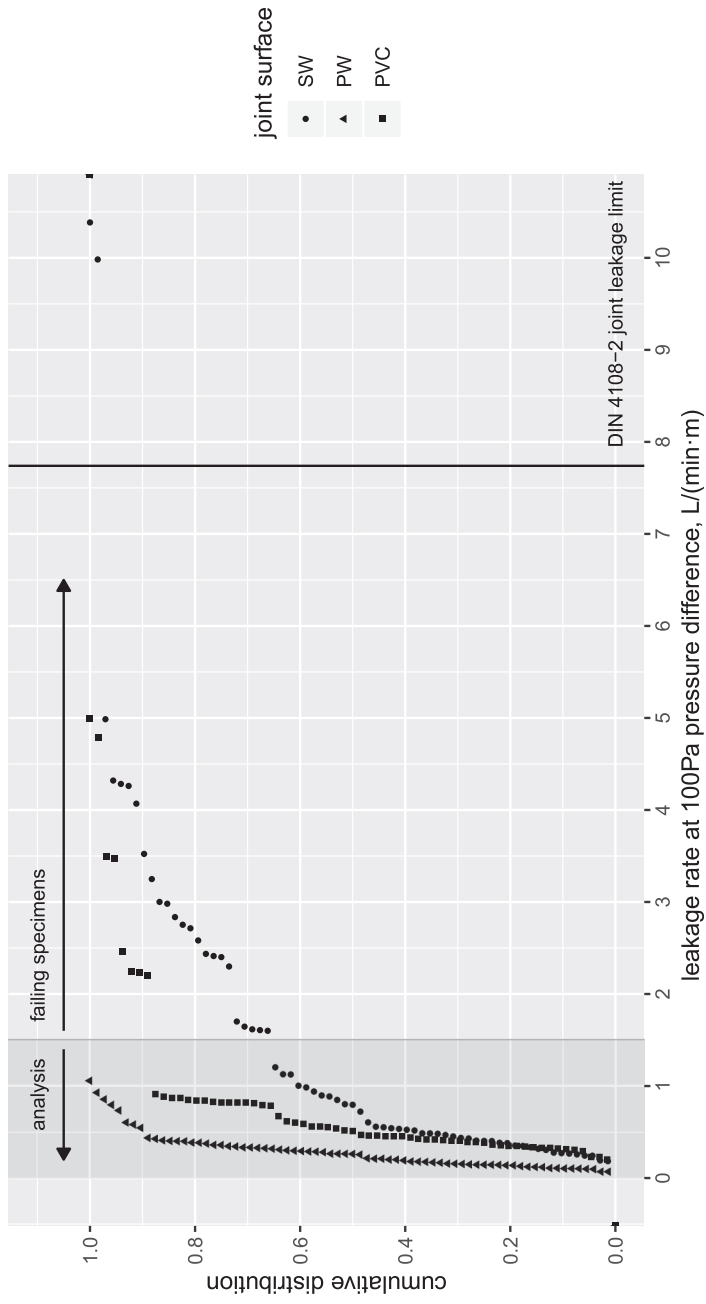
Figure 6. Cumulative distribution of leakage rates for different joint surface types at 100 Pa pressure difference and the limiting value for the failing specimens.

3. Results

The proportion of the test specimens with failed airtightness (significantly larger air leakage compared to test specimens with exactly the same configuration or excessive air leakage of all test specimens with visible cracks) depended greatly on lath surface treatment. Figure 7 shows that in the case of planed timber, the airtightness did not fail. In the case of the PVC surface, the proportion of failed test specimens was 16% and 28%, respectively, for 10 mm and 30 mm joint widths. Joints with a sawed wooden surface performed significantly worse, with a failure rate of 33% and 50% for 10 mm and 30 mm joint widths, respectively.
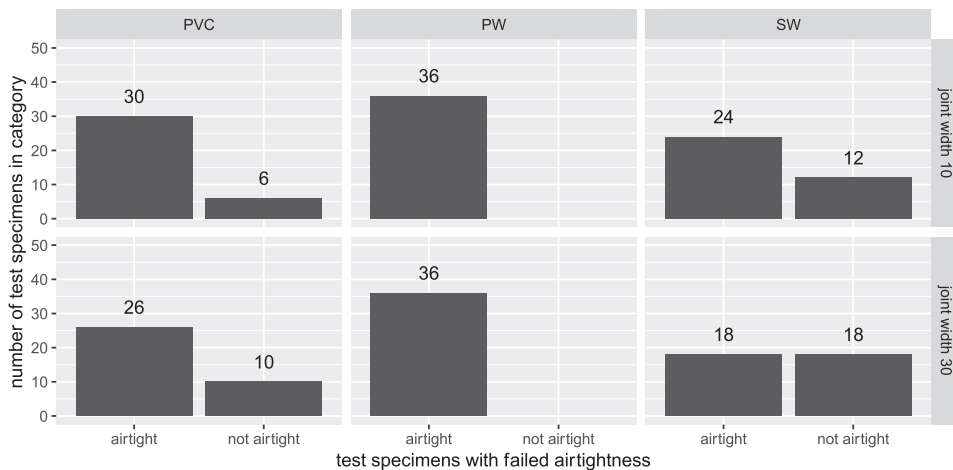
Figure 7. Number of test specimens with failed airtightness depending on lath surface treatment grouped by joint width (10 mm or 30 mm).

A larger joint width also contributed to a higher failure rate of airtightness. Grouping by specific foam product did not have a significant effect on the failure rate of the test specimens.

The mean air leakage rates at 400 Pa and 50 Pa pressure differences grouped by foam product, joint width and lath surface treatment are given in Table 1 along with the variations (standard deviation) among the test specimens and in under- and overpressure conditions. For statistical testing, air leakage rates at 400 Pa pressure difference were used.

Figure 8 shows that the mean air leakage rate for joints with a planed wood surface (V_{400} = 0.549 L/(min·m)) was significantly ($p < 0.0001$) lower by a factor of two or more than that of joints with sawn wood surfaces (V_{400} = 1.132 L/(min·m)) and plastic surfaces (V_{400} = 1.438 L/(min·m)). Also, the deviation was lower for joints with a planed wooden surface (σ_{V400} = 0.501 L/(min·m)) compared to those with sawn wooden surfaces (σ_{V400} = 0.635 L/(min·m)) and plastic surfaces (σ_{V400} = 0.524 L/(min·m)), meaning a better reliability in achieving the target result. It was expected that the smooth timber surface would enable better bonding between the timber surface and the PU foam, in contrast to the sawn timber surface, for which the foam would not fill all the small grooves etc.

For plastic-coated laths, the foam can expand similarly to planed laths, but the humidity transport from surface to foam is limited, and therefore the foam expansion is inhibited. This is usually compensated by moistening the plastic surface before applying the foam; however, exact guidelines regarding the quantities to be used are not provided by the foam producers. If the plastic surface is moistened before the foam is applied, water droplets on the plastic surface may cause random leakage pathways depending on the spraying technique and the amount of water used. The difference between PVC coating and sawed timber was small (but still significant, with $p < 0.01$) contributing to approximately a 27% increase of leakage, on average, in the case of plastic coating.
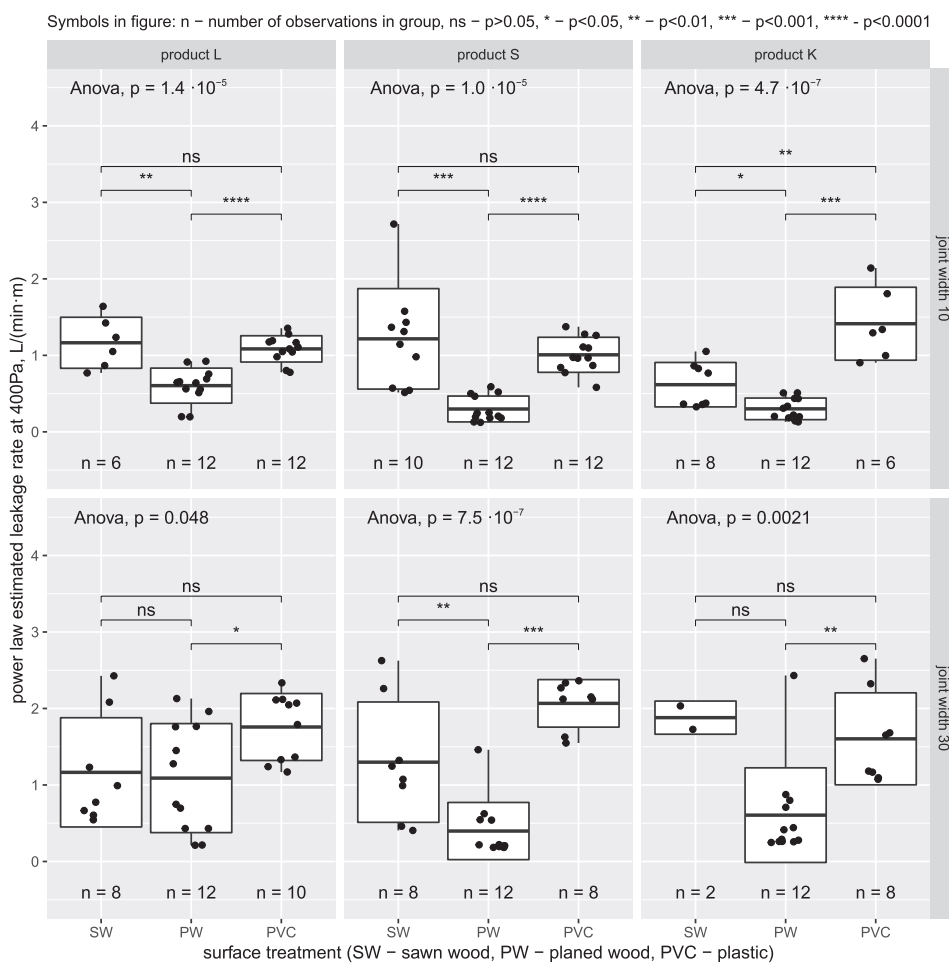
Table 1. Power curve-estimated air leakage rates and standard deviation at 400 Pa and 50 Pa pressure differences. PW: planed wood, PVC: plastic surface, SW: sawn wood.

Joint Type			V_{400}, L/(min·m)		V_{50}, L/(min·m)	
			Mean	σ_{V400}	**Mean**	σ_{V50}
PW	10	K	0.301	0.141	0.203	0.109
		L	0.604	0.229	0.203	0.076
		S	0.299	0.169	0.156	0.054
	30	K	0.606	0.618	0.214	0.092
		L	1.090	0.713	0.404	0.191
		S	0.398	0.374	0.172	0.068
PVC	10	K	1.413	0.477	0.293	0.118
		L	1.084	0.172	0.233	0.078
		S	1.007	0.229	0.251	0.070
	30	K	1.603	0.601	0.313	0.134
		L	1.758	0.438	0.441	0.123
		S	2.067	0.311	0.483	0.071
SW	10	K	0.616	0.290	0.252	0.097
		L	1.164	0.334	0.381	0.129
		S	1.216	0.657	0.329	0.147
	30	K	1.880	0.217	0.565	0.027
		L	1.165	0.714	0.392	0.207
		S	1.298	0.787	0.402	0.195

The comparison between different surface treatments within groups, for the same foam product and joint with is shown in Figure 9.
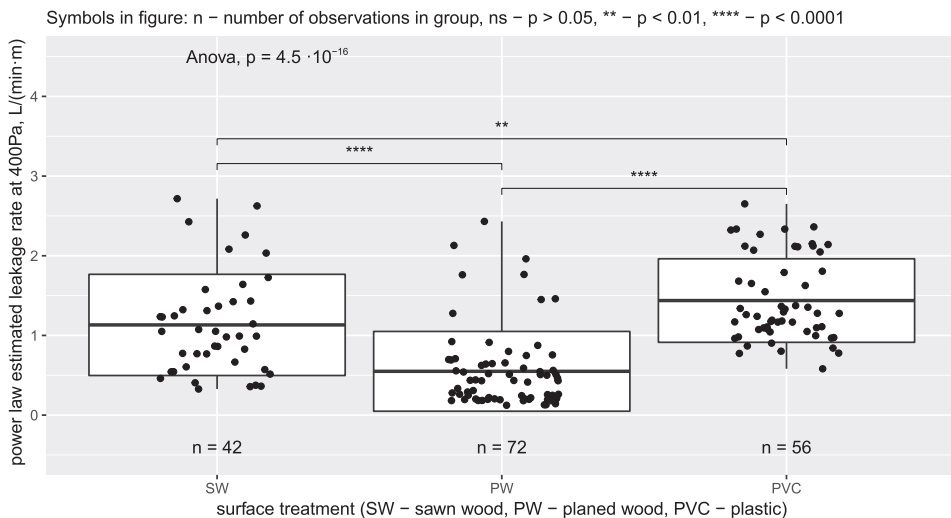
Figure 8. Mean air leakage rate (bold line) and standard deviation (white box) at 400 Pa depending on lath surface treatment (both joint widths are included).

Symbols in figure: n − number of observations in group, ns − p>0.05, * − p<0.05, ** − p<0.01, *** − p<0.001, **** - p<0.0001

Figure 9. Mean air leakage rate (bold line) and standard deviation (white box) at 400 Pa depending on lath surface treatment grouped by joint width (10 mm or 30 mm) and foam product (K, L and S).

The air leakage rate in the case of the planed timber remained significantly lower than those measured for the two other surface treatment groups, even when considering the effect of joint width (10 mm versus 30 mm) and specific foam products, except for the test specimens with 30 mm-wide joints treated with the foam product "L", for which all measurements had large variations, and the average air flow difference between all foam products were small. The difference between the sawn wooden surface and the plastic surface was not significant in most cases.

The mean air leakage rate and its variation increased with the increase in joint width (Figure 10). The mean air leakage through a 10 mm joint with all surfaces filled with all foams ($V_{400} = 0.801$ L/(min·m)) was significantly lower ($p < 0.0001$) than mean air leakage through a 30 mm joint ($V_{400} = 1.194$ L/(min·m)). The same phenomena were observed in the case of different lath surface treatments, although for sawn wooden surfaces, the difference was not statistically significant (Figure 11).

Although different analysed foam products performed slightly differently in the case of wider joints, an overall difference between these products was not statistically significant (Figure 12), mainly due to a large variation in the measured performance of the test specimens.
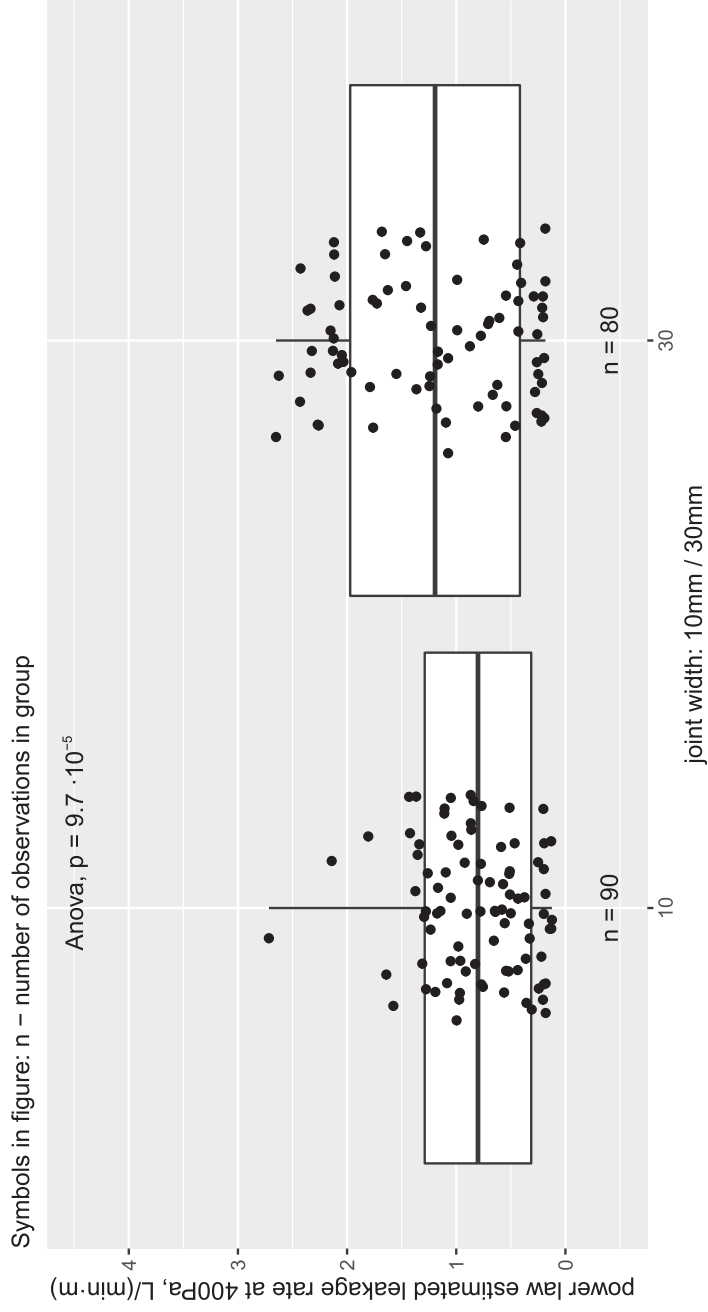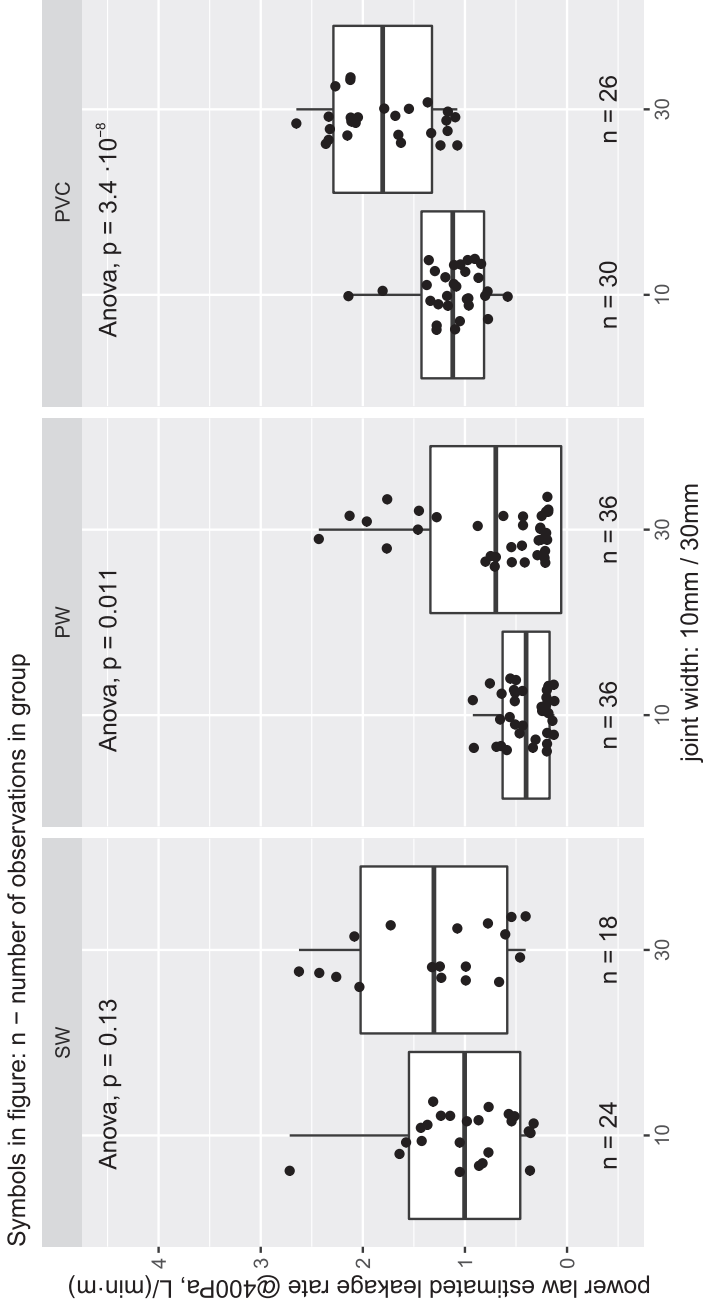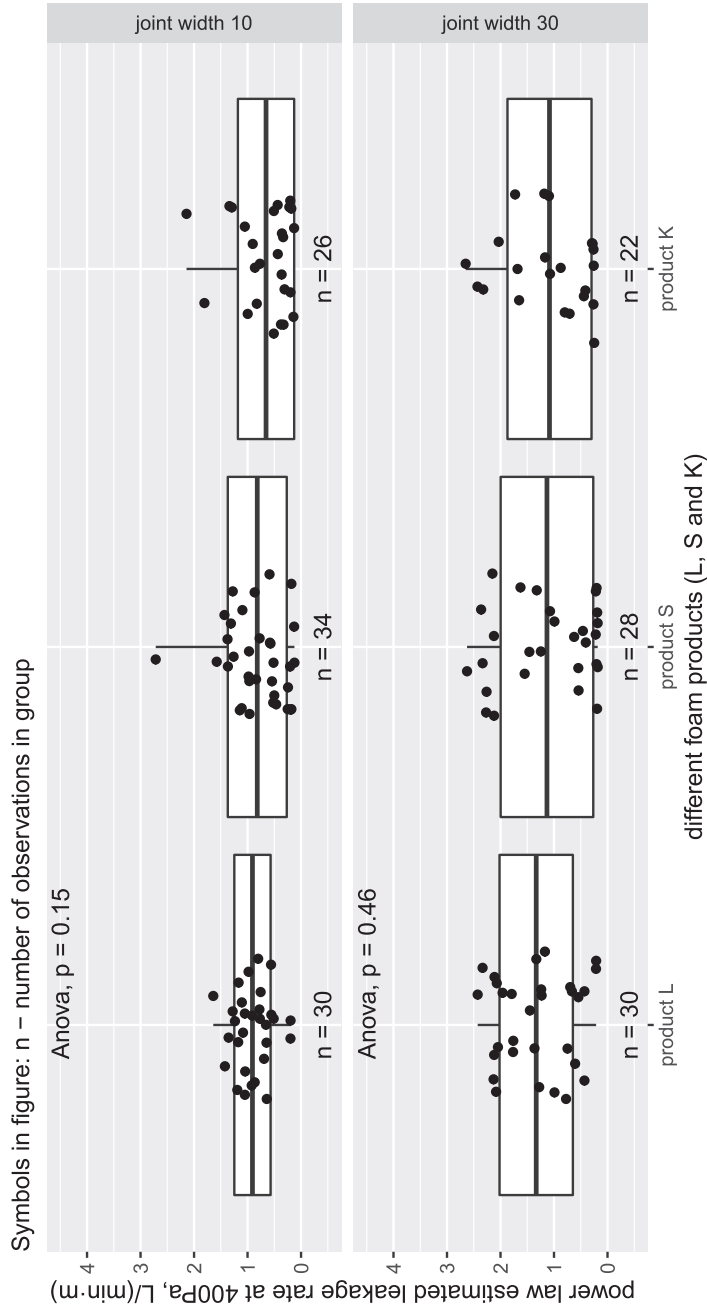
Figure 10. Mean air leakage rate (bold line) and standard deviation (white box) at 400 Pa depending on the joint width (10 mm (**left**) or 30 mm (**right**)).

Figure 11. Mean air leakage rate (bold line) and standard deviation (white box) at 400 Pa depending on the joint width (10 mm or 30 mm), grouped by lath surface treatment.

Figure 12. Mean air leakage rate (bold line) and standard deviation (white box) at 400 Pa depending on foam product, grouped by joint width (10 mm (**a**) or 30 mm (**b**)).

4. Discussion

Although the airtightness properties of foam joints have been previously tested and these foams have been proved to be almost airtight [13] and perform satisfactorily at the window–wall interface in cavity brick walls [14], the current study showed that the airtightness of actual joints could vary a lot and depends strongly on many parameters. A previous study in Belgium [14] assessed the airtightness joints filled with PU foam, among other insulating and sealing materials (tapes, mineral wool). Several joints with PU foam filling half of the cavity, full cavity and full cavity with plaster coating were measured for airtightness. Air leakage rates in the range of 1.06 to 1.77 m^3/(h·m) were measured at 50 Pa pressure difference for the test specimens treated with pure PU foam, which corresponds to 17.6 to 29.5 L/(min·m). Additional coating with plaster or additional sealing with caulking lowered the air leakages below 0.10 m^3/(h·m), which corresponds to 1.67 L/(min·m). In this study, the air leakages at 50 Pa pressure difference remained in the range of 0.156 to 0.565 L/(min·m) depending on the surface treatment and joint width. Other studies of window-to-wall interfaces sealed with PU foam have also shown somewhat higher air leakages in the range of 0.0 to 0.155 (mean 0.03) m^3/(h·m) [15] and 0.10 m^3/(h·m) [16].

Expanding montage foams need additional moisture from air and through adjacent surfaces to fully expand and fill the grooves and concavities. It was expected that the smooth planed surface of timber joints would provide good conditions for foam bonding, and the measured results confirmed this. The air leakages in the case of planed timber surfaces were significantly lower, averaging $V_{400} = 0.549$ L/(min·m) at 400 Pa pressure difference. During repetitive testing with three identical test specimens for each configuration, no airtightness failures were observed. The joints with sawn timber laths performed worse by more than a factor of two, averaging $V_{400} = 1.132$ L/(min·m) at 400 Pa pressure difference, and the fail rate under repetitive testing was huge, totalling 33% and 50% for 10 mm and 30 mm joint widths, respectively. This shows that the studied foams were often unable to bond with the uneven surface and, although some test specimens had air leakages comparable to those of planed timber surfaces, the foam–timber interface is systematically not airtight.

The failure rate of plastic-coated laths was significantly lower compared to that of sawn timber but, nonetheless, showed some bonding problems in the case of the wider joint, which had a failure rate of more than 28%. The surface of PVC-coated laths is smooth, but the inhibited transport of moisture through the plastic surface and the water droplets caused by surface moistening can, in some cases, create pathways for air leakages. Although this does not always cause major air leakages, it contributes to even higher average air leakage rates compared to sawn timber ($V_{400} = 1.438$ L/(min·m) at 400 Pa pressure difference).

The leakage rate through the window–wall interface can be compared to the leakage rate of the window itself to assess the additional effect of leakages on the overall airtightness. A large number of window products were tested in Belgium to assess the distribution and average airtightness of different window types [17]. Although the variation within the test specimens was high, the median airtightness of single and double windows (independently of the material) was 0.82 m^3/(h·m^2) and 1.36 m^3/(h·m^2), respectively, for 50 Pa pressure difference. For a hypothetical window with a size of 1.0 m × 1.0 m (joint length of 4.0 m), this corresponds to air leakage of 0.82 and 1.36 m^3/(h·m^2), respectively, for single and double windows at 50 Pa pressure difference. The average air leakage rate of joints in the range of 0.156 to 0.565 L/(min·m) according to this study would add 0.04 m^3/(h·m^2) to 0.14 m^3/(h·m^2), corresponding to a 5% to 17% increase in the case of a single window, and a 5% to 10% increase in the case of a double window. For larger windows with a favourable aspect ratio, the additional effect of window–wall interface will be lower.

Similarly, the potential effect of the measured joint air leakage can be calculated for an entire building envelope. For this, a cumulative joint length for all connections between the building envelope elements was calculated for a prefabricated two-storey wooden reference building with very good airtightness and optimised window connections [18]. The airtightness was achieved with the systematic use of special tapes and on-site quality assurance measures. The building was included

in a larger study about airtightness of Estonian wooden buildings [1] and had an average measured air leakage rate $q_{50} = 0.24$ m^3/(h·m^2) at 50 Pa pressure difference corresponding to the measured air flow rate $V_{50} = 91$ m^3/h. With cumulative joint length of 206 m and external envelope area of 373.5 m^2, the average air leakage rate of the joints in the range of 0.156 to 0.565 L/(min·m) at 50 Pa pressure difference according to this study would contribute to additional 1.93 m^3/h to 6.98 m^3/h, respectively, corresponding to less than 0.02 m^3/(h·m^2) increase in air leakage of the entire building envelope. A previous study has shown that the actual average air leakage rate of the building envelope in newer wooden buildings is around 1.1 m^3/(h·m^2), with very high variation (standard deviation 1.6 m^3/(h·m^2)) [1]. This strongly suggests that the actual air leakage of the building envelope is mainly dependent on the 'failure rate' of the sealing measures rather than on the leakage properties of the sealing measure and its influencing factors. Previous studies have found that workmanship quality plays a critical role in achieving airtightness. Kalamees et al. [19] showed that a comparison between air leakage readings measured in field conditions and those calculated based on laboratory measurements showed significant differences.

The joint width and, accordingly, the volume of the joint are important factors when considering the use of expanding polyurethane foam to achieve airtightness of these connections. Although more foam is used for wider joints, the pressure during foam expansion is expected to be higher in the case of a smaller volume. This can be systematically seen from our measurements, where the 10 mm-wide joints performed significantly better for all surface types. The variation of the measured air leakages along with the failure rate during repetitive testing was always higher with a 30 mm joint width compared to a 10 mm joint. The effect of long-term expansion and periodic movement of the building elements has to be further studied, as a larger joint width with the same elasticity can withstand larger movements. It is shown that PU foams are prone to fast chemical degradation [20], which changes the mechanical properties of the foam. In this study, the measurements were carried out within a few months after the foam was applied, and the effect of ageing and chemical degradation was not considered.

Different foam products were compared in this study, and although our detailed analysis within subgroups of different lath surfaces and joint widths indicated some differences between specific foam products in some cases, statistically significant differences were not found. It has to be noted that top-of-the-line high-quality polyurethane foams from each producer applied by skilled workers in a laboratory setup were measured in this study. The skill level of the workers and real-life application conditions can significantly influence the performance of different foams and cause higher air leakages compared to those measured in the laboratory, although this has to be further studied.

5. Conclusions

Based on the measurement results, the surface properties have the most significant effect on the air leakage of joints filled with polyurethane montage foam. In everyday construction practice, it should be considered that the airtightness of foam-filled joints with a sawn timber surface finish can be very variable, with a failure rate up to 50%. On the other hand, the airtightness of foam-filled joints with a planed wood surface is better, characterized by much lower average air leakage rates and a 0% failure rate. Increasing the joint width increases the air leakage and its variation within all analysed factors. Contrary to the assumption, significant differences between different premium-class foam products could not be shown. A comparison of the estimated and previously measured overall airtightness of an entire building envelope showed a dependency on 'failure rate' rather than on average measured leakage rate. It should be taken into consideration that the results obtained in laboratory conditions may be better than the ones obtained on site; also, the effect of aging has to be further studied.

Conflicts of Interest: The authors declare no conflict of interest.

References

1. Hallik, J.; Kalamees, T. Development of airtightness of Estonian wooden buildings. *J. Sustain. Archit. Civ. Eng.* **2019**, *24*, 36–43. [CrossRef]

2. Górzeński, R.; Szymański, M.; Górka, A.; Mróz, T. Airtightness of buildings in Poland. *Int. J. Vent.* **2014**, *12*, 391–400. [CrossRef]

3. Relander, T.O.; Holøs, S.; Thue, J.V. Airtightness estimation—A state of the art review and an en route upper limit evaluation principle to increase the chances that wood-frame houses with a vapour- and wind-barrier comply with the airtightness requirements. *Energy Build.* **2012**, *54*, 444–452. [CrossRef]

4. Vinha, J.; Manelius, E.; Korpi, M.; Salminen, K.; Kurnitski, J.; Kiviste, M.; Laukkarinen, A. Airtightness of residential buildings in Finland. *Build. Environ.* **2015**, *93*, 128–140. [CrossRef]

5. Cuce, E. Role of airtightness in energy loss from windows: Experimental results from In-Situ tests. *Energy Build.* **2017**, *139*, 449–455. [CrossRef]

6. CEN. *EN 12114. Thermal Performance of Buildings—Air Permeability of Building Components and Building Elements—Laboratory Test Method*; CEN: Brussels, Belgium, 2000.

7. Kalamees, T.; Kurnitski, J.; Jokisalo, J.; Eskola, L.; Jokiranta, K.; Vinha, J. Measured and simulated air pressure conditions in Finnish residential buildings. *Build. Serv. Eng. Res. Technol.* **2010**, *31*, 177–190. [CrossRef]

8. CEN. *ISO 9972:2015 Thermal Performance of Buildings—Determination of Air Permeability of Buildings—Fan Pressurization Method*; CEN: Geneva, Switzerland, 2015.

9. CEN. *EN 12207 Windows and Doors—Air Permeability—Classification*; CEN: Brussels, Belgium, 2016.

10. Beuth-Verlag. *DIN 4108-2:2013-02 Wärmeschutz und Energie-Einsparung in Gebäuden—Teil 2: Mindestanforderungen an den Wärmeschutz*; Beuth-Verlag: Berlin, Germany, 2013.

11. R Core Team. R: A Language and Environment for Statistical Computing. Available online: https://www.r-project.org/ (accessed on 11 July 2019).

12. Kassambara, A. Ggpubr: "Ggplot2" Based Publication Ready Plots. Available online: https://cran.r-project.org/package=ggpubr (accessed on 11 July 2019).

13. Ift Rosenheim. *Air Permeability of Montage Foam. Test Report 10533428*; Ift Rosenheim: Rosenheim, Germany, 2007.

14. Van Den Bossche, N.; Huyghe, W.; Moens, J.; Janssens, A.; Depaepe, M. Airtightness of the window-wall interface in cavity brick walls. *Energy Build.* **2012**, *45*, 32–42. [CrossRef]

15. Proskiw, G. *Air Leakage Characteristics of Various Rough-Opening Sealing Methods for Windows and Doors*; ASTM International: West Conshohocken, PA, USA, 1995.

16. Höglund, I.; Bengt, J. *Joint Sealing between Window (Door) Frames and Walls—Development of New Types of Synthetic Rubber Stuffing Strips*; Swedish Council for Building Research: Stockholm, Sweden, 1984.

17. Van Den Bossche, N.; Janssens, A. Airtightness and watertightness of window frames: Comparison of performance and requirements. *Build. Environ.* **2016**, *110*, 129–139. [CrossRef]

18. Kalbe, K.; Kalamees, T. Influence of Window Details on the Energy Performance of an nZEB. *J. Sustain. Archit. Civ. Eng.* **2019**, *1*, 61–70. [CrossRef]

19. Kalamees, T.; Alev, Ü.; Pärnalaas, M. Air leakage levels in timber frame building envelope joints. *Build. Environ.* **2017**, *116*, 121–129. [CrossRef]

20. Pellizzi, E.; Lattuati-Derieux, A.; Lavédrine, B.; Cheradame, H. Degradation of polyurethane ester foam artifacts: Chemical properties, mechanical properties and comparison between accelerated and natural degradation. *Polym. Degrad. Stab.* **2014**, *107*, 255–261. [CrossRef]

PUBLICATION III

III

Hallik, J.; Kalamees, T. (2020). A new method to estimate point thermal transmittance based on combined two-dimensional heat flow calculation. 12th Nordic Symposium on Building Physics, NSB 2020, Tallinn; Estonia; 6 September + 9 September 2020. Ed. Kurnitski, J., Kalamees, T. EDP Sciences, #08005. (E3S Web of Conferences; 172). DOI: 10.1051/e3sconf/202017208005.

A new method to estimate point thermal transmittance based on combined two-dimensional heat flow calculation

Jaanus Hallik[1,*] and *Targo* Kalamees[2,1]

[1] nZEB Research Group, Tallinn University of Technology, Estonia
[2] Smart City Center of Excellence (Finest Twins), Tallinn University of Technology, Estonia

Abstract. A well-insulated, airtight and thermal bridge free building envelope is a key factor for nearly zero energy buildings (nZEB). However, increased insulation thickness and minimized air leakages increase the effect of thermal bridges on overall energy efficiency of the nZEBs. Although several more prominent linear thermal bridges are accounted for in the practice the three-dimensional heat flow through vast array of fixation elements, mounting brackets and other point thermal bridges are usually neglected due to time-consuming model preparation routine, lack of input data as well as high number of different thermal bridges that have to be assessed for a single project. In this study a new method was proposed for predicting three-dimensional heat flow and the point thermal transmittance of thermal bridges caused by full or partial penetration of the building envelope with metal elements with uniform geometry in third dimension based on multiple two-dimensional numerical heat flow calculations. A new parameter (equivalent length of thermal bridge) was defined which incorporates the effect of additional thermal transmittance in third dimension when multiplied by the difference of two thermal coupling coefficients derived for two-dimensional cross section. Multiple linear regression model was fitted on database with 102 cases and verified with separate case of window to wall connection incorporating metal penetration at fixation points. The proposed methodology can be useful in general practice where the design team lacks the skills or software tools for conducting detailed numerical analysis in three dimensions.

1 Introduction

A well-insulated, airtight and thermal bridge free building envelope is a key factor for nearly zero energy buildings that becomes mandatory from year 2021. Minimising heat losses and combining a thermally optimised building envelope with the passive use of solar energy allows a significant reduction in the heat load and heating energy demand of residential buildings. However, increased insulation thickness and minimized air leakages increase the effect of thermal bridges on overall heat loss nZEB building envelope. The contribution of thermal bridges to overall heat loss is highly dependent on architectural and structural solution but can easily be as high as 30 – 40% of total heat loss of the building envelope [1–5] and influence of moisture safety [6]. Although several more prominent linear thermal bridges are accounted for in the practice the three-dimensional heat flow through vast array of fixation elements and other point thermal bridges are usually neglected. Based on experience with less insulated structures it is usually expected that various point thermal bridges have small contribution to overall heat loss, but several recent studies have shown that within highly insulated building envelope the highly conductive metal fixing elements and cladding systems have considerable effect on effectiveness of thermal insulation layers [7]. Although the detailed numerical calculation methodology for steady state three-dimensional heat flow is described in European standard ISO 10211:2017 [8] along with other connected standards it is not implemented in general practice due to time-consuming model preparation routine, lack of input data as well as high number of different thermal bridges that have to be assessed for a single project. Additionally, the selection of software tools for three-dimensional numerical heat flow modelling is limited due to high price and steep learning curve (ANSYS [9], COMSOL Multiphysics [10], PHYSIBEL Trisco and Solido [11]) compared to numerical heat flow calculation tools in two dimensions where several open source or free to use tools (LBNL Therm [12] etc) are generally available.

Omitting numerical calculation of point thermal transmittances for different point thermal bridges introduces great uncertainty in estimating the overall heat loss of highly insulated building envelope and different parametric or simplified calculation procedures are needed for general practice to describe the overall thermal transfer value of entire building envelope close to reality. There have been several efforts to generalize the thermal bridge effects of different fixation elements inside the insulating layer with sensitivity analysis to show the effect of different technical parameters contributing to heat flow

---

*Corresponding author: jaanus.hallik@taltech.ee

through these thermal bridges such as thermal conductivity of bridging element and surrounding insulation layer, thermal resistances of adjoining layers etc [7,13,14]. Additionally several methods have been proposed how to estimate two-dimensional thermal bridge effects from one-dimensional building envelope data, such as thermal transmittances etc [4,15].

A very rough estimation of point thermal transmittance can be made by multiplying the length of thermal bridging element with the heat flow difference per unitary temperature difference derived from two distinct two-dimensional calculations. One cross section with thermal bridge element and other without it. This always underestimates the actual three-dimensional heat flow because the heat flow from third dimension to the bridging element is neglected.

Current study proposes a new methodology for estimating the three-dimensional heat flow caused by point thermal bridge based on multiple two-dimensional numerical heat flow calculations by using a multiple regression model to estimate the equivalent length of point thermal bridge based on several parameters related to heat flow through the building envelope.

The hypothesis of the study is that the difference between actual length of thermal bridge and the equivalent length of thermal bridge is strongly correlated to difference in thermal coupling coefficients derived from respective cross sections (i.e. central plane of thermal bridge and reference plane without it) and that difference partially involves the effect of varying geometry and conductivities to the heat flow in the third dimension.

The proposed methodology can be useful in general practice where the design team lacks the skills or software tools for conducting detailed numerical analysis in three dimensions.

2 Materials and methods

2.1 Finite element analysis

Thermal bridges are defined as part of the building envelope where the otherwise uniform thermal resistance is significantly changed by full or partial penetration of the building envelope by materials with higher thermal conductivity [8]. The point thermal transmittance (χ), which represents the additional heat flow per 1 K air temperature difference between the internal and the external environment, of this kind of penetrations is calculated as in equation 1.

$$\chi = L_{3D} - \sum_{i=1}^{N_i} U_i \cdot A_i - \sum_{k=1}^{N_k} \psi_k \cdot l_k \qquad (1)$$

where L_{3D} is the thermal coupling coefficient obtained from a three-dimensional numerical calculation, U_i is the thermal transmittance of the building envelope adjoining the thermal bridge, A_i is the respective area of the adjoining part of the building envelope in the calculation model, ψ_k is the linear thermal transmittance of additional

thermal bridge if present and l_k is the respective length of additional linear thermal bridge.

The linear thermal transmittance of additional thermal bridge is calculated as described in equation 2.

$$\psi = L_{2D} - \sum_{j=1}^{N_j} U_j \cdot l_j \qquad (2)$$

where L_{2D} is the thermal coupling coefficient obtained from a separate two-dimensional numerical calculation, U_j is the thermal transmittance of the building envelope adjoining the thermal bridge and l_j is the respective length of adjoining part of the building envelope described in the calculation model.

The point thermal transmittance of assessed thermal bridge can also be derived as in equation 3 when three-dimensional reference calculation without assessed penetrating element already contains the effect of additional linear thermal bridge.

$$\chi = L_{3D} - L_{3Dref} \qquad (3)$$

where L_{3Dref} is the thermal coupling coefficient obtained from a separate three-dimensional numerical calculation model with identical boundary conditions, cut-off planes etc, but without considering the presence of assessed point thermal bridge. The thermal coupling coefficients L_{2D} and L_{2Dref} as well as L_{3D} and L_{3Dref} obtained from two- and three-dimensional numerical models are calculated as respective heat flows divided by the temperature difference used in the model.

The heat flow and thermal bridge calculations in this study was carried out according to methodology, boundary conditions and modelling rules described in ISO 10211:2017 using software package Physibel Trisco [11], which utilizes finite difference method to numerically calculate three-dimensional heat flows in complex geometrical models.

For each assessed point thermal bridge case four heat flows were numerically calculated:

- three-dimensional heat flow for actual point thermal bridge;

- three-dimensional reference heat flow for same model omitting the thermal point penetration;

- two-dimensional heat flow for horizontal cross section taken from the central plane of point thermal bridge element and

- two-dimensional reference heat flow for horizontal cross section omitting the thermal point penetration.

To avoid the uncertainty generated by the use of different numerical software tools for two- and three-dimensional calculation the two-dimensional heat flow was obtained from three-dimensional calculation model, where third dimension was set to unitary length (1 m) and modelled with uniform geometry in that dimension.

2.2 Description of assessed thermal bridging elements

In current study an external wall construction with external insulation layer, wind barrier and ventilated cladding with penetrating metal bracket fixed to vertical timber elements was assessed. Schematic horizontal cross sections for thermal bridge cases and reference cases are shown in figure 1.
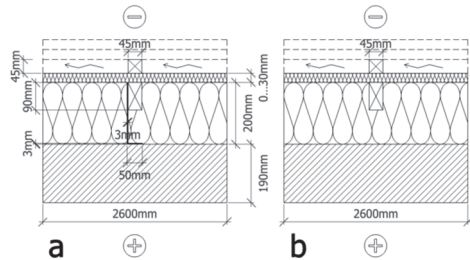
Fig. 1. Schematic cross section (horizontal) of assessed external wall for calculating the thermal coupling coefficient L_{2D} with thermal bridge (a) and thermal coupling coefficient L_{2Dref} for reference cases (b) without point thermal bridge.

Previous studies have shown that along with thermal conductivity of penetrating element itself the thermal conductivity of insulation material and its layer thickness used in building envelope as well as the resistances of the layers covering the penetrating element on internal and external sides have significant effect on point thermal transmittance [7,13]. In current study thermal conductivity (λ, W/(mK)) of internal load bearing structure, insulation layer and wind barrier layer along with metal thermal bridging element was varied as described in Table 1. Assessed different insulation materials correspond to two different typical mineral wool types along with polyurethane foam insulation that are used in this kind of construction for nearly zero energy buildings.

Table 1. Variable parameters used in heat flow analysis.

|	Description	λ, W/(mK)
Load bearing structure	0.19 m reinforced concrete	2.50
	0.19 m aerated concrete	0.15
Insulation layer	typical mineral wool	0.040
	good mineral wool	0.031
	polyurethane foam	0.023
Wind barrier	0.009 m gypsum board	0.250
	0.030 m gypsum board	0.250
	0.030 m mineral wool board	0.031
	0.030 m fibreboard	0.055
	only wind barrier membrane	(-)
Metal bracket	Regular steel	55.0
	Reinforced steel	17.0
	Aluminium	160.0

In addition to variable thermal conductivity and layer thickness the length of metal bracket in third dimension was varied to include brackets with following length: 0.06 m, 0.12 m and 0.18 m. The thickness of metal

brackets in all calculated cases was set to 0.003 m. Altogether 102 different combinations were calculated.

The cut-off planes for two- and three-dimensional models were selected according to ISO 20211:2017 to eliminate the effect of thermal bridge on heat flow distribution near the cut-off planes of the calculation model. The total with of two-dimensional calculation model was 2.60 m while the width and height of the three-dimensional calculation model were both 2.60 m as shown in figure 2 and figure 3.
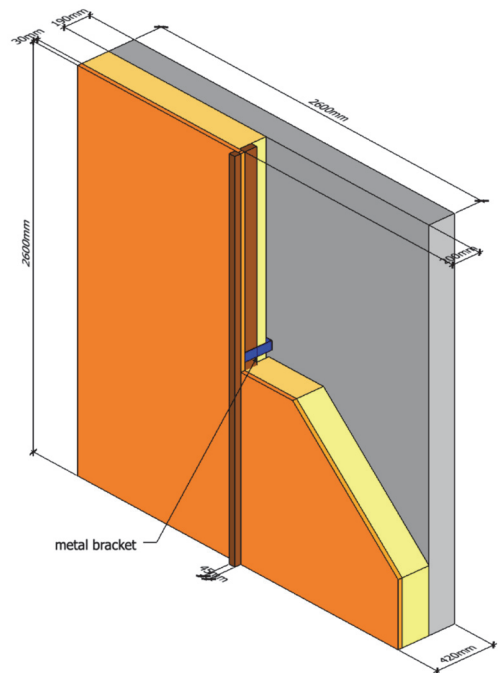
Fig. 2. Geometric model of assessed external wall part containing the thermal bridge (the parts of wind barrier and insulation layers are cut off for visualizing purpose).
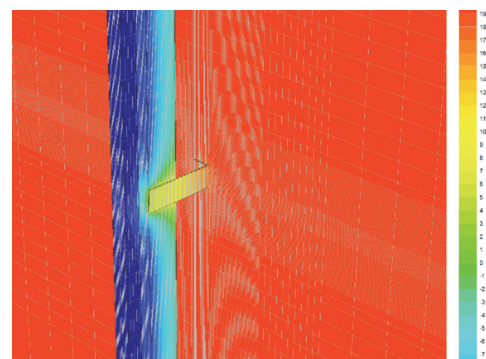

Fig. 3. Three-dimensional FED model of assessed external wall part containing the thermal bridge with indicated mesh density and temperature distribution (the external wind barrier and insulation layers are hidden for visualizing purpose).

Based on three-dimensional thermal coupling coefficients the point thermal transmittance was calculated as in equation 3. The acquired point thermal transmittance was divided by the difference of two-dimensional thermal coupling coefficients to obtain the equivalent length of the thermal bridge. As the point thermal transmittance of the bridging element is directly related to actual thermal bridge length this effect is omitted from further analysis by subtracting the actual length of thermal bridge (h_{TB}) from the equivalent length of thermal bridge (h_{eq}) so the effect of different parameters is tested against the additional length of the thermal bridge (h_{add}) as in equation 4.

$$h_{add} = h_{eq} - h_{TB} \qquad (4)$$

The half amount of additional length of thermal bridge can be considered as extra length on both side of the bridging element to compensate for the heat flows in third dimension as shown in figure 4.
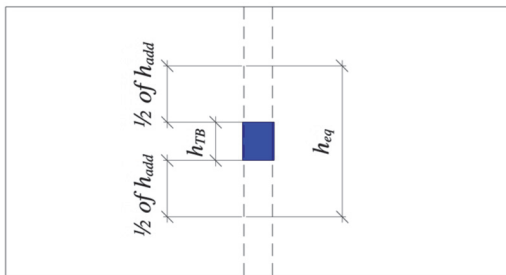
Fig. 4. Schematic cross section (vertical) of assessed external wall with actual length (h_{TB}), equivalent length (h_{eq}) and additional length (h_{add}) of thermal bridge in third dimension.

2.3 Statistical analysis

The heat flows and thermal coupling coefficients for each combination of input variables were combined into a database. Based on the calculated point thermal transmittances and difference of two-dimensional thermal coupling coefficients several multiple linear regression models were fitted to the numerically calculated data. As first step simple linear regression was fitted as in equation 5, but additional terms to basic multiple linear regression equation were added to improve the model fit as given in equations 6, 7 and 8 based on preliminary numerically calculated data (altogether 12 different equations were fitted, but only 4 most relevant are given here).

$$h_{add} = c_1 \cdot (L_{2D} - L_{2Dref}) + c_n \qquad (5)$$

$$h_{add} = c_1 \cdot (L_{2D} - L_{2Dref}) + c_2 \cdot \lambda_{TB} + c_3 \cdot R_{il} + c_4 \cdot R_{el} + c_n \qquad (6)$$

$$h_{add} = c_1 \cdot (L_{2D} - L_{2Dref}) + c_2 \cdot \lambda_{TB} + c_3 \cdot h_{TB} + c_4 \cdot R_{el} \cdot (L_{2D} - L_{2Dref}) + c_n \qquad (7)$$

$$h_{add} = c_1 \cdot (L_{2D} - L_{2Dref}) + c_2 \cdot \lambda_{TB} + c_3 \cdot h_{TB} + c_4 \cdot R_{el} \cdot (L_{2D} - L_{2Dref}) + c_5 \cdot R_{il} + c_n \qquad (8)$$

where R_{il}, R_{el} are the thermal resistances of the layers adjoining the thermal bridging element from internal and external side, λ_{TB} is the thermal conductivity of thermal bridging element, h_{tb} is the actual length of thermal bridging element and c_1, c_2, c_3, c_4, c_5 and c_n are the estimated coefficients.

The goodness of fit was assessed by considering the adjusted R-squared for each model and the p-value for each coefficient estimate. For the analysis and model fitting by least squares method the statistical analysis software R (version 3.5.1) [16] was used with several add-on packages to allow statistical analysis and data visualisation.

3 Results

## 3.1. Correlation of main parameters

Altogether 102 different combination of thermal bridging situations were numerically calculated. For testing the effect of thermal bridge length in third dimension, a concrete wall with regular steel fixation bracket with 60 mm length combined with three alternative insulation materials and 9 mm gypsum wind barrier layer was selected as the base case. Other variable parameters were tested in all possible combinations. The correlation between point thermal transmittance and the difference of two-dimensional thermal coupling coefficients can be seen in figure 5.
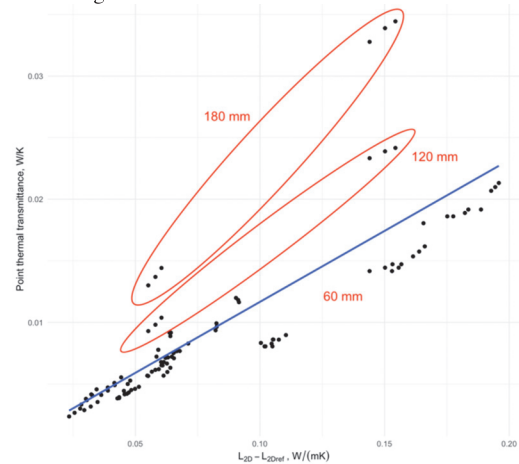

Fig. 5. Correlation between point thermal transmittance and the difference of two-dimensional thermal coupling coefficients.

It can be seen from the figure that despite reasonable correlation there are some variation depending on other input variables. The difference caused by bracket length is expected as the thermal bridge itself has more length, but other factors need further analysis. Additional thermal bridge length is used instead of point thermal transmittance to omit direct effect of bracket length and test the correlation between different input variables and the additional heat loss from the third dimension. It can be seen from figure 6 that the additional length of thermal

bridge increases when the difference between two-dimensional thermal coupling coefficients gets smaller, but the variation due to other factors is high. The variation is mainly described by the thermal conductivity of the bridging element (figure 7a) and the thermal resistance of the external (i.e. the wind barrier) layers (figure 7b).
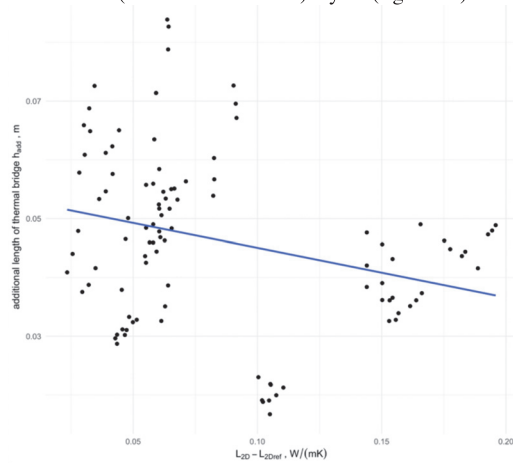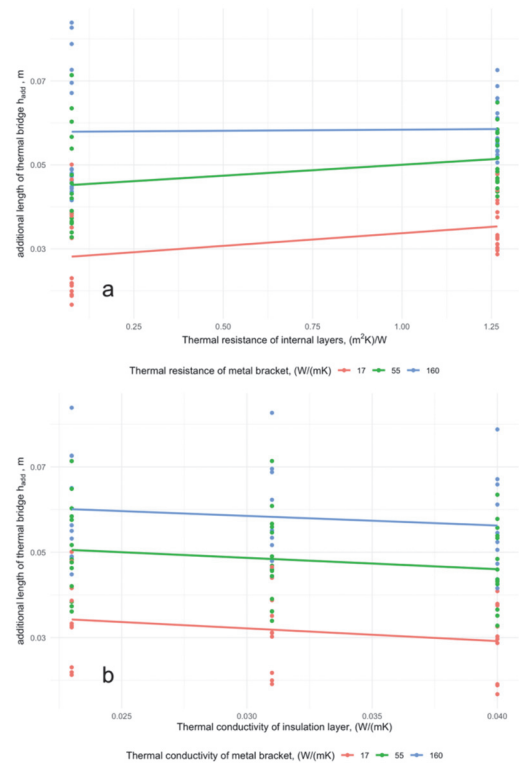

Fig. 6. Correlation between additional thermal bridge length and the difference of two-dimensional thermal coupling coefficients.
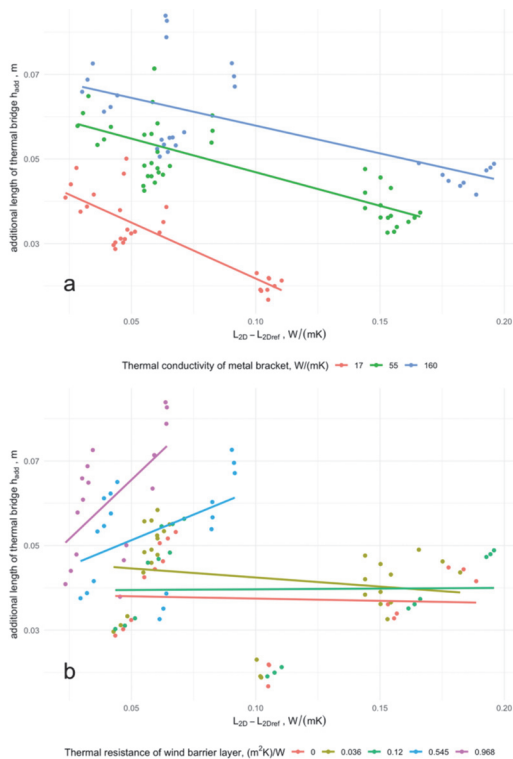
Fig. 7. Correlation between additional thermal bridge length and the difference of two-dimensional thermal coupling coefficients grouped by thermal conductivity of bridging element (a) or thermal resistance of external wind barrier layer (b).

Depending on the thermal conductivity of the bridging element the correlation between the additional length of thermal bridge and the difference of thermal coupling coefficients have roughly similar slope, but the correlation is shifted. The effect of the external wind barrier layer is different as the correlation between additional length and difference between thermal coupling coefficients is strongly affected by the thermal resistances of the outermost layers. With higher thermal resistances (mineral wool or wood fibre wind barrier) the additional length of the thermal bridge is significantly affected by the difference between respective thermal coupling coefficients. With low thermal resistance (wind barrier membrane or gypsum board) this effect is not present. This means that the variables have to be described with mutual interaction when fitting the model.

Surprisingly the thermal resistance of load bearing layer and other internal layers adjoining the thermal bridge (figure 8a) and the thermal conductivity of the insulation layer with the thermal bridge (figure 8b) have no significant effect on the additional thermal bridge length.

Fig. 8. Correlation between additional thermal bridge length and the thermal conductivity of insulation layer grouped by thermal conductivity of bridging element (a) or thermal resistance of external wind barrier layer (b).

Although it has been previously shown that the point thermal transmittance depends on these parameters [13] the effect is already included in the thermal coupling coefficients and the additional length of thermal bridge is

not directly affected. This allows more simplification in the multiple regression model fitting as those parameters can be omitted.

3.2 Model fitting

Altogether 12 different model fits were tested to find a good balance with good fit and minimum amount of terms in multiple linear regression equation. As the difference between two-dimensional thermal coupling coefficients and the additional model length is strongly related to thermal conductivity of point thermal bridge and the thermal resistance of the wind barrier layer, it was expected that the simple correlation as in equation 5 has no predictive power (adjusted $R^2 = 0.072$). Other model equations had better predictive power as can be seen from table 2. Although the last model equation had highest predictive power, the p-values of some coefficient estimates were a lot higher than 0.05.

Table 2. The goodness of fit for models assessed in this study.

|	Adjusted R^2	Root mean square error	p-value for coefficient estimates
Model based on equation 5	0.072	0.014	$c_1, p < 0.01$ $c_n, p < 0.001$
Model based on equation 6	0.734	0.007	$c_1, p > 0.1$ $c_2, p < 0.001$ $c_3, p > 0.1$ $c_4, p < 0.001$ $c_n, p < 0.001$
Model based on equation 7	0.860	0.005	$c_1, p < 0.001$ $c_2, p < 0.001$ $c_3, p < 0.001$ $c_4, p < 0.001$ $c_n, p < 0.001$
Model based on equation 8	0.893	0.005	$c_1, p > 0.1$ $c_2, p > 0.1$ $c_3, p < 0.001$ $c_4, p < 0.001$ $c_5, p < 0.001$ $c_n, p < 0.001$

Final fitted equation and estimated coefficients (all parameters with p-value < 0.001)

$$h_{add} = -1.078 \cdot 10^{-1} \cdot (L_{2D} - L_{2Dref}) + 1.732 \cdot 10^{-4} \cdot \lambda_{TB} + 1.480 \cdot 10^{-1} \cdot h_{TB} + 4.162 \cdot 10^{-1} \cdot R_{el} \cdot (L_{2D} - L_{2Dref}) + 2.529 \cdot 10^{-2} \quad (9)$$

Estimated additional thermal bridge length can be used to calculate the point thermal transmittance of given thermal bridge as in equation 10.

$$\chi = (h_{add} + h_{TB}) \cdot (L_{2D} - L_{2Dref}) \quad (10)$$

Point thermal transmittances retrieved from three-dimensional numerical calculations are plotted against estimated point thermal transmittances in figure 9 for the same thermal bridges.
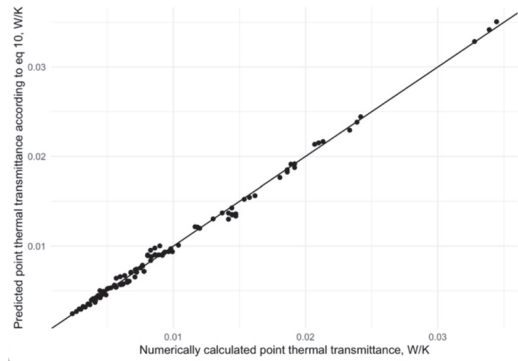

Fig. 9. Correlation between calculated and estimated point thermal transmittance (the black line represents x=y).

The relative error varies between -9.2% (underestimation) and +15.1% (overestimation) although typical deviation from the numerically calculated values were significantly lower with 0.25 and 0.75 quantiles at -2.7% and +3.2% respectively.

The equation and the calculation methodology can be used for thermal bridges which incorporate similar situations with local point thermal bridges incorporating metal penetrations through insulation layer, such as metal brackets supporting or fixing the window frame to the load bearing structure etc. The analysis showed that the thermal conductivity of the insulation material of the layer that is penetrated and the thermal resistance of the internal (load bearing) structure has no significant effect on the equivalent length of thermal bridge, which makes it possible to use the method on wide array of different envelope configurations.

3.3 Calculation example

As an example, a calculation procedure according to the developed methodology is given for a plastic window connection to the lightweight steel sandwich wall panel with 160 mm mineral wool insulation (thermal conductivity 0.039 W/(mK)). The point thermal bridge is created by 1 mm thick steel sheet that connects the internal and external layers. The length of connecting metal sheet is 200mm. The schematic cross section is given in figure 10.
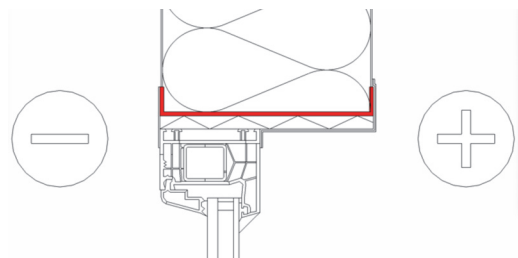
Fig. 10. Schematic cross section of assessed window connection featuring a steel penetration between window frame and sandwich wall element.

For this junction a two-dimensional heat flow was calculated for cross section with thermal bridge element (figure 11a) and a reference case without thermal bridge element (figure 11b) by using LBNL Therm finite element calculation software [12].
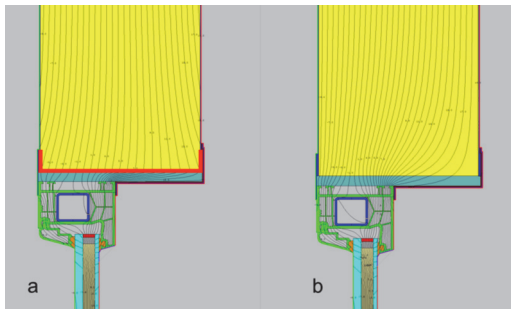
Fig. 11. Isotherms on a window connection to wall element cross section with (a) a thermal bridge and a reference case without (b) thermal bridge.

Respective thermal coupling coefficients were L_{2D} = 0.9008 W/(mK) and L_{2Dref} = 0.6834 W/(mK). The thermal conductivity of thermal bridge element λ_{TB} = 50.0 W/(mK). According to the geometric model the length of the thermal bridge is 0.200 m and the resistance of the wind barrier layer R_{el} = 0 (m²K)/W as thermal bridge connects directly the internal and external environment. Using equation 9 the additional thermal bridge length for this junction is h_{add} = 0.040 m. The equivalent thermal bridge length is h_{eq} = 0.240 m accordingly. Multiplication with difference in thermal coupling coefficients derived from respective cross sections predicts point thermal transmittance χ = 0.052 W/K. In comparison the point thermal transmittance derived from numerical three-dimensional calculation was χ = 0.048 W/K. For this case the point thermal transmittance was overestimated by 0.004 W/K (8.3%) compared to detailed calculation following rules in ISO 10211:2017.

For comparison, in practice a very rough estimation of point thermal transmittance is sometimes calculated as the actual length of the thermal bridge (h_{TB}) multiplied by the difference (L_{2D} - L_{2Dref}) in thermal coupling coefficients derived from two-dimensional numerical calculations based on respective cross sections. As this alternative calculation disregards the heat flow from third dimension, it always underestimates the point thermal transmittance of the bridging element. For this calculation example this rough estimation would lead to point thermal transmittance of 0.043 W/K, which underestimates the actual point thermal transmittance by 0.005 W/K (10.4%). The underestimation of rough calculation is in the same magnitude as the overestimation by suggested new method for this example.

3.4 Possible limitations of new method

The new method is expected to work accurately for thermal bridges with small point thermal transmittance such as façade mounting brackets, fixation elements and other small metal elements inside building envelopes. The exact values of multiple linear model coefficients used in final equation are based on large number of numerical calculations for thermal bridges with point thermal transmittance in the range between 0.002 and 0.034 W/K. The equation is expected to work outside this range up to 0.2 W/K, but the estimation accuracy for significantly larger thermal bridges such as concrete columns protruding external floor elements or roof construction etc has to be systemically assessed during further research. It is expected that same underlying model structure can be used, but different model coefficients have to be derived for thermal bridges with significantly higher point thermal transmittance.

Additionally, the multiple linear regression model was based on dataset of thermal bridges with uniform geometry in third dimension. The point thermal transmittances for non-uniform bridging elements such as steel beams with C-shaped, H-shaped, L-shaped or tubular cross sections cannot be therefore predicted. The further research is planned to see if several simplifications for heat flows in third dimension can be used, such as the use of area-weighed cross sections, using additional two-dimensional numerical calculations for different adjacent cross sections etc.

4 Conclusions

In this study a new method was proposed for predicting three-dimensional heat flow and the point thermal transmittance of thermal bridges caused by full or partial penetration of the building envelope with metal elements with uniform geometry in third dimension using two-dimensional numerical calculation. This enables the possibility to estimate the point thermal transmittance of different mounting brackets etc in cases, where three-dimensional calculation procedure is not possible due to lack of time, software tools or skills within design team.

A new parameter (equivalent length of thermal bridge) was defined which incorporates the effect of additional thermal transmittance when multiplied by the difference of two thermal coupling coefficients derived from two-dimensional numerical calculations. The difference between equivalent length and actual length of thermal bridge can be estimated based regression model fitted to numerical data.

Altogether 102 three-dimensional cases were numerically assessed, and the effect of different parameters were analysed by varying the thermal conductivities of bridging element, insulation layer and both internal and external layers surrounding the bridging element. Based on the analysis the effect of insulation material as well as the thermal resistance of the internal layers (load bearing part of the building envelope) did not have significant effect on linear regression between the additional length of thermal bridge and the difference in thermal coupling coefficients derived from respective cross sections. Several multiple regression models were fitted to numerical data and best fit included the thermal resistance (R_{el}) of the wind barrier layers and the thermal conductivity of the bridging element itself (λ_{TB}) along

with the actual length of the thermal bridge (h_{TB}) and the difference (L_{2D} - L_{2Dref}) in thermal coupling coefficients derived from two-dimensional numerical calculations based on respective cross sections.

References

1. S. A. Al-Sanea and M. F. Zedan, Applied Energy **98**, 584 (2012)
2. B. Berggren and M. Wall, Energy and Buildings **65**, 331 (2013)
3. B. Berggren and M. Wall, Buildings **8**, 154 (2018)
4. A. Capozzoli, A. Gorrino, and V. Corrado, Applied Energy **107**, 229 (2013)
5. S. Ilomets, K. Kuusk, L. Paap, E. Arumägi, and T. Kalamees, Journal of Civil Engineering and Management **23**, 96 (2017)
6. S. Ilomets and T. Kalamees, Journal of Building Pathology and Rehabilitation **1**, 11 (2016)
7. T. Theodosiou, K. Tsikaloudaki, S. Tsoka, and P. Chastas, Journal of Cleaner Production **214**, 62 (2019)
8. CEN committee ISO/TC 163/SC, *ISO 10211:2017 Thermal Bridges in Building Construction. Heat Flows and Surface Temperatures. Detailed Calculations* (2017)
9. ANSYS inc., (2020)
10. Comsol inc., (2020)
11. PHYSIBEL, (2020)
12. Lawrence Berkley National Laboratory, (2020)
13. T. G. Theodosiou, A. G. Tsikaloudaki, K. J. Kontoleon, and D. K. Bikas, Energy and Buildings **109**, 377 (2015)
14. A. Lorenzati, S. Fantucci, A. Capozzoli, and M. Perino, Energy and Buildings **111**, 164 (2016)
15. A. Ben Larbi, Energy and Buildings **37**, 945 (2005)
16. R Core Team, (2018)

PUBLICATION IV

IV

Hallik, J.; Kalamees, T. (2021). The effect of flanking element length in thermal bridge calculation and possible simplifications to account for combined thermal bridges in well insulated building envelopes. Energy and Buildings, 252 (111397). DOI: 10.1016/j.enbuild.2021.111397.
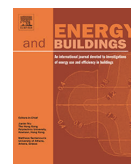
The effect of flanking element length in thermal bridge calculation and possible simplifications to account for combined thermal bridges in well insulated building envelopes

Jaanus Hallik [a,b,*], Targo Kalamees [a,b]

[a] nZEB Research Group, Department of Civil Engineering and Architecture, Tallinn University of Technology, Estonia
[b] Smart City Center of Excellence (Finest Twins), Tallinn University of Technology, Estonia

ARTICLE INFO

ABSTRACT

A well-insulated, airtight, thermal bridge free building envelope is a key factor for nearly zero energy buildings (nZEB). However, increased insulation thickness and minimised air leakages increase the effect of thermal bridges on the overall energy efficiency of the nZEBs. Currently, the calculation of linear thermal transmittance follows ISO 10211, which requires the separate numerical assessment of combined thermal bridges, where two or more junctions are positioned in close proximity within delimiting cut-off planes. This poses a practical problem, as the number of different combinations (mainly related to window to wall connections in combination with corners, intermediate ceiling etc) is too large in practice to follow the standard procedure.

In this study, a parametric numerical assessment of different thermal bridges in well-insulated constructions showed that with linear thermal transmittance up to 0.2 W/(mK) in lightweight construction and up to 0.1 W/(mK) in heavyweight construction the reduction of flanking element length from 1.440 m to 0.288 m (80% reduction) had no effect on numerically calculated linear thermal transmittance in steady-state conditions. For thermal bridges inside heavyweight construction with linear thermal transmittance below 1.1 W/(mK) the flanking element length could be reduced by 50% without any effect and by 70% with marginal effect (<2%) on linear thermal transmittance.

The shorter flanking element length, roughly equal to its thickness, can then be used to minimise the amount of combined thermal bridges in complex building envelopes. Compared to ISO 10211 requirements, the amount of different combined thermal bridges in two exemplary building envelopes was reduced by 35% to 76%, depending on the building type, and allowed deviation of 0.5%, 1.0% or 2.0%, thus significantly reducing the working hours of practitioners.

© 2021 Elsevier B.V. All rights reserved.

1. Introduction

A well-insulated, airtight and thermal bridge free building envelope is a key factor for nearly zero energy buildings (nZEB) that becomes mandatory from year 2021. Minimising heat losses and combining a thermally optimised building envelope with the passive use of solar energy allows a significant reduction in the heat load and heating energy demand of residential buildings. However, increased insulation thickness and minimised air leakages in modern energy efficient buildings and nZEBs increase the effect of thermal bridges on the overall heat loss of the building envelope [1]. The fraction of heat loss due to thermal bridge effects is highly dependent on architectural complexity and constructional solutions used in the building envelope, but is usually significant in nZEBs and can be as high as 30% or more [2].

Currently the calculation of linear thermal transmittance follows procedures described in ISO 10211 [3], however a detailed guideline is given only for straightforward geometrical situations. In complex situations where multiple thermal bridges are in close proximity, the calculation of linear thermal transmittance should be conducted separately for each such combination. This poses a practical problem as the number of different combinations (mainly related to window to wall connections in combination with corners, intermediate ceiling etc) is too large in practice to follow the standardised procedure. Furthermore, most whole building energy simulation tools do not usually have an interface for the

---

* Corresponding author at: nZEB Research Group, Department of Civil Engineering and Architecture, Tallinn University of Technology, Estonia.
E-mail address: jaanus.hallik@taltech.ee (J. Hallik).

highly fragmented input of linear thermal transmittances which is required to realistically model the overall thermal transfer value of an entire building envelope.

Over the years there has been a lot of research to propose different ways to reduce the workload related to thermal bridge effects in building envelopes. Robust coefficients for increasing the thermal transmittances have been used [4], but these can underestimate the actual heat loss [5–7]. A large number of thermal bridge catalogues has been developed for typical or approximate geometries (both national and international) [8] along with specific attention to optimised window to wall connections [9–11], special construction types [12,13], etc. Alternatively, there have been attempts to generate statistical models for typical junctions that would allow the estimation of linear thermal transmittance based on other building envelope parameters [14–16], but these are bound to specific geometrical and constructional solutions and are not universally applicable. Despite this collective effort, in lot of cases a standardised numerical calculation is still mandatory and in the case of complex building geometry and window layout, the number of combined thermal bridges is too large in practice to follow the standardised procedure. Moreover, for very complex junctions where highly conductive elements create a need for very fine meshing of the finite element model, it can be the case that larger models with multiple combined junctions cause extended simulation duration as well as models reaching the maximum mesh size limitations.

In practice, junctions with two or more combined thermal bridges are sometimes handled as the sum of individual thermal bridges, but this is not allowed by ISO 10211 and not backed up by previous studies. It is expected that building envelope parts with variable layer properties related to thermal resistances as well as geometric dimensions need different minimal flanking element lengths to reach a uniform thermal distribution at the cut-off boundary condition. In ISO 10211 methodology, it is defined that for all regular building envelope elements (excluding ground coupled elements) the minimum flanking element length is at last 1.0 m or 3 times the thickness of the flanking element itself. Previous studies related to simplification of dynamic properties of thermal bridges through the equivalent wall [17] and mixed equivalent wall methods [18] have shown that shorter flanking element lengths for those specific junctions can be used to describe the heat loss and surface temperatures without significant loss of accuracy compared to ISO 10211 methodology The current study builds on these findings to detect the minimal flanking element lengths through parametric numerical assessment of different well insulated constructions and use these shorter lengths to simplify the assessment of combined thermal bridges.

The hypothesis of the study is that for well insulated constructions (which are used in the nZEBs) the minimum flanking element lengths required in the numerical model to achieve necessary accuracy are significantly lower than described in ISO 10211. This, in turn, might enable the possibility of simplifying the assessment of combined thermal bridges by arithmetically combining the linear thermal transmittances of unitary thermal bridges and thus reducing the required working hours of practitioners and reducing the time and computing power for more complex numerical finite element (FE) or finite difference (FD) models due to smaller model geometry.

2. Material and methods

The current study uses parametric steady-state FE calculation to assess the effect of flanking element length on numerically derived linear thermal transmittance values of different junctions with different insulation materials in lightweight timber construction as well as constructions with heavyweight concrete and lightweight concrete layers as the load bearing structure. All the main types of thermally good junctions were assessed across these variations, as well as some additional junctions with higher linear thermal transmittances for reference, totalling some 570 numerical models altogether.

2.1. Finite element analysis

Thermal bridges are defined as part of the building envelope where the otherwise uniform thermal resistance is significantly changed by full or partial penetration of the building envelope by materials with higher thermal conductivity. The linear thermal transmittance Ψ, W/(m·K) of an additional thermal bridge is calculated as described in equation (1).

$$\Psi = L_{2D} - \sum_{j=1}^{N_j} U_j \cdot l_j \qquad (1)$$

where L_{2D}, W/(m·K) is the thermal coupling coefficient obtained from a separate two-dimensional numerical calculation, U_j, W/(m²·K) is the thermal transmittance of the building envelope adjoining the thermal bridge and l_j, m is the respective length of the adjoining part of the building envelope (i.e flanking element) described in the calculation model.

The thermal coupling coefficients L_{2D} for each case were obtained from two-dimensional numerical models as respective heat flows divided by the temperature difference used in the model. The heat flow and thermal bridge calculations in this study were carried out according to methodology, boundary conditions and modelling rules described in ISO 10211 [3] using software package LBNL Therm [19], which utilises steady state finite element methods to numerically calculate two-dimensional heat flows in complex geometrical models. This software package was selected because the authors have developed pre- and post-processing workflows to enable parametric study.

2.2. Description of geometric models

In the current study, three well insulated construction types with three different insulation materials were used for assessment, with an equal overall wall thickness of 480 mm:

A. Lightweight timber construction with a 417 mm layer of insulation and repeating wooden c-beams as load bearing structures (Fig. 1 - A; Figs. 2 - 1, 2, 5, 6) with thermal transmittance between 0.060 and 0.094 W/(m²K) depending on thermal conductivity of the insulation material.
B. Lightweight concrete (thermal conductivity 0.24 W/(mK)) sandwich element with a 200 mm layer of insulation (Fig. 1 – B, Figs. 2 – 3,4,7,8) with thermal transmittance between 0.096 and 0.158 W/(m²K) depending on the insulation material.
C. Heavyweight concrete (thermal conductivity 2.3 W/(mK)) sandwich element with a 200 mm layer of insulation (Fig. 1 - C, Figs. 2 – 3, 4, 7, 8) with thermal transmittance between 0.106 and 0.189 W/(m²K) depending on thermal conductivity of the insulation material.

Assessment was carried out on 5 main types of thermal bridges connected to the external wall part for each construction type. The slab on ground construction and foundation geometry below the ground was similar for all assessed cases with 200 mm of heavyweight concrete on top of 250 mm insulation with thermal conductivity corresponding to the external wall insulation layer. In the case of ground coupled junctions the length of terrain and soil
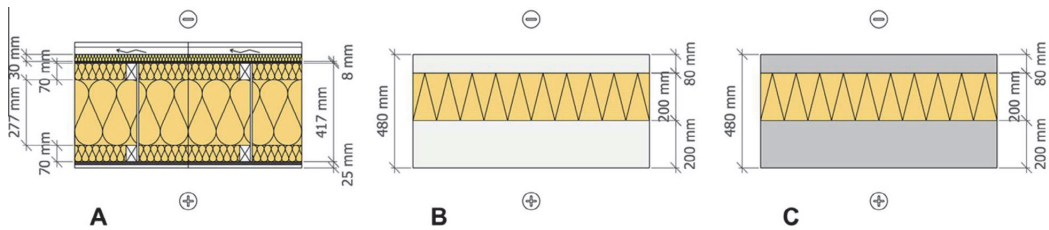
Fig. 1. Three different wall construction types used in numerical analysis, A – lightweight timber construction, B – lightweight concrete sandwich element, C – heavyweight concrete sandwich element.
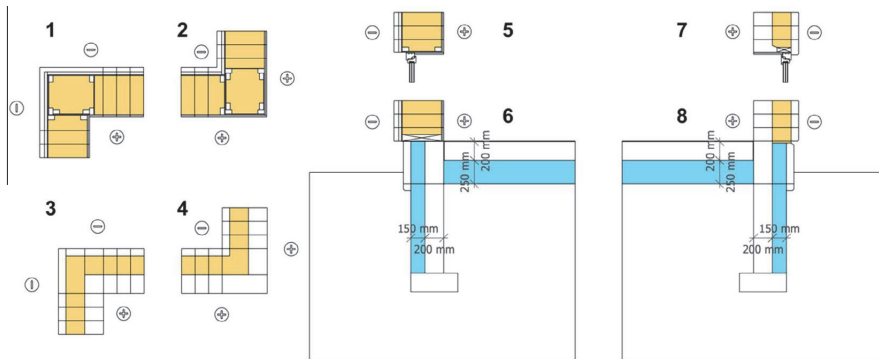

Fig. 2. Assessed geometric cases in main analysis, 1 and 3 – regular corner, 2 and 4 – inverted corner, 5 and 7 – window to wall connection, 6 and 8 – slab on ground to external wall connection.

depth was set to 20 m and the length of floor slab inside the building to 4 m according to ISO 10211 and the characteristic dimension of the floor for exemplary buildings used in this study. The overview of assessed geometries is shown in Fig. 2:

- Regular external wall to external wall connection (Figs. 2 – 1 and 3)
- Inverted external wall to external wall connection (Figs. 2 – 2 and 4)
- Window to external wall connection (Figs. 2 – 5 and 7)
- External wall to slab on ground connection (Figs. 2 – 6 and 8)
- External wall to intermediate ceiling connection

The flanking element length for each assessed thermal bridge was varied between 100% (corresponds to 3 times the thickness of flanking element length) and 10% (corresponds to one third of flanking element thickness) with steps of 10% (i.e., 0.144 m) totalling 10 different numerical models with flanking element lengths between 0.144 m and 1.44 m.

Additional geometry was included for further numerical analysis for the external wall with heavyweight concrete sandwich elements to study thermal bridges with significantly higher linear thermal transmittances. For this, two suboptimal levels ("medium" and "high") of thermal bridges were described for the external wall to window connection and external wall to balcony connection, as described in Fig. 3. The balcony connection junction with "high" thermal bridge corresponds to a fully protruding balcony slab while the junction with "medium" thermal bridge has a special decoupling element (ISOKORB) [20] with an effective thermal conductivity of 0.124 W/(mK) separating the balcony slab and intermediate floor slab. The window connection with "medium" and "high" thermal bridges corresponds to suboptimal positioning of

the window frame halfway or fully into the internal load bearing layer.

The thermal conductivities (λ, W/(mK)) used in the numerical analysis are described in Table 1. The assessed different insulation materials correspond, for example, to two different typical mineral wool types, along with the polyurethane foam insulation, that are used in this kind of construction for nZEBs. In the scope of this study alternative insulation materials with same thermal conductivities can be considered as interchangeable.

2.3. Description of example building geometry

In order to assess the potential for simplifications in real life situations, two existing buildings with different sizes and geometry were described, featuring several combined thermal bridges in the thermal envelope. A large non-residential four-storey office building (Fig. 4 A) with mixed construction was used as an example building for bigger and more complex building geometry featuring 11 regular junctions with a single linear thermal bridge and 73 junctions with two or more combined thermal bridges according to the minimum flanking element length required by ISO 10211 [3]. A prefabricated two-storey wooden reference building (Fig. 4 B) with a well-insulated lightweight timber frame wall and roof elements was used as an alternative example of detached house featuring 8 regular junctions with a single linear thermal bridge and 26 junctions with two or more combined thermal bridges. For both buildings, the number of combined thermal bridges was calculated based on the minimum distance between the different junctions according to ISO 10211.

Subsequently, a new minimum distance between all junctions were defined based on numerical cases with relative deviation of linear thermal transmittance up to 0.5%, 1.0% or 2.0% and the
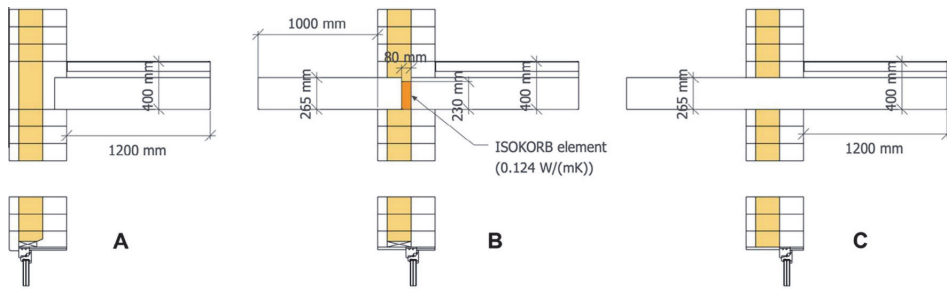
Fig. 3. Additional geometric cases for follow up analysis, A – junctions with "low" thermal bridge from main analysis, B – junctions with "medium" thermal bridge, C – junctions with "high" thermal bridge.

Table 1
Variable layer properties in assessed geometric cases.

Construction type	Material layer	Thermal conductivity λ, W/(mK)
Lightweight timber construction	0.03 m wind barrier board	0.031
	0.008 m fibreboard (OSB)	0.130
	0.417 m insulation layer	0.022/0.031/0.040
	0.012 m fibreboard (OSB)	0.130
	0.013 m gypsum board	0.210
Heavyweight concrete sandwich element	0.08 m heavyweight concrete	2.300
	0.2 m insulation layer	0.022/0.031/0.040
	0.2 m heavyweight concrete	2.300
Lightweight concrete sandwich element	0.08 m lightweight concrete	0.240
	0.2 m insulation layer	0.022/0.031/0.040
	0.2 m lightweight concrete	0.240
Slab on ground	0.2 m heavyweight concrete	2.300
	0.25 m insulation layer	0.022/0.031/0.040
	20.0 m soil layer	2.000
	0.15 m edge insulation layer	0.022/0.031/0.040

reduced number of combined thermal bridges were calculated while using these shorter flanking element lengths. This allows estimating the reduction of working hours for general practitioners when unitary linear thermal transmittances are combined for overall heat loss calculation.

3. Results and discussion

3.1. Linear thermal transmittances of assessed junctions

Altogether, 5 typical junctions with 3 different insulation materials and 3 construction types were numerically assessed, with 10 different flanking element lengths, totalling 450 models. The linear thermal transmittance of these junctions considering the flanking element length corresponding to ISO 10211 requirements was

between −0.130 and 0.341 W/(mK) depending on the junction, construction type and thermal conductivity of the insulation layer.

Additional analysis included two levels of more severe thermal bridges of window to wall connection and balcony slab to wall connection (Fig. 3) with 3 different insulation materials and with 10 different flanking element lengths for single construction type (heavyweight concrete as internal load bearing layer) totalling to 120 additional numerical models with linear thermal transmittances between 0.101 and 1.111 W/(mK).

3.2. The effect of flanking element length

The numerical analysis of different junctions showed that the minimum flanking element lengths for well insulated wall construction is significantly lower than defined in the ISO 10211
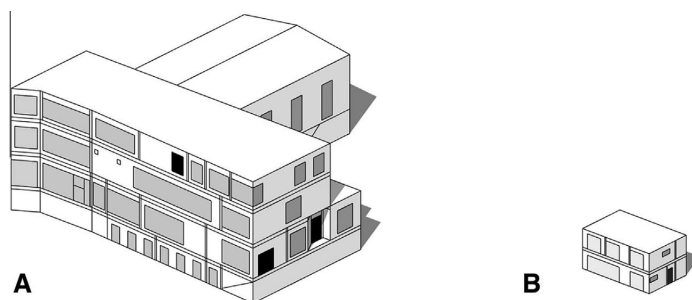

Fig. 4. Example building envelope geometry of large non-residential office building (A, 3 storeys + basement) and detached house (B, 2 storeys) used for assessment.
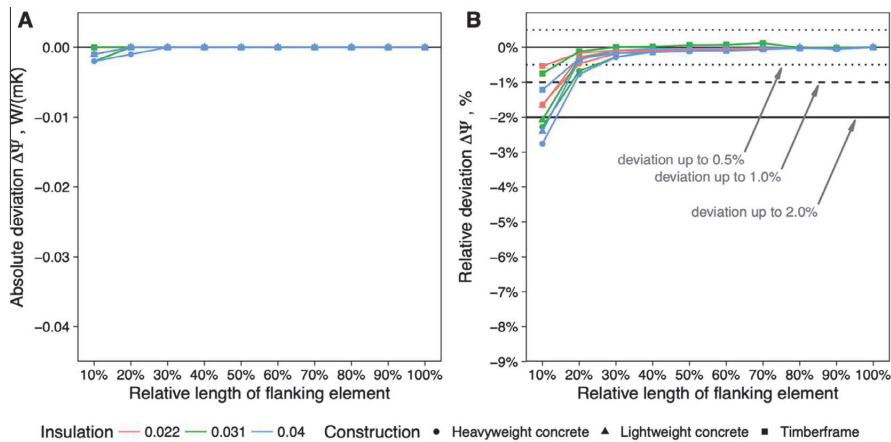
Fig. 5. The effect of flanking element lengths on linear thermal transmittance of external wall corner (absolute deviation on the left, relative deviation on the right).

standard. The deviation of linear thermal transmittance of all combinations compared to a reference case according to ISO 10211 for all assessed external wall to external wall connections is less than 3%. For a regular wall corner (Fig. 5), the construction with a highly conductive internal structural layer (200 mm heavyweight concrete) had a higher deviation compared to the lightweight timber construction with thin and less conductive internal layers. In the case of an inverted (inward) corner with a highly conductive internal structural layer (Fig. 6) the effect was also inverted and negligible. For both junctions, the insulation material with higher thermal conductivity caused a slightly higher deviation from the standardised calculation results. The absolute deviation of linear thermal transmittance $\Delta\Psi$ for all assessed cases was less than 0.002 W/(mK).

In the case of window to external wall connections (Fig. 7), the deviation from the standardised calculation was less than 2% for construction with a highly conductive internal structural layer (heavyweight concrete) and similar for all assessed insulation materials. In the case of lightweight timber frame construction, the relative deviation varied more and for very short flanking element lengths (10% of the standardised flanking element length) the deviation was in the range of 6% to 8%. However, the absolute deviation for all cases was 0.002 W/(mK) or less.

If a ground coupled element such as slab on ground is part of the numerical model, the deviation from the standardised case is significantly higher. When both flanking element lengths (i.e., external wall part and slab on ground part) decrease (Fig. 8) there seems to be at least two different processes affecting the heat flows.

The steady increase of calculated linear thermal transmittance is caused by the increasing edge effect when the length of the slab on ground part is reduced, which is expected [21]. Nevertheless, for all assessed material and construction combinations, the deviation of linear thermal transmittance is rapidly decreasing when ground slab length in the model is 30% or less from the standardised slab length (i.e., 4 m). This can be caused by the mutual effect of vertical foundation insulation and very short geometric boundaries of the floor slab and the ground domain, meaning that in these small models, the heat has to travel a significantly longer path to reach exterior conditions. This is highly dependent on the foundation geometry and the subsoil insulation, and shows that it is not possible to decrease the length of ground coupled flanking elements without introducing a lot of uncertainty.

To exclude this effect another set of calculations were performed with a constant slab on ground length of 4 m and only the flanking element length of the external wall was altered. The results can be seen in Fig. 9. As expected, the effect of ground losses is eliminated and only the effect of wall part length is seen.

The effect is similar to other junctions where linear thermal transmittance in the case of short flanking element lengths is lower than for the full-size model, however the difference between different construction types is significant. For lightweight timber frame construction, the deviation is less than 1% for all cases. On the other hand, a highly conductive internal structural layer (heavyweight concrete) coupled to the floor slab and foundation causes deviations of up to 8% at very short wall lengths (0.144 m) due to limited heat flow at the internal boundary condition compared to standard geometry of the model. Absolute values of deviation are in the range of 0.02 to 0.03 W/(mK). The linear thermal transmittance of all assessed thermal bridge combinations are given in Table 2 in full detail, along with the corresponding deviation at different relative flanking element lengths.

To confirm these findings for thermal bridges with higher thermal transmittance, a wall construction with a highly conductive internal load bearing layer was further assessed, in combination with junctions where the insulation layer was significantly reduced by a protruding balcony slab or by suboptimal positioning of the window frame as described in chapter 2.2. The results are given in Table 3 along with linear thermal transmittances and corresponding deviations for all assessed junctions and combinations.

The deviation of linear thermal transmittance for medium thermal bridges was similar to previous results with deviations occurring at 30% relative length of the flanking element compared to ISO 10211 requirements. Although the absolute deviation of linear thermal transmittance of the worse thermal bridges was higher at very short flanking element lengths, the deviation at 40% and 50% of the required flanking element was negligible compared to a very high linear thermal transmittance of the junction itself.

These findings indicate that for a well insulated building envelope and for a wide range of thermal bridges and construction types, the minimum flanking element length can be significantly lower than required by ISO 10211. For the majority of the assessed junctions, using 50% of the standard flanking element length provided the same numerical results for linear thermal transmittance. In Fig. 10 the required length of flanking element is shown for each assessed combination of connection, construction and insulation
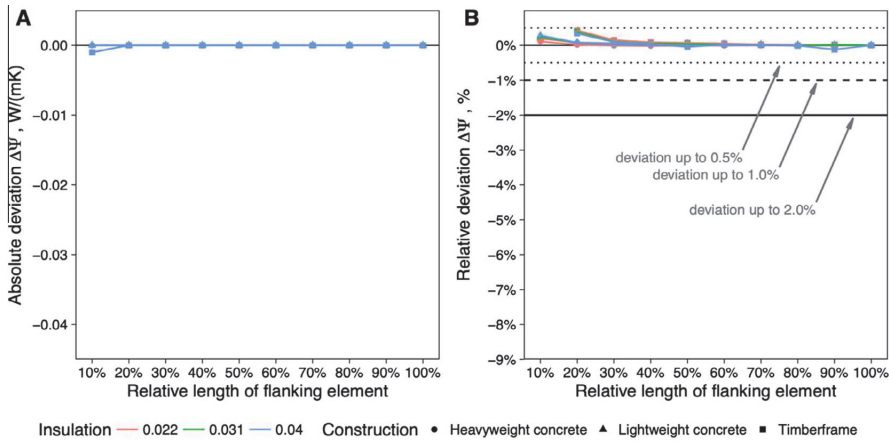
Fig. 6. The effect of flanking element lengths on linear thermal transmittance of inverted external wall corner (absolute deviation on the left, relative deviation on the right).
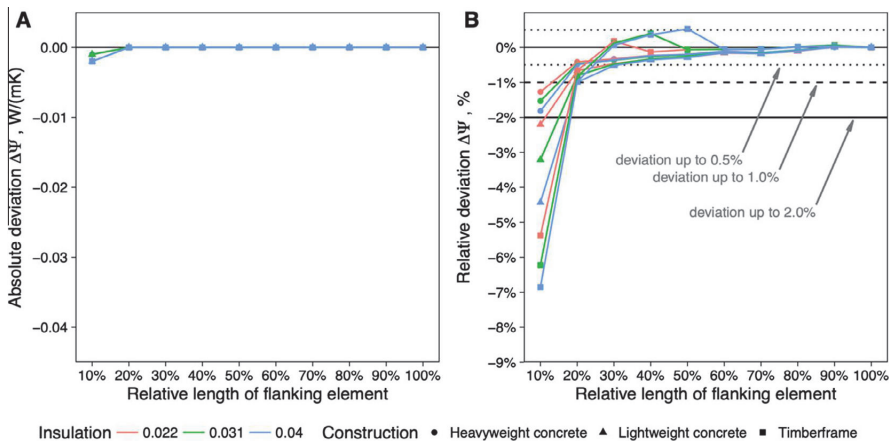

Fig. 7. The effect of flanking element lengths on linear thermal transmittance of window to wall connection (absolute deviation on the left, relative deviation on the right).

that keeps the deviation of linear thermal transmittance $\Delta\Psi$ below a certain limit depending on the linear thermal transmittance of the assessed junction. Side by side comparison is given for same combinations at three limiting values – i.e., allowed deviation from the standard calculation for the same junctions is less than 0.5%, 1.0% or 2.0%.

For minimal deviation, a flanking element length around 40% to 50% has to be used compared to ISO 10211 requirements. If a deviation up to 2% is allowed, then a junction with a minimum flanking element length of 20% can be used for junctions with linear thermal transmittance <0.2 W/(mK) and 30% for junctions with higher linear thermal transmittance. In this case, the required flanking element length in the numerical model corresponds roughly to the flanking element thickness or less. This shows that for well insulated building envelopes, the effect of thermal bridges seems to be localised near the junction and interaction of multiple thermal bridges is very small at distances corresponding roughly to wall or roof thickness. This is to be expected as thicker insulation layer and higher thermal resistance of the wall or roof part reduce the proportion of perpendicular heat flow through the flanking elements regarding the theoretical heat flow limited by surface resis-

tances as well as provide higher and more even surface temperatures along flanking element length.

3.3. Simplification of combined thermal bridges

Based on these findings, the linear thermal transmittances of single connections can be arithmetically combined to estimate the linear thermal transmittance of combined thermal bridges with good accuracy. For ground coupled flanking elements such as slab on grade etc this simplification is not possible and flanking element length according to ISO 10211 has to be used.

To estimate the potential of this simplification on time and effort for general practitioners the number of regular and combined thermal bridges were identified on two different building geometries as described in chapter 2.3. Altogether 84 (office building) and 34 (single family home) different junctions were present in these building envelopes. Using shorter flanking element lengths based on the previous chapter corresponding to three alternative levels of accuracy, the number of different junctions was recalculated. It can be seen from Table 4 that in the case of office building the numerical calculation of linear thermal transmittance is
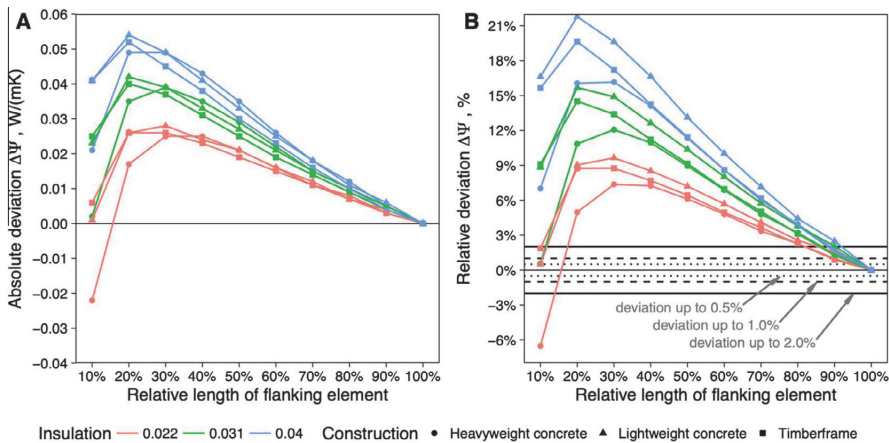
Fig. 8. The effect of flanking element lengths on linear thermal transmittance of ground floor slab to wall connection (the flanking element length both for external wall and ground floor slab was changed).
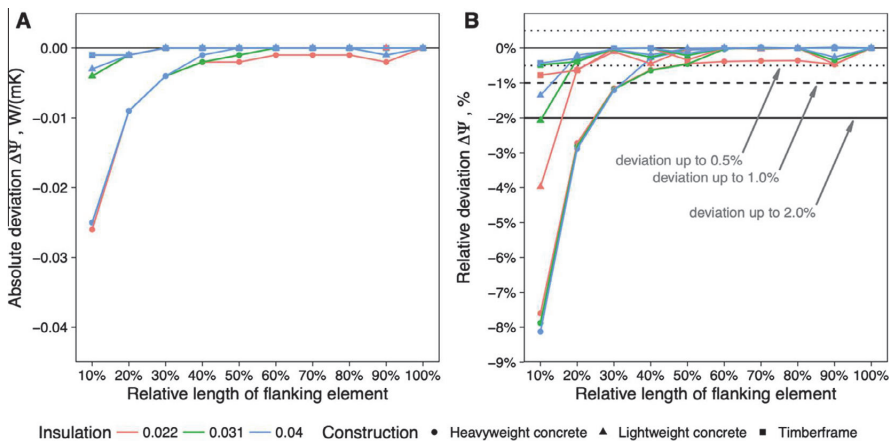

Fig. 9. The effect of flanking element lengths on linear thermal transmittance of ground floor slab to wall connection (absolute deviation on the left, relative deviation on the right).

needed for only 45 different junctions (46% reduction) when deviation up to 0.5% is allowed. If deviation up to 2.0% is allowed the reduction in the number of different junctions is 76%, significantly reducing the time needed for thermal bridge calculation. For the single family home, the reduction in number of different thermal bridge combinations is lower as expected, but still between 35% and 50%.

In conclusion, the current study confirmed that for well insulated constructions, the minimum flanking element length required in the numerical model is significantly lower than described in ISO 10211, without compromising the accuracy of steady state calculations of linear thermal transmittance. Similar findings have been seen in previous studies related to dynamic modelling of thermal bridges with equivalent wall and mixed equivalent wall methods where new shorter flanking element lengths were identified by limited change in surface temperature along the flanking element [17,18,22]. The length of equivalent wall parts in these studies were strictly related to fixed geometry and material layers, but nevertheless showed that only 40% to

50% of flanking element length was needed [1] to define equivalent wall parts, compared to the requirements of ISO 10211.

The current study showed that even shorter flanking element lengths are possible for most junctions. In the case of regular junctions adjacent to external air within well-insulated constructions with linear thermal transmittance below 0.1 W/(mK), the reduction of flanking element length from 1.44 m to 0.288 m (80% reduction) had no effect on numerically calculated linear thermal transmittance. For junctions with significantly higher linear thermal transmittance, especially above 0.3 W/(mK) and up to 1.1 W/(mK), a reduction of only half of the flanking element length (0.72 m) was possible without a change in calculated linear thermal transmittance, although this phenomenon was only present in constructions with a highly conductive internal load bearing layer (heavyweight concrete). The junctions within lightweight concrete or timber frame construction behaved similarly to thermally good junctions, with deviation of linear thermal transmittance $\Delta\Psi$ within 0.001 W/(mK) when the flanking element length was reduced from 1.44 m to 0.288 m (80% reduction). The

Table 2
Deviation of linear thermal transmittance Ψ depending on flanking element length in numerical model for thermal bridges with low linear thermal transmittance.

Junction	Construction	$\lambda_{insulation}$, W/(mK)	Ψ, W/ (mK)	ΔΨ, W/(mK) at different relative lengths of flanking element l_j									
				10%	20%	30%	40%	50%	60%	70%	80%	90%	100%
External wall to external wall connection	Heavyweight concrete	0.022	0.052	−0.001	0	0	0	0	0	0	0	0	0
		0.031	0.072	−0.002	0	0	0	0	0	0	0	0	0
		0.040	0.090	−0.002	−0.001	0	0	0	0	0	0	0	0
	Lightweight concrete	0.022	0.041	−0.001	0	0	0	0	0	0	0	0	0
		0.031	0.052	−0.001	0	0	0	0	0	0	0	0	0
		0.040	0.060	−0.001	0	0	0	0	0	0	0	0	0
	Timber frame	0.022	0.034	0	0	0	0	0	0	0	0	0	0
		0.031	0.038	0	0	0	0	0	0	0	0	0	0
		0.040	0.042	−0.001	0	0	0	0	0	0	0	0	0
Inverted external wall to external wall connection	Heavyweight concrete	0.022	−0.073	0	0	0	0	0	0	0	0	0	0
		0.031	−0.102	0	0	0	0	0	0	0	0	0	0
		0.040	−0.130	0	0	0	0	0	0	0	0	0	0
	Lightweight concrete	0.022	−0.067	0	0	0	0	0	0	0	0	0	0
		0.031	−0.090	0	0	0	0	0	0	0	0	0	0
		0.040	−0.110	0	0	0	0	0	0	0	0	0	0
	Timber frame	0.022	−0.028	0.001	0	0	0	0	0	0	0	0	0
		0.031	−0.042	0.001	0	0	0	0	0	0	0	0	0
		0.040	−0.056	0.001	0	0	0	0	0	0	0	0	0
Window to external wall connection	Heavyweight concrete	0.022	0.047	−0.001	0	0	0	0	0	0	0	0	0
		0.031	0.045	−0.001	0	0	0	0	0	0	0	0	0
		0.040	0.043	−0.001	0	0	0	0	0	0	0	0	0
	Lightweight concrete	0.022	0.039	−0.001	0	0	0	0	0	0	0	0	0
		0.031	0.038	−0.001	0	0	0	0	0	0	0	0	0
		0.040	0.037	−0.002	0	0	0	0	0	0	0	0	0
	Timber frame	0.022	0.028	−0.002	0	0	0	0	0	0	0	0	0
		0.031	0.030	−0.002	0	0	0	0	0	0	0	0	0
		0.040	0.032	−0.002	0	0	0	0	0	0	0	0	0
External wall to slab on ground connection	Heavyweight concrete	0.022	0.341	−0.026	−0.009	−0.004	−0.002	−0.002	−0.001	−0.001	−0.001	−0.002	0
		0.031	0.322	−0.025	−0.009	−0.004	−0.002	−0.001	0	0	0	0	0
		0.040	0.306	−0.025	−0.009	−0.004	−0.001	0	0	0	0	0	0
	Lightweight concrete	0.022	0.108	−0.004	−0.001	0	0	0	0	0	0	0	0
		0.031	0.182	−0.004	−0.001	0	0	0	0	0	0	−0.001	0
		0.040	0.248	−0.003	−0.001	0	0	0	0	0	0	−0.001	0
	Timber frame	0.022	0.118	−0.001	−0.001	0	0	0	0	0	0	0	0
		0.031	0.194	−0.001	−0.001	0	0	0	0	0	0	0	0
		0.040	0.263	−0.001	−0.001	0	0	0	0	0	0	0	0

Table 3
Deviation of linear thermal transmittance Ψ depending on flanking element length in the numerical model for thermal bridges with medium and high linear thermal transmittance.

Junction	Construction	$\lambda_{insulation}$, W/(mK)	Ψ, W/ (mK)	ΔΨ, W/(mK) at different relative lengths of flanking element l_j									
				10%	20%	30%	40%	50%	60%	70%	80%	90%	100%
Window to external wall connection with medium TB	Heavyweight concrete	0.022	0.105	−0.006	−0.002	−0.001	0	0	0	0	0	0	0
		0.031	0.104	−0.006	−0.002	−0.001	0	0	0	0	0	0	0
		0.040	0.101	−0.006	−0.002	−0.001	0	0	0	0	0	0	0
Window to external wall connection with high TB	Heavyweight concrete	0.022	0.422	−0.076	−0.025	−0.009	−0.003	−0.001	0	0	0	0	0
		0.031	0.418	−0.074	−0.025	−0.008	−0.003	−0.001	0	0	0	0	0
		0.040	0.415	−0.073	−0.024	−0.008	−0.003	−0.001	0	0	0	0	0
External wall to inter. ceiling connection with medium TB	Heavyweight concrete	0.022	0.300	−0.006	−0.002	−0.001	0	0	0	0	0	0	0
		0.031	0.308	−0.006	−0.002	−0.001	0	0	0	0	0	0	0
		0.040	0.316	−0.005	−0.002	−0.001	0	0	0	0	0	0	0
External wall to inter. ceiling connection with high TB	Heavyweight concrete	0.022	1.111	−0.089	−0.029	−0.01	−0.003	−0.001	0	0	0	0	0
		0.031	1.104	−0.086	−0.028	−0.01	−0.003	−0.001	0	0	0	0	0
		0.040	1.097	−0.082	−0.027	−0.009	−0.003	−0.001	0	0	0	0	0

thermal conductivity of insulation material had no significant effect on $\Delta\Psi$ for all assessed cases.

Contrary to the objective of the equivalent wall method, the shorter distance to the adiabatic cut-off plane in this study was used to disaggregate more complex thermal bridges with multiple combined junctions, allowing the separation of the bridges, which can then be summed up arithmetically. The results show that when minimum flanking element lengths identified in this study are used instead of standard values, the amount of different complex thermal bridges in two exemplary buildings can be reduced

between 35% and 76% depending on the allowed deviations in the range of 0.5% to 2.0%, thus significantly reducing the working hours of practitioners.

A previous study regarding the application of infrared thermography for assessment of combined thermal bridges has also referred that despite ISO 10211 requirements the adjacent thermal bridges can be assumed to interact only if the surface temperature between the thermal bridges remains lower than the uniform surface temperature and shorter flanking elements are possible depending on the detail [23] referring to remark in BRE report that
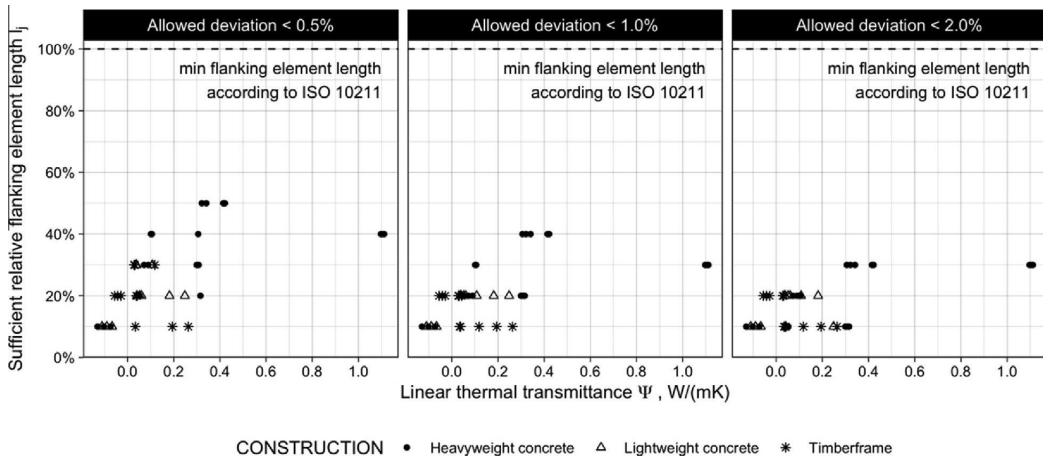
Fig. 10. Minimal relative length of flanking elements in all assessed junctions that keep deviation of linear thermal transmittance below 0.5% (left), 1.0% (middle) or 2.0% (right) compared to ISO 10211 reference case depending on linear thermal transmittance of the junction.

Table 4
Reduction in number of thermal bridges considering shorter flanking element length.

	Allowed relative deviation	Office building	Detached house
Regular thermal bridges	According to ISO 10211	11	8
Combined thermal bridges	According to ISO 10211	73	26
	<0.5%	34	14
	<1.0%	28	10
	<2.0%	19	9

allows separate assessment of combined thermal bridges if these are more than the thickness of the building element apart from each other [24].

4. Conclusion

A large number of different thermal bridges in lightweight and heavyweight constructions were numerically assessed in this paper to propose a way to simplify the procedure to combine linear thermal transmittances of separate simple junctions, such as window connection to intermediate ceiling, ground floor slab and several short wall segments in between. The results show that in the case of a well insulated building envelope, the sufficient length of the flanking element to adequately describe the linear thermal transmittance in a steady state situation, is equal to approximately its thickness. Compared to ISO 10211 requirements, this makes it possible to reduce the amount of different complex thermal bridges from between 35% and 76%, depending on the allowed deviations in the range of 0.5% to 2.0%, thus significantly reducing the working hours of practitioners.

The results of this study can be used as input to further research on this topic to generate a generalized set of requirements for a future version of ISO 10211 and provide a more detailed workflow for the assessment of combined thermal bridges in steady state calculations.

Author Contributions

The conceptualisation of this study, project administration and funding acquisition for the tasks carried out was performed by T.K., compilation of methodology by J.H and T.K., preparation of calcula-

tion models and numerical calculations by J.H. Data visualisation and original draft preparation by J.H., review and editing by J.H. and T.K.

Declaration of Competing Interest

The authors declare that they have no known competing financial interests or personal relationships that could have appeared to influence the work reported in this paper.

References

[1] H. Ge, F. Baba, Dynamic effect of thermal bridges on the energy performance of a low-rise residential building, Energy Build. 105 (2015) 106–118, https://doi.org/10.1016/j.enbuild.2015.07.023.

[2] H. Erhorn, H. Erhorn-Kluttig, M. Citterio, M. Cocco, D. Van Orshoven, A. Tilmans, P. Schild, P. Bloem, K.E. Thomsen, J. Rose, An effective Handling of Thermal Bridges in the EPBD Context, (2010). www.asiepi.eu.

[3] CEN committee ISO/TC 163/SC, ISO 10211:2017 Thermal bridges in building construction. Heat flows and surface temperatures. Detailed calculations, 2017. https://www.iso.org/standard/65710.html.

[4] CEN committee ISO/TC 163/SC 2, ISO 13790:2008 Energy performance of buildings − Calculation of energy use for space heating and cooling, 2008.

[5] S. Bergero, A. Chiari, The influence of thermal bridge calculation method on the building energy need: a case study, Energy Procedia. 148 (2018) 1042–1049, https://doi.org/10.1016/J.EGYPRO.2018.08.056.

[6] T. Theodosiou, K. Tsikaloudaki, K. Kontoleon, C. Giarma, Assessing the accuracy of predictive thermal bridge heat flow methodologies, Renew. Sustain. Energy Rev. 136 (2021), https://doi.org/10.1016/j.rser.2020.110437 110437.

[7] T.G. Theodosiou, A.M. Papadopoulos, The impact of thermal bridges on the energy demand of buildings with double brick wall constructions, Energy Build. 40 (11) (2008) 2083–2089, https://doi.org/10.1016/j.enbuild.2008.06.006.

[8] CEN committee ISO/TC 163/SC 2, ISO 14683:2017 Thermal bridges in building construction — Linear thermal transmittance — Simplified methods and default values, 2017.

[9] K. Kalbe, T. Kalamees, Influence of Window Details on the Energy Performance of an nZEB, J. Sustain. Archit. Civ. Eng. 1 (2019) 61–70, https://doi.org/10.5755/j01.sace.24.1.22052.

[10] J. Adamus, M. Pomada, Analysis of heat flow in composite structures used in window installation, Compos. Struct. 202 (2018) 127–135, https://doi.org/10.1016/j.compstruct.2017.12.077.

[11] F. Cappelletti, A. Gasparella, P. Romagnoni, P. Baggio, Analysis of the influence of installation thermal bridges on windows performance: The case of clay block walls, Energy Build. 43 (6) (2011) 1435–1442, https://doi.org/10.1016/j.enbuild.2011.02.004.

[12] H. Viot, A. Sempey, M. Pauly, L. Mora, Comparison of different methods for calculating thermal bridges: Application to wood-frame buildings, Build. Environ. 93 (2015) 339–348, https://doi.org/10.1016/j.buildenv.2015.07.017.

[13] S.J. Chang, S. Wi, S. Kim, Thermal bridging analysis of connections in cross-laminated timber buildings based on ISO 10211, Constr. Build. Mater. 213 (2019) 709–722, https://doi.org/10.1016/J.CONBUILDMAT.2019.04.009.

[14] A.B. Larbi, Statistical modelling of heat transfer for thermal bridges of buildings, Energy Build. 37 (9) (2005) 945–951, https://doi.org/10.1016/j.enbuild.2004.12.013.

[15] A. Capozzoli, A. Gorrino, V. Corrado, A building thermal bridges sensitivity analysis, Appl. Energy. 107 (2013) 229–243, https://doi.org/10.1016/j.apenergy.2013.02.045.

[16] D. Borelli, P. Cavalletti, A. Marchitto, C. Schenone, A comprehensive study devoted to determine linear thermal bridges transmittance in existing buildings, Energy Build. 224 (2020), https://doi.org/10.1016/j.enbuild.2020.110136 110136.

[17] K. Martin, C. Escudero, A. Erkoreka, I. Flores, J.M. Sala, Equivalent wall method for dynamic characterisation of thermal bridges, Energy Build. 55 (2012) 704–714, https://doi.org/10.1016/j.enbuild.2012.08.024.

[18] J. Quinten, V. Feldheim, Mixed equivalent wall method for dynamic modelling of thermal bridges: Application to 2-D details of building envelope, Energy Build. 183 (2019) 697–712, https://doi.org/10.1016/J.ENBUILD.2018.11.004.

[19] Lawrence Berkley National Laboratory, Therm, (2020).

[20] , Building Physics Analyses and Isokorb Specifications (2012). https://www.laros.com.au/wp-content/uploads/2017/03/LAROS-Schöck-Isokorb-BuildingPhysicsReportNo1_Mar12.pdf.

[21] C.-E. Hagentoft, Heat loss to the ground from a building : slab on the ground and cellar, Byggnadsfysik LTH, Lunds Tekniska Högskola, 1988, https://lup.lub.lu.se/search/ws/files/4896022/8056211.pdf.

[22] J. Quinten, V. Feldheim, Dynamic modelling of multidimensional thermal bridges in building envelopes: Review of existing methods, application and new mixed method, Energy Build. 110 (2016) 284–293, https://doi.org/10.1016/j.enbuild.2015.11.003.

[23] M. O'Grady, A.A. Lechowska, A.M. Harte, Application of infrared thermography technique to the thermal assessment of multiple thermal bridges and windows, Energy Build. 168 (2018) 347–362, https://doi.org/10.1016/J.ENBUILD.2018.03.034.

[24] T. Ward, G. Hannah, C. Sanders, Conventions for Calculating Linear Thermal Transmittance and Temperature Factors: (br 497), IHS BRE Press, 2016.

PUBLICATION V

V

Hallik, J.; Klõšeiko, P.; Piir, R.; Kalamees, T. (2022). Numerical analysis of additional heat loss induced by air cavities between insulation boards due to non-ideality. (Under review, submitted to: Journal of Building Engineering 06.04.2022)

Article

Numerical analysis of additional heat loss induced by air cavities between insulation boards due to non-ideality

Jaanus Hallik [1, 2,]*, Paul Klõšeiko [1], Reimo Piir [1], Targo Kalamees [2, 1]

[1]   nZEB Research Group, Department of Civil Engineering and Architecture, Tallinn University of Technology

[2]   Smart City Center of Excellence (Finest Twins), Tallinn University of Technology

*   Correspondence: jaanus.hallik@taltech.ee

Abstract: This study uses the numerical steady-state three-dimensional CFD calculation method to assess parametrically the thermal transmittance of a building envelope with partially and fully penetrating air cavities within 20cm thick layer of insulation. Heat flux measurements from climate chamber experiment were used to validate numerical model and estimated heat flux at different height of penetrating air cavity. Focus is on the effect of different cavity geometry and cavity location within a building envelope, including the effect of temperature difference across the building envelope. Fully penetrating horizontal air cavities in the wall construction and vertical air cavities inside the floor construction were found to have an insignificant effect on thermal transmittance. The vertical air cavities in the wall and the roof construction significantly increase the convective heat transfer through the insulation layer, well over the normative correction levels defined by EN ISO 6946. The effect is strongly dependent on the temperature difference and cavity thickness. At 40 K temperature difference, the penetrating air cavities with 5, 10 and 20 mm thickness will increase the thermal transmittance up to 10, 33 and 59% respectively; the simplified procedure in EN ISO 6946 was unable to describe this effect adequately. For an upward heat flow in the roof construction, the effect was even more adverse. Using dual layer insulation with rebate, tongue and groove edge or expanding montage foam to tighten the external side of the air cavity, additional heat loss is reduced roughly by half and the dependency of additional heat loss on the temperature difference between internal and external environments is decreased.

Keywords: *air voids, air cavities, natural convection, thermal transmittance, heat loss, insulation*

1. Introduction

A well-insulated, airtight, and thermal bridge free building envelope is a key factor to minimize the heat loss in energy efficient buildings. The planning process of nearly zero energy buildings (nZEB) includes careful optimization and detailed assessment of heat loss through insulation layers; however, the quality of workmanship on the construction site can have significant effect on the actual performance of a well-insulated building envelope. One specific issue with rigid insulation boards, such as many common external thermal insulation composite systems (ETICS), is the irregular air voids and cavities caused by the varying

tolerances of the boards during the production process, on-site cutting and assembling as well as due to poor workmanship, especially in the case of more complex building geometry. These air cavities inside an insulation layer can vary in size, shape and may lack filling or tightening with montage foam or similar agent. Depending on the product classification according to EN 13163 [1] and EN 825 [2] regarding the production quality, the allowed tolerances of board width and length are up to 5 mm and of board squareness up to 1, 2 and 5 mm/m, which in the worst case can lead up to 15 mm wide cavity where 3 m long insulation boards are installed vertically, corresponding to the full building floor height of approx. 3 m. Similar issues with manufacturing tolerances occur in the case of mineral wool boards. A study in Lithuania looked at dual density rockwool boards whereas their allowed deviations in the manufacturing process related to observed deviations in the roof construction and deviation in the board length were up to 20 mm and board width up to 5 mm. A deviation from squareness according to the width and the length up to 3 mm/m was observed [3]. The width of actual vertical air cavities forming due to these deviations was up to 5 mm [3]. When an insulation layer is installed between timber or steel battens, additional cavities can occur due to non-ideal cutting and placement of insulation material.

Additionally, the expanded polystyrene (EPS) is prone to shrinkage due to aging as well as thermal expansion and contraction [4]. The alternating heating and cooling cycles cause changes in the cavity width between boards with increasing permanent deformation [4,5]. Altogether, the heat loss through a building envelope featuring all the irregularities of that kind is higher due to radiation and natural convection that occur inside these cavities and is highly dependent on cavity dimensions as well as the temperature difference between internal and external environment.

There have been several empirical studies that give insight into the approximate effect of penetrating cavities inside insulation layers. In 1972, in the first study conducted in Sweden, heat flow plates were used to test a change in local thermal resistance caused by penetrating cavities with 5, 10 and 30 mm width within an insulation layer; although the study concentrated mainly on natural convection inside the insulation material itself, the overall effect of air cavities on the thermal transmittance was not quantified [6]. Under the heat flow plate, the thermal resistance decreased up to 8% at a 5 mm wide cavity, up to 21% at a 10 mm wide cavity, and up to 64% at a 30 mm wide cavity locally [6]. Although the effect on the entire wall area with lower fraction of cavities will be significantly lower, the study showed that natural convection inside that kind of air cavities can have a significant impact on the thermal transmittance that depends strongly on the cavity width.

Similarly, it has been shown through field measurements in Great Britain that differently sized and shaped air cavities caused by poor workmanship can increase the observed thermal transmittance by a factor of two [7–9] and the effect is strongly dependent on actual observed non-idealities and their distribution.

In another study in Finland [10], hot-box measurements were used to study the natural convection inside the exterior wall with air-permeable insulation and to assess the effect of horizontal cavities within an insulation layer caused by material displacement after installation or by non-ideal workmanship, resulting in the rounded edges of insulation wool batts that form vertical air cavities between the edge of the insulation wool batt and the structural timber element. It was reported that negligent installation of insulation wool can cause horizontal air cavities at the upper or lower edges of the wall insulation layer and in the case of wet-sprayed cellulose insulation, these may be formed due to creep of the material [10]. Contrary to previous studies, it was concluded that air cavities formed due to poor

workmanship do not dramatically increase (observed increase 5% to 10%) the thermal transmittance at no provision of air circulation from hot side to cold side, which refers to rounded edges of wool batts [10]. The effect of creeps at the edge of wet-sprayed cellulose, which enables air circulation between hot and cold side, showed significantly greater effect [10], up to 34% increase in the thermal transmittance calculated according to EN ISO 6946 [11]. However, the dimensions of the air cavities and their effect compared to standardized installation quality levels were not quantified and the current study seeks to solve this problem.

Our study uses numerical simulation tools of computational fluid dynamics (CFD) to parametrically assess the additional heat loss caused by natural convection and radiation inside air cavities with different cavity width, geometry, and location in a well-insulated building envelope. The hypothesis of the study is that for a well-insulated structure, the simplified method described in EN ISO 6946, annex F [11], underestimates the effect of cavities on actual thermal transmittance and the additional heat loss is highly dependent on the temperature difference between internal and external environments. The aim of the study is to quantify the effect of different air cavities with different width and geometry on the thermal transmittance depending on the temperature difference as well as to describe the cavity types and geometries with respective dimensions that correspond to simplified correction factors assigned to each installation level given in EN ISO 6946 [11].

2. Material and methods

2.1. Observed cavity widths in practice

In order to select typical cavity types, widths and locations for further analysis, hundreds of photos taken on building sites and in prefabrication factories were qualitatively assessed. The most typical situations selected are presented in the results section for each main construction type.

2.2. Experimental study in climate chamber

To validate the numerical CFD model a measurement data from a climate chamber experiment was used to gather temperature and heat flux data with penetrating cavity with 10mm thickness. The test-wall incorporated 200 mm thick insulation boards with thermal conductivity of 0.019 W/(m2K) and 0.3 mm thick duct tape covering used to seal the cavities between insulation boards and to form a closed space. Interior and exterior temperatures along with interior surface heat flux was measured at cavity location as well as at one reference point away from the joints corresponding to one-dimensional situation using following sensors and loggers:

- Temperature sensor Onset Hobo TMC20-HD (accuracy ±0.15°C) fastened using tape and hot glue with logger UX120-006M
- Heat flux plate greenTEG gSKIN-XP (accuracy ±3%) fastened using thermal paste and tape with logger Grant Squirrel SQ2020 1F8
- Heat flux plate Hukseflux HFP03 (accuracy ±6%) fastened using thermal paste with logger Grant Squirrel SQ2020 1F8 for PIR 1D conductivity measurements
- Temperature sensor Pico PT100 1/10 DIN (accuracy ±0.03°C) with logger Pico PT-104 for calibration of the Onset temperature sensors
- Temperature sensor Siemens QFA3171 (accuracy ±0.6°C) built-in to the climate chamber for boundary condition measurements

The temperature and heat flux measurements were taken at central plane of penetrating cavity at different heights measured from bottom of the cavity. Heat flux values were recorded at 20 mm, 100 mm, 800 mm, 2110 mm and 2360 mm height. Exterior chamber temperatures ranged from -30 °C to +10 °C (with 10 °C intervals), interior chamber temperature was set at +20 °C. Measurement results were averaged over periods of stable ambient temperatures for analysis. The scheme of experimental setup is shown in *Figure 1*.
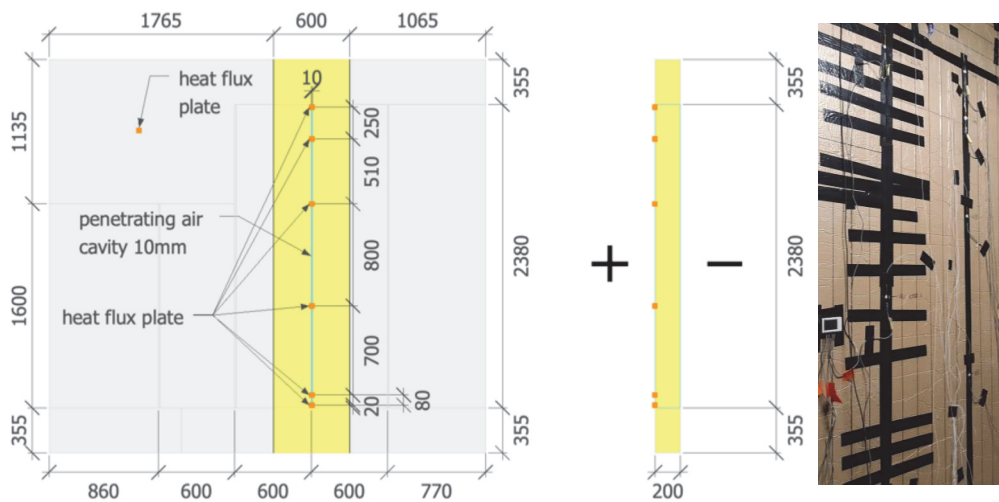
Figure 1. View of test wall – sensor placement on internal chamber side (left); cross-section of test wall (middle); photo of test wall (right)

The measurements regarding the air cavity with metal diagonal tie and additional filling with mineral wool, foam tape and PU foam were part of study related to thermal bridge effects of vertical diagonal tie connectors in precast concrete sandwich panels and are published in *Klõšeiko et. al 2020* [12].

2.3. Simplified thermal transmittance correction (EN ISO 6946)

European standard EN ISO 6946 [11] describes a simplified method to account for the effect of air cavities within an insulation layer. Three levels of installation quality are defined with appropriate correction factors $\Delta U''$ with values of 0.00 W/(m²·K), 0.01 W/(m²·K) and 0.04 W/(m²·K) for installation level 0 (IL 0), 1 (IL 1) and 2 (IL 2). These correction factors are used to calculate the correction term for air cavities ΔU_g (equation 1).

$$\Delta U_g = \Delta U'' \cdot \left(\frac{R_1}{R_{tot}}\right)^2 \tag{1}$$

where

R_1 *is the thermal resistance of the layer containing the cavities, (m²·K)/W;*

R_{tot} *is the total thermal resistance of the component ignoring any thermal bridging (thermally homogeneous building envelope), (m²·K)/W;*

$\Delta U''$ *is the correction factor based on the level of insulation installation quality, W/(m²·K).*

166   The correction term is then used to estimate the corrected thermal transmittance U_c
167 (equation 2) of the building envelope.
168

169    $$U_c = U + \Delta U_g \qquad\qquad (2)$$

170   *where*
171   U *is the thermal transmittance of a component ignoring any air cavities and*
172 *thermal bridging, W/(m²·K);*
173   ΔU_g *is the correction term for air cavities in accordance with equation 1, W/(m²·K).*
174

175   It is difficult to implement this simplified method correctly in real life conditions as the
176 descriptions given for each installation level are limited in detail, have changed in different
177 redactions of the same standard and do not quantify the amount and location of air cavities.
178 For example, depending on the width of the installed insulation panels, the recurring distance
179 between the penetrating air cavities differs and therefore also the average length per unitary
180 envelope area is different. Additionally, the convective heat flow inside penetrating cavities
181 is caused by buoyancy-driven air flow, but it is not clearly described if and in which range of
182 temperature differences this flow is accounted for in tabulated correction factors.
183   In our study, the numerical modelling is used to calculate detailed values for
184 correction factors $\Delta U''$ depending on the temperature difference, thermal transmittance of
185 the penetrated insulation material as well as the geometric characteristics of the assessed air
186 cavities.

2.4. Description of geometric models
188   We used a simplified construction type of a single insulation layer with a thickness of
189 200 mm for the assessment with alternative thermal conductivity of 0.019 W/(m·K),
190 0.031 W/(m·K) and 0.040 W/(m·K), corresponding to the typical range of insulation materials
191 used in nZEBs. The numerical domain is 600 mm wide, corresponding to the typical ETICS
192 panel and 3110 mm long, corresponding to the full storey height of a building (*Figure 2*). The
193 numerical domain encloses one cavity between insulation boards along the length of the
194 domain and symmetric to cut-off planes, corresponding to an average cavity length-to-area
195 ratio of 1.67 m/m². The dimensions of numerical domain for the roof and floor construction
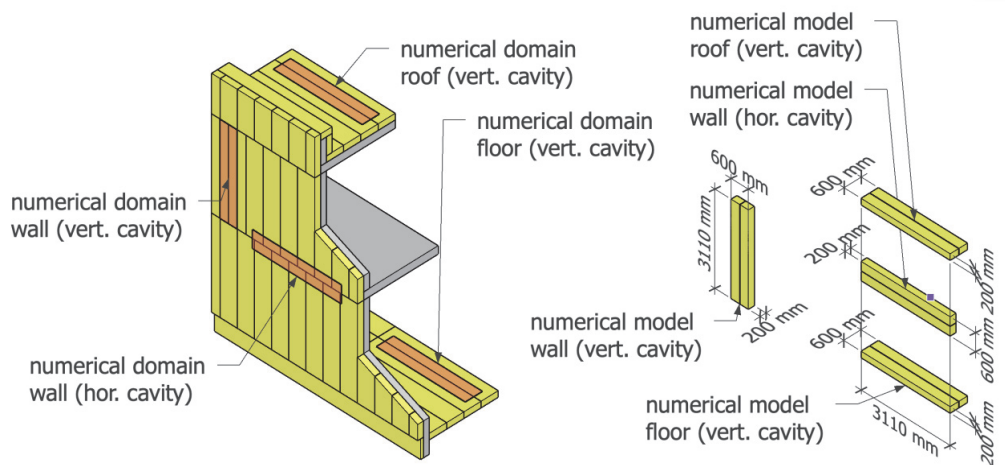196 were kept the same for comparative purposes.

197
198   *Figure 2. Location of numerical domains and respective calculation models with dimensions.*

200   The thermal transmittance of this building component without the effect of thermal
201 bridging and air cavities corresponding to ISO 6946 installation level 0 is $U_{c0} = 0.194$ W/(m²·K)
202 for the thermal conductivity of 0.040 W/(m·K). The simplified normative method suggests
203 corrected thermal transmittance $U_{c1} = 0.203$ W/(m²·K) and $U_{c2} = 0.231$ W/(m²·K) respectively
204 for installation levels 1 and 2 with the same insulation material. For the thermal conductivity
205 of 0.031 W/(m·K), $U_{c0} = 0.151$ W/(m²·K), $U_{c1} = 0.161$ W/(m²·K) and $U_{c2} = 0.189$ W/(m²·K) and
206 for the thermal conductivity of 0.019 W/(m·K), $U_{c0} = 0.094$ W/(m²·K), $U_{c1} = 0.103$ W/(m²·K),
207 and $U_{c2} = 0.132$ W/(m²·K) respectively.
208   For each location in the building envelope, the CFD analysis was carried out on five
209 main types of potential air cavities, as seen in *Figure 3*, totalling 483 numerical models:
210   a) Penetrating cavity with rectangular cross-section
211   b) Rectangular cavity filled by PU foam (50 mm) from external side
212   c) Cavities on 2-layer insulation with rebate, tongue and groove edge
213   d) Penetrating cavity with wedge shaped cross-section
214   e) Penetrating cavity with additional triangular cut-outs
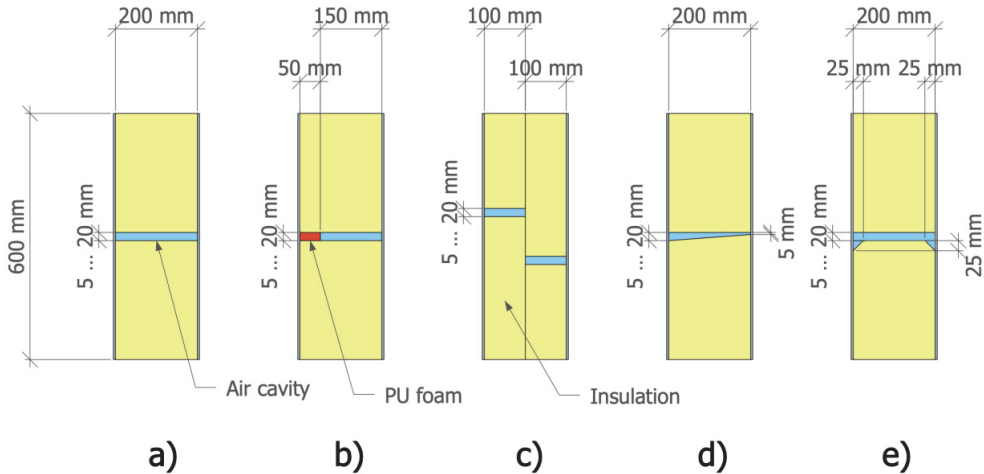
215
216 *Figure 3. Assessed geometric cases of different cavities.*

217   *2.5. CFD analysis*

218   We used the numerical parametric steady-state three-dimensional CFD calculation
219 (ANSYS® Fluent Academic Student 2021 R2 [13]) to assess the effect of radiation and gravity
220 induced natural convection on heat and particle transfer inside cavities between rigid
221 insulation boards and within the insulation material.
222   The calculation model with 10 mm penetrating air cavity with uniform cross-section
223 was validated with climate chamber measurements described in more detail in our previous
224 study [12]. The thermal resistances $R_{si} = 0.08$ (m²·K)/W and $R_{se} = 0.08$ (m²·K)/W for all
225 calculations were defined according to the values measured in that study. Incompressible
226 ideal gas and laminar flow was assumed for each calculation.
227   The models were set up with adaptive computational mesh with very fine element
228 size inside the air cavity and its vicinity and coarser elements near the cut-off surfaces (*Figure*
229 *4*) of the model as the number of finite elements was limited by the used software package.
230 Convergence criterion defined in EN ISO 10211 [14] was used to limit the number of

iterations, i.e., the sum of all heat flows entering the object, divided by half the sum of the absolute values of all heat flows, shall be less than 0.0001. Continuity, velocity and energy absolute residual criteria were set to ≤ 10E-6.
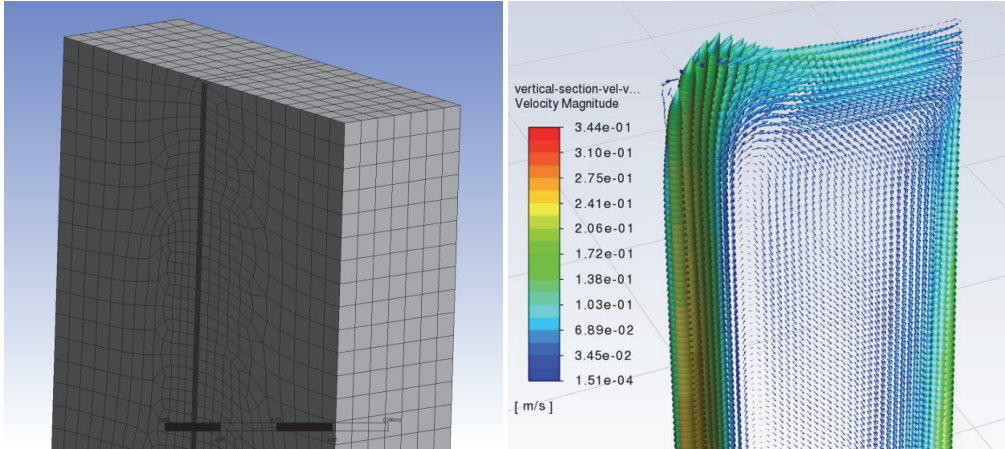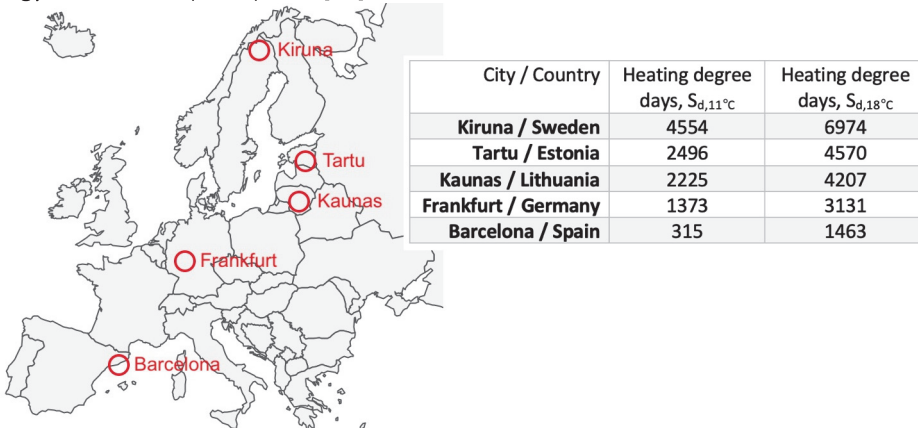

Figure 4. An example of adaptive computational mesh and calculated air velocities inside penetrating air cavity. Screenshots courtesy of ANSYS, Inc.

The sum of all heat flows entering the object was then divided by the reference area of the geometric model to quantify respective heat flux for each assessed case. The heat flux was then divided by the temperature difference used between opposite boundary conditions to quantify corrected thermal transmittance U_{CFD} for each case and calculate the correction factor ΔU_g by subtracting the nominal thermal transmittance U_{c0} without air cavities.

2.6. Calculation of heat loss in different climate conditions

As the increase in the thermal transmittance of a building envelope due to natural convection inside penetrating air cavities is strongly related to the temperature difference, the effect on overall heat loss of the building envelope is different in different climates. To assess this difference, a simplified heat loss calculation utilizing heating degree days was used for five different locations across Europe, as shown in *Figure 5*. For Estonian climate (Tartu), hourly temperature data from national test reference year for energy calculations were used [15], for all other locations, hourly temperature data from ASHRAE International Weather for Energy Calculations (IWEC) data [16] were used.

City / Country	Heating degree days, $S_{d,11°C}$	Heating degree days, $S_{d,18°C}$
Kiruna / Sweden	4554	6974
Tartu / Estonia	2496	4570
Kaunas / Lithuania	2225	4207
Frankfurt / Germany	1373	3131
Barcelona / Spain	315	1463

Figure 5. Locations with different heating degree days on a typical year used for the
253 *assessment.*
254   For each assessed cavity type and insulation combination, a linear regression was used
255 to retrieve slope and intercept for the numerically derived relationship between U_{CFD} and the
256 temperature difference in the range of 10 K to 40 K. Based on regression parameters, the
257 temperature dependent thermal transmittance U_{Ch} was calculated for each hour of the typical
258 year and respective heat loss through the unitary area of the building envelope was
259 accumulated for all hours where exterior temperature is below thermal balance point
260 according to equation 3. The thermal balance point was defined at 11 °C corresponding to 10
261 K below the interior temperature of 21 °C.

262

263 $$Q_H = 0.001 \cdot \sum(\Theta_i - 10 - \Theta_e) \cdot U_{Ch} \text{ if } \Theta_e < (\Theta_i - 10) \qquad\qquad (3)$$

264   *where*
265   Q_H *annual heat loss through 1 m^2 of building envelope, kWh/(m²·a);*
266   Θ_i *interior temperature, °C;*
267   Θ_e *exterior temperature, °C;*
268   U_{Ch} *variable thermal transmittance of the building envelope depending on the*
269 *temperature difference between interior and exterior temperatures W/(m²·a).*

3. Results

3.1. Installation conditions

272   Based on observations, typical situations for different kinds of insulation materials and
273 construction types are presented in *Figure 6*, *Figure 8* and *Figure 9* to show ideal workmanship
274 compared to typical non-idealities commonly found in construction sites or in prefabrications.
275

276 *Figure 6. Ideal workmanship (left) and typical non-idealities (right) for a timber framed*
277 *construction with mineral wool insulation batts.*

Most typical non-idealities in the case of wool insulation batts with a lightweight timber frame construction are rounded corners that form when a slightly wider insulation batt is tucked between the timber frames. According to previous research, when the formed cavity is not penetrating the entire layer and does not enable air circulation between warm and cold side, the effect on measured thermal transmittance is not high, corresponding to an increase of 5 to 10% at the 35 K temperature difference [10]. If the air circulation between warm and cold side is enabled, the effect increases by a factor of 2 or more. Other non-idealities associated with wool insulation solutions, such as shown in *Figure 7*, are not typical and should be classified as defective work. The effect of that kind of cavities is not covered by EN ISO 6946 and not assessed in this study.

Figure 7. Non-acceptable installation of mineral wool insulation batts in timber framed construction.

An example of non-idealities for rigid insulation boards used in an ETICS system on masonry or a similar structural layer contains vertical and horizontal cavities that will occur due to several factors. Smaller cavity widths up to 5 to 10 mm can be caused by material shrinkage through aging or cycling exposure to high temperatures in dark coloured facades or roof construction or by squareness tolerances of the insulation boards. Wider cavities are typically caused by poor workmanship as well as in the case of complex building envelope with curved or otherwise non-uniform geometry when insulation boards must be precisely cut to a specific size on the building site. It is recommended to use the polyurethane (PU) foam to fill the cavities between the rigid insulation boards during the installation (*Figure 8* left), but this is often omitted in practice (*Figure 8* right). The most typical non-ideality observed on-site occurs within a wall insulation layer where up to 10 mm wide vertical cavities between insulation boards are not filled with foam running along with full floor height.

Figure 8. Ideal workmanship (left) and typical non-idealities (right) for rigid insulation boards of walls (above) and roof (below).

When PU foam is used to close these cavities, it is not technically possible to fill the entire cavity in a well-insulated building envelope. The nozzle of the foam gun does not fit properly into thinner cavities and due to a thicker insulation layer, only a small external part of the cavity can be filled. According to montage foam manufacturers, the polyurethane foam applied through the nozzle to the cavity between insulation boards can fill approximately 50 mm deep outermost part of the cavity if the cavity width is below 20 mm. A typical penetrating air cavity formed due to cyclic thermal expansion and shrinkage is shown in *Figure 9.*

Figure 9. Penetrating air cavity formed due to aging and cyclic thermal expansion and shrinkage in the roof insulation layer.

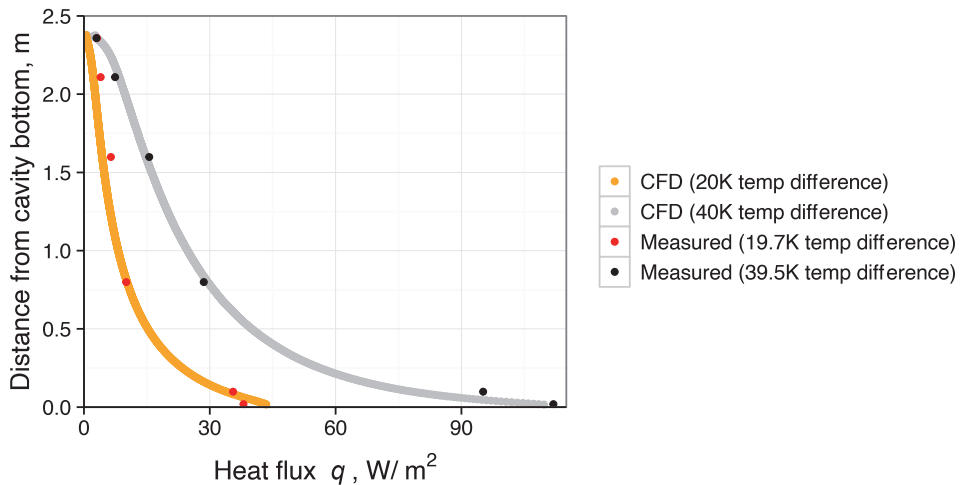The measured heat fluxes are given in Table 1. The heat flux at the top of the penetrating cavity is small but increases significantly towards the lower part of the cavity. Due to natural convection occurring inside the penetrating cavity the cooling air moves downwards at external side of the cavity and creates large temperature gradient on the bottom end corresponding to maximum measured heat flux. The heat flux on the bottom part of the cavity depends significantly on the temperature difference between internal and external environments. In the case of approximately 10K temperature difference the maximum heat flux was 16.1 W/m^2 while in the case of approximately 50K temperature difference the maximum heat flux increased up to 151.2 W/m^2.

Table 1. Average measured heat fluxes through penetrating air cavity between insulation boards.

Temperature difference, K	Measured average heat flux at different height from bottom of cavity, W/m^2					
	at 20mm	at 100mm	at 800mm	at 1600mm	at 2110mm	at 2360mm
9.8	16.1	14.0	3.5	2.8	2.1	2.6
19.7	38.0	35.6	10.1	6.4	4.0	3.1
29.5	61.6	59.5	18.8	10.9	6.1	4.0
39.5	111.9	95.2	28.6	15.5	7.4	3.0
49.3	151.2	122.2	35.9	19.0	8.6	2.6

The experimental and computational heat fluxes through the penetrating air cavities of the test wall were found to be in relatively good agreement as shown on *Figure 10*.

Figure 10. Comparison of simulated and measured interior surface heat fluxes at different heights of the penetrating air cavity at 20 K and 40 K ambient temperature difference.

3.3. Convective heat loss of penetrating air cavities

The results from numerical models show that the heat loss through penetrating air cavity within the insulation layer is strongly dependent on the temperature difference across the building envelope. *Figure 11* shows the numerically derived thermal transmittance U_{CFD} for a wall, roof, and floor construction with 200 mm of insulation with the thermal conductivity of 0.040 W/(mK), including the effect of 5, 10 and 20 mm penetrating rectangular air cavity.
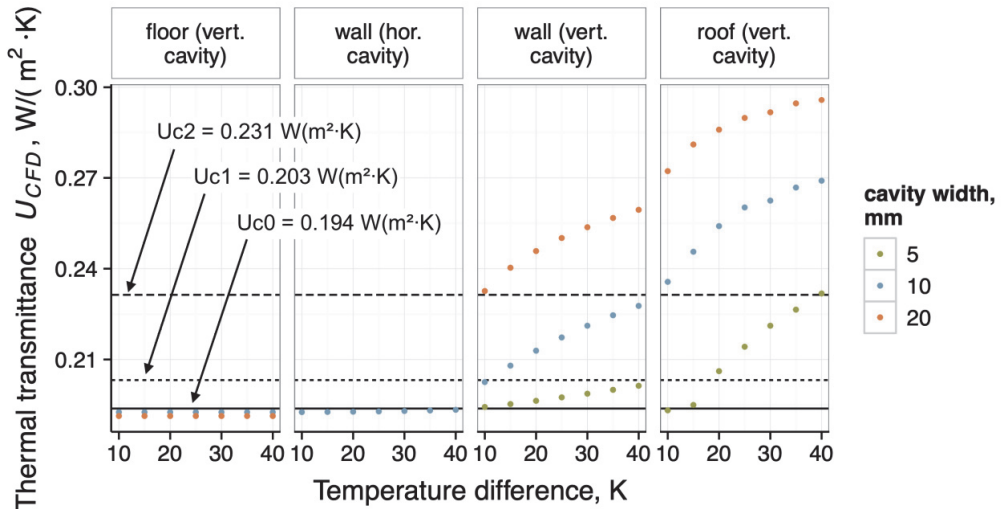

Figure 11. Corrected thermal transmittance U_{CFD} of a building envelope (insulation thermal conductivity 0.040 W/(m²·K)) incorporating the effect of air cavities depending on the temperature difference and penetrating cavity width and location.

The results from numerical models show that penetrating vertical air cavities inside the floor construction and horizontal air cavities in the wall construction have no significant effect on the thermal transmittance, but in the case of vertical air cavity inside the wall and the roof construction, the convective heat flow inside the cavity increases the corrected thermal transmittance U_{CFD} well over normative correction level at higher temperature differences. At 40 K temperature difference and 20 mm vertical cavity width, the corrected thermal transmittance is U_{CFD} = 0.296 W/(m²·K) for the roof construction and U_{CFD} = 0.259 W/(m²·K) for the wall construction, which corresponds to 53% and 34% increase in respective thermal transmittances.

In favour of better comparison, the correction factors $\Delta U''$ for the thermal transmittance instead of corrected thermal transmittances were derived from the numerical models for penetrating air cavities in different locations and are given in *Figure 12* depending on the cavity width, insulation material and temperature difference across the entire building envelope.
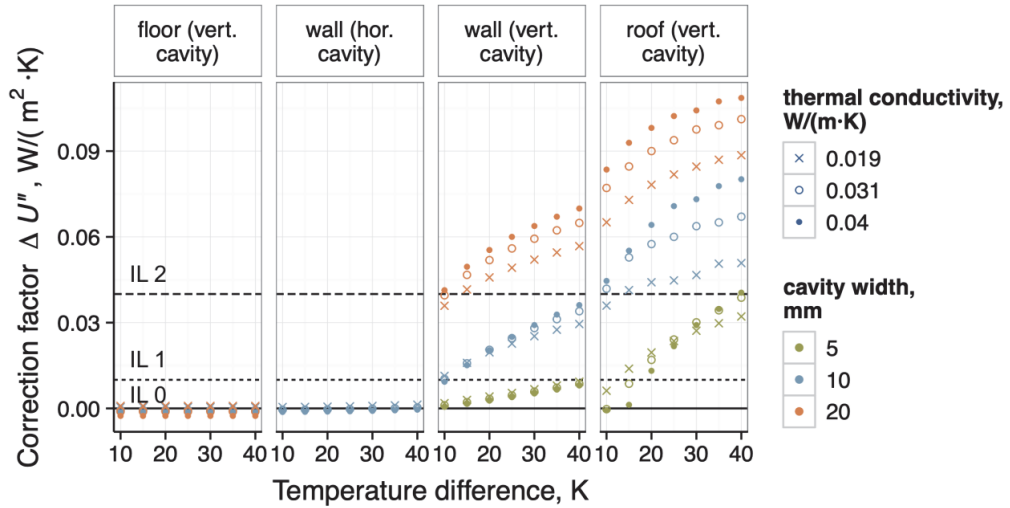
Figure 12. Correction factor of air cavities ΔU'' depending on the temperature difference, the thermal conductivity of insulation layer and penetrating cavity width and location.

It can be seen from *Figure 12* that horizontal penetrating cavities within the wall insulation layer do not affect the thermal conductivity of the wall because the convective air flow between warm internal and cold external side is not taking place due to very small height of the air cavity. In the case of insulation material with higher thermal conductivity, the air cavity even slightly decreases the heat loss due to the lower thermal conductivity of still air. A similar situation can be seen with vertical air cavity in the floor construction, where thermal stratification takes place between warm boundary on the top and cold boundary at the bottom and convective air flow is not possible. Similar to horizontal air cavity, the still air with lower thermal conductivity decreases the heat loss in cases with inferior insulation materials.

In the case of vertical air cavities within a wall insulation layer, the convective heat flow is strongly dependent on the temperature difference and cavity width. At the 10 K temperature difference, the correction factor $\Delta U''$ was similar to simplified values according to EN ISO 6946 [11] but increased from 0.002 to 0.010 W/(m²·K) for 5 mm and from 0.010 to 0.035 W/(m²·K) for 10 mm wide air cavities at the 40 K temperature difference, corresponding approximately to one level of increase in the installation level. For a wider cavity, the correction factor increases from 0.040 up to 0.070 W/(m²·K) and at the 40 K temperature difference, is well over maximum correction level proposed by EN ISO 6946. The increase of the thermal transmittance due to a higher temperature difference is higher in the roof construction for all assessed cases with the correction factor $\Delta U''$ value over 0.1 W/(m²·K) in a worst case. The simplified procedure defined in EN ISO 6946 [11] is unable to describe this for any of the cases with a cavity of >5 mm.

The effect of the insulation material is small for cavity widths of 5 and 10 mm. For wider cavities (20 mm), the heat loss increases with the increase in the thermal conductivity. This effect is more prominent in vertical cavities inside the roof construction.

3.4. The effect of air cavities at dual layer insulation with rebate edge or partial filling with PU foam

400   Additionally, the cases with non-penetrating cavities were assessed to see if the effect
401   on the thermal transmittance is significantly lower when the air circulation between internal
402
403   and external boundaries is prevented by partial filling with PU foam or with the use of dual
404   layer insulation with rebate edge (*Figure 3*). The results from both geometrics cases in
405   comparison with fully penetrating air cavity are given in *Figure 13*.
406
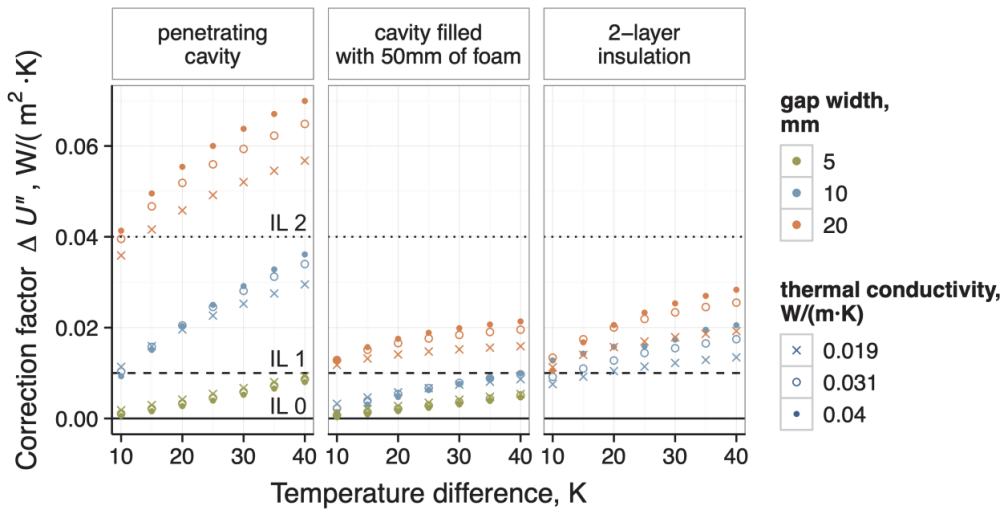
407
408   *Figure 13. Correction factor of air cavities ΔU'' depending on the temperature difference, the*
409   *thermal conductivity of the insulation layer and penetrating cavity width at a dual insulation*
410   *layer or partially foamed cavity.*
411

412   Both alternatives to penetrating air cavity decreased the correction factor $\Delta U''$ by a
413   factor of two or more depending on the temperature difference; however, at the
414   temperature difference of $\Delta t = 35$K, the numerically derived correction factor was above
415   normative installation levels 0 and 1, although both alternatives are listed as level 0
416   installation solution in ISO 6946. Nevertheless, compared to the penetrating cavity, the
417   additional heat loss through these cavities is only slightly depending on the temperature
418   difference across the entire building envelope which is to be expected.
419

3.5. The effect of irregular shape of air cavities

421   Additionally, the effect of an irregular shape (*Figure 3*) of penetrating air cavity on the
422   thermal conductivity was assessed. Cases with wedge-shaped air cavity and cases with
423   additional triangular cut-out at the edges of penetrating air cavity are compared in *Figure 14*.
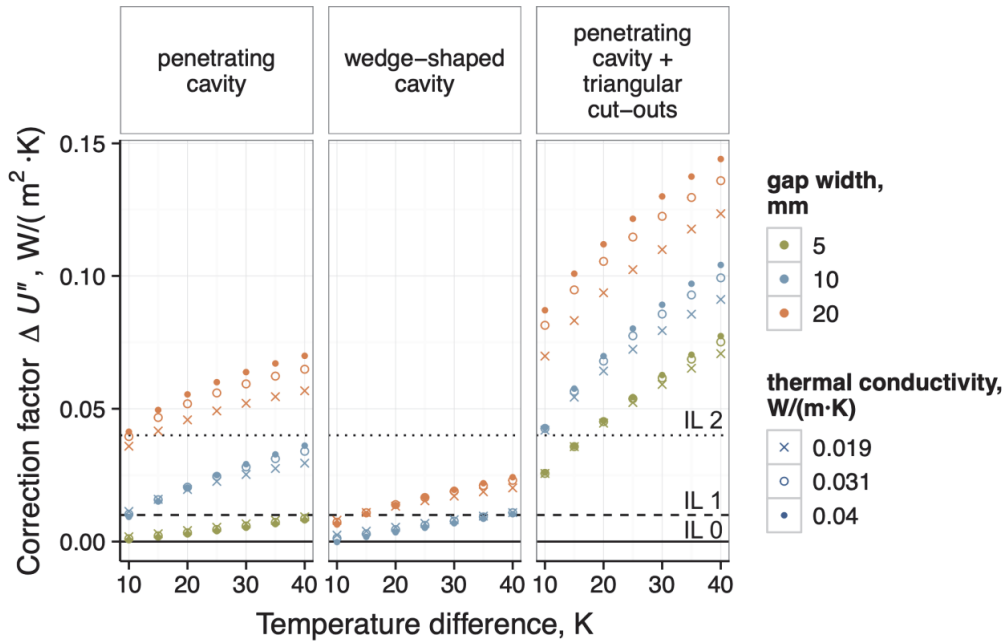424

Figure 14. Correction factor of air cavities ΔU'' depending on the temperature difference, the thermal conductivity of the insulation layer in the case of irregularly shaped cavities.

It can be seen from the figure that if the penetrating air cavity is wedge shaped so that the width decreases perpendicular to the insulation layer down to 5 mm, the additional heat loss is strongly reduced. The effect of the vertical 10 mm cavity in the wall construction is in the range of normative installation level 1 and the effect of the vertical 20 mm cavity well below normative installation level 2 where the correction factor will remain between 0.01 and 0.025 W/(m²·K) in the wall insulation layer. This is roughly reduction by one level compared to a rectangular penetrating air cavity. Compared to the penetrating cavity, the additional heat loss through the wedge-shaped cavity only slightly depends on the temperature difference across the entire building envelope.

If additional triangular cut-outs are added to the penetrating air cavity, the correction factor is increased significantly and for all cases, the additional thermal transmittance is well above normative correction values, suggesting that errors of that kind during installation should be classified as inadequate workmanship.

3.6. Heat loss of a building envelope in different climate conditions

The natural convection and radiation inside assessed air cavities was found to be strongly dependent on the temperature difference between warm and cold side; therefore, the actual increase in the heat loss will vary depending on the location and climate. To account for cumulative temperature differences and their effect on different climates, the heat loss through a wall or roof construction with a unitary area including vertical penetrating air cavity was calculated for five different locations in Europe, including Barcelona (Spain) from Southern Europe, Kiruna (Sweden) from cold Northern Europe and Tartu (Estonia), Kaunas (Lithuania), and Frankfurt (Germany) in between those locations.

453 The linear model was fitted using the results from previous sections for each assessed
454 case, and the intercept along with slope parameter from regression model was used to
455 calculate the corrected thermal transmittance U_{ch} for each hour of the year based on outdoor
456 temperature on a typical year on each location. The estimated heat losses using corrected
457 thermal transmittances in the case of an insulation material with the thermal conductivity of
458 0.019 W/(m·K) are given below as an example.

459
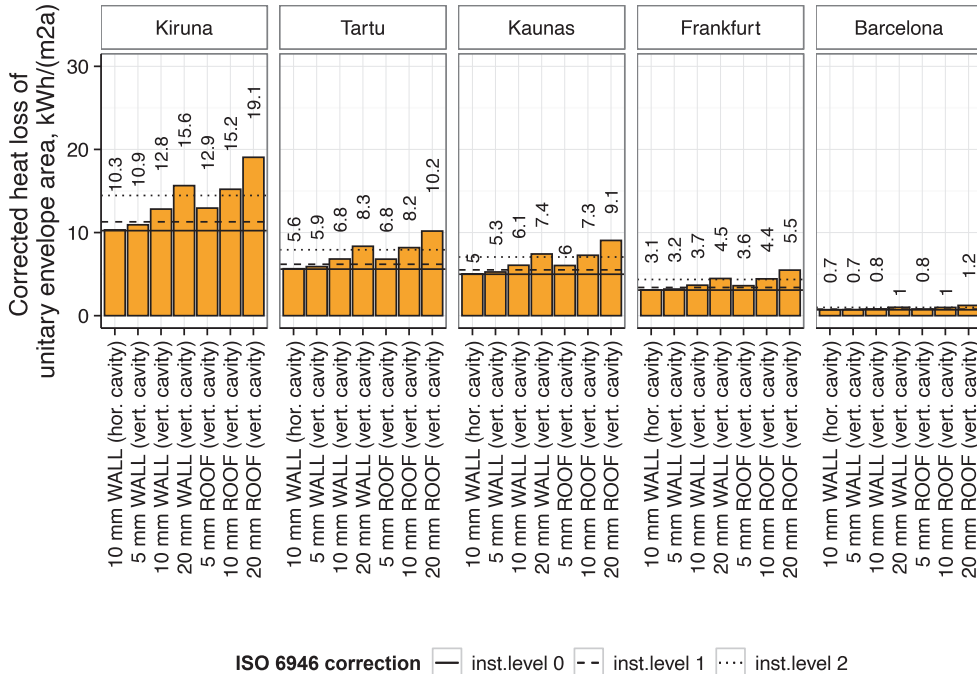
Figure 15. Heat loss of unitary envelope area with vertical penetrating air cavity in different climates depending on the air cavity configuration inside the insulation layer.

It can be seen from *Figure 15* that in Barcelona with warm climate, the difference in the estimated annual heat loss is marginal. For Frankfurt (Germany) and Kaunas (Lithuania), the heat loss through the unitary envelope area is in the range of 3.1 to 9.1 kWh/(m²·a), depending on the air cavity configuration. In Tartu (Estonia), the estimated annual heat loss on a typical year is between 5.6 to 10.2 kWh/(m²·a) and in Northernmost part of Europe, it will be in the range of 10.3 to 19.1 kWh/(m²·a). The relative increase of the heat loss for a worst-case scenario (20 mm wide air cavity in the roof construction) is from 74.9 to 86.3%, depending on the climate (*Figure 16*) and the absolute increase of the heat loss in Kiruna (Sweden) is 8.8 kWh/(m²·a) for each m² of the envelope area.
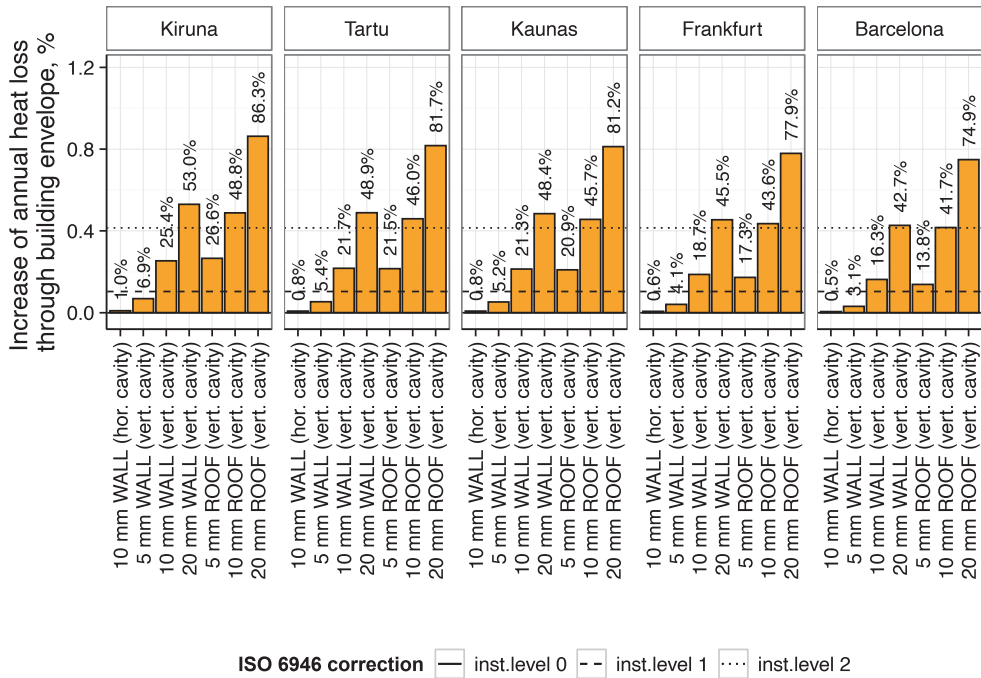
Figure 16. Relative increase of the heat loss of the unitary envelope area in different climates depending on the air cavity configuration inside the insulation layer.

Compared to a regular penetrating 10 mm and 20 mm wide air cavity, the use of polyurethane montage foam to fill the outermost 50 mm of the cavity will reduce the heat loss by 0.8 and 1.9 kWh/(m²·a) in Estonian climate.

4. Discussion

The study showed that in a fully penetrating vertical air cavity within a wall insulation layer, the convective heat flow is strongly dependent on the temperature difference and cavity width. At low temperature differences (Δt = 10K), the correction factor $\Delta U''$ was similar to simplified values defined in EN ISO 6946 but increased temperature difference (Δt = 40 K) increases the heat loss significantly, corresponding approximately to one level of increase in standardized installation level. For a 20 mm wide fully penetrating cavity, the correction factor at the 40 K temperature difference is well over maximum correction level proposed by EN ISO 6946. Although direct comparison is not possible, an older empirical study in Sweden [6] measured the reduction of thermal resistance under heat flow plate over vertical and horizontal 5, 10 and 30 mm cavities in a 95 mm thick insulation layer and found similar effects. At the temperature difference around 20 K, the thermal resistance decreased approximately up to 5, 21 and 55% on average under the heat flow plate respectively to the cavity width of 5 mm to 30 mm [6], based on the 100 mm diameter of the measurement plate and cavity width, the approximate length-to-area ratio of the cavity is 12.7 m/m². In our study, the relative cavity length-to-area-ratio for an assessed typical situation was 1.67 m/m²

corresponding to insulation boards with full building floor height and repeating cavities with 600 mm step. Approximately estimated correction factors for vertical air cavity $\Delta U''$ based on Swedish data but scaled to the length-to-area-ratio used in our study are 0.003, 0.014, 0.063 W/(m²·K) respectively for 5, 10 and 30 mm wide air cavities. In the current study, the numerically calculated correction factors for vertical air cavities $\Delta U''$ were 0.004 and 0.015 W/(m²·K) for 5 and 10 mm wide air cavities and 0.055 W/(m²·K) for 20 mm wide air void, which are very similar.

Unexpectedly in the Swedish study, the results for penetrating horizontal cavities in the insulation layer did not differ from vertical cavities, which could not be reproduced in our study. Similarly, another study conducted in Finland featuring cavity length-to-area-ratio around 2.1 m/m² found that horizontal air cavities have no significant effect on the overall thermal transmittance [10].

The increase of the thermal transmittance due to higher temperature difference is higher in the roof construction for all assessed cases. The simplified procedures defined in ISO 6946 are unable to describe this problem for all cases with cavity above 5 mm. Previous research from Lithuania on cavities in roof insulation has shown that cavity widths below 5 mm have no significant effect on the thermal transmittance [3], but the measurements were conducted only with the temperature difference of $\Delta t = 20$ K. Our study shows that with the increasing temperature difference, the additional heat loss due to convection increases significantly. In the case of a roof, the external surface temperature may be even higher, and the temperature difference may be even greater [3]. For wider cavities in the roof insulation, the measured thermal transmittance in the Lithuanian study increased up to 20% when considering the least favourable estimated combination of air cavity length-to-area-ratios of 0.25 m/m² (1.3 mm wide cavity), 0.25 m/m² (3.0 mm wide cavity), 0.556 m/m² (9.0 mm wide cavity), and 0.556 m/m² (18.0 mm wide cavity). Our study determined the correction factor for 10 mm and 20 mm air cavities for the thermal conductivity of 0.040 W/(m·K) around 0.07 and 0.10 W/(m²·K), when the cavity length-to-area-ratio is 1.67 m/m². For three times lower cavity length-to-area-ratio, this means approximately 12% increase in the thermal transmittance due to 10 mm cavity and 17% increase due to 20 mm cavity. In total, the increase is similar to previous findings [3]. In the case of circular use of materials [17], the possible deviation from nominal material dimensions could be larger than set for new materials up to 2% for mineral wool [18] or 3% for expanded polystyrene [1]. Therefore, the construction of the building envelope from materials from urban mines or reused material banks should be even more conservative when estimating crack dimensions.

The effect of insulation material is small for cavity widths of 5 and 10 mm. For wider cavities (20 mm), the heat loss increases with the increase in the thermal conductivity. This effect is more prominent in vertical cavities inside the roof construction. This also suggests that in wider penetrating cavities occurring between the edge of the insulation board and the timber frame or steel battens, an additional heat loss can be even higher.

Two types of non-penetrating cavities were assessed to see if the effect on the thermal transmittance is significantly lower when air circulation between internal and external boundaries is prevented by partial filling with PU foam or with the use of dual layer insulation with rebate edge. Both alternatives decreased the correction factor $\Delta U''$ by a factor of two or more depending on the temperature difference with 10 mm wide cavity staying slightly below normative installation level 1, which corresponds to 4.6 to 9.5% increase in the thermal transmittance depending on the insulation material. A previous study has shown that cavities

545 formed due to poor workmanship do not dramatically increase (observed increase 5 to 10%)
546 the thermal transmittance if they prevent air circulation from hot side to cold side [10].
547   Nevertheless, at the temperature difference of Δt = 35K, the numerically derived
548 correction factor for a 10 mm wide cavity was above the normative installation level 0 and
549 20 mm wide cavity above the normative installation level 1, although both alternatives are
550 listed as level 0 installation solution in EN ISO 6946 [11], which should be updated.
551   The current study and previous studies have shown that along with the temperature
552 difference, the length-to-area-ratio has a significant effect on additional heat loss through the
553 building envelope. Our study was based on typical dimensions of insulation boards and typical
554 timber frame step size with an approximate width of 600 mm corresponding to the cavity
555 length-to-area-ratio of 1.67 m/m^2 when only vertical cavities are accounted for. If the step
556 size between timber or steel battens is smaller due to architectural or structural constraints,
557 the length-to-area-ratio will increase along with additional heat loss. The average step size of
558 400 mm, for example, increases the additional losses through vertical cavities by 50%.
559 Currently, the correction factors for air cavities defined in EN ISO 6946 do not quantify the
560 number of cavities and should be updated.
561   Our study showed that there are smaller or larger cavities present between the
562 insulation boards and batts installed on construction sites in the factory of the prefabricated
563 building elements - the insulation does not always fill the space provided. Our results showed
564 that the actual heat loss due to cracks and cavities is higher than the calculated ideal situation.
565 Hamburg [19] showed that the performance gap between the measured and the calculated
566 energy consumption was 2–30%, and the delivered energy for room heating after
567 refurbishment works was on average more than 35% larger than the calculated values in the
568 design phase. In addition to higher room temperature [20], energy for heating depends
569 directly also on the heat loss of the building envelope. The standard EN ISO 6946 [11] is based
570 on the ideal electrical-thermal analogy; therefore, it is necessary to consider corrections to
571 the thermal transmittance in the calculations of the heat loss of the building envelope. In their
572 review about building wall thermal characterization, Evangelisti et al. [21] showed that the
573 measured thermal transmittance is about 20% higher than that of the calculated.
574   Although our study showed that from the energy use perspective, the horizontal air
575 cavities inside the wall construction and vertical air cavities inside the floor construction have
576 no significant effect on the heat loss, the transport of moisture due to diffusion and
577 convection can still be problematic regarding the performance and durability of the building
578 envelope.

5. Conclusion

580   The cavities inside an insulation layer increase the thermal transmittance and the heat
581 loss of the building envelope due to additional convection and radiation inside the cavity. The
582 effect is dependent on different physical conditions, some of which are not currently taken
583 into account in ISO 6946 [11].
584   Due to low natural convection, the additional heat loss through penetrating horizontal
585 air cavity is insignificant in the wall insulation layer. In vertical air cavities, the additional heat
586 loss was found highly dependent on the cavity diameter and temperature difference. In the
587 case of 10 K temperature difference, the additional heat loss was marginal, but at 40 K
588 temperature difference, the penetrating air cavities with 5, 10 and 20 mm diameter will
589 increase the thermal transmittance up to 10, 33 and 59% respectively; however, the
590 simplified procedure in EN ISO 6946 was unable to describe this effect adequately. In total,

591 the increase of the temperature difference from 10 to 40 K increased the correction factor
592 for air cavities one level up compared to the normative suggestion. For an upward heat flow
593 (roof construction), the effect was even more adverse. Using dual layer insulation with rebate,
594 tongue and groove edge or expanding montage foam to tighten the external side of the air
595 cavity reduced the additional heat loss roughly by half and reduced the dependency of
596 additional heat loss on the temperature difference between internal and external
597 environments. In conclusion, the results are summed up in Table 2, where for each assessed
598 situation, the suitable normative installation level is given, which does not underestimate the
599 actual heat loss.

600 *Table 2. Standardized installation levels (ISO 6946) for each assessed case (cc 600 mm)*
601 *that can be used and will not underestimate the actual thermal transmittance caused by air*
602 *cavities inside the insulation layer in well-insulated building envelopes.*

Cavity width	Standardized installation levels (ISO 6946) according to cavity geometry (see *Figure 3*) for floor wall and roof construction										
	Penetrating cavity with rectangular cross-section				Cavity filled by PU foam (50 mm) from external side		Cavities in 2-layer insulation with rebate, tongue and groove edge		Penetrating cavity with wedge shaped cross-section		Penetrating cavity with additional triangular cut-outs
	Floor	Wall (hor.)	Wall (vert.)	Roof	Wall	Roof	Wall	Roof	Wall	Roof	Wall
= 5 mm	0	0	1	2	1	1	1	2	1	2	n/a
≤ 10 mm	0	0	2	n/a	1	2	2	2	1	2	n/a
> 10 mm (20 mm)	0	0	n/a	n/a	2	n/a	2	n/a	2	n/a	n/a

603 n/a - not applicable
604

605 Previous research has stated that in the case of impermeable insulation
606 materials convective heat transfer can take place in air gaps wider than 5 mm [3,22], but the
607 influence of natural convection on general heat transfer is insignificant when a joining small
608 air gap up to 3 mm thickness occurs around the thermal-insulating layer and therefore
609 cavities with thickness below 5 mm is not assessed in this study. In practice, insulation
610 installation level 0 (i.e., no-effect due to cavities) is not achievable with most insulation
611 solutions, where the formation of vertical cavities with thickness around 5mm or more is
612 expected. A few notable exceptions to this in practice would be spray-on foam insulation and
613 blown-in cellulose insulation inside wall and roof elements when high density blow in
614 insulation is used to avoid forming of creeps and cavities through vibration and aging. Many
615 other insulation solutions should be reclassified (currently level 0) to levels 1 or 2: dual layer
616 insulation, sealed or partly foamed cavities within single insulation layers. The effect is
617 strongly climate dependent, however, the current definition of the thermal transmittance
618 neglects this. Insulation material has only marginal effect (higher thermal conductivity

619 contributes to slightly higher additional heat loss). Penetrating cavities with thickness more
620 than 10 mm inside roof insulation have a huge effect and should be classified as inadequate
621 workmanship and a non-appropriate solution. Similarly, additional cut-out corners combined
622 with penetrating cavity have a significant effect and should be classified also as inadequate
623 workmanship and non-appropriate solution.

624 The results of this study can be used as input to further research on this topic to
625 generate a generalized set of requirements for a future version of EN ISO 6946, including the
626 effect of temperature difference and quantification of cavities through the length-to-area-
627 ratio or a similar measure.

6. Acknowledgements

7. Conflicts of Interest

636 The authors declare no conflict of interest. The funders had no role in the design of
637 the study; in the collection, analyses, or interpretation of data; in the writing of the
638 manuscript, or in the decision to publish the results.

8. Author Contributions

640 Compilation of methodology by J.H and T.K., preparation of calculation models and
641 numerical calculations by J.H. Experimental climate chamber measurements by R.P and
642 numerical calculations of validation cases by P.K, Data visualization and original draft
643 preparation by J.H., review and editing by J.H., P.K and T.K. The conceptualization of this
644 study, project administration and funding acquisition for the completed tasks were
645 performed by T.K.

9. References

648 [1] EN 13163, Thermal insulation products for buildings - Factory made expanded
649 polystyrene (EPS) products - Specification, EN 13163:2, European committee of
650 Standardization, Brussels, Belgium, 2016.
651 [2] EN 825, Thermal insulating products for building applications - Determination of
652 flatness, EVS-EN 825, European committee of Standardization, Brussels, Belgium, 2013.
653 [3] J. Šadauskiene, A. Buska, A. Burlingis, R. Bliūdžius, A. Gailius, The effect of vertical air
654 gaps to thermal transmittance of horizontal thermal insulating layer, J. Civ. Eng. Manag.
655 15 (2009) 309–315. https://doi.org/10.3846/1392-3730.2009.15.309-315.
656 [4] J. Tatara, L. Ricketts, Impact of Heating and Cooling of Expanded Polystyrene and Stone
657 Wool Insulations on Conventional Roof Performance, in: IMPACT Heat. Cool. Expand.
658 Polystyr. STONE WOOL Insul. Conv. ROOF Perform., Vancouver, BC, 2017: pp. 1–16.
659 [5] L. Ricketts, Impact of Insulation Dimensional Stability on Conventional Roof
660 Performance, in: 33rd RCI Int. Conv. Trade Show, 2018: pp. 161–173.
661 [6] C.G. Bankwall, Natural convective heat transfer in insulated structures, ASME Pap.

662   (1972).

663   [7]   D. Miles-Shenton, C. Gorse, F. Thomas, External walls partially filled with insulation,
664   and the potential to "top-up" the residual cavity., (2015).
665   http://eprints.leedsbeckett.ac.uk/5067/.

666   [8]   R.J. Lowe, J. Wingfield, M. Bell, J.M. Bell, Evidence for heat losses via party wall cavities
667   in masonry construction, Build. Serv. Eng. Res. Technol. 28 (2007) 161–181.
668   https://doi.org/10.1177/0143624407077196.

669   [9]   D. Miles-Shenton, J. Wingfield, R. Sutton, M. Bell, Temple Avenue field trial – Evaluation
670   of design & construction process and measurement of fabric performance of new build
671   dwellings, (2010) 1–32.

672   [10] P. Huttunen, J. Vinha, Effect of natural convection on the thermal transmittance of
673   exterior walls with air-permeable insulation, Therm. Perform. Exter. Envel. Whole
674   Build. - 12th Int. Conf. (2013).

675   [11] EN ISO 6946, Building components and building elements — Thermal resistance and
676   thermal transmittance — Calculation Method, 2017th ed., ISO Copyright office,
677   Geneva, 2017. www.iso.org.

678   [12] P. Klõšeiko, R. Piir, M. Jeltsov, T. Kalamees, Thermal bridge effect of vertical diagonal
679   tie connectors in precast concrete sandwich panels: An experimental and
680   computational study, E3S Web Conf. 172 (2020) 1–7.
681   https://doi.org/10.1051/e3sconf/202017208001.

682   [13] ANSYS inc., ANSYS finite element analysis software, (2020).
683   https://www.ansys.com/products (accessed January 27, 2020).

684   [14] CEN committee ISO/TC 163/SC, ISO 10211:2017 Thermal bridges in building
685   construction. Heat flows and surface temperatures. Detailed calculations, 2017.
686   https://www.iso.org/standard/65710.html.

687   [15] T. Kalamees, J. Kurnitski, Estonian climate analysis for selecting the test reference year,
688   in: HB 2006 - Heal. Build. Creat. a Heal. Indoor Environ. People, Proc., 2006: pp. 207–
689   212.

690   [16] R. of Heating, Ashrae, International Weather for Energy Calculations (Iwec), Amer
691   Society of Heating, 2001. https://books.google.ee/books?id=tcaVuAAACAAJ.

692   [17] K. Kuusk, K. Kullerkupp, P. Pihelo, M. Ritzen, A. Tisov, T. Kalamees, Circularity concepts
693   for offsite prefabricated energy renovation of apartment buildings, in: 8th Int. Build.
694   Phys. Conf., Copenhagen, Denmark, 25-27 August 2021, 2021.

695   [18] EN 13162, Thermal insulation products for buildings - Factory made mineral wool (MW)
696   products - Specification, Brussels, 2016.

697   [19] A. Hamburg, T. Kalamees, How well are energy performance objectives being achieved
698   in renovated apartment buildings in Estonia?, Energy Build. 199 (2019) 332–341.
699   https://doi.org/https://doi.org/10.1016/j.enbuild.2019.07.006.

700   [20] A. Hamburg, T. Kalamees, The Influence of Energy Renovation on the Change of Indoor
701   Temperature and Energy Use, Energies. 11 (2018) 3179.
702   https://doi.org/10.3390/en11113179.

703   [21] L. Evangelisti, C. Guattari, F. Asdrubali, Influence of heating systems on thermal
704   transmittance evaluations: Simulations, experimental measurements and data post-
705   processing, Energy Build. 168 (2018) 180–190.
706   https://doi.org/10.1016/j.enbuild.2018.03.032.

707   [22] V. Stankevičius, V. Paukštys, R. Bliudžius, J. Šadauskiene, Z. Turskis, R. Samajauskas,
708   Convection in mineral wool used as insulation for buildings, J. Civ. Eng. Manag. 19

709   (2013) 296–304. https://doi.org/10.3846/13923730.2013.775182.

Curriculum vitae

Personal data

Name:	Jaanus Hallik
Date of birth:	14.12.1981
Place of birth:	Võru, Estonia
Citizenship:	Estonian

Contact data

E-mail:	jaanus.hallik@taltech.ee

Education

2017–…	Tallinn University of Technology, Department of Civil Engineering and Architecture: Nearly Zero Energy Buildings Research Group, PhD studies in Civil and Environmental Engineering
2005–2008	University of Tartu, Faculty of Biology and Geography, MSc degree in environmental technology (ecological engineering)
2000–2005	University of Tartu, Faculty of Biology and Geography, BSc degree in environmental technology (ecological engineering)
1997–2000	Gustav Adolf Grammar School, specialization in mathematics and physics

Special courses

12.04.2021 – 16.04.2021	RILEM EACCOURSE "Computational Methods for Building Physics and Construction Materials" in Darmstadt, Germany
02.10.2017 – 07.10.2017	IDA ICE simulation software advanced course "EQUA Academýs 3rd Simulation Summit" in Vilifau, Austria

Language competence

Estonian	Native speaker
English	Fluent
Finnish	Average

Professional employment

2019–…	Tallinn University of Technology, School of Engineering, Department of Civil Engineering and Architecture, Expert
2015–2021	Modular building factory Sense OÜ, specialist of energy efficiency
2009–2015	Energy efficiency in buildings consultancy company PassiveHouse OÜ, consultant
2007–2017	University of Tartu, Energy efficient building core lab, specialist
2004–2007	Alkranel LCC, environmental consultant

Scientific publications and conference proceedings

Hallik, J.; Klõšeiko, P.; Piir, R.; Kalamees, T. (2022). Numerical analysis of additional heat loss induced by air cavities between insulation boards due to non-ideality. (Submitted to: *Journal of Building Engineering* 06.04.2022)

Hallik, J.; Kalamees, T. (2021). The effect of flanking element length in thermal bridge calculation and possible simplifications to account for combined thermal bridges in well insulated building envelopes. *Energy and Buildings, 252*. DOI: 10.1016/j.enbuild.2021.111397.

Klõšeiko, P.; Arumägi, E.; Hallik, J.; Kalamees, T. (2021). Dependence of measured specific air leakage rate (qE50) on envelope pressure measurement position: a case study in an apartment building in winter conditions. *Journal of Physics: Conference Series: 8th International Buildings Physics Conference 2021, Copenhagen, 25-27 August 2021*. IOP Publishing, #012229. DOI: 10.1088/1742-6596/2069/1/012229.

Hallik, J.; Kalamees, T. (2020). A new method to estimate point thermal transmittance based on combined two-dimensional heat flow calculation. *12th Nordic Symposium on Building Physics, NSB 2020, Tallinn; Estonia; 6 September + 9 September 2020. Ed. Kurnitski, J.,,Kalamees, T. EDP Sciences, #08005. (E3S Web of Conferences; 172)*. DOI: 10.1051/e3sconf/202017208005.

Hallik, J.; Kalamees, T. (2019). Development of Airtightness of Estonian Wooden Buildings*. Journal of Sustainable Architecture and Civil Engineering, 24 (1), 36–43.* DOI: 10.5755/j01.sace.24.1.23231.

Hallik, J.; Gustavson, H.; Kalamees, T. (2019). Air Leakage of Joints Filled with Polyurethane Foam. *Buildings, 9 (7), 172.* DOI: 10.3390/buildings9070172.

Kuusk, K.; Kaiser, A.; Lolli, N.; Johansson, J.; Hasu, T.; Gunnarshaug Lien, A.; Arumägi, E.; Kalbe, K.; Hallik, J.; Kurnitski, J.; Kalamees, T. (2019). Energy Performance, Indoor Air Quality and Comfort in New Nearly Zero Energy Day-care Centres in Northern Climatic Conditions*. Journal of Sustainable Architecture and Civil Engineering, 24 (1), 7–16.* DOI: 10.5755/j01.sace.24.1.23228.

Kuusk, K.; Hallik, J.; Kalamees, T.; Mauring, T. (2015). Performance of Heat Recovery Ventilation System with Ground Source Brine Heat Exchanger Pre-Heating System in the Context of nZEB. *Proceedings of REHVA Annual Conference: Latvia, Rīga, 6-9 May, 2015.* RTU Press, 17–22. DOI: 10.7250/rehvaconf.2015.002.

Hallik, J.; Kalbe, K.; Mauring, T. (2014). The performance of subsoil frost protection system of mechanical heat recovery ventilation unit in a cold climate in the context of net zero energy building. *10th Nordic Symposium on Building Physics, Lund, Sweden, 15-19 June 2014.*

Mauring, T., Hallik, J., Kalbe, K., Valge, M. (2014). Winter performance of certified Passive House building in Northern European cold climate. *18th International Passive House Conference, Aachen, Germany, 25-26 April 2014.*

Mauring, T.; Reinberg, GW.; Hallik, J.; Valge, M.; Kalbe, K. (2013). A prototype architecture for passive and plus energy building in Estonia. *Proceedings of 6th Passive House Conference in the Nordic Countries, 6: 6th Passive House Conference in the Nordic Countries; Göteborg, Sweden; 15.-17. Oct 2013. Ed. Jan-Olof Dalenbäck. Göteborg, Sweden: Chalmers University of Technology, 18–29.*

Reinberg, G. W.; Mauring, T.; Hallik, J.; Valge, M.; Kalbe, K. (2013). First Certified Passive House in Estonia. *Proceedings of 17th International Passive House Conference, 17: 17th International Passive House Conference; Frankfurt, Germany; 19.-20. April 2013. Ed. Feist, Wolfgang. Darmstadt: Passivhaus Institut Darmstadt.*

Elulookirjeldus

Isikuandmed

Nimi:	Jaanus Hallik
Sünniaeg:	14.12.1981
Sünnikoht:	Võru, Eesti
Kodakondsus:	Eesti

Kontaktandmed

E-post:	jaanus.hallik@taltech.ee

Hariduskäik

2017–…	Tallinna Tehnikaülikool, Inseneriteaduskond, Ehituse ja arhitektuuri instituut, doktoriõpe ehituse ja keskkonnatehnika erialal
2005–2008	Tartu Ülikool, Bioloogia-geograafiateaduskond, keskkonnatehnoloogia magistriõpe
2000–2005	Tartu Ülikool, Bioloogia-geograafiateaduskond, keskkonnatehnoloogia bakalaureuseõpe
1997–2000	Gustav Adolfi Gümnaasium, matemaatika ja füüsika süvaõpe

Erikursused

12.04.2021 – 16.04.2021	RILEM EACCOURSE "Computational Methods for Building Physics and Construction Materials" in Darmstadt, Germany
02.10.2017 – 07.10.2017	IDA ICE simulation software advanced course "EQUA Academy's 3rd Simulation Summit" in Vilifau, Austria

Keelteoskus

Eesti keel	Emakeel
Inglise keel	Kõrgtase
Soome keel	Kesktase

Teenistuskäik

2019–…	Tallinna Tehnikaülikool, Inseneriteaduskond, Ehituse ja arhitektuuri instituut, ekspert
2015–2021	Sense OÜ, energiatõhususe spetsialist PassiveHouse
2009–2015	OÜ, konsultant
2007–2017	Tartu Ülikool, Energiatõhusa ehituse tuumiklabor, spetsialist
2004–2007	Alkranel OÜ, keskkonnaspetsialist

Teaduspublikatsioonid ja konverentsiettekanded

Hallik, J.; Klõšeiko, P.; Piir, R.; Kalamees, T. (2022). Numerical analysis of additional heat loss induced by air cavities between insulation boards due to non-ideality. (Submitted to: *Journal of Building Engineering* 06.04.2022)

Hallik, J.; Kalamees, T. (2021). The effect of flanking element length in thermal bridge calculation and possible simplifications to account for combined thermal bridges in well insulated building envelopes. *Energy and Buildings, 252*. DOI: 10.1016/j.enbuild.2021.111397.

Klõšeiko, P.; Arumägi, E.; Hallik, J.; Kalamees, T. (2021). Dependence of measured specific air leakage rate (qE50) on envelope pressure measurement position: a case study in an apartment building in winter conditions. *Journal of Physics: Conference Series: 8th International Buildings Physics Conference 2021, Copenhagen, 25-27 August 2021.* IOP Publishing, #012229. DOI: 10.1088/1742-6596/2069/1/012229.

Hallik, J.; Kalamees, T. (2020). A new method to estimate point thermal transmittance based on combined two-dimensional heat flow calculation. *12th Nordic Symposium on Building Physics, NSB 2020, Tallinn; Estonia; 6 September + 9 September 2020. Ed. Kurnitski, J.,,Kalamees, T. EDP Sciences, #08005. (E3S Web of Conferences; 172)*. DOI: 10.1051/e3sconf/202017208005.

Hallik, J.; Kalamees, T. (2019). Development of Airtightness of Estonian Wooden Buildings*. Journal of Sustainable Architecture and Civil Engineering, 24 (1), 36−43.* DOI: 10.5755/j01.sace.24.1.23231.

Hallik, J.; Gustavson, H.; Kalamees, T. (2019). Air Leakage of Joints Filled with Polyurethane Foam. *Buildings, 9 (7), 172.* DOI: 10.3390/buildings9070172.

Kuusk, K.; Kaiser, A.; Lolli, N.; Johansson, J.; Hasu, T.; Gunnarshaug Lien, A.; Arumägi, E.; Kalbe, K.; Hallik, J.; Kurnitski, J.; Kalamees, T. (2019). Energy Performance, Indoor Air Quality and Comfort in New Nearly Zero Energy Day-care Centres in Northern Climatic Conditions*. Journal of Sustainable Architecture and Civil Engineering, 24 (1), 7−16.* DOI: 10.5755/j01.sace.24.1.23228.

Kuusk, K.; Hallik, J.; Kalamees, T.; Mauring, T. (2015). Performance of Heat Recovery Ventilation System with Ground Source Brine Heat Exchanger Pre-Heating System in the Context of nZEB. *Proceedings of REHVA Annual Conference: Latvia, Rīga, 6-9 May, 2015.* RTU Press, 17−22. DOI: 10.7250/rehvaconf.2015.002.

Hallik, J.; Kalbe, K.; Mauring, T. (2014). The performance of subsoil frost protection system of mechanical heat recovery ventilation unit in a cold climate in the context of net zero energy building. *10th Nordic Symposium on Building Physics, Lund, Sweden, 15-19 June 2014.*

Mauring, T., Hallik, J., Kalbe, K., Valge, M. (2014). Winter performance of certified Passive House building in Northern European cold climate. *18th International Passive House Conference, Aachen, Germany, 25-26 April 2014.*

Mauring, T.; Reinberg, GW.; Hallik, J.; Valge, M.; Kalbe, K. (2013). A prototype architecture for passive and plus energy building in Estonia. *Proceedings of 6th Passive House Conference in the Nordic Countries, 6: 6th Passive House Conference in the Nordic Countries; Göteborg, Sweden; 15.-17. Oct 2013. Ed. Jan-Olof Dalenbäck. Göteborg, Sweden: Chalmers University of Technology, 18−29.*

Reinberg, G. W.; Mauring, T.; Hallik, J.; Valge, M.; Kalbe, K. (2013). First Certified Passive House in Estonia. *Proceedings of 17th International Passive House Conference, 17: 17th International Passive House Conference; Frankfurt, Germany; 19.-20. April 2013. Ed. Feist, Wolfgang. Darmstadt: Passivhaus Institut Darmstadt.*